Univerzita Karlova

Přírodovědecká fakulta

Studijní program:

Environmentální vědy

Mgr. Jitka Sikorová

Měření a toxicita nanočástic ze spalovacích procesů
Measurement and toxicity of combustion generated nanoparticles

Dizertační práce

Školitel:
Ing. Jan Topinka, DrSc.
Prof. Martin Braniš, CSc.

Školitel-konzultant:
doc. Michal Vojtíšek, Ph.D.

Praha 2019

Prohlašuji, že jsem tuto dizertační práci vypracovala samostatně s využitím uvedené literatury a informací, na něž odkazuji. Tato práce ani její podstatná část nebyla předložena k získání jiného nebo stejného akademického titulu.

V Praze dne .....

Mgr. Jitka Sikorová

Poděkování

Ráda bych poděkovala všem, kteří mi v průběhu tvorby disertační práce poskytli pomoc, především svému vedoucímu ing. Janu Topinkovi DrSc., který mě laskavě a lidsky vedl po dobu doktorského studia. Také bych chtěla poděkovat prof. RNDr. Martinu Branišovi CSc. který ovlivnil mé vysokoškolské studium a navedl mě na problematiku znečištěného ovzduší a jeho dopad na lidské zdraví.

Díky patří všem spoluautorům článků, především Doc. Michalovi Vojtíškovi Ph.D., ing Vítu Beránkovi Ph.D., RNDr. Pavlu Rössnerovi, Jr. Ph.D., mgr. Heleně Líbalové Ph.D., mgr. et ing. Táňě Závodné, mgr. Kristýně Vrbové, mgr. Aleně Milcové a dalším. Bez nich by články nikdy nedosahovaly takové kvality a práce na nich by nebyla ani z poloviny tak zábavná.

V neposlední řadě bych chtěla poděkovat členům rodiny, kteří se snažili pomoci, jak to bylo možné, jmenovitě manželovi především za trpělivost, mámě a tchýni za možnost odpočinku a mému synu Vladimíru Sikorovi, že někdy dokonce i spal.

Abstrakt

Předložená dizertační práce se komplexně věnuje problematice nanočástic vznikajících ve spalovacích motorech používaných v dopravě. Zabývá se prostorovou distribucí nanočástic v lidských sídlech, dopadem použití alternativních paliv na produkci a toxicitu nanočástic a také otázkou samotného toxikologického testování částic.

V rámci dizertační práce byl proveden monitoring nanočástic v ovzduší a doprava byla identifikovaná jako hlavní zdroj nanočástic nejen v silně zatíženém městě (Praha), ale i ve městě s nízkým stupněm dopravy (Čelákovice). Většina částic pravděpodobně vznikla během krátkých epizod vysokých emisí (např. akcelerace vozidel do kopce). Během měření byla identifikována vozidla s vysokými emisemi, která se podílí velkou měrou na znečistění ovzduší. Na straně druhé jsou provozovány spalovací motory, u kterých emise nejsou regulovány, jako např. motorová sekačka, která byla v provozu poblíž místa měření a generovala velké množství nanočástic.

Množství a vlastnosti částic vytvářených spalováním jsou závislé na technologii spalování a složení paliva. Velká část dizertační práce se zabývá vlivem alternativních paliv na množství a kvalitu produkovaných částic a na toxicitu organické složky adsorbované na částice. Nejnižší toxicitu pro vznětové motory vykazoval hydrogenovaný rostlinný olej (HVO, z anglického hydrotreated vegetable oil), ale pokles počtu a hmotnosti částic nebyl takový jako u klasické bionafty (metylestery nenasycených mastných kyselin z řepky olejky). Nevýhodou HVO je vysoká cena. Oba tyto problémy by se daly vyřešit přimícháním výrazně levnějšího butanolu do HVO, který zároveň snižuje množství částic. Jako nejvhodnější příměs do benzínu pro zážehové motory se ukázal být isobutanol, jak z toxikologického hlediska, tak i pro nízké množství vyprodukovaných částic.

Toxikologické účinky emisí byly stanoveny pomocí organických extraktů z částic, tedy toxicita samotných částic nebyla sledována, neboť samotné vzorkování částic tak, aby v jeho důsledku nedošlo ke změně morfologie a velikosti částic, je technicky velmi obtížné. Také převedení částic do buněčného média s sebou nese další proměnné, které ovlivňují výsledky testování toxicity. Na modelu nanočástic TiO_2 bylo ukázáno, že na toxicitu má vliv stabilita suspenze, která je ovlivněna laboratorním postupem

resuspendace částic v médiu, a tvorba proteinové korony v buněčném mediu. Tyto charakteristiky závislé na zvoleném laboratorním postupu by mohly vysvětlit nesourodé výsledky toxikologických analýz nanočástic.

Práce přispěla k pochopení složité problematiky nanočástic z dopravy, nastínila možnou cestu k redukci toxických účinků emitovaných nanočástic a identifikovala možnou příčinu nesourodých výsledků v toxikologii nanočástic.

Klíčová slova: alternativní paliva, biopaliva, nanočástice, TiO_2, toxicita nanočástic, ultra-jemné částice

Abstract

This thesis is focused on nanoparticles produced by internal combustion engines utilized in vehicles. It deals with spatial distribution of nanoparticles within urban areas, impact of alternative fuels usage on particle production and toxicity, and a particle toxicological testing methodology.

Monitoring of airborne nanoparticles identified traffic as the main source of airborne nanoparticles in places with heavy traffic load (Prague), as well as in a small city with only local traffic (Čelákovice). Most particles were likely emitted during short episodes of high emissions (e.g. uphill acceleration). During the measurements, high-emission vehicles responsible for a large fraction of the air pollution were also identified. On the other hand, small non-road internal combustion engines, which are not subject to any limit on particle emissions, such as a lawn mower, were operated during the measurement and generated a large number of nanoparticles.

The amount and characteristics of the particles produced by combustion depend on the combustion technology and the fuel composition. A large part of the thesis deals with alternative fuels and their effects on the quantity of produced particles and toxicity of organic matter adsorbed on the particles. Hydrotreated vegetable oil (HVO) exhibited the lowest toxicity among tested fuels for diesel engines, but it did not reduce the mass of particles as much as biodiesel. Another disadvantage of HVO is its high price. Both issues could be solved by blending significantly cheaper butanol into the HVO that reduces particulate matter emissions. A blend of gasoline and isobutanol was shown to be the best alternative fuel for spark-ignition engines from both toxicological and particle emission points of view.

Toxicological effects were determined in organic extracts of particles. Thus, the toxicity of the particles themselves was omitted, since sampling of intact particles without morphological and size changes is technically difficult. Moreover, transferring the particles into the cell culture medium affects characteristics of the particles important for their toxicity. Using TiO_2 nanoparticles as a model nanomaterial, it has been shown that the stability of the suspension affects the toxicity of particles; suspension stability is dependent on the operation procedure of particle resuspension in the medium and formation of the protein corona within the cell culture medium. These characteristics,

dependent on a laboratory procedure, could explain inconsistent results in toxicological analyses of nanoparticles.

The thesis contributed to understanding of combustion generated nanoparticles, showed a possible way for toxicity reduction of traffic related nanoparticles, and identified a possible cause of ambiguous results in nanoparticles toxicity.

Key words: alternative fuels, biofuels, Nanoparticles, nanotoxicity, ultra fine particles, TiO_2

Obsah

1. Úvod

Nanočástice, jako částice s průměrem menším nebo rovným 100 nm, jsou nejjemnější frakcí částic v prostředí. Přirozeně se nanočástice vyskytují například v sopečném popelu, vznikají při lesních požárech, jsou vytvářeny v atmosféře reakcí těkavých organických látek uvolňovaných rostlinami nebo např. viry jsou biologické částice o nanorozměrech. V současné době jsou nanočástice zmiňované hlavně v souvislosti s rozvojem nanotechnologií. Lidmi vytvářené nanočástice můžeme dělit na záměrně vyráběné a na ty, které doprovázejí lidskou činnost jako její vedlejší produkt.

Vyráběné nanočástice jsou navržené s určitým cílem využití a jsou tedy produkovány záměrně. Jejich složení, tvar a velikost jsou kontrolované. Takto vytvořené nanočástice mnohdy mívají vlastnosti, které původní makromateriál neměl (Gwinn et Vallyathan, 2006). Vyráběné nanočástice našly uplatnění v celé řadě oblastí jako je elektronika, biomedicína, farmakologie, kosmetika, energetika, životní prostředí nebo katalýza (Missaoui et al., 2018). Právě díky velkému potenciálu a množnému ekonomickému dopadu jsou do nanotechnologií investovány nemalé peníze a rozvoj těchto technologií je obrovský (Shapira et Wang, 2010). I přes rozsáhlé využití cíleně vyráběných nanomateriálů je s ohledem na jejich množství potřeba sledovat jejich osud v životním prostředí v rámci jejich celého životního cyklu.

Na druhé straně je investováno do technologií, které snižují množství nanočástic vznikajících jako vedlejší produkt lidské činnosti. Typickým příkladem jsou nanočástice vytvářené hořením paliva ve spalovacích motorech vozidel, kde se pro snížení emisí těchto částic instalují filtry pevných částic. I přes postupné zavádění filtrů pevných částic, zůstává doprava hlavním zdrojem nanočástic ve velkých městech (Kumar *et al*., 2014; Brines *et al*., 2015), kde se soustřeďuje značná část lidské populace.

Nanočásticím ze spalovacích motorů vozidel jsou lidé vystaveni již po desetiletí, na druhé straně expozice lidí vyráběným nanočásticím je relativně nová problematika. Není proto divu, že nanotoxikologie zabývající se vyráběnými nanočásticemi čerpá ze studií zabývajícími se toxikologií částic ze spalovacích motorů vozidel (Hesterberg *et al*., 2010), a zároveň nové poznatky o účincích přesně definovaných nanočástic, mohou být použity v toxikologii nanočástic ze spalovacích motorů. Hranice mezi

vyráběnými nanočásticemi a těmi ze spalovacích procesů se stala více nejasnou objevem nanotrubic, typicky vyráběných nanočástic, v dieselových emisích (Evelyn *et al*., 2003).

1.1 Velikostní distribuce částic v ovzduší

Částicemi v ovzduší rozumíme částice veliké několik nanometrů až desítky mikrometrů. Jakmile jsou uvolněné do atmosféry, mohou měnit svoji velikost a chemické složení kondenzací (nebo odpařováním) těkavých sloučenin na svém povrchu, koagulací s dalšími částicemi nebo chemickými reakcemi. Koncentrace částic je časově i prostorově velmi variabilní, jejich počty se pohybují od několika desítek částic po stovky tisíc částic × cm^3 ve znečištěném městském prostředí (Hinds, 1998). Velikostní distribuce částic má typicky několik módů, teoretické distribuce částic jsou znázorněny na Obrázek 1.

Nukleační mód tvoří částice s průměrem do 100 nm (nanočástice, ultra jemné částice). Vznikají při vysokoteplotních procesech a fotochemických reakcích v atmosféře (Hinds, 1998). Vzhledem k jejich malé velikosti, zřídka tvoří více než několik procent v celkové hmotnosti částic. Jejich doba setrvání v atmosféře je krátká díky jejich reaktivitě, kdy vzájemnou koagulací vytvářejí částice větší nebo se deponují na částice větší.

Akumulační mód tvoří částice přibližně od 100 nm po 1 μm. Vznikají především koagulací částic nukleačního modu a kondenzací par na jejich povrchu. Mechanismy odstraňování částic z atmosféry jsou u částic akumulačního modu nejméně účinné a hromadí se v atmosféře. Jejich doba setrvání je poměrně dlouhá, 1-2 týdny (Willeke *et* Whitby, 1975).

Mód hrubých částic obsahuje částice, které přesahují velikost 1 μm. Vznikají mechanickými procesy, jako jsou zvíření prachu větrem, mořský sprej, vulkanický popel aj. (Willeke *et* Whitby, 1975). Vzhledem k jejich velikosti hrubé částice rychle sedimentují a jejich doba setrvání v atmosféře je tedy krátká, mimo větrné dny, kdy jsou částice opětovně strhávány do ovzduší.

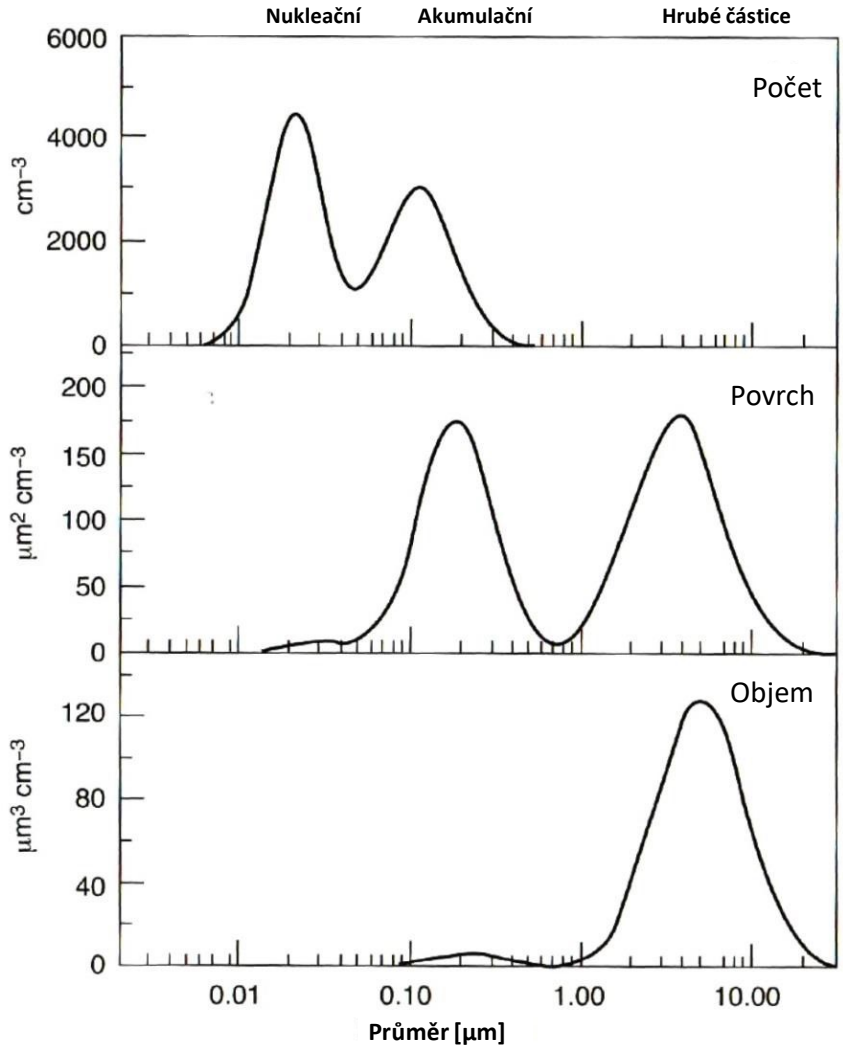

Obrázek 1 Teoretická početní, povrchová a objemová distribuce městského aerosolu. Většina částic v atmosféře jsou částice nukleačního modu, ale díky své malé velikosti přispívají jen několika procenty do celkové hmotnosti částic. Částice akumulačního modu významně přispívají do celkového objemu, a tedy i hmotnosti částic, a mají velký celkový povrch. Tyto částice jsou díky povrchu velmi důležité pro depozici částic nukleačního modu, adsorpci plynných sloučenin a heterogenní chemické reakce probíhající na jejich povrchu. Hrubé částice vytvářejí podstatnou část objemu a hmotnosti všech částic. Převzato z Colbeck *et al*., 2008.

1.2 Nanočástice ze spalovacích motorů

Tvorba nanočástic ve spalovacích motorech závisí především na typu motoru, ale také na kvalitě paliva, teplotě motoru, zatížení motoru aj. Částice ze vznětových motorů jsou složeny z uhlíkových částic a popelu s těkavými a sirnými sloučeninami. Uhlíkové částice jsou vytvářeny v průběhu hoření paliva v místech s bohatou směsí paliva. Většina takto vytvořených částic je následně oxidována. Nespálené částice pak opouštějí motor. (Kittelson, 1998)

Zážehové motory s nepřímým vstřikováním vytvářejí zanedbatelné množství částic ve srovnání se vznětovými motory (Kittelson, 1998). Částice v zážehových motorem vznikají hlavně spalováním oleje, odtrháváním úsad a porušováním povrchu dílů. Novější technologie zážehových motorů s přímým vstřikováním, která snižuje spotřebu paliva ve srovnání s konvenčními motory, vytváří částice podobně jako motory vznětové, a to v místech s bohatou směsí paliva za nedostatku kyslíku. Nedostatkem této technologie je, že vytváří znatelně více částic než motory s nepřímým vstřikováním (Tripathy *et al*., 2017).

Primární částice a jsou vytvářeny přímo v motoru. Jsou to aglomeráty v drtivé většině menší než mikrometr, tvořené pevným uhlíkatým materiálem (saze). V ovzduší přetrvávají především v akumulačním módu. Tyto částice mohou obsahovat popel a mít na svém povrchu adsorbované nebo zkondenzované uhlovodíky a sirné sloučeniny (Morawska *et al*., 2008). Uhlovodíky v motorech jsou výsledkem nedokonalého hoření malé frakce paliva a odpařeného mazacího oleje. Tyto látky jsou tvořeny také polycyklickými organickými uhlovodíky (PAH, z anglického polyaromatic hydrocarbons) a jejich deriváty obsahujícími skupiny s kyslíkem, dusíkem a sírou. Kovové sloučeniny z paliva a mazacího oleje vytváří pak malé množství částic popelu ve výfukových plynech (Kittelson, 1998). Vznětové motory většinou vytvářejí částice o velikostech v rozmezí 20-130 nm. Rozměry částice vytvořených zážehovými motory se pohybují v rozmezí 20-60 nm (Morawska *et al*., 2008).

Sekundární částice vznikají v atmosféře z prekurzorů. Motory ve vozidlech vypouští množství částečně těkavých organických látek, které vznikají nedokonalým prohořením paliva ve válci. Tyto látky se ve volné atmosféře ochladí a kondenzují ve velké množství několika nanometrových částic. Tyto částice jsou tvořeny zejména

uhlovodíky a hydratovanou kyselinou sírovou. Byly pozorovány poblíž rušných silnic nebo při měření za provozu, kdy mobilní laboratoř měří jednotlivé složky atmosféry za vozidlem. Vznik takových částic je velmi závislý na podmínkách ředění výfukových plynů. Měření vozidla na dynamometru tedy nemusí takové částice ukázat díky odlišné teplotě a nastavení ředícího poměru v ředícím tunelu. Plynné prekurzory se mohou také adsorbovat na povrch uhlíkatých primárních částic. Tedy vozidla vypouštějící velké množství částic, typicky vznětové motory bez filtrů částic, sekundární částice téměř nevytváří, kdežto vozidla osazena filtry částic již mohou. Tyto částice se řadí do nukleačního módu. Koncentrace těchto částic je velmi nestabilní a obtížně předvídatelná. (Morawska *et al*., 2008). Distribuce částic ze spalovacího motoru je znázorněna na Obrázek 2.

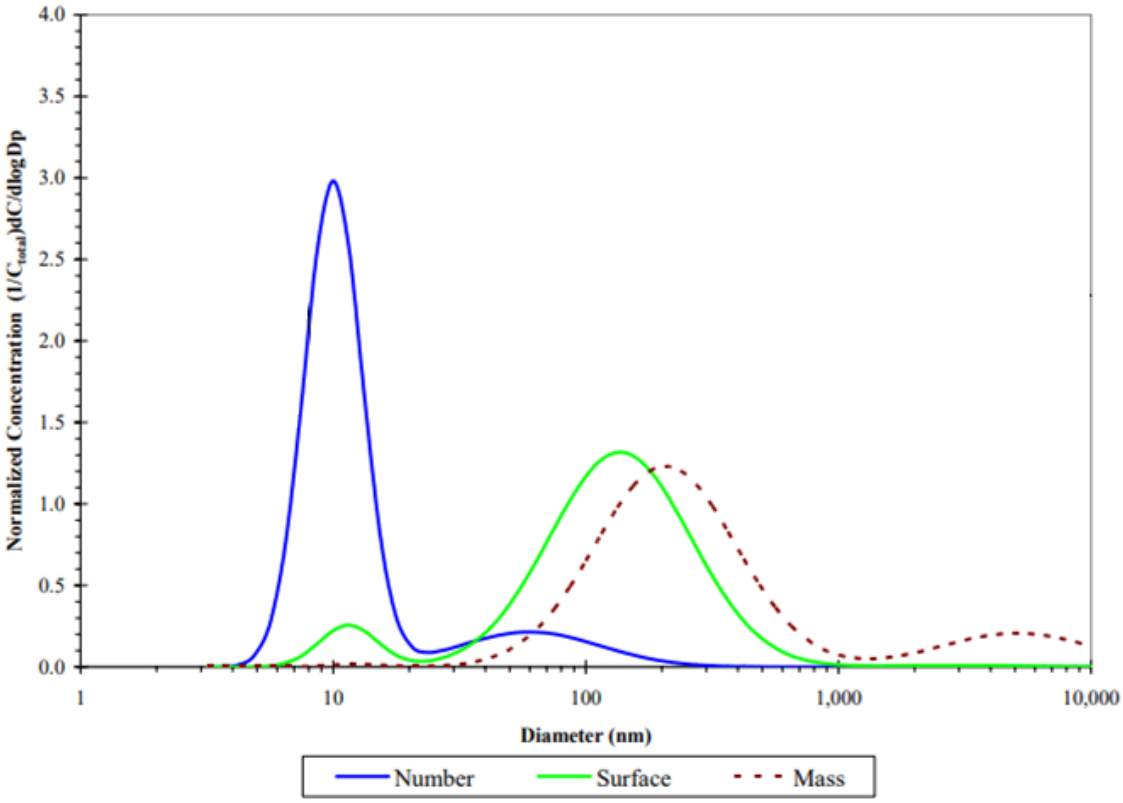

Obrázek 2 Velikostní distribuce částic emitovaných typickým spalovacím motorem (Kittelson *et al*., 2002); početní distribuce – modrá, distribuce dle velikosti povrchu – zelená, hmotnostní distribuce – přerušovaná hnědá. Na obrázku je znázorněna typická bimodální distribuce částic spalovacího motoru. Sekundární částice, veliké několik nanometrů, vytvářejí velmi výrazný vrchol v početní koncentraci, ale do celkové hmotnosti přispívají zanedbatelnou vahou. Většina primárních částic má průměr menší než 100 nm, ale většinu hmotnosti nesou částice větší než 100 nm.

Vznik a charakter částic je silně ovlivněn složením paliva. Klasická paliva vyráběná z ropy jsou často nahrazovaná obnovitelnými nejen kvůli změně klimatu, ale také kvůli energetické bezpečnosti a nezávislosti.

Obnovitelné náhrady paliva pro stávající vznětové motory jsou obvykle vyráběné z rostlinných olejů. Bionafta vzniká zpracováním tuků transesterifikací, v EU se typicky vyrábí palivo na bázi metylesterů nenasycených mastných kyselin z řepky olejky. Hydrodeoxidací tuků vzniká hydrogenovaný rostlinný olej (HVO, z anglického hydrotreated vegetable oil), také nazýván „zelená nafta“. Obě obnovitelné náhrady postrádají síru a neobsahují aromatické uhlovodíky jako klasická nafta. Bionafta je na rozdíl od HVO a nafty obohacena o kyslík (Aatola *et al*., 2009). Obě náhražky čisté i

ve směsi s naftou výrazně snižují emise částic, ale často lehce zvyšují emise NO_2 (Szybist *et al*., 2007; Knothe, 2010; Prokopowicz *et al*., 2015).

Jako obnovitelná složka benzínu pro běžná vozidla se v drtivé většině přimíchává v malém procentu (5-15 %) etanol. Vznětové motory jsou schopny provozu na 95% etanol s aditivy, avšak až po určité modifikaci motoru. Nevýhody etanolu jsou hygroskopické vlastnosti a agresivita vůči materiálům (Awad *et al*., 2018). Jako alternativa k etanolu se nabízí butanol a jeho izomery. Butanol je méně hygroskopický a není tolik agresivní vůči materiálu motoru (Andersen *et al*., 2010). Obnovitelné náhrady benzínu snižují emise částic a uhlovodíků, vliv na emise NOx je nejednoznačný (Lattimore *et al*., 2016; Awad *et al*., 2018).

Vznik částic v reálném provozu velmi záleží na osazení vozidla prvky následného zpracování výfukových plynů (filtr pevných částic, katalyzátory) a nastavení řídící jednotky vozidla. U novějšího, správně pracujícího vozidla se pak nemusí rozdíly v palivu odrazit na emisích (Suarez-Bertoa *et al*., 2019). Emise částic z motorů vozidel nejsou rovnoměrně rozděleny mezi vozový park, ale malé množství vozidel je zodpovědné za velkou část emisí částic (Wang *et al*., 2011; Kumar *et al*., 2011). Emise těchto částic také nejsou rovnoměrně rozptýlené po celé délce trasy daného vozidla, ale velká část emisí je soustředěna do krátkých epizod vysokých emisí, jako jsou akcelerace nebo běh studeného motoru. (Vojtisek-Lom *et al*., 2015).

1.3 Depozice nanočástic v lidských plicích

Existují tři hlavní mechanismy depozice

- Impakce – takto se deponují především hrubé částice, které mají díky vyšší hmotnosti i velkou hybnost
- Sedimentace – uplatňuje se pro částice v oblastech plicních sklípků a respiračních bronchiol
- Difúze – nanočástice difundují na stěny dýchacích cest a plicních sklípků.

Depozice částic v lidských plicích úzce souvisí s jejich stabilitou v ovzduší. Hrubé částice (> 1 μm) s relativně velkou hmotností se zachytávají v horních cestách dýchacích, kde se nedokážou přizpůsobit proudění a narazí do překážky díky své velké

hybnosti. Jemné částice (0,1 – 1 μm), které snadno následují proudnice vdechovaného vzduchu, se dostanou hluboko do plic, následně je většina těchto částic opět vydechnuta. Ještě menší částice (< 0,1 μm) jsou už výrazněji ovlivňovány Brownovým pohybem. Ty nejmenší z nanočástic se zachytávají již v horních cestách dýchacích. Větší těžší nanočástice (30 - 100 nm) se dostávají hluboko do plic, kde se deponují difúzí, na rozdíl od částic nad 100 nm, které jsou těžší, difúze není tolik efektivní a jsou vydechovány zpět do ovzduší (Obrázek 3). Při zrychleném dýchání (např. při cvičení) dochází často k nádechu ústy, kdy nos neslouží jako fyziologický filtr. Zvyšuje se celkové množství vdechovaného vzduchu, který přináší více částic, a zvyšuje se depozice nanočástic v plicních sklípcích (US EPA, 2019).

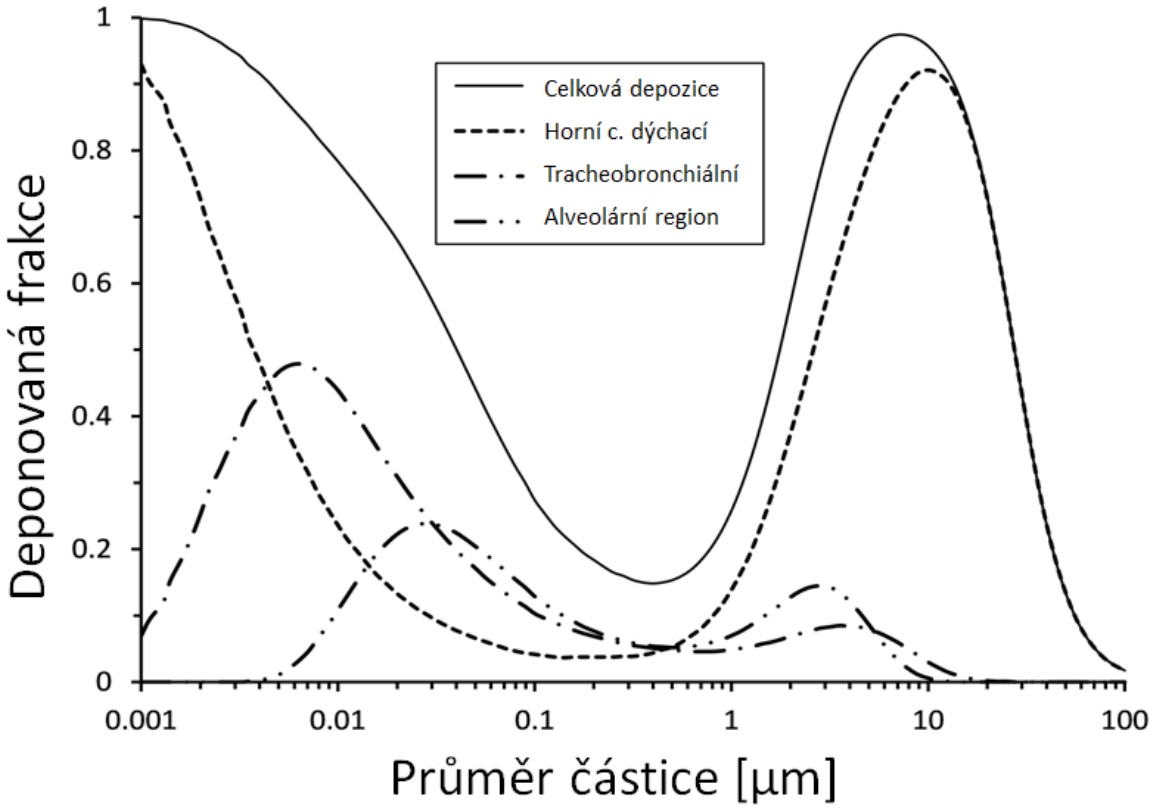

Obrázek 3 Matematický model depozice částic při nadechování nosem, dechový objem 500 ml, četnost nádechů 15x za minutu a rychlost nádechu je 250 ml/s. Částice v rozmezí 300-500 nm vykazují nejmenší depozici. (US EPA, 2019)

Částice deponované v plicích jsou odstraňovány pomocí mukociliárního eskalátoru nebo fagocytózou. Mukociliární eskalátor funguje v tracheobronchiální oblasti, kterou je u zdravých lidí schopen vyčistit od nerozpustných částic do 24 hodin. Fagocytózou jsou odstraňovány částice z alveolární oblasti. Zvláště důležité jsou alveolární makrofágy, které se společně s fagocytovanými částicemi přesouvají do tracheobronchiálního regionu nebo cestují do lymfatických uzlin (US EPA, 2019). Studie ukazují, že efektivita alveolárních makrofágů je nižší pro nanočástice ve srovnání s většími částicemi. Další cesty odstraňování nanočástic z plic, např. přestup do krve, nejsou jednoznačně potvrzené u lidí a často jsou výsledky studií navzájem v rozporu. (Oberdörster *et al*., 2005; US EPA, 2019).

1.4 Expozice nanočásticím ze spalovacích motorů a její vliv na zdraví lidské populace

Již v 90 letech 20. století se předpokládalo, že nejjemnější frakce z polétavých částic v ovzduší, nanočástice, je zodpovědná za akutní dýchací a kardiovaskulární účinky. Tento předpoklad byl brzy potvrzen epidemiologickou studií (Peters *et al*., 1997). Následovaly studie zaměřené především na městské ovzduší, kde jsou koncentrace částic vyšší než na venkově a zároveň je zde vyšší hustota osídlení.

Hlavním zdrojem nanočástic v městském ovzduší je doprava (Kumar et al., 2014; Brines *et al*., 2015). Není proto divu, že nejvyšším koncentracím jsou lidé vystaveni při dojíždění do práce/školy, kdy se pohybují v blízkosti zdrojů nanočástic (Gu et *al*. 2015; Panella *et al*., 2017; de Kluizenaar *et al*., 2017). Lidé tráví většinu času uvnitř budov, kde jsou koncentrace nanočástic závislé na intenzitě větrání, venkovní koncentraci a činnostech probíhajících v budově (de Kluizenaar *et al*., 2017). Právě venkovní koncentrace nanočástic je v prostoru velmi proměnlivá, a to díky krátké době setrvání nanočástic atmosféře.

Doba setrvání nanočástic v atmosféře se pohybuje od několika sekund po jednotky hodin, protože jakmile se nanočástice uvolní do ovzduší, tak vzájemnou koagulací vytvoří větší agregáty nebo koagulují s většími částicemi. Vyskytují se tedy hlavně v blízkosti svého zdroje, jako jsou dopravní tepny. Koncentrace rychle klesá s horizontální vzdáleností od silnice. Ve vzdálenosti 150 m od silnice byl zjištěn pokles

koncentrace o více než polovinu (Karner *et al*., 2010; Buonanno et al., 2009; Zhu et al., 2002). Rozdíly v koncentracích mohou být dokonce zřetelné na stranách chodníku sousedící se silnicí a s budovou (Buonanno *et al*., 2011). Méně jasný je vertikální profil koncentrací nanočástic ve městě. Většinou je viditelný pokles s výškou (Li *et al*., 2007; Sajani *et al*. 2018). Zároveň byla zpozorována maxima nanočástic výšce 2-3 m nad zemí (Kumar *et al*. 2008; Zhu *et* Hinds 2005). V jiné studii není vertikální profil patrný (Morawska *et al*., 1999).

Kromě proměnlivosti koncentrace nanočástic v ovzduší, epidemiologické studie čelí další výzvě, jak odlišit účinky nanočástic v ovzduší na zdraví od účinků větších částic a směsice plynných polutantů. Přesto byl prokázán negativní vliv expozice zvýšeným koncentracím nanočástic v ovzduší na kardiovaskulární sytém, který zahrnuje sníženou variabilitu srdečního rytmu, zvýšení výskytu, doby trvání a závažnosti arytmie, zhoršení ischemie myokardu, zesílený tonus cév, zvýšený krevní tlak a zvětšená krevní srážlivost (Stone *et al*., 2017; Magalhaes *et al*., 2018; Ohlwein *et al*., 2019). Velmi dobře je také dokumentovaný vliv na dýchací soustavu. Studie zaměřené na citlivou populaci astmatiků shledaly, že nanočástice ze spalování zhoršují funkce plic a vyvolávají zánět (McCreanor *et al*., 2007). Rozvoj zánětu v dýchacích cestách byl vícekrát prokázán i u zdravých jedinců exponovaných ovzduší znečištěnému nanočásticím (Stone *et al*., 2017; Ohlwein *et al*., 2019).

K hlavním mechanismům, přes který účinkují nanočástice ze spalovacích procesů na lidské zdraví, jsou zánět a oxidační stres. Poté může následovat kaskáda událostí, která vede k smrti buněk (Traboulsi *et al*., 2017). Tyto mechanismy jsou podepřeny o epidemiologické studie, které pozorují markery systémového zánětu vyvolaného nanočásticemi ze spalování (Ohlwein *et al*., 2019). Systémový zánět je již delší dobu spojován s neurodegenerativními onemocněními, mechanismus účinku zatím ale není zcela znám (Perry, 2004; Stone *et al*., 2017). Několik epidemiologických studií, našlo souvislost mezi a neurodegenerativními procesy a částicemi v ovzduší nebo znečištěním ovzduší spojeným s dopravou, které je hlavním zdrojem částic v nanorozměrech (Heusinkveld *et al*., 2016).

1.5 Testování toxicity nanočástic

Epidemiologické studie již velmi dobře zmapovaly některé účinky nanočástic v ovzduší na lidské zdraví. Mají však řadu nedostatků, pro které jsou toxikologické testy na modelových organismech nebo tkáních nezastupitelné. Takové testy dokážou měřit charakteristiky, které v živém člověku jsou neměřitelné, díky standardním postupům se vyloučí množství ovlivňujících faktorů, které mohou mít efekt na dané onemocnění, a hlavně pracují s jasně danou délkou expozice a koncentrací, které jsou u nanočástic velice složitě odhadovány.

In vivo testy toxicity jsou stále hojně používané, model zahrnuje celý organismus, a tedy i všechny toxikodynamické a toxikokinetické procesy (metabolismus, exkrece, všechny tkáně v organismu atd.). Nevýhodou je nutnost extrapolace výsledků na člověka, kdy mezidruhové rozdíly mohou způsobit značné zkreslení výsledků. Stejně tak moc složité pro studování mechanismu působení látky, protože *in vivo* modely obsahují příliš mnoho faktorů, které znesnadňují interpretaci. Je zde také etická rovina používání živých organismů (Page *et al*., 2012).

In vitro modely jsou alternativou k *in vivo* modelům, vedle mikroorganismů používají tkáňové nebo orgánové kultury z vyšších organismů včetně člověka. Jsou levnější, rychlejší, snadno dostupné, je možné je miniaturizovat a automatizovat. Lépe se na buněčných kulturách studují mechanismy procesů cizorodých látek. Na druhou stranu in vitro modely nedokáží simulovat chod celého organismu (interakce mezi tkáněmi, vylučování, přestup cizorodé látky přes sliznice nebo kůži, metabolismus aj.). Ačkoli se použijí lidské kultury, výsledek testování nemusí být relevantní pro celý lidský organismus. Často jsou používány nádorové linie nebo jinak geneticky upravené buněčné kultury a kultivační podmínky nikdy plně nenahradí fungující organismus. Mnoho světových laboratoří pracuje na modelech, které by měly tyto a další problematické aspekty in vitro testování minimalizovat. Kromě klasických 2D modelů jsou dnes k dispozici 3D modely, které již do jisté míry simulují fungování určité tkáně (Page *et al*., 2012; Haycock *et al*., 2011).

Do problematiky in vitro modelů při testování nanočástic ze spalovacích procesů vstupuje navíc významný faktor, převedení částic do buněčného média. Často používaný postup spočívá v extrakci látek z částic nachytaných na filtr. Extrahuje se

zpravidla do vodné nebo organické fáze. Látky adsorbované na částicích jsou zodpovědné za podstatnou část toxicity, obsahují karcinogenní PAH a další vedlejší produkty spalování v závislosti na palivu a použité technologii. Tato organická složka tvoří nejméně polovinu hmotnosti částic menších než 1 μm v ovzduší (Hallquist *et al*., 2009). Extrahováním organické složky se částice, stejně jako jiné neuvolněné sloučeniny, vynechávají při testování, což vede k potenciálnímu podhodnocení biologických účinků částic ze spalování. Převedení částic do buněčného media se nejčastěji provádí uvolněním částic z filtru pomocí ultrazvuku. Tento krok zároveň znamená, že částice složené původně z několika primárních částic (drtivá většina), se rozbijí na jednotlivé primární částice, které se pak v mediu shluknou v závislosti na podmínkách panující právě v daném mediu (koncentrace, tvorba proteinové korony atd.). Vlastnosti ani toxicita takových částic již nemusí odpovídat původním částicím (Lenz *et al*., 2013; Schmidt *et al*., 2019). Alternativou je vzorkování částice přímo do vodného prostředí (systém VACES, virtuální impaktory, upravený impaktor v tandemu s kondenzačním zařízením. aj.) (Kim *et al*., 2001, Wang *et al*., 2013). To sice zjednodušuje a celý postup, ale ke změnám částic v suspenzi dochází dál.

Nejvhodnější modelem pro testování toxicity inhalovaných částic jsou buněčné epitelové kultury, jejichž bazální povrch je v kontaktu s mediem a horní část buněčné kultury je vystavena ovzduší; kultura ve formě systému na rozhraní vzduch / kapalina (anglicky Air-liquid interface cell culture, ALI). Takové buněčné kultury mohou být za pomoci expoziční komory vystaveny nezměněným částicím. Výzkumy naznačují, že tyto kultury vykazují méně falešně negativních výsledků ve srovnání s klasickými kulturami zcela ponořenými v mediu (Upadhyay *et* Palmberg, 2018; Lenz *et al*., 2013).

Tato dizertační práce je založena na souboru šesti článků zabývajících se nanočásticemi ze spalování v dopravě. Článek 1 se zabývá koncentracemi nanočástic, které byly měřeny ve 3 lokalitách lišící se intenzitou dopravy. Články 2-5 se věnují změně charakteristik a toxicity částic v závislosti na použitém palivu (konvenční x alternativní). Toxicita byla měřena *in vitro* z extraktů organické hmoty navázané na částice. Poslední článek je věnován cytotoxicitě nanočástic oxidu titanu, látce inertní,

který odhalil další úskalí u měření toxicity, když se částice převádí do media (Článek 6).

2. Cíle práce

Nanočásticím z ovzduší jsou lidé vystaveni denně. Jedním z hlavních zdrojů jsou spalovací motory používané v automobilové dopravy. Technologický pokrok, který vede ke snižování spotřeby paliva, spolu se změnou složení paliv se s velkou pravděpodobností odrazí i ve vlastnostech částic produkovaných spalovacími motory. Předložená dizertační práce si klade tyto základní cíle:

- Zmapovat koncentrace nanočástic v lokalitách, které se liší v intenzitě automobilové dopravy a určit zdroj těchto nanočástic.
- Zjistit, jak alternativní paliva ovlivní produkci částic ve spalovacích motorech a jak se změní jejich toxicita.
- Vzhledem ke komplikovanosti toxikologického testování částic ze spalování, zjistit na jednodušším modelu, jak samotné částice ovlivňují toxicitu.

3. Výsledky – publikace a podíl autorky

Vědecké články publikované v periodicích s impakt faktorem vzniklé v průběhu doktorského studia jsou k nahlédnutí v kapitole Odborné články na konci dizertační práce. Přispění řešitelky k jednotlivým článkům je:

Článek 1 – Internal Combustion Engines as the Main Source of Ultrafine Particles in Residential Neighborhoods: Field Measurements in the Czech Republic
Jitka Stolcpartova, Martin Pechout, Lubos Dittrich, Martin Mazac, Michael Fenkl, Kristyna Vrbova, Jakub Ondracek, Michal Vojtisek-Lom

Atmosphere, 6 (2015), 1714-1735 (IF 2,046)

- Měření v terénu s mobilními přístroji
- Zpracování a interpretace dat
- Sepsání článku

Článek 2 – Comparative Analysis of Toxic Responses of Organic Extracts from Diesel and Selected Alternative Fuels Engine Emissions in Human Lung BEAS-2B Cells
Helena Libalova, Pavel Rossner, Jr., Kristyna Vrbova, Tana Brzicova, Jitka Sikorova, Michal Vojtisek-Lom, Vit Beranek, Jiri Klema, Miroslav Ciganek, Jiri Neca, Katerina Pencikova, Miroslav Machala, Jan Topinka

International Journal of Molecular Sciences, 17 (2016) 1833 (IF 4,183)

- Vzorkování a měření emisí z motoru
- Zpracování a interpretace výsledků z měření částic (hmotnosti částic a distribuce)

Článek 3 – Transcriptional response to organic compounds from diverse gasoline and biogasoline fuel emissions in human lung cells

Helena Libalova, Pavel Rossner Jr., Kristyna Vrbova, Tana Brzicova, Jitka Sikorova, Michal Vojtisek-Lom, Vit Beranek, Jiri Klema, Miroslav Ciganek, Jiri Neca, Miroslav Machala, Jan Topinka

Toxicology in Vitro 48 (2018) 329 – 341 (IF 3,067)

- Vzorkování a měření emisí z automobilů
- Zpracování a interpretace výsledků z měření částic (hmotnosti částic a distribuce)

Článek 4 – Toxic Effects of the Major Components of Diesel Exhaust in Human Alveolar Basal Epithelial Cells (A549)

Pavel Rossner Jr., Simona Strapacova, Jitka Stolcpartova, Jana Schmuczerova, Alena Milcova, Jiri Neca, Veronika Vlkova, Tana Brzicova, Miroslav Machala, Jan Topinka

International Journal of Molecular Sciences, 17 (2016) 1393 (IF 4,183)

- Analýza oxidačního poškození proteinů a lipidů

Článek 5 – Blends of butanol and hydrotreated vegetable oils as drop-in replacement for diesel engines: Effects on combustion and emissions

Michal Vojtisek-Lom, Vít Beránek, Pavel Mikuška, Kamil Křůmal, Pavel Coufalík, Jitka Sikorová, Jan Topinka

Fuel, 197 (2017) 407 – 421 (IF 5,128)

- Vzorkování a měření emisí z motoru
- Zpracování a interpretace výsledků z měření částic (hmotnosti částic a distribuce) a z plynných emisí

Článek 6 – Nano-TiO_2 stability in medium and size as important factors of toxicity in macrophage-like cells

Tana Brzicova 1, Jitka Sikorova 1, Alena Milcova, Kristyna Vrbova, Jiri Klema, Petr Pikal, Zuzana Lubovska, Vlada Philimonenko, Fernanda Franco, Jan Topinka, Pavel Rossner Jr

Toxicology in Vitro 54 (2019) 178 – 188 (IF 3,067)

- Charakterizace nanočástic ve vodě a v buněčném mediu
- Zpracování a interpretace výsledků
- Statistická analýza
- Podíl na sepsání článku

Vedoucí práce/školitel, ing. Jan Topinka, DrSc., souhlasí v plném rozsahu s výše uvedenými publikačními podíly autorky, Mgr. Jitky Sikorové.

ing. Jan Topinka, DrSc.

4. Shrnutí

Předložená práce se zaměřuje na nanočástice ze spalovacích procesů. Obsahuje studii (Článek 1) o měření nanočástic v obydlených oblastech lišících se dopravním zatížením, hlavním zdrojem nanočástic v ovzduší v městských oblastech, čtyři studie (Článek 2-5) zabývající se vlivem konvenčního a obnovitelného paliva na emise částic, složení organické složky navázané na částice a toxicitu této organické složky a toxikologickou studii (Článek 6) nanočástic TiO_2, které sledovala toxicitu nanočástic v buněčném mediu, s výsledky relevantními pro toxikologické testy s nanočásticemi ze spalovacích procesů. Kapitolu je tedy možné pro větší přehlednost rozdělit do 3 částí.

4.1 Článek 1: Měření nanočástic v obydlených oblastech lišících se dopravním zatížení

Aby měření reflektovalo rychlost, se kterou se koncentrace mění (projíždějící auto), a zároveň bylo mobilní, byl sestaven aparát navzájem se doplňujících přístrojů, které byly připevněny na ruční vozík společně s napájením. Vozík se pohyboval po třech lokalitách lišících se intenzitou dopravy; Spořilov (vysoká intenzita osobní i nákladní dopravy), Líbeznice (obec s komunikací zatíženou dojížděním do Prahy), Čelákovice (obec s nízkou intenzitou dopravy).

Na Spořilově byly pozorovány výrazné rozdíly mezi koncentracemi nanočástic naměřenými u hlavních silnic a koncentracemi měřenými dále v sídlišti. Koncentrace klesaly se zvyšující se rychlosti větru. Ale i za velmi dobrých rozptylových podmínek koncentrace překračovaly pozaďové koncentrace Prahy. Měření na lávce přes hlavní silnici 5.května ukázalo velmi vysoké koncentrace nanočástic, které byly výsledkem emisí nákladních vozidel, která zrychlovala po delší době strávené v silné dopravní zácpě.

V Líbeznicích byly pozorovány vyšší koncentrace kolem hlavní silnice. Mimo tuto silnice byla zaznamenaná velmi vysoká koncentrace velmi malých nanočástic (<20 nm) způsobená benzínovou sekačkou. Sekačky na trávu jsou poháněny benzínovými motory bez elektronického řízení a bez následné úpravy výfukových plynů. Malé nesilniční motory o výkonu do 19 kW nepodléhají žádnému omezení emisí částic.

V Čelákovicích byly k dispozici dvě mobilní zařízení, která měřila simultánně poblíž a dále od silnice. Vzdálenější přístroj zaznamenával nižší koncentrace nanočástic s velmi podobnou velikostní distribucí jako přístroj u silnice.

Pozorované vysoké koncentrace nanočástic odpovídají emisím vozidel při dlouhém volnoběhu, při akceleracích a vozidlům s vysokými emisemi. Koncentrace nanočástic ve vzdálenějších částech od silnic byly relativně nízké a podíl částic větších než 100 nm byl malý ve všech měřených početních distribucích. Většinu částic v úrovni dýchací zóny tvořily tedy nanočástice pocházející z automobilové dopravy.

4.2 Články 2 – 5: Vliv konvenčního a obnovitelného paliva

Články 2 a 3 pojednávají o toxicitě a chemickém složení organické složky částic a ze spalovacích motorů poháněných konvenčními a obnovitelnými palivy. Přehled testovaných paliv spolu s množstvím produkovaných částic na kg paliva je na Obrázek 4. Hmotnost částic na kilogram paliva klesala, pokud motor spaloval alternativní palivo nebo jeho příměs, kromě benzínu s příměsí 15 % etanolu. Technologie přímého vstřikování u zážehového motoru produkuje několikanásobně více částic nežli než technologie bez přímého vstřikování. I tak produkoval vznětový motor o řád více částic na kilogram paliva než motor zážehový s přímým vstřikováním, ani jeden motor nebyl osazen filtrem tuhých částic.

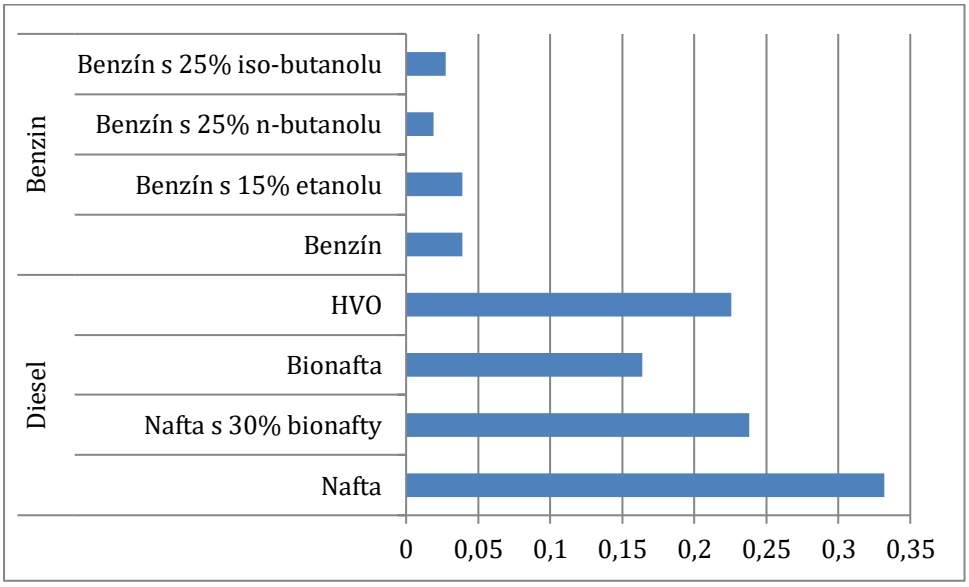

Obrázek 4 Hmotnost částic [g] na kg paliva (data z článků 2 a 3, upravena, aby mohla být porovnávána).

Distribuce částic u zážehového motoru byla u všech paliv bimodální, tedy obsahovala částice jak akumulačního, tak nukleačního módu, které početně převažují. U vznětového motoru jsou částice nukelačního módu téměř neznatelné, pravděpodobně díky adsorpci organických látek, které by jinak vytvořily sekundární částice, na velké množství primárních částic.

Analýzou PAH adsorbovaných na částicích bylo zjištěno, že ze zkoumaných druhů naftových paliv bylo nejméně PAH na hmotnost částic při spalování HVO. Naopak zvýšená emise PAH na hmotnost částic byla pozorovaná při spalování čisté bionafty nebo její směsi s konvenční naftou, a to především u nízkomolekulárních PAH (fluoranthen a pyren). U směsi benzínu s 15 % etanolu nebyl pozorován žádný podstatný rozdíl u emisí PAH. Isobutanol měl příznivý vliv na množství PAH, ale n-butanol množství PAH na částicích zvyšoval.

Analýza celogenomové exprese na modelových buňkách A549 určila hlavní mechanismy účinku extraktů částic ze spalovacích motorů, jako oxidační stres a procesy spojené s metabolismem PAH. Jako nejpříznivější palivo pro vznětový motor se ukázalo být HVO. Nejvhodnější obnovitelnou příměsí v benzínu se ukázal být z hlediska toxicity isobutanol. Reakce buněk do jisté míry odráží množství PAH v extraktech, což naznačuje, že nejen genotoxicita, ale i změny v celkové genové expresi jsou ovlivněny přítomností PAH ve vzorcích. Tato zjištění jsou v souladu se starší studií (článek 4), která zkoumala vliv 3 PAH spojovaných se spalováním ve vznětovém motoru, kde byly pozorovány nejen genotoxické účinky PAH, ale i oxidační poškození makromolekul v buňkách.

Palivo produkující emise s nejméně toxickými účinky se ukázalo být HVO, které je ale výrazně dražší, něž konvenční nafta anebo klasická bionafta. Ačkoli HVO snižuje produkci částic, nedosahuje takových výsledků v jejich snížení, jako bionafta. Řešením obou problémů, by mohlo být naředění HVO levnějším butanolem, který se ukázal, jako vhodnou alternativní příměsí benzínu (Článek 3). Článek 5 se zabývá rozdíly v emisích plynných polutantů, částic a organickou složkou při spalování nafty, bionafty, HVO a směsí HVO s 30 % n-butanolu nebo isobutanolu. Směsi HVO s butanolem vykazovaly nižší emise částic i PAH ve srovnání s ostatními palivy bez zvýšení oxidů dusíku.

4.3 Článek 6: Cytotoxicita nano-TiO_2: Vliv velikosti a stability nanočástic v buněčném mediu na toxicitu

Článek 6 si kladl za cíl odhalit, které vlastnosti jsou zodpovědné za cytotoxicitu u nanočástic. Jedinou statisticky významnou veličinou kromě koncentrace byla hodnota polydiperzity. Hodnota polydiperzity určuje míru, do jaké jsou částice v kapalině agregované. Nízká hodnota odpovídá suspenzi s částicemi, které neagregují nebo vytvářejí jen malé agregáty. Naopak vysoká hodnota odpovídá nestálé suspenzi, kde částice rychle agregují a vytvářejí agregáty o různých velikostech. Velikost částic pravděpodobně také hraje roli, nejmenší a největší částice nebyly toxické, ale částice mezi 20 – 60 nm vykazovaly toxicitu.

Oba tyto parametry jsou ovlivněné při expozici buněk částicemi ze spalovacích procesů resuspendovanými v buněčném mediu. Toxicita částic bude ovlivněná výslednou velikostí částic v mediu (sonikace rozbíjí větší agregáty částic na menší nebo na primární částice) a jejich stabilitě, která do jisté míry závisí na použitém mediu a tvorbě proteinové korony na částicích. Jako nejvhodnějším modelem *in vitro*, který v sobě zahrnuje jak toxikologii sloučenin adsorbovaných na částicích, tak i účinky samotných částic bez převedení do buněčného media, jsou buněčné kultury ALI.

5. Závěry

Disertační práce prokázala, že:

- Množství, složení a toxicita nanočástic produkovaných dopravu jsou závislé především na technických parametrech motoru, zpracování výfukových plynu (např. filtry pevných částic) a použitém palivu.
- Některá paliva mohou redukovat množství emitovaných částic a zároveň snížit toxicitu těchto částic.
- Jsou velké rozdíly v koncentracích nanočástic mezi obydlenými oblastmi způsobené různou vzdáleností od hlavní silnice. Zároveň byla zachycena vozidla s vysokými emisemi, která jsou zodpovědná za

podstatnou část emisí nanočástic. Snížení počtu takových vozidel by rychle vedlo ke snížení zátěže populace.

- Toxikologické účinky organických extraktů z částic emitovaných dieselovým motorem nebo motorem benzínového osobního automobilu zahrnují zejména oxidační stres a procesy spojené s metabolismem PAH.
- Pro toxicitu částic je důležitá jejich velikost a stabilita v buněčném mediu. Obě tyto vlastnosti jsou ovlivněny resuspendací nanočástic v mediu. Různý postup při resuspendaci částic v buněčném mediu může stát za nesourodými výsledky v toxicitě nanočástic napříč laboratořemi.

Práce přispěla k pochopení složité problematiky nanočástic z dopravy, nastínila možnou cestu k redukci toxických účinků emitovaných nanočástic a identifikovala možnou příčinu nesourodých až kontroverzních výsledků v toxikologii nanočástic.

6. Literatura

Aatola, H.; Larmi, M.; Sarjovaara, T. and Mikkonen, S. (2009) „Hydrotreated vegetable oil (HVO) as a renewable diesel fuel: Trade-off between nox, particulate emission, and fuel consumption of a heavy duty engine“, *SAE International Journal of Engines*, 2009, 1(1): 1251–1262.

Andersen, V.F.; Anderson, J.E.; Wallington, T.J.; Mueller, S.A and Nielsen, O.J. (2010) “Vapor Pressures of Alcohol-Gasoline Blends”, *Energy & Fuels*, 24(6): 3647-3654.

Awad, O.I.; Mamat, R.; Ibrahim, T.K.; Hammid, A.T.; Yusri, I.M.; Hamidi, M.A.; Humada, A.M. and Yusop, A.F. (2018) “Overview of the oxygenated fuels in spark ignition engine: Environmental and performance“, *Renewable & Sustainable Energy Reviews*, 91: 394-408.

Brines, M.; Dall’Osto, M.; Beddows, D.C.S.; Harrison, R.M.; Gómez-Moreno, F.; Núñez, L.; Artíñano, B.; Costabile, F.; Gobbi, G.P.; Salimi, F.; Morawska L.; Sioutas, C. and Quero X. (2015) „Traffic and nucleation events as main sources of ultrafine particles in high-insolation developed world cities“, *Atmospheric Chemistry and Physics*, 15: 5929–5945.

Buonanno, G.; Fuoco, F.C. and Stabile, L. (2011) „Influential parameters on particle exposure of pedestrians in urban microenvironments“, *Atmospheric Environment*, 45(7), 1434–1443.

Buonanno, G.; Lall, A.A. and Stabile, L. (2009) „Temporal size distribution and concentration of particle near a major highway“, *Atmospheric Environment*, 43(5): 1100–1105.

Colbeck, I., Turner, J., Laaksonen, A., Lehtinen, K.E.J., Clement, C.F., Lazaridis, M., Grgi´c, I., Topping, D., MacKenzie, R., Baltensperger, U. and Furger, M. (2008) „Environmental Chemistry of Aerosols“, 1st ed. Blackwell Publishing Ltd., Oxford.

de Kluizenaar, Y.; Kuijpers, E.; Eekhout, I.; Voogt, M.; Vermeulen, R.C.H.; Hoek, G.; Sterkenburg, R.P.; Pierik, F.H.; Duyzer, J.H.; Meijer, E.W. and Pronk, A. (2017)

„Personal exposure to UFP in different micro-environments and time of day“, *Building and Environment*, 122: 237-246.

Evelyn, A.; Mannick, S. and Sermon, P.A. (2003) „Unusual carbon-based nanofibers and chains among diesel-emitted particles“, *Nano Letters*, 3(1): 63–64.

Gu, J.; Kraus, U.; Schneider, A.; Hampel, R.; Pitz, M.; Breitner, S.; Wolf, K.; Hänninen, O.; Peters, A. and Cyrys, J. (2015) „Personal day-time exposure to ultrafine particles in different microenvironments“, *International Journal of Hygiene and Environmental HealthI,* 218(2):188-95.

Gwinn, M.R. and Vallyathan V. (2006) „Nanoparticles: health effects—pros and cons“, *Environmental Health Perspectives*, 114(12): 1818-1825.

Haycock, J. (2011) „3D cell culture: a review of current approaches and techniques“, *Methods in molecular biology*, 695, 1-15.

Hallquist, M.; Wenger, J. C.; Baltensperger, U.; Rudich, Y.; Simpson, D.; Claeys, M.; Dommen, J.; Donahue, N. M.; George, C.; Goldstein, A. H.; Hamilton, J. F.; Herrmann, H.; Hoffmann, T.; Iinuma, Y.; Jang, M.; Jenkin, M. E.; Jimenez, J. L.; Kiendler-Scharr, A.; Maenhaut, W.; McFiggans, G.; Mentel, Th. F.; Monod, A.; Prévôt, A. S. H.; Seinfeld, J. H.; Surratt, J. D.; Szmigielski, R.; and Wildt, J. (2009) „The formation, properties and impact of secondary organic aerosol: current and emerging issues“, Atmospheric Chemistry and Physics, 9(14), 5155-5236.

Hesterberg, T.W.; Long, C.M.; Lapin, C.A.; Hamade A.K. and Valberg P.A. (2010) „Diesel exhaust particulate (DEP) and nanoparticle exposures: What do DEP human clinical studies tell usabout potential human health hazards of nanoparticles?“ *Inhalation Toxicology*, 22(8): 679-694.

Heusinkveld, H.J.; Wahle, T.; Campbell, A.; Westerink, R.H.S.; Tran, L.; Johnston, H.; Stone, V.; Cassee, F.R. and Schins, R.P.F. (2016) „Neurodegenerative and neurological disorders by small inhaled particles“, *Neurotoxicology*, 56: 94-106.

Hinds, W.C. (1998). Aerosol Technology-Properties, Behavior, and Measurement of Airborne Particles, 2nd ed. John Wiley & Sons, Inc., New York.

Karner, A.A.; Eisinger, D.S. and Niemeier, D.A. (2010) „Near-Roadway Air Quality: Synthesizing the Findings from Real-World Data“, *Environmental Science & Technology*, 44(14): 5334–5344.

Kim, S.; Jaques, P.A.; Chang, M.C.; Barone, T.; Xiong, C.; Friedlander, S.K. and Sioutas, C. (2001) „Versatile aerosol concentration enrichment system (VACES) for simultaneous in vivo and in vitro evaluation of toxic effects of ultrafine, fine and coarse ambient particles - Part II: Field evaluation“, *Journal of Aerosol Science*, 32(11): 1299-1314.

Kittelson, D. (1998) „Engines and nanoparticles: a review“, *Journal of Aerosol Science*, 29 (5-6), 575-588.

Kittelson, D.; McMurry, P; Park, k.; Sakurai, H.; Tobias, H. and Ziemann P. (2002) „Chemical and Physical Characteristics of Diesel Aerosol“, *Cambridge Particle Conference*, 23 April 2002.

Knothe, G. (2010) „Biodiesel and renewable diesel: a comparison“, *Progress in Energy and Combustion Science*, 36(3): 364-373.

Kumar, P.; Fennell, P. and Britter, R.E. (2008) „Pseudo-simultaneous measurements for the vertical variation of coarse, fine and ultra-fine particles in an urban street Canon“, *Atmospheric Environment*, 42(18): 4304-4319.

Kumar, P.; Gurjar, B.R.; Nagpure, A. and Harrison, R.M. (2011) „Preliminary estimates of nanoparticles number emissions from road vehicles in megacity Delhi and associated health impacts“, *Environmental Science & Technology*, 45(13): 5514-5521.

Kumar, P.; Morawska, L.; Birmili, W.; Paasonen, P.; Hu, M.; Kulmala, M.; Harrison, R.M.; Norford, L. and Britter, R. (2014) „Ultrafine particles in cities“, *Environment International*, 66: 1–10.

Lattimore, T.; Herreros, J.M.; Xu, H. and Shuai, S. (2016) „Investigation of compression ratio and fuel effect on combustion and PM emissions in a DISI engine“, *Fuel*, 169: 68-78.

Lenz, A. G.; Karg, E.; Brendel, E.; Hinze-Heyn, H.; Maier, K. L.; Eickelberg, O.; Stoeger, T. and Otmar, S. (2013) „Inflammatory and oxidative stress responses of an alveolar epithelial cell line to airborne zinc oxide nanoparticles at the air-liquid interface: A comparison with conventional, submerged cell-culture conditions“, *Biomed Research International*, 652632.

Li, X.L.; Wang, J.S.; Tu, X.D.; Liu, W. and Huang Z. (2007) „Vertical variations of particle number concentration and size distribution in a street canyon in Shanghai, China“, *Science of the Total Environment*, 378(3): 306-316.

Magalhaes, S.; Baumgartner, J. and Weichenthal, S. (2018) „Impacts of exposure to black carbon, elemental carbon, and ultrafine particles from indoor and outdoor sources on blood pressure in adults: A review of epidemiological evidence“, *Environmental Research*, 161: 345-353.

McCreanor, J.; Cullinan, P.; Nieuwenhuijsen, M.J.; Stewart-Evans, J.; Malliarou, E.; Jarup, L.; Harrington, R.; Svartengren, M.; Han, I.; Ohman-Strickland, P.; Chung, K.F. and Zhang, J.F. (2007) „Respiratory effects of exposure to diesel traffic in persons with asthma“, *New England Journal of Medicine*, 357(23):2348–2358.

Missaoui, W.N.; Arnold, R.D. and Cummings, B.S. (2018) „Toxicological status of nanoparticles: What we know and what we don't know“, *Chemico-Biological Interactions*, 295: 1-12.

Morawska, L.; Ristovski, Z.; Jayaratne, E.R.; Keogh, D.U. and Ling, X. (2008) „Ambient nano and ultrafine particles from motor vehicle emissions: Characteristics, ambient processing and implications on human exposure“, *Atmospheric Environment*, 42(35): 8113-8138.

Morawska, L.; Thomas, S.; Gilbert, D.; Greenaway, C. and Rijnders E. (1999) „A study of the horizontal and vertical profile of submicrometer particles in relation to a busy road“, *Atmospheric Environment*, 33 (8): 1261-1274.

Oberdörster, G.; Oberdörster, E. and Oberdörster, J. (2005) „Nanotoxicology: an emerging discipline evolving from studies of ultrafine particles“, *Environmental Health Perspectives*, 113(7): 823-39.

Ohlwein, S.; Kappeler, R.; Joss, M.K.; Kunzli, N. and Hoffmann, B. (2019) „Health effects of ultrafine particles: a systematic literature review update of epidemiological evidence“, *International Journal of Public Health*, 64(4): 547-559.

Page, H.; Flood, P. and Reynaud, E.G. (2012) „Three-dimensional tissue cultures: current trends and beyond“, *Cell and Tissue Research*, 352(1): 123-131.

Panella, P.; Casas, M.; Donaire-Gonzalez, D.; Garcia-Esteban, R.; Robinson, O.; Valentin, A.; Gulliver, J.; Momas, I.; Nieuwenhuijsen, M.; Vrijheid, M. and Sunyer, J. (2017) „Ultrafine particles and black carbon personal exposures in asthmatic and non-asthmatic children at school age“, *Indoor Air*, 27(5): 891-899.

Perry, V.H. (2004) „The influence of systemic inflammation on inflammation in the brain: implications for chronic neurodegenerative dinase“, *Brain Behavior And Immunity*, 18(5): 407-413.

Peters, A.; Wichmann, H.E.; Tuch, T.; Heinrich, J. and Heyder, J. (1997) „Respiratory effects are associated with the number of ultrafine particles“, *American Journal of Respiratory and Critical Care Medicine*, 155(4):1376–1383. PMID: 9105082.

Prokopowicz, A.; Zaciera, M.; Sobczak, A.; Bielaczyc, P. and Woodburn, J. (2015) „The effects of neat biodiesel and biodiesel and HVO blends in diesel fuel on exhaust emissions from a light duty vehicle with a diesel engine“, *Environmental Science & Technology*, 49(12)“ 7473–7482.

Sajani, S.Z.; Marchesi, S.; Trentini, A.; Bacco, D.; Zigola, C.; Rovelli, S.; Ricciardelli, I.; Maccone, C.; Lauriola, P.; Cavallo, D.M.; Poluzzi, V.; Cattaneo, A. and Harrison, R.M. (2018) „Vertical variation of PM2.5 mass and chemical composition, particle size distribution, NO2, and BTEX at a high rise building“, *Environmental Pollution*, 235: 339-349.

Shapira, P. and Wang, J. (2010) „Follow the money“, *Nature*, 468(7324): 627-628.

Schmidt, S.; Altenburger, R. and Kühnel, D. (2019) „From the air to the water phase: implication for toxicity testing of combustion-derived particles“, *Biomass Conversion and Biorefinery*, 9(1): 213–225.

Stone, V.; Miller, M.R.; Clift, M.J.D.; Elder, A.; Mills, N.L.; Moller, P.; Schins, R.P.F.; Vogel, U.; Kreyling, W.G.; Jensen, K.A.; Kuhlbusch, T.A.J.; Schwarze, P.E.; Hoet, P.; Pietroiusti, A.; De Vizcaya-Ruiz, A.; Baeza-Squiban, A.; Teixeira, J.P.; Tran, C.L. and Cassee, F.R. (2017) „Nanomaterials Versus Ambient Ultrafine Particles: An Opportunity to Exchange Toxicology Knowledge“, *Environmental Health Perspectives*, 125(10): 106002.

Suarez-Bertoa, R.; Kousoulidou, M.; Clairotte, M.; Giechaskiel, B.; Nuottimaki, J.; Sarjovaara, T. and Lonza, L. (2019) „Impact of HVO blends on modern diesel passenger cars emissions during real world operation“, *Fuel*, 235: 1427-1435.

Szybist, J.P.; Song, j.; Alam, M. and Boehman, A.L. (2007) „Biodiesel combustion, emissions and emission kontrol“, *Fuel Processing Technology*, 88(7): 679-69.

Traboulsi, H.; Guerrina, N.; Iu, M.; Maysinger, D.; Ariya, P. and Baglole C.J. (2017) „Inhaled Pollutants: The Molecular Scene behind Respiratory and Systemic Diseases Associated with Ultrafine Particulate Matter“, *International Journal of Molecular Sciences*, 18(2), 243.

Tripathy, S.; Sahoo, S.; Srivastava, D.K.; (2017) „Gasoline direct injection—challenges“, In: Agarwal, A.K.; De, S.; Pandey, A. and Singh, A.P. *Combustion for Power Generation and Transportation: Technology, Challenges and Prospects. Springer Singapore*, Singapore, pp. 367–379.

Upadhyay, S. and Palmberg, L. (2018) „Air-Liquid Interface: Relevant In Vitro Models for Investigating Air Pollutant-Induced Pulmonary Toxicity“, *Toxicological Sciences*, 164(1): 21–30.

US EPA (United States Environmental Protection Agency) (2019) „Particle Pollution Exposure“, availible online: https://www.epa.gov/pmcourse/particle-pollution-exposure (accessed 30.4. 2019)

Vojtisek-Lom, M.; Pechout, M.; Dittrich, L.; Beranek, V.; Kotek, M.; Schwarz, J.; Vodicka, P.; Milcova, A.; Rossnerova, A.; Ambroz, A. and Topinka, J. (2015) „Polycyclic aromatic hydrocarbons (PAH) and their genotoxicity in exhaust emissions from a diesel engine during extended low-load operation on diesel and biodiesel fuels“, *Atmospheric Environment*, 109, 9–18.

Wang, D.B.; Pakbin, P.; Saffari, A.; Shafer, M.M.; Schauer, J.J. and Sioutas, C. (2013) „Development and Evaluation of a High-Volume Aerosol-into-Liquid Collector for Fine and Ultrafine Particulate Matter“, *Aerosol Science and Technology*, 47(11): 1226-1238.

Wang, X.; Westerdahl, D.; Wu, Y.; Pan, X. and Zhang, K.M. (2011) „On-road emission factor distributions of individual diesel vehicles in and around Beijing, China“, *Atmospheric Environment*, 45(2): 503–513.

Willeke K. and Whitby K.T. (1975), Atmospheric Aerosols: Size Distribution Interpretation, *Journal of the Air Pollution Control Association*, 25(5): 529-534.

Zhu, Y. and Hinds, W.C. (2005) „Predicting particle number concentrations near a highway based on vertical concentration profile“, *Atmospheric Environment*, 39(8): 1557-1566.

Zhu, Y.; Hinds, W.C.; Kim, S. and Sioutas, C. (2002) „Concentration and size distribution of ultrafine particles near a major highway“, *Journal of the Air & Waste Management Association*, 52(9), 1032–1042.

7. Odborné články

Článek 1

Atmosphere **2015**, *6*, 1714-1735; doi:10.3390/atmos6111714

OPEN ACCESS

atmosphere

ISSN 2073-4433

www.mdpi.com/journal/atmosphere

Article

Internal Combustion Engines as the Main Source of Ultrafine Particles in Residential Neighborhoods: Field Measurements in the Czech Republic

Jitka Stolcpartova [1,2,*], Martin Pechout [3], Lubos Dittrich [3], Martin Mazac [3], Michael Fenkl [4], Kristyna Vrbova [2], Jakub Ondracek [5] and Michal Vojtisek-Lom [6]

1 Institute for Environmental Studies, Faculty of Science, Charles University, Benatska 2, 128 01 Prague 2, Czech Republic

2 Institute of Experimental Medicine, Academy of Sciences of the Czech Republic v.v.i., Videnska 1083, 142 20 Prague, Czech Republic; E-Mail: kristyna.vrbova@biomed.cas.cz

3 Department of Vehicles and Engines, Technical University of Liberec, Studentska 2, 461 17 Liberec, Czech Republic; E-Mails: martin.pechout@tul.cz (M.P.); lubos.dittrich@tul.cz (L.D.); martin.mazac@tul.cz (M.M.)

4 Department of Energy Engineering, Technical University of Liberec, Studentska 2, 461 17 Liberec, Czech Republic; E-Mail: michael.fenkl@tul.cz

5 Institute of Chemical Process Fundamentals, Academy of Sciences of the Czech Republic v.v.i., Rozvojova 2/135, 165 02 Praha 6, Czech Republic; E-Mail: ondracek@icpf.cas.cz

6 Department of Automotive, Combustion Engine and Railway Engineering, Czech Technical University in Prague, Technicka 4, 166 07 Prague, Czech Republic; E-Mail: michal.vojtisek@fs.cvut.cz

* Author to whom correspondence should be addressed; E-Mail: jitka.stolcpartova@biomed.cas.cz; Tel.: +420-241-062-663; Fax: +420-241-062-785.

Academic Editor: Pasquale Avino

Received: 31 August 2015 / Accepted: 29 October 2015 / Published: 5 November 2015

Abstract: Ultrafine particles (UFP, diameter < 100 nm) exposure has already been associated with adverse effects on human health. Spatial distribution of UFP is non-uniform; they concentrate in the vicinity of the source, e.g. traffic, because of their short lifespan. This work investigates spatial distribution of UFP in three areas in the Czech Republic with different traffic load: High traffic (Prague neighborhood—Sporilov), commuter road vicinity (Libeznice), and a small city with only local traffic (Celakovice). Size-resolved measurements of particles in the 5–500 nm range were taken with a particle

classifier mounted, along with batteries, GPS and other accessories, on a handcart and pushed around the areas, making one-minute or longer stops at places of interest. Concentrations along main roads were elevated in comparison with places farther from the road; this pattern was observed in all sites, while particle number distributions both close and away from main roads had similar patterns. The absence of larger particles, the relative absence of higher concentrations of particles away from the main roads, and similar number distributions suggest that high particle number concentrations cannot be readily attributed to sources other than internal combustion engines in vehicles and mobile machinery (*i.e.*, mowers and construction machines).

Keywords: ultrafine particles; nanoparticles; UFP; air pollution; traffic load; spatial distribution; UFP source; mobile measurement; field study

1. Introduction

Ultra fine particles (UFP, <100 nm in diameter) are the smallest fraction of particles. They are formed directly within combustion processes such as within internal combustion engines and/or they arise in the air from precursors. Traffic is currently the biggest source of UFP in big cities [1,2]. UFP represent a small fraction of the total particle mass due to their small size; however, they dominate the total particle counts or number concentrations. Their lifespan ranges from seconds to a few hours because of condensation and coagulation into larger particles. Thus, they are concentrated near their sources such as roadways, while the number concentration of UFP rapidly decays (>50% at 150 m) along with the distance from the busy road [3–5], there are even differences between particle concentrations measured kerbside and building side [6].

UFP exposure has already been associated with some adverse health effects involving respiratory and cardiovascular systems in humans [7–10]. There is also evidence that urban UFP, in comparison with larger particles, induced grater systemic oxidative stress in rats, which was enhanced by an inhibition of the anti-inflammatory capacity and subsequently led to larger atherosclerotic lesions [11]. Epidemiological studies have found association between residence location near the busy road and pulmonary impairments [12,13] as well as increase in the risk of cardiovascular disease [14].

With vehicle fleet turnaround along with the tightening of emissions limits for new on-road vehicles sold in the European Union, the relative contribution of other sources, namely home heating appliances, to the total particle mass in the Czech Republic is increasing [15], and often, improperly designed, maintained or operated stoves are the dominant sources of visible smoke. Such appliances, however, produce larger particles, typically hundreds of nanometers in diameter [16–18], and their exhaust is released from chimneys, while engines produce rather small particles, mostly on the order of 10 nm to tens of nm diameter [19,20], which are released directly in the streets. In addition, real driving emissions measurements show that engine UFP emissions are not evenly distributed among vehicles or along the path of travel, but rather, a small number of vehicles is responsible for a large fraction of the total emissions from the vehicle fleet [21,22], and a large fraction of UFP emissions from a given vehicle is attributable to short episodes with high emissions [23].

In this study, the UFP concentrations at the breathing levels on the streets were investigated in multiple residential neighborhoods in the Czech Republic with a hand-pushed instrument cart, with the goal of using particle size distributions and geographic distributions to investigate the spatial distribution of UFP and to provide a rough source apportionment between road traffic and local heating.

All measurements were conducted during the heating season, and it was assumed that home heating devices as well as their operation and emissions are distributed randomly (and on a large scale, evenly) throughout the neighborhood, and that high emitters will be spotted by visible smoke.

2. Experimental Section

The fast mobility particle sizer was used for measurements because it is, in contrast with scanning mobility particle sizer (SMPS), able to record rapid changes in particle number distribution caused by traffic, which SMPS could miss [24]. Therefore two fast mobility particle sizers, EEPS (Engine Exhaust Particle Sizer, model 3090, TSI, measurement of 32 channels distributed over 5–560 nm range, 1 Hz sampling frequency), and one condensation UFP counter (UF-CPC, model 200, Palas, 50% sensitivity at 5 nm, using butanol as working fluid), all already modified and mounted for in-vehicle operation, were mounted on 60 cm wide hand-operated carts, along with batteries (12 V 90 Ah LiFePo), inverters, GPS (eTrex 10, Garmin, 1 Hz sampling rate), and notebook computers (Figure 1).

Figure 1. Installed mobile measurement apparatus; EEPS—Engine Exhaust Particle, CPC—condensation particle counter.

Prior to the study, both EEPS instruments were co-located with a reference SMPS (SMPS 3034, TSI) for multiple days to assess their ambient air monitoring capabilities. The reference SMPS is owned by the Institute of Chemical Process Fundamentals, Academy of Sciences of the Czech Republic v.v.i. and was operated within the UFIREG Quality Assurance Program [25]. The SMPS measured particles in range of 10–500 nm and its scanning interval was set to 5 min.

The carts with instruments were pushed on different days through a residential neighborhood with local traffic (a small city of Celakovice), a neighborhood intersected by an arterial road frequented by commuter traffic to and from Prague (village of Libeznice), and an urban neighborhood surrounded by high-traffic motorways (Sporilov neighborhood in the city of Prague). Site details are given in Figure 2 and below. The carts were pushed through the neighborhoods to places of interest identified by representatives of local citizens and by the authors. Logging intervals of all instruments (EEPS, CPC and GPS) were set to 1 s. As the EEPS has shown increased noise during transportation due to vibrations (see Section 3.1), only data measured during frequent stops were used. A typical stop took one minute; this interval was extended in the case of unstable concentrations or anomalies due to the passage of individual vehicles.

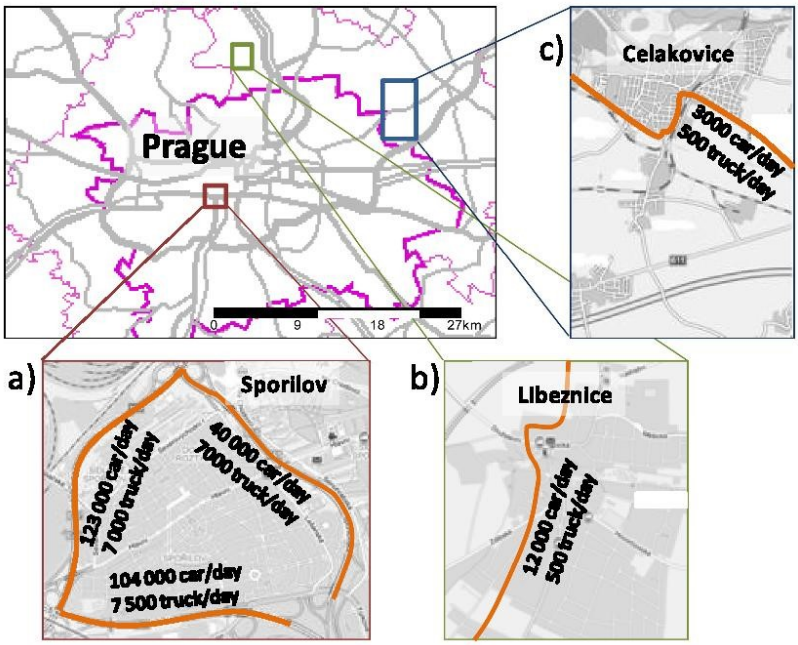

Figure 2. Location of measurement sites with given traffic density: (**a**) Spořilov, (**b**) Libeznice, and (**c**) Celakovice. Map sources: Geofond, Czech Geological Survey; Mapy.cz, Seznam.cz a.s.

Meteorological data from nearby observatories were used to supplement the data about temperature, humidity, and wind speed and direction.

High traffic location: Sporilov is a Prague residential neighborhood with 14,000 inhabitants completely surrounded by three freeways that are major heavy truck thoroughfares. Traffic intensity on two roads exceeded 100,000 cars per day in 2014 and each of the main roads is travelled by 7000 trucks per day [26] (Figure 2a). Measurements in this area were performed within weekdays on 20 February, and 6, 12 and 26 March 2014. Meteorological conditions were acquired of meteorological station Sporilov operated by Institute of Atmospheric Physic, Academy of Sciences of the Czech Republic.

Commuter traffic location: Libeznice is a village with 2000 inhabitants situated nearby Prague border. A road that goes through Libeznice is congested during morning and afternoon traffic peaks because the road is a feeder for many drivers coming into and out of Prague. There is a bypass away from Libeznice but that way is longer, therefore many drivers still go through the village. The daily traffic load is 12,000 cars and 500 trucks [27] (Figure 2b). Meteorological conditions were obtained from meteorological station Kojetice. The station is 5 km North from Libeznice.

Local traffic location: Celakovice is a small city situated 15 km northeast of Prague's built up area, and 3 km from the closest highway. Inhabitants commute daily to work to Prague by public transportation and many of them by car. This situation is typical for the most small cities and satellites around larger cities. Traffic intensity is relatively low, 3000 cars and around 500 trucks per day [28] (Figure 2c). Meteorological conditions were obtained from a station operated by Celakovice city.

3. Results

3.1. Effects of Vibrations

The online particle classifiers EEPS and reference SMPS size distributions and total particle count were in general agreement during a co-location exercise during the UFIREG Quality Assurance Program [25]. The EEPS, normally used for engine exhaust measurement, uses, however, electrometers as opposed to condensation particle counter, and exhibits a higher detection limit as well as zero drift of units of thousands of particles per cm^3, which may be significant at ambient levels. This drift was determined by periodically placing a HEPA filter on the EEPS inlet and recording the "zero" size distribution, which was then subtracted from all measured size distributions (Figure 3). In addition, during the operation of a handcart, the EEPS was exposed to different vibrations than those encountered in the vehicle, resulting in increased noise. While this noise could be suppressed by improved suspension system (designed for the mass of the handcart as opposed to the mass of a vehicle), the effects of vibrations on EEPS measurement artifacts are not well quantified, and a decision was made to treat the data while moving and for about 10 s afterwards as indicative only. For this reason, EEPS data were considered to be quantitative only at standstill, and were frequently compared against the UF-CPC data. The effects of instrument travel on the measurement noise are shown in Figure 4.

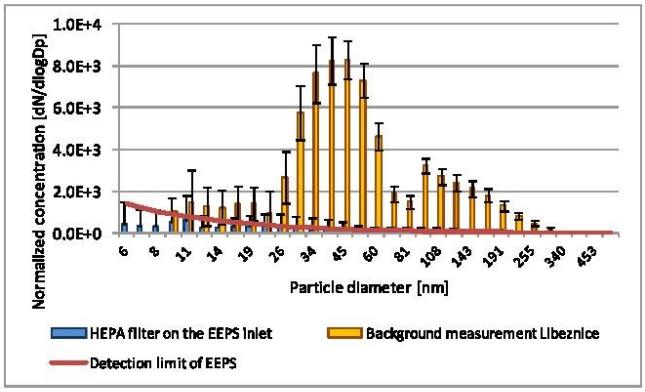

Figure 3. Comparison of manufacturer-supplied detection limit of EEPS, instrument electrometer noise (High-efficiency particulate arrestance (HEPA) filter on EEPS inlet) and the lowest measured number concentrations (Libeznice background) with standard deviations. The data representing the lowest measured concentration among campaigns (4.2×10^3 #/cm^3, Libeznice background—best dispersion conditions) show that particles with diameter >25 nm are well above the detection limit. Concentrations measured on the other sites were several times/orders of magnitude higher. Measured concentrations were above detection limit of the instrument.

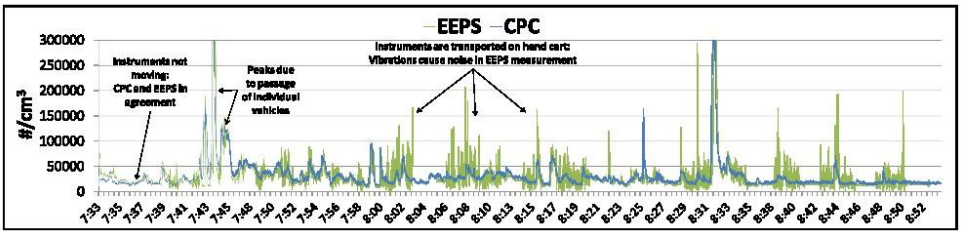

Figure 4. Comparison of particle number concentrations measured by CPC and EEPS; EEPS noise due to handcart vibration during its movement to another measurement stop and measurement stops are indicated on 30 January, EEPS and CPC are in agreement in total particle counts.

Measurements were carried out with one or two mobile apparatuses, which were pulled around the site making one-minute or longer stops at various places of interest. Measurements always took several hours, involving both peak and off-peak traffic, so that the intensity of traffic emissions was changing over the course of measurement. Presented concentrations include particles with electric mobility diameter between 5–100 nm. Distributions include all measured sizes and demonstrate a very small contribution of particles larger than 100 nm to the total particle counts.

3.2. Sporilov—Effects of Distance from Major Roads

Measurements in Sporilov were performed within weekdays on 20 February, and 6, 12 and 26 March 2014 with one mobile apparatus. Sporilov is a part of Prague with very high traffic load.

Morning and afternoon traffic peaks were recorded on 6 March (7:15–11:15 a.m.) and 20 February (1:15–6:00 p.m.), respectively. During both days the wind was stable and moderate (Figure 5). Near the road, *circa* 50 m away from the road, averaged concentrations were 3.4×10^4 #/cm^3 (median 2.3×10^4 #/cm^3) and 3.1×10^4 #/cm^3 (median 3.1×10^4 #/cm^3) for 20 February and 6 March, respectively. Further from the main roads the concentration decreased to average values 1.2×10^4 #/cm^3(median 9×10^3 #/cm^3) on 20 February and 1.5×10^4 #/cm^3 (median 1.3×10^4 #/cm^3) on 6 March. Anomalous value 3.3×10^5 #/cm^3 in the middle of building area was caused by a passing scooter. This value was not involved in average and median calculation (Figure 5). Distributions for both days are shown in Figure 6. There are strong peaks in particle concentration for 10 nm particles and less visible for particles with 40 nm diameter.

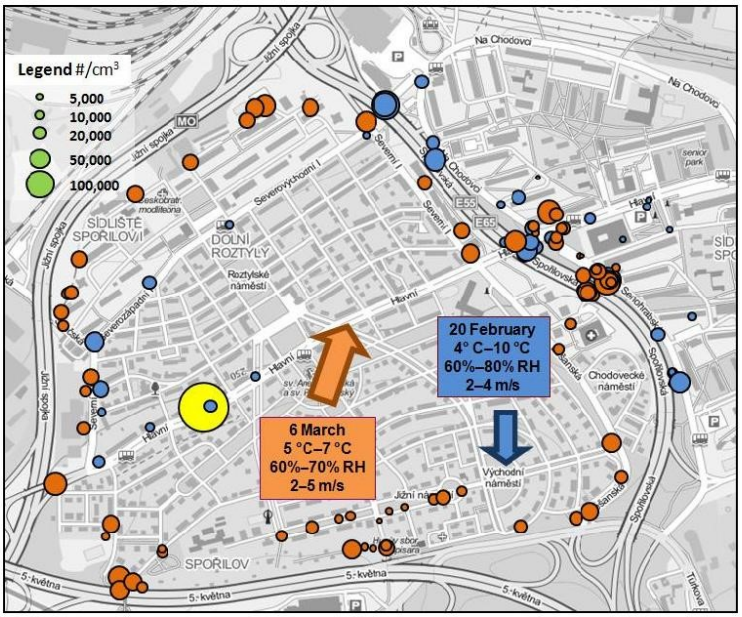

Figure 5. Measured average UFP concentrations and meteorological conditions in Sporilov on 20 February—blue, 6 March—orange. There can be seen substantial difference between higher concentrations measured closed to main roadways and lower concentrations measured deeper in a housing estate. Anomalous concentration due to scooter passing was indicated as a yellow dot; Map sources: Mapy.cz, Seznam.cz a.s.

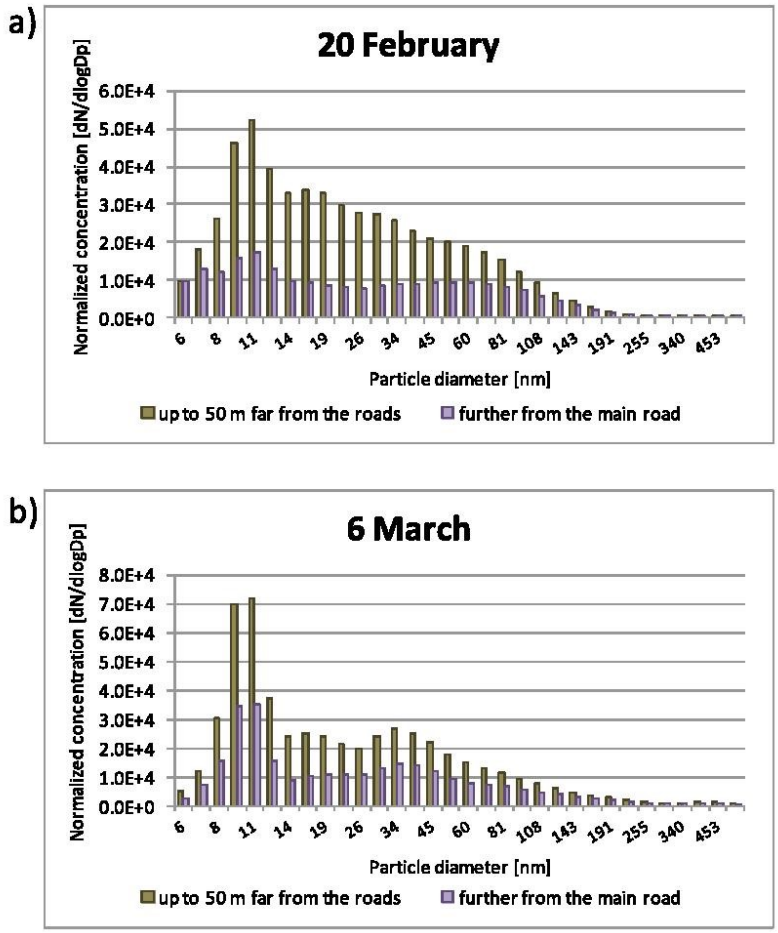

Figure 6. Particle number distribution measured in Sporilov on 20 February (**a**) and 6 March (**b**) according to distance from the main road. The highest peaks for both measurements were observed in 10 nm diameter particles, the second smaller peaks were formed in 20 and 40 nm particles for 20 February and 6 March, respectively. Similarity in distributions near and away from the main roadways and relative shift of smaller particles to larger ones in places further from the main roadways in comparison with places near the roadways indicated that particles measured deeper in a housing estate had a traffic origin.

3.3. Sporilov—Effects of Wind Direction

Measurement on 12 March was performed from 7:20 a.m. to 11:30 a.m. During this campaign the temperature and wind velocity gradually increased. Along with better dispersion condition, measured concentrations were decreasing. Meteorological conditions were recognized as the main determinant of number concentrations. Data were divided into three datasets: measurement 7:20–8:30 a.m. windless

condition, 8:30–10:00 a.m. moderate wind along a main road, and 10:00–11:30 a.m. measurements upwind from a major road where the emissions were blown away (Figure 7). Windless condition, while traffic culminated, led to averaged concentration 8.9×10^4 #/cm^3 (median 8.6×10^4 #/cm^3), distance from a main road was between 10–200 m. Moderate wind along a main road resulted in averaged concentration 3.8×10^4 #/cm^3 (median 3.5×10^4#/cm^3), distance from a main road was between 50–170 m. Situation when emissions were blown away occurred after 10:00 a.m., under this condition, concentrations were the lowest with average 1.3×10^4 #/cm^3 (median 1.0×10^4 #/cm^3), however, still above the Prague urban background of 7.3×10^3 #/cm^3 [29]. Particle number distributions have been changing with dispersion conditions. The highest peak seen under windless condition with maximum around 11 nm particles decreased and an almost imperceptible peak in bigger sizes (*ca.* 100 nm) increased in comparison with the peak in smaller sizes (Figure 8).

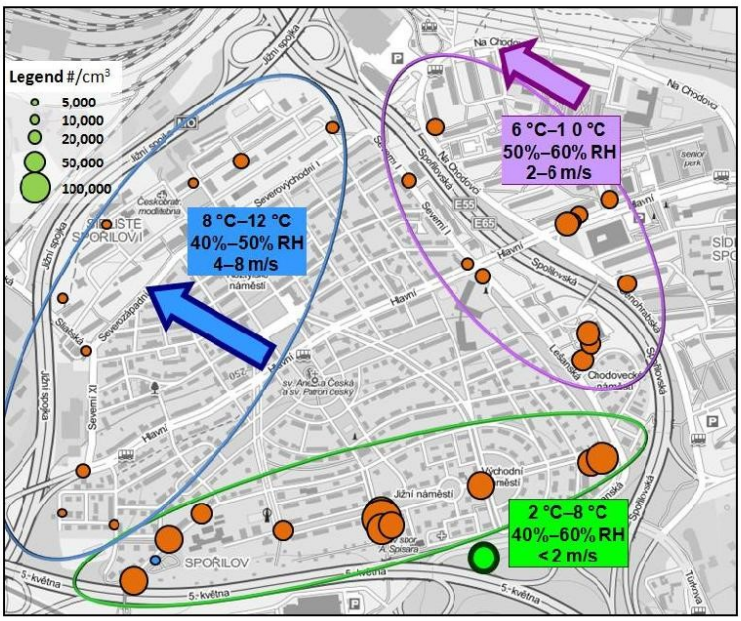

Figure 7. Measured average UFP concentrations within changing meteorological conditions in Sporilov on 12 March; during windless conditions, the highest averaged concentrations were measured in a building estate. Along with increasing wind speed measured particle number concentrations were gradually decreasing. Even within good dispersion conditions the particle number concentrations exceeded Prague background. Dots in a green ellipse represent measurement between 7:20–8:30 a.m.; purple, 8:30–10:00 a.m.; and blue, and 10:00–11:30 a.m.; Map sources: Mapy.cz, Seznam.cz a.s.

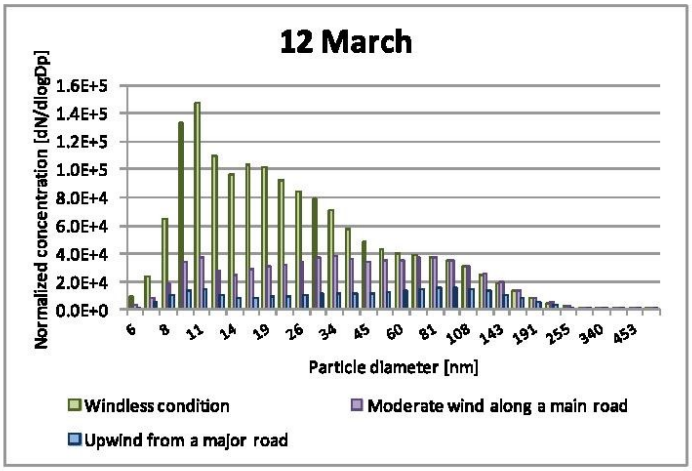

Figure 8. Particle number distribution within changing meteorological conditions in Sporilov on 12 March. Within windless condition a particle number distribution showed similar patter as measured on other days (20 February and 26 March; Figure 3) close to main roadways although this measurements involving places even further from the main roadway. Along with increasing wind speed relative proportion of smallest particles decreased while larger particles increased relatively.

3.4. Sporilov—Effects of Truck Acceleration Hotspot

Additional measurement was performed on 26 March from 10:45 a.m. to 1:20 p.m. after dilution of morning inversion. The highest concentrations, with a peak of 1.0×10^6 #/cm^3, were measured on the footbridge over a freeway. The eastbound section of the freeway is traveled by trucks, which have made a transit through Prague, often through extended periods of heavy congestion, entered the freeway on a ramp located just west of the footbridge, and are accelerating from the ramp while negotiating an incline. Earlier simulation of such conditions in an engine laboratory by this group [23] has demonstrated that extended low load leads to the cooling of the combustion chamber and of the exhaust system, which in turn results in worsened combustion, formation of deposits within the engine and the exhaust system, and loss of efficiency of catalytic devices due to low exhaust temperature. When such engine is subsequently operated at higher load, the deposits are driven off, and the emissions of particulate matter and temporarily increased; the emissions of carcinogenic polyaromatic hydrocarbons are increased an order of magnitude during such conditions over a stabilized high load operation.

The concentrations on the footbridge, nominally in hundreds of thousands of particles per cubic cm, were fluctuating, with peaks attributed to the passage of individual vehicles (Figure 9). The concentrations decreased markedly with the distance from the freeway to around 5.0×10^4 #/cm^3 50 meters away from the main road. Except for this acceleration site and related main road, the concentrations were relatively low thanks to good dispersion condition, average 7.0×10^3 #/cm^3, median 6.0×10^3 #/cm^3 (Figure 10). Distributions are shown in Figure 11. A bimodal distribution (10 nm and 20 nm peaks) was observed for site on/around the footbridge, with concentrations

decreasing with the distance from the road. Farther places had low particle concentration, even though a peak in 10 nm particles was still noticeable. These results contain only particles in range 5–100 nm; instrument channels counting larger particles were affected by a measurement artifact (a dog hair lodged on an EEPS electrometer).

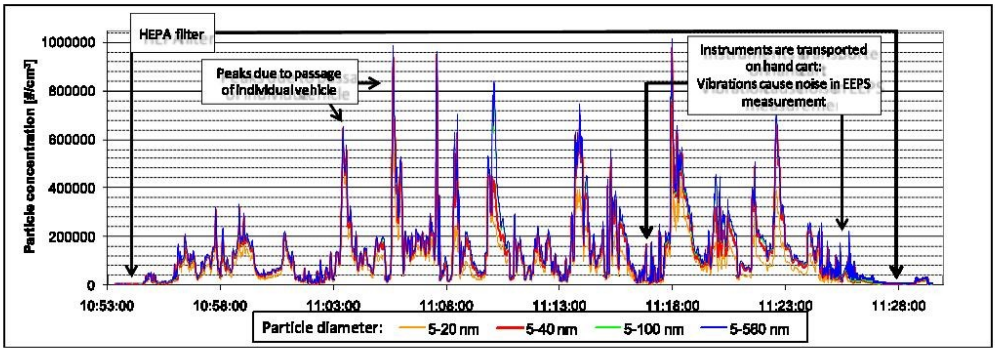

Figure 9. Number particle concentration time course within hotspot measurement in Sporilov on 26 March. Truck acceleration is peculiar for this measurement site. Additionally, before the trucks reach this place, they often spend some time in congestion. Under congestion condition extended low load leads to the cooling of the combustion chamber and of the exhaust system, which in turn results in worsened combustion, formation of deposits within the engine and the exhaust system, and loss of efficiency of catalytic devices due to low exhaust temperature. When such engine is subsequently operated at higher load, the deposits are driven off, and the emissions of particulate matter and temporarily increased.

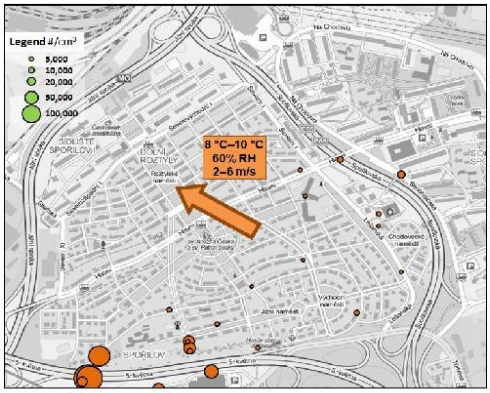

Figure 10. Measured average UFP concentrations near a hotspot and around in Sporilov on 26 March; High concentrations measured on a footbridge over a freeway were a result of emissions from truck accelerations after extended periods of heavy congestion. Impact of this hotspot can be seen in a near buildup area. Due to good dispersion conditions majority locations of housing estate showed low concentrations. Map sources: Mapy.cz, Seznam.cz a.s.

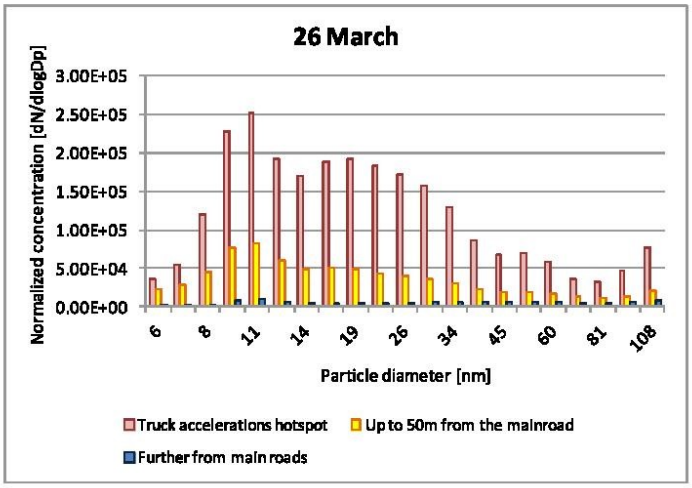

Figure 11. Particle number distributions near a hotspot and around according to distance from the hotspot and a main road measured in Sporilov on 26 March; Truck accelerations hotspot showed bimodal distribution with peaks at 10 and 20 nm. There should probably be another peak in larger particles; however, those data are not available because of the contamination of the corresponding instrument channels. Particles concentrations decreased with the distance from the road (up to 50 m), while the size distribution pattern remained similar. Farther places had low particle concentrations, even though a peak in 10 nm particles is still noticeable.

3.5. Libeznice

Measurement was performed during morning traffic peak on 15 May 2014 (6:20–8:15). Particles with diameter <10 nm were excluded because of periodically recurring artifact affecting the smallest two channels, resembling a nucleation event, which was considered improbable. Actual concentrations varied from tens of thousands to hundreds of thousands with peaks exceeding a million particles in cubic centimeter after passing of a high emitting vehicle. Average concentrations are plotted in Figure 12 and were 2.7×10^4 #/cm^3 (median 2.5×10^4 #/cm^3) next to the main road. Further from the main road, the number concentrations decreased rapidly to 7.5×10^3 #/cm^3 at 100 m and 4.5×10^3 #/cm^3 at 150 m.

A local and temporary hotspot was created by a small riding lawnmower. Lawnmowers are powered by gasoline engines with no electronic controls and no exhaust after treatment, and are, up to 19 kW power, not subject to any limit on particle emissions. As such, they can be a considerable source of particle emissions in residential neighborhoods. Further, the particles are emitted in the immediate vicinity of the operator, and therefore could pose significant health risk to the workers using such equipment on a regular basis.

The concentrations of particles were in the order of hundreds of thousands of particles per cm^3 *circa* ten meters away from the mower (Figure 12), a higher than expected value considering favorable

dispersion conditions. Background concentration was measured in the outskirts between rapeseed fields, concentration were around 3.8×10^3 #/cm^3.

Number distributions revealed difference between two sources of excess emissions: smoking vehicles and a lawn mower (Figure 13). Smoking vehicles (automobiles, buses and trucks typically in unsatisfactory technical condition) emitted particles with larger diameter, which is consistent with the visual observation of smoke. The lawn mower was responsible for similar amount of particles by count, but those particles were much smaller than the wavelength of the visible light and therefore practically invisible.

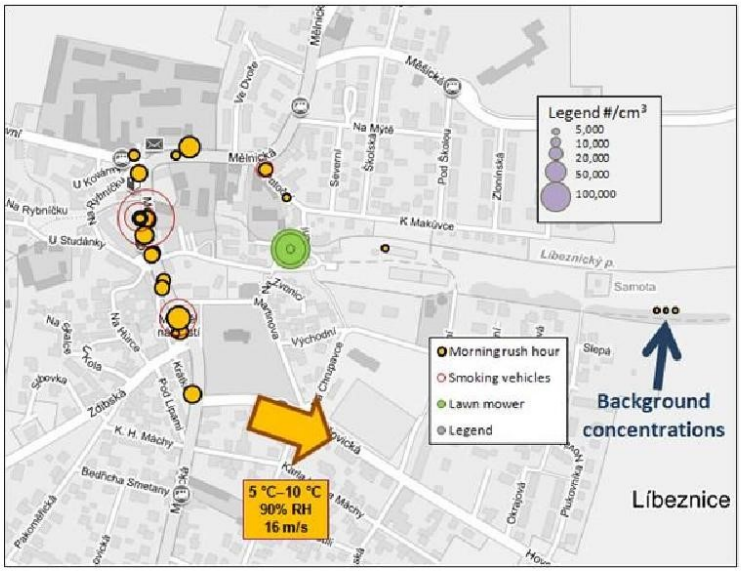

Figure 12. Measured average UFP concentrations and meteorological conditions on 15 May in Libeznice; UFP number concentrations closed to a main road were higher than concentrations measured further from the main road. Attention should be paid to concentrations measured near riding lawn mower (green dots), which are comparable with concentrations measured within passing smoking vehicle (red rings). Operating lawn mower created temporary local UFP hotspot. Lawnmowers are powered by gasoline engines with no electronic controls and no exhaust after-treatment, which are, up to 19 kW power, not subject to any limit on particle emissions. Particles with diameter <10 nm were excluded because of periodically recurring artifact affecting the smallest two channels, resembling a nucleation event, which was considered improbable; Map sources: Mapy.cz, Seznam.cz a.s.

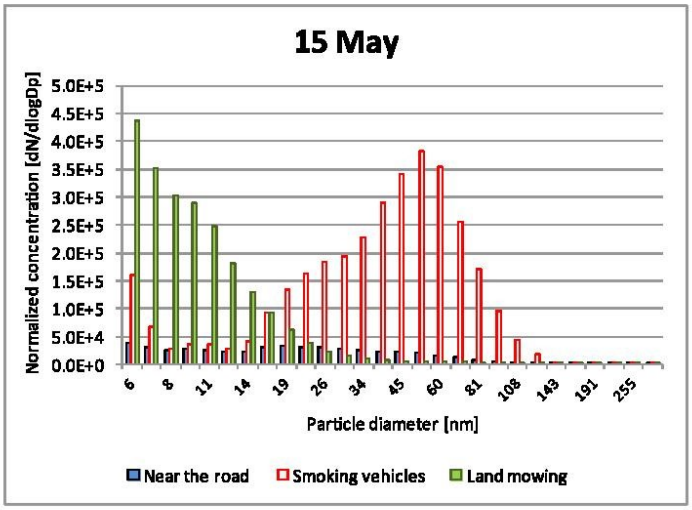

Figure 13. Particle number distribution measured in Libeznice on 15 May according to source of particles (road traffic excluding high emitters, smoking vehicles, lawn mower). Smoking vehicles emitted particles with larger diameter, which is consistent with the visual observation of smoke. The lawn mower is responsible for similar amount of particles by count, but those particles are much smaller than the wavelength of the visible light and therefore practically invisible. Particles with diameter <10 nm were excluded because of periodically recurring measurement artifacts affecting the smallest two channels.

3.6. Celakovice

Measurement in Celakovice city was carried out with two mobile apparatuses measuring in parallel; the first apparatus equipped with EEPS and CPC measured concentrations next to the main road, the second measured further form the road (*ca.* 100–150 m). Measurements were performed on two days, 30 January (morning and afternoon measurement) and 3 February (all day measurement). Data presented herein comprise all measured particles (5–500 nm) due to inconsistence results obtained from CPC and EEPS. On 3 February, particle number concentrations from the EEPS were consistently lower by about 6500 #/cm^3 compared to the CPC during campaign on 3 February, an offset attributed to an erroneous zeroing of the EEPS. As CPC can be considered the ultimate source of total particle number concentrations, total counts calculated from EEPS size distributions were corrected for the zero drift to match the CPC. The UF-CPC measures particles with diameter between 4 nm–10 μm, while the EEPS range is 5–500 nm; difference in instrument ranges on the upper end was considered to be insignificant because vast majority of the urban particles, from particle number concentration point of view, fell within the EEPS range. However, we were not able to reconstructed particle number distribution due to the shifted zero offset on 3 February, therefore distribution is presented only for 30 January measurement.

During traffic peaks concentrations next to the road varied around 2×10^4 #/cm^3 with typical peaks after passing older vehicles around 4×10^4 #/cm^3; together average particle number concentrations for

morning traffic peaks were 3.6×10^4 #/cm^3 (median 3.0×10^4 #/cm^3) on 30 January and 3.2×10^4 #/cm^3 (median 2.0×10^4 #/cm^3) on 3 February. Maximal measured concentration, more than 5×10^5 #/cm^3, occurred after the passages of high emitters (a tractor and several automobiles) The influence of the main road was not noticeable at 150 m from the road, where the concentrations were mainly around 1.5×10^4 #/cm^3 or lower (Figure 14). Particle number distributions measured next to the road on 30 January and 150 m away from the road are shown in (Figure 15) and are similar for both places. It suggests that traffic, even in small city with low traffic load, is a key contributor to the ambient UFP concentrations.

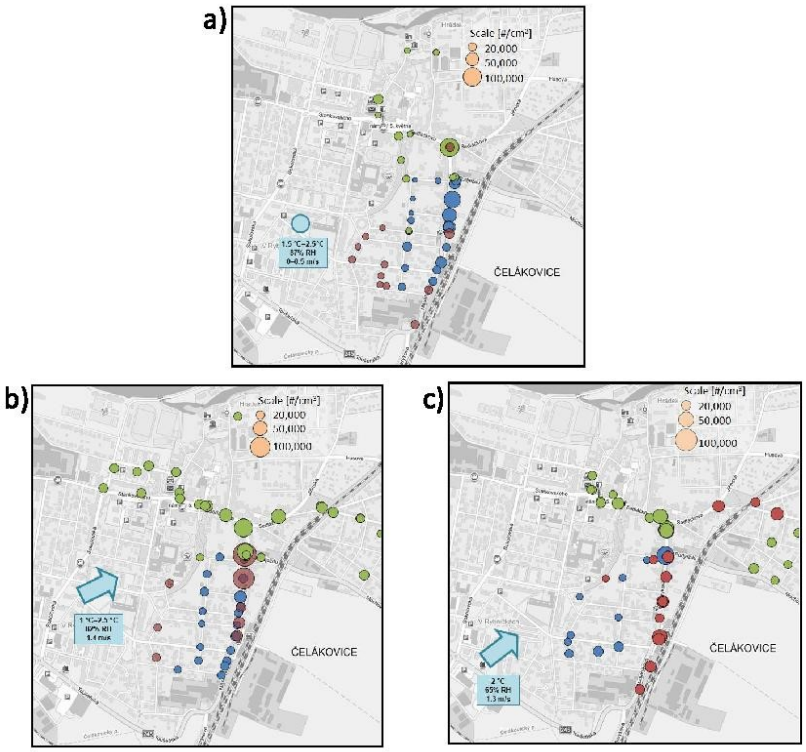

Figure 14. Simultaneous particles number concentration measurements with two mobile apparatuses. Dot colors indicate time intervals. The first apparatus measured closed to a main road while the second measured parallel away from the main road. Concentrations along main roads were elevated in comparison with places further from the road. (**a**) Particle number concentrations 30 January; simultaneous measurement at 7:30–8:00 a.m. blue points, 8:00–8:20 a.m. red points, and 8:20–9:00 a.m. green points.(**b**) Particle number concentrations on 3 February; simultaneous measurement at 6:45–7:20 a.m. blue points, 7:20–7:35 a.m. red points, and 7:35–9:00 a.m. green points.(**c**) Particle number concentrations on 3 February; simultaneous measurement at 5:10–5:15 p.m. blue points, 5:15–5:50 p.m. red points, 5:50–6:30 p.m. green points; Map sources: Mapy.cz, Seznam.cz a.s.

Afternoon traffic peak was measured on 3 February, while one apparatus stayed on an intersection and the second operated away from the main road. The intersection represents a hotspot of the Celakovice city, it is the part of the main road and many cars have to slow down or stop and then accelerate to common city speed. Average particle number concentration was 6.1×10^4 #/cm^3 (median 5.7×10^4 #/cm^3) next to the intersection. The apparatus measured away from the crossroad (*ca.* 150–250 m) measured average concentration 1.4×10^4 #/cm^3 (median 1.2×10^4 #/cm^3) during the traffic peak.

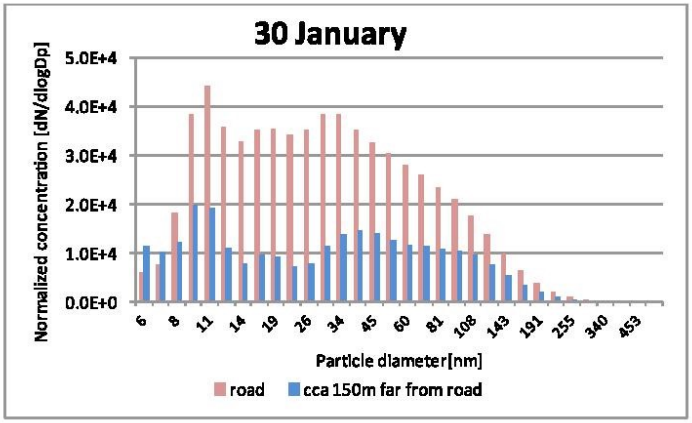

Figure 15. Particle number distributions during simultaneous measurement by two instruments sets, one near the main road, the second *ca.* 150 m away from the road on 30 January, 7:30–8:00 a.m., corresponding to blue dots in Figure 14a. Concentrations measured away from a main road in Celakovice had similar distribution as particles measured next to the main road.

Concentrations after morning traffic peaks were stable around 1.5×10^4 #/cm^3 up to 10:00 a.m., then gradually decreased to concentrations 1.0×10^4 #/cm^3 (3 February) and 7.0×10^3 #/cm^3 (30 January) at midday. Lower concentrations on 30 January were not likely to have been caused by better dispersion conditions because wind speed were around 0.5–2 m/s, while on 3 February the wind speed varied between 0.5–3 m/s (Figure 16).We expected lower concentrations in comparison with other studies, so there should be other sources of ultrafine particles, but no such sources were identified during the measurements. A heavily traveled freeway to Prague is 3 km from the measurement site. UFP generated by vehicles going on the highway should have already coagulated into large particles before they reached Celakovice; however, at this time, the measurement was downwind from the freeway.

After the afternoon traffic peak, 3 February 6:00–6:30 p.m., concentrations were stabilized around 2.0×10^4 #/cm^3 with some exceeding values, while the source was always vehicle e.g., idling diesel vehicle in front of a house or a high emitting vehicle passage. Together, average particle number concentration was 2.2×10^4 #/cm^3 (median 1.8×10^4 #/cm^3).

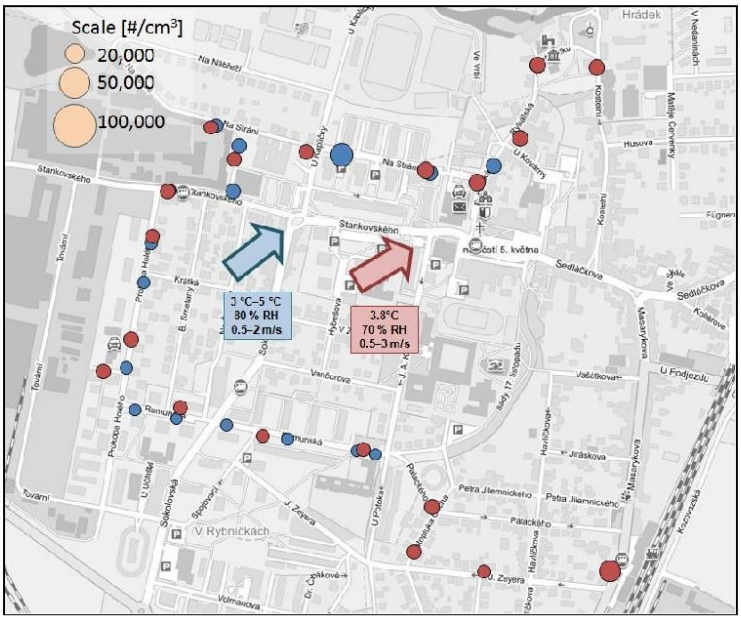

Figure 16. Particle number concentrations measured after traffic peaks on 30 January—blue, and 3 February—red; Vehicles on the main road going through the city were not proved as the main source due to very low traffic load after morning peak. Other source of UFP emissions is a motorway, about 3 km and upwind from the measurement site. Map sources: Mapy.cz, Seznam.cz a.s.

4. Discussion

4.1. Instrumentation

The results confirmed that fast particle classifiers are useful for mobile measurements [24], as the size information is helpful in the explanation of the origin of the particles, and the time resolution allows for detection of temporary or localized sources such as passing high emitting vehicles. The particle classifiers closely matched both SMPS data during a stationary co-location exercise, and condensation particle data during field measurements when not moving. The classifiers were subject to increased noise in data when traveling on a small cart, and to a non-negligible zero drift, suggesting that they should be complemented by a CPC as a data validation tool. Mounting the particles on a handcart has allowed much more detailed measurements that could have been accomplished by instrumented motor vehicles.

4.2. Effects of Traffic

In all locations, elevated UFP concentrations associated with the proximity of internal combustion engines (mostly vehicular traffic, but also a lawn mower) were found. The size distribution was generally bi-modal, with nucleation peak around 10 nm, and a second accumulation mode peak in the

tens of nm range, corresponding to, for example, thermodenuded diesel exhaust [20]. The particles were generally smaller compared to the size distributions measured at background stations throughout Europe [30] as well as at the Czech background station in Košetice [31], but well in agreement in terms of size and concentration with observations in the center of Milano [32]. The nucleation peak was more pronounced, and the accumulation mode peak shifted towards smaller particles, in the proximity of the source, except for high emitting vehicles, where the accumulation mode has dominated the size distribution. Farther from the source, the concentration diminished, in agreement with [5], the nucleation peak was smaller or not present, and the accumulation mode peak was shifted to larger particles. The contribution of high emitting vehicles was readily noticeable. Highest concentrations were observed in an area where truck engines were operated at high load which was likely to have immediately followed extended periods of low load, which is in agreement with earlier results of engine tests showing detrimental effects of extended low load [23].

It is the opinion of the authors that avoiding overloading of the roads (seen in Sporilov and Libeznice), during which both the engine combustion efficiency and the catalyst efficiency can decrease, improved vehicle emissions inspection program eliminating high emitting vehicles (smoking vehicles were observed in all places), support of public transit and non-motorized passenger transport, shifting transit road transport to more ecological railways, and other means are some relatively low-cost measures that would bring a relatively fast reduction in ambient UFP concentrations.

4.3. Effects of Local Heating Appliances

Virtually all measurements were done at temperatures when regular ordinary use of home heating appliances was expected. In the Czech Republic, large apartment buildings often use central heating or have their own natural gas furnaces, while family houses are heated by a mix of natural gas, wood and coal. The mix is dependent on the economic situation of the families; in economically depressed areas, the use of poor-quality coal, waste products, and other inferior fuels is not uncommon.

In the Sporilov neighborhood, particles originating from residential houses in the central and southern parts of the triangle would be expected to be present (a) in the central part of the triangle formed by the freeways in Figure 5; (b) downwind of the central part of the triangle along its northwest border in Figure 7, and (c) throughout the southern part of the triangle in Figure 9. Further, such particles would be expected to be observed at least at some points in Libeznice and Celakovice. No substantially elevated concentrations and no hotspots (it was recognized that hotspots from heating appliances would be broader than from engines), which were not attributed to internal combustion engines, were, however, found at any of the places examined. The domination of traffic sources is consistent with ambient measurement in schools in Australia [33] and ambient measurements in Pittsburgh [34]. The large contrast between busy streets and urban background was also observed in a Copenhagen study, which concluded that a "significant underestimation of disease burden may occur when relying too much on the regulated components" [35].

However, when emissions limits of heating appliances and engines are compared either on a PM mass per kg of fuel or PM mass per cubic meter of exhaust, the currently allowed maximum emissions of heating appliances exceed heavy duty on-road engines by orders of magnitude. It therefore appears that while local heating appliances might be a significant source of particulate matter in general, and

notably total particle mass, they were not found to be a noticeable contributor to UFP at street level, possibly as they produce larger particles which are also less available at the street level due to smokestacks.

5. Conclusions

This work investigated the spatial distribution of UFP in three areas in the Czech Republic with different traffic load by fast mobility particle sizers (EEPS) mounted on a handcart and pushed around the areas. Utilization of a fast mobility particle sizer was appropriate for UFP measurement influenced by traffic, because it was able to record rapid changes in particle number distribution.

In all locations, the highest concentrations were observed in the vicinity of vehicular traffic (or operation of non-road engines), and observed particle number distributions both close to and away from main roads had similar patterns consistent with size distributions observed in engine exhaust. Further, the observed patterns corresponded to findings from vehicle emissions studies, attributing high emissions to extended idling, transient operation, and high emitting vehicles. On the contrary, the particle number concentrations in other parts of the neighborhoods were relatively small, and the share of particles larger than 100 nm was relatively low in all number size distributions. Therefore, it appears that the number counts of UFP at breathing level are dominated by UFP originating from vehicular traffic. Vehicles, while contributing only tens of percent to the total emissions of total particulate mass, could therefore bear much larger share in the total health effects of particulate matter, due to a combination of high share of UFP and proximity of sources to citizens. The study reiterates the need to further reduce vehicle emissions through reduction in vehicular traffic, improvements in vehicle maintenance, cleaner fuels and technologies, and other measures.

Acknowledgments

This project was partly supported by Czech Science Foundation (13-01438S and P503-12-G147). The salary of the authors was funded by the EU LIFE+ program, project LIFE10 ENV/CZ/651: MEDETOX—"Innovative Methods of Monitoring of Diesel Engine Exhaust Toxicity in Real Urban Traffic" (J.S., M.F., L.D., M.P., M.V.), by the European Social Fund, project CZ.1.07/2.3.00/30.0034 "Support of inter-sectoral mobility and quality enhancement of research teams at the Czech Technical University in Prague" (M.V. in part). Loan of one of the EEPS and its operation was funded by the Czech Ministry of Education, Youth and Sports program NPU I (LO), project LO1311 "Development of Vehicle Centre of Sustainable Mobility". The P-trak was loaned by Institute for Environmental Studies, Faculty of Science, Charles University in Prague. The remaining instrumentation (EEPS, UF-CPC, GPS, power electronics) was provided by, and special parts funded by, the MEDETOX project.

The authors thank Jana Růžičková, Pavla Kačabová and Zdravý Spořilov citizen group, and Anna Šindelářová, Libor Semotán and SOS Spořilov citizen group from Spořilov, Jan Vondráš from Libeznice, and Jan and Věra Topinka from Celakovice for insights and for local support.

Author Contributions

All authors participated in transport and operation of the instrumentation during the measurement campaigns. Lubos Dittrich and Martin Pechout designed and fabricated the carts and instrument

mounting. Jakub Ondracek ran the reference SMPS and took part in the collocation exercise. Jitka Stolcpartova and Michal Vojtisek-Lom analyzed and interpreted the data. Michal Vojtisek-Lom was the visionary behind the measurement setup and methods and leader of the project.

Conflicts of Interest

The authors declare no conflict of interest.

References

1. Kumar, P.; Morawska, L.; Birmili, W.; Paasonen, P.; Hu, M.; Kulmala, M.; Harrison, R.M.; Norford, L.; Britter, R. Ultrafine particles in cities. *Environ. Int.* **2014**, *66*, 1–10.
2. Brines, M.; Dall'Osto, M.; Beddows, D.C.S.; Harrison, R.M.; Gómez-Moreno, F.; Núñez, L.; Artíñano, B.; Costabile, F.; Gobbi, G.P.; Salimi, F.; *et al.* Traffic and nucleation events as main sources of ultrafine particles in high-insolation developed world cities. *Atmos. Chem. Phys.* **2015**, *15*, 5929–5945.
3. Karner, A.A.; Eisinger, D.S.; Niemeier, D.A. Near-Roadway Air Quality: Synthesizing the Findings from Real-World Data. *Environ. Sci. Technol.* **2010**, *44*, 5334–5344.
4. Buonanno, G.; Lall, A.A.; Stabile, L. Temporal size distribution and concentration of particles near a major highway. *Atmos. Res.* **2009**, *43*, 1100–1105.
5. Zhu, Y.; Hinds, W.C.; Kim, S.; Sioutas, C. Concentration and size distribution of ultrafine particles near a major highway. *J. Air Waste Manag. Assoc.* **2002**, *52*, 1032–1042.
6. Buonanno, G.; Fuoco, F.C.; Stabile, L. Influential parameters on particle exposure of pedestrians in urban microenvironments. *Atmos. Res.* **2011**, *45*, 1434–1443.
7. Peters, A.; Wichmann, H.E.; Tuch, T.; Heinrich, J.; Heyder, J. Respiratory effects are associated with the number of ultrafine particles. *Am. J. Respiratory Crit. Care Med.* **1997**, *155*, 1376–1383.
8. Politis, M.; Lekkas, T.D. Ultrafine particles (UFP) and health effects. Dangerous. Like no other PM? Review and analysis. *Glob. NEST J.* **2008**, *10*, 439–452.
9. Devlin, R.B.; Smith, C.B.; Schmitt, M.T.; Rappold, A.G.; Hinderliter, A.; Graff, D.; Carraway, M.S. Controlled Exposure of Humans with Metabolic Syndrome to Concentrated Ultrafine Ambient Particulate Matter Causes Cardiovascular Effects. *Toxicol. Sci.* **2014**, *140*, 61–72.
10. Lanzinger, S.; Schneider, A.; Breitner, S.; Erzen, I.; Dostal, M.; Pastorkova, A.; Bastian, S.; Cyrys, J.; Zscheppang, A.; Kolodnitska, T.; *et al.* Health Effects of Ultrafine and Fine Particles in Central Europe—Results from the UFIREG study. In Proceedings of the HEI Annual Conference, Philadelphia, PA, USA, 3–5 May 2015. Available online: http://www.healtheffects.org/Pubs/AnnualConferenceProgramAbstracts2015.pdf (accessed on 1 June 2015).
11. Araujo, J.A.; Barajas, B.; Kleinman, M.; Wang, X.; Bennett, B.J.; Gong, K.W.; Navab, M.; Harkema, J.; Sioutas, C.; Lusis, A.J.; *et al.* Ambient particulate pollutants in the ultrafine range promote early atherosclerosis and systemic oxidative stress. *Circ. Res.* **2008**, *102*, 589–596.
12. Lindgren, A.; Stroh, E.; Montnemery, P.; Nihlen, U.; Jakobsson, K.; Axmon, A. Traffic-related air pollution associated with prevalence of asthma and COPD/chronic bronchitis. A cross-sectional study in Southern Sweden. *Int. J. Health Geogr.* **2009**, *8*, doi:10.1186/1476-072X-8-2.

13. Nuvolone, D.; della Maggiore, R.; Maio, S.; Fresco, R.; Baldacci, S.; Carrozzi, L.; Pistelli, F.; Viegi, G. Geographical information system and environmental epidemiology: A cross-sectional spatial analysis of the effects of traffic-related air pollution on population respiratory health. *Environ. Health* **2011**, *10*, doi:10.1186/1476-069X-10-12.
14. Lewtas, J. Air pollution combustion emissions: Characterization of causative agents and mechanisms associated with cancer, reproductive, and cardiovascular effects. *Mutat. Res. Rev. Mutat. Res.* **2007**, *636*, 95–133.
15. Czech Hydrometeorological Institute, Annual Tabular Overview 2013: Air quality in the Czech Republic. Available online: http://portal.chmi.cz/files/portal/docs/uoco/isko/grafroc/13groc/gr13cz/IV1_PM_CZ.html (accessed on 19 October 2015).
16. Buonanno, G.; Stabile, L.; Morawska, L. Particle emission factors during cooking activities. *Atmos. Environ.* **2009**, *43*, 3235–3242.
17. Tiwari, M.; Sahu, S.K.;Bhangare, R.C.; Yousaf, A.; Pandit, G.G. Particle size distributions of ultrafine combustion aerosols generated from household fuels. *Atmos. Pollut. Res.* **2014**, *5*, 145–150.
18. Janhall, S.; Andreae, M.O.; Poschl, U. Biomass burning aerosol emissions from vegetation fires: Particle number and mass emission factors and size distributions. *Atmos. Chem. Phys. Discuss.* **2009**, *9*, 17183–17217.
19. Kittelson, D.B. Engines and nanoparticles: A review. *J. Aerosol Sci.* **1998**, *29*, 575–588.
20. Ronkko, T.; Lahde, T.; Heikkila, J.; Pirjola, L.; Bauschke, U.; Arnold, F.; Schlager, H.; Rothe, D.; Yi-Ojanpera, J.; Keskinen, J. Effects of Gaseous Sulphuric Acid on Diesel Exhaust Nanoparticle Formation and Characteristics. *Environ. Sci. Technol.* **2013**, *47*, 11882–11889.
21. Wang, X.; Westerdahl, D.; Wu, Y.; Pan, X.; Zhang, K.M. On-road emission factor distributions of individual diesel vehicles in and around Beijing, China. *Atmos. Environ.* **2011**, *45*, 503–513.
22. Kumar, P.; Gurjar, B.R.; Nagpure, A.; Harrison, R.M. Preliminary estimates of nanoparticle number emissions from road vehicles in megacity Delhi and associated health impacts. *Environ. Sci. Technol.* **2011**, *45*, 5514–5521.
23. Vojtisek-Lom, M.; Pechout, M.; Dittrich, L.; Beranek, V.; Kotek, M.; Schwarz, J.; Vodicka, P.; Milcova, A.; Rossnerova, A.; Ambroz, A.; *et al.* Polycyclic aromatic hydrocarbons (PAH) and their genotoxicity in exhaust emissions from a diesel engine during extended low-load operation on diesel and biodiesel fuels. *Atmos. Environ.* **2015**, *109*, 9–18.
24. Manigrasso, M.; Stabile, L.; Avino, P.; Buonanno, G. Influence of measurement frequency on the evaluation of short-term dose of sub- micrometric particles during indoor and outdoor generation events. *Atmos. Environ.* **2013**, *67*, 130–142.
25. UFIREG, Data Collection and Methods: Report. Available online: http://www.ufireg-central.eu/files/Downloads/UFIREG_Data_collection_and_methods.pdf (accessed on 28 August 2015).
26. Technical Administration of Roadways of the Capital of Prague (TSK), Automotive Transport Intensity: Transport Intensity in the Monitored Network for Traffic Count TSK-ÚDI 2012 (XLSX) (CZ). Available online: http://www.tsk-praha.cz/wps/wcm/connect/www.tsk-praha.cz20642/46097abd-b458–4c48-a73d-02f46196d262/tsk-udi-intenzity-2014.xlsx?MOD=AJPERES (accessed on 22 July 2015).

27. AF-CITYPLAN S.R.O., Study of Traffic Calming in village Libeznice (in Czech: "Dopravní Studie Zklidnění Průjezdu Obcí LIBEZNICE"). Available online: http://www.libeznice.cz/sites/default/files/2012/12/dopravni_pruzkum_2012_finalni_verze_pdf_52449.pdf (accessed on 22 July 2015).
28. Road and Motorway Directorate of the Czech Republic (RSD), National Traffic Counts (in Czech: "Celostátní Sčítání Dopravy"). Available online: http://scitani2010.rsd.cz/pages/results/section/default.aspx?l=St%C5%99edo%C4%8Desk%C3%BD%20kraj (accessed on 23 July 2015).
29. Rimnacova, D.; Zdimal, V.; Schwarz, J.;Smolik, J.; Rimnac, M. Atmospheric aerosols in suburb of Prague: The dynamics of particle size distributions. *Atmos. Environ.* **2011**, *101*, 539–552.
30. Asmi, A.; Wiedensohler, A.; Laj, P.; Fjaeraa, A.-M.; Sellegri, K.; Birmili, W.; Weingartner, E.; Baltensperger, U.; Zdimal, V.; Zikova, N.; *et al*. Number size distributions and seasonality of submicron particles in Europe 2008–2009. *Atmos. Chem. Phys.* **2011**, *11*, 5505–5538.
31. Zikova, N.; Zdimal, V. Long-Term Measurement of Aerosol Number Size Distributions at Rural Background Station Kosetice. *Aerosol Air Qual. Res.* **2013**, *13*, 1464–1474.
32. Lonati, G.; Crippa, M.; Gianelle, V.; van Dingenen, R. Daily patterns of the multi-modal structure of the particle number size distribution in Milan, Italy. *Atmos. Environ.* **2011**, *45*, 2434–2442.
33. Guo, H.; Morawska, L.; He, C.R.; Zhang, Y.L.L.; Ayoko, G.; Cao, M. Characterization of particle number concentrations and PM2.5 in a school: Influence of outdoor air pollution on indoor air. *Environ. Sci. Pollut. Res.* **2010**, *17*, 1268–1278.
34. Stanier, C.O.; Khlystov, A.Y.; Pandis, S.N. Ambient aerosol size distributions and number concentrations measured during the Pittsburgh Air Quality Study (PAQS). *Atmos. Environ.* **2004**, *38*, 3275–3284.
35. Boogard, H.; Kos, G.P.A.; Weijers, E.P.; Janssen, N.A.H.; Fischer, P.H.; van der Zee, S.C.; de Hartog, J.J.; Hoek, G. Contrast in air pollution components between major streets and background locations: Particulate matter mass, black carbon, elemental composition, nitrogen oxide and ultrafine particle number. *Atmos. Environ.* **2011**, *45*, 650–658.

Článek 2

International Journal of
Molecular Sciences

MDPI

Article

Comparative Analysis of Toxic Responses of Organic Extracts from Diesel and Selected Alternative Fuels Engine Emissions in Human Lung BEAS-2B Cells

Helena Libalova [1], Pavel Rossner, Jr. [1], Kristyna Vrbova [1], Tana Brzicova [1,2], Jitka Sikorova [1,3], Michal Vojtisek-Lom [4], Vit Beranek [4], Jiri Klema [5], Miroslav Ciganek [6], Jiri Neca [6], Katerina Pencikova [6], Miroslav Machala [6] and Jan Topinka [1,*]

1 Department of Genetic Toxicology and Nanotoxicology, Institute of Experimental Medicine AS CR, Videnska 1083, 142 20 Prague, Czech Republic; libalova@biomed.cas.cz (H.L.); prossner@biomed.cas.cz (P.R.Jr.); kristyna.vrbova@biomed.cas.cz (K.V.); tana.brzicova@biomed.cas.cz (T.B.); jitkastolcpartova@seznam.cz (J.S.)
2 Faculty of Safety Engineering, VSB–Technical University of Ostrava, Lumirova 13, 700 30 Ostrava, Czech Republic
3 Institute for Environmental Studies, Faculty of Science, Charles University in Prague, Benatska 2, 128 01 Prague 2, Czech Republic
4 Center of Vehicles for Sustainable Mobility, Faculty of Mechanical Engineering, Czech Technical University in Prague, Technicka 4, 166 07 Prague, Czech Republic; michal.vojtisek@fs.cvut.cz (M.V.-L.); vit.beranek@fs.cvut.cz (V.B.)
5 Department of Cybernetics, Faculty of Electrical Engineering, Czech Technical University in Prague, Karlovo namesti 13, 121 35 Prague, Czech Republic; klema@fel.cvut.cz
6 Department of Chemistry and Toxicology, Veterinary Research Institute, Hudcova 296/70, 621 00 Brno, Czech Republic; ciganek@vri.cz (M.C.); neca@vri.cz (J.N.); pencikova@vri.cz (K.P.); machala@vri.cz (M.M.)
* Correspondence: jtopinka@biomed.cas.cz; Tel.: +420-241-062-675; Fax: +420-241-062-785

Academic Editor: Marcello Iriti
Received: 9 August 2016; Accepted: 25 October 2016; Published: 3 November 2016

Abstract: This study used toxicogenomics to identify the complex biological response of human lung BEAS-2B cells treated with organic components of particulate matter in the exhaust of a diesel engine. First, we characterized particles from standard diesel (B0), biodiesel (methylesters of rapeseed oil) in its neat form (B100) and 30% by volume blend with diesel fuel (B30), and neat hydrotreated vegetable oil (NEXBTL100). The concentration of polycyclic aromatic hydrocarbons (PAHs) and their derivatives in organic extracts was the lowest for NEXBTL100 and higher for biodiesel. We further analyzed global gene expression changes in BEAS-2B cells following 4 h and 24 h treatment with extracts. The concentrations of 50 μg extract/mL induced a similar molecular response. The common processes induced after 4 h treatment included antioxidant defense, metabolism of xenobiotics and lipids, suppression of pro-apoptotic stimuli, or induction of plasminogen activating cascade; 24 h treatment affected fewer processes, particularly those involved in detoxification of xenobiotics, including PAHs. The majority of distinctively deregulated genes detected after both 4 h and 24 h treatment were induced by NEXBTL100; the deregulated genes included, e.g., those involved in antioxidant defense and cell cycle regulation and proliferation. B100 extract, with the highest PAH concentrations, additionally affected several cell cycle regulatory genes and p38 signaling.

Keywords: diesel; alternative fuels; diesel exhaust particles; organic extracts; gene expression profiles

1. Introduction

Diesel engines are popular not only for trucks but also in passenger cars and a wide range of mobile machinery due to lower fuel consumption and consequently lower CO_2 emissions, relatively

low production and operating costs, reliability, and overall practicality. Awareness of global climate change and the need to reduce CO_2 emissions have led to renewable diesel fuels with significantly lower emissions of fossil carbon (as CO_2) compared to conventional fossil diesel fuels. Drop-in replacement fuels for existing diesel engines are typically produced from vegetable oils and other fatty acids, either by transesterification into n-alkyl-esters of fatty acids, called biodiesel (in the EU, typically rapeseed oil methylesters), or by thermal hydrodeoxynation or similar processes into mostly paraffinic fuels, termed hydrotreated vegetable oil (HVO). The chemical composition and properties of renewable diesels are dependent on the production technique; e.g., biodiesel is enriched with oxygen in comparison with HVO and conventional diesel, biodiesel and HVO lack sulfur and do not contain aromatic hydrocarbons as diesel [1,2].

Renewable diesel fuels produce less particulate matter, carbon monoxide and total hydrocarbons due to reduced aromatics content, higher cetane number (HVO), or oxygen content (biodiesel); the same property, however, could lead to higher emissions of nitrogen oxides (NO_x) [3–8]. A disadvantage specific for biodiesel is its lower energy density, leading to a higher fuel consumption and a decrease in torque and power at full load conditions [9]. HVO, however, has no or minor negative influence on fuel consumption and engine power [3,10]. Particle number size distributions were mostly shifting toward smaller sizes with an increased portion of biodiesel in the fuel [4,11]. All presented emission patterns for biodiesel strongly depend on operating regime and engine type, therefore there are also opposite findings, e.g., an increase in particulate mass during idling on biodiesel [12] or opposite results in particle number concentrations in exhaust between two engines under the same conditions on the same biodiesel/diesel mixtures [13].

Diesel exhaust, along with air pollution, was categorized by the International Agency for Research on Cancer (IARC) as carcinogenic to humans [14,15]. However, the different chemical composition of diverse blends of diesel and renewable fuels also influences exhaust emission characteristics. In recent years, more attention has been paid to diesel exhaust particles (DEP) (reviewed in [16]), as DEP is a carrier of polycyclic aromatic hydrocarbons (PAHs) that exert most of the genotoxic activity. Benzo[a]pyrene (BaP) is carcinogenic to humans and several other PAHs have been classified as probable or possible human carcinogens [14]. Although secondary genotoxicity elicited by the interaction of the particles with the immune system resulting in inflammation is believed to be an important factor in the negative health effects of DEP exposure [17], primary genotoxicity directly caused by organic compounds adsorbed onto DEP may substantially contribute to the carcinogenicity of DEP. As the content of PAHs between different fuels' DEPs varies, the genotoxicity of their organic extracts also depends on the fuel used [12,18]. It has been reported that toxic effects of DEP and DEP extracts from identical fuels differ [19,20]. Therefore, ideally, a battery of tests including both particles and extracts should be applied. However, to specifically reveal the potential carcinogenic effects of PAHs, application of organic extracts is more relevant. Although the genotoxicity of DEP extracts may be easily tested by standardized, well-established tests including cytotoxicity measurement [20], Ames test [20,21], analysis of double strand DNA breaks [21], apoptosis, frequency of micronuclei [22], bulky DNA adducts formation or oxidative DNA damage [12], for a comprehensive assessment of the biological processes induced by the DEP extracts the treatment of the whole genome gene expression analysis is a valuable tool.

The objective of the present study was to compare the toxicity of organic compound mixtures extracted from DEPs produced by diverse fuels (conventional fossil diesel, 100% biodiesel, a blend of diesel/biodiesel and HVO) with the special focus on characterization of the complex cellular response. A fuel marketed as "renewable diesel" under the name of NEXBTL (Neste Oil, Espoo, Finland) was used as a HVO representative. An IVECO Tector 5.9 L, 176 kW engine was used to generate DEPs as it is commonly used in the EU in smaller trucks. We aimed to investigate the whole-genome gene expression changes following the exposure to organic compounds extracted from different diesel/renewable diesel fuel exhaust particles and to reveal common genes and processes similarly affected upon all DEP extracts treatment as well as the specific molecular signatures linked

to the activity of individual extracts. A detailed chemical analysis of PAHs and their derivatives was employed to clarify the differences in toxicity of individual extracts. To support gene expression data, the oxidative potential of DEP extracts was evaluated by intracellular reactive oxygen species (ROS) assay and glutathione assay upon 4 h exposure and expressions of selected genes were confirmed by RT-qPCR.

2. Results

2.1. Characteristics of Collected Exhaust Particles; Chemical Analysis of Organic Extracts

Figure 1A shows particle number distributions for individual fuels. Although the size of most of the DEPs for all fuels was between 25 and 100 nm, B100 also generated a substantial amount of particles smaller than 10 nm. The total mass of particles emitted, calculated per kg of fuel, differed among diesel, biodiesel and NEXBTL100 (Figure 1B). While standard diesel fuel generated more than 11 mg particles/kg, for B100 the production was almost halved (6 mg/kg). NEXBTL100 and B30 fuels produced similar amount of particles (8.2 and 8.7 mg/kg, respectively). Next, we determined the content of PAHs and their derivatives in dichloromethane extracts of DEPs from individual fuels. In general, the content of PAHs was the lowest in the NEXBTL100 extract and highest in the extracts from DEPs from fuels containing biodiesel (B30 or B100) (Table 1). The sum of PAH concentrations classified by IARC as carcinogenic, or probably/possibly carcinogenic to humans (c-PAHs; Group 1, 2A or 2B) including benzo[a]pyrene, benz[a]anthracene, chrysene, benzo[b]fluoranthene, benzo[k]fluoranthene, dibenz[a,h]anthracene, and indeno[1,2,3-cd]pyrene, expressed in ng of cPAH per mg of particulate matter, ranged from 7.5 ng/mg for NEXBTL100 to 51.7 ng/mg for B100. Interestingly, although concentrations of most of the c-PAHs were lowest in the NEXBTL100 extract, this was not confirmed for BaP, a known human carcinogen. On the other hand, high concentrations of low-molecular-weight PAHs fluoranthene and pyrene were found in the B30 and B100 extracts (Table 1).

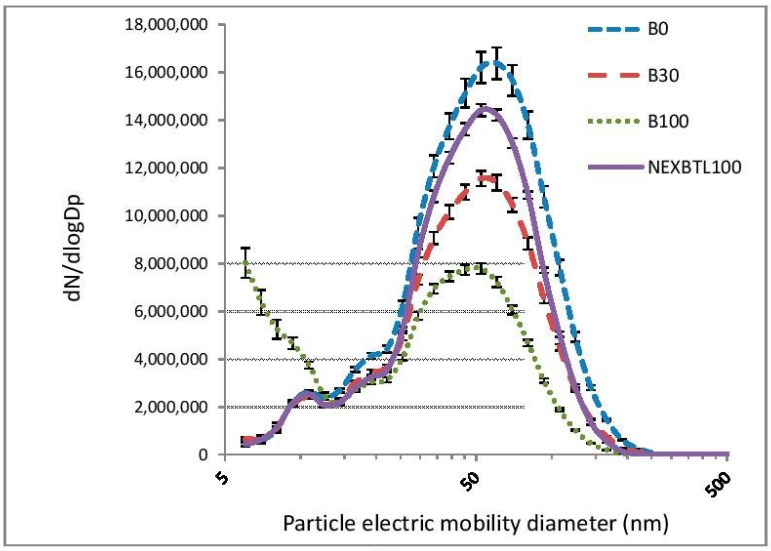

(A)

Figure 1. *Cont.*

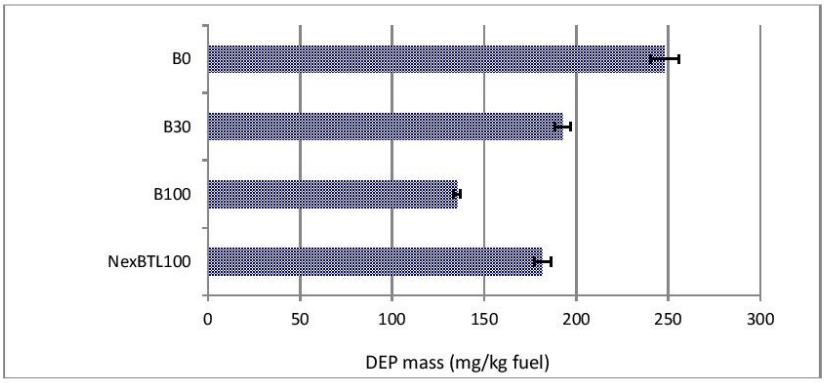

(**B**)

Figure 1. Characterization of collected particles: (**A**) number of particles per second as a function of their size (nm) for undiluted emissions from the tested fuels; and (**B**) the amount of particles (mg) per kg of individual fuels (average mass collected over 10 runs of WHTC cycle, see Materials and Methods). DEP, diesel exhaust particles.

Table 1. Results of chemical analysis.

PAHs				
Compound (ng/mg DEP)	**B0**	**B30**	**B100**	**NEXBTL100**
Fluoranthene	41.9	110	117	39.4
Pyrene	67.7	152	144	43.1
Benz[a]anthracene *	6.6	9.8	26.1	5.0
Chrysene *	5.1	6.0	12.5	1.0
Benzo[b]fluoranthene *	1.2	1.4	7.0	0.3
Benzo[k]fluoranthene *	n.d.	n.d.	2.6	n.d.
Benzo[a]pyrene *	0.6	0.9	1.7	1.2
Benzo[g,h,i]perylene	2.2	2.8	3.8	2.0
Dibenz[a,h]anthracene *	n.d.	n.d.	n.d.	n.d.
Indeno[1,2,3-cd]pyrene *	0.7	0.8	1.8	n.d.
4H-Cyclopenta[d,e,f]phenathrene	2.8	3.8	4.3	9.4
Benzo[c]phenanthrene	1.9	3.8	4.0	1.3
Benzo[j]fluoranthene	2.4	2.8	6.4	2.0
Benzo[e]pyrene	0.7	0.6	3.6	0.3
Triphenylene	9.0	3.6	4.0	1.1
Benzo[c]chrysene	n.d.	n.d.	0.2	n.d.
Coronene	0.8	0.7	0.7	0.6
Methylated PAHs				
Compound (ng/mg DEP)	**B0**	**B30**	**B100**	**NEXBTL100**
1-Methylpyrene	5.1	7.2	3.9	1.4
2-Methylpyrene	8.5	11.0	8.0	2.9
4-Methylpyrene	10.0	13.4	12	3.7
1-Methylchrysene	0.3	0.3	1.2	n.d.
7-Methylbenz[a]anthracene	0.3	n.d.	n.d.	0.2

Table 1. *Cont.*

Oxygenated PAHs				
Compound (ng/mg DEP)	**B0**	**B30**	**B100**	**NEXBTL100**
1,8-Naphthalic Anhydride	25.4	29.5	29.7	19.8
Phenanthrene-9,10-dione	1.3	0.8	0.8	0.5
9H-Fluoren-9-one	4.3	2.8	1.7	4.7
Anthrone	n.d.	n.d.	n.d.	n.d.
Anthracene-9,10-dione	2.7	4.5	4.0	2.6
7H-Benz[d,e]anthracene-7-one	1.4	1.5	2.4	0.28
9-Hydroxybenzo[a]pyrene	0.06	0.07	0.09	0.07
Benz[a]anthracene-7,12-dione	0.02	0.04	0.15	0.01
3-Hydroxybenzo[a]pyrene	0.05	0.05	0.10	0.02
Nitrated PAHs				
Compound (pg/mg DEP)	**B0**	**B30**	**B100**	**NEXBTL100**
1-Nitropyrene	314	539	1504	126
2-Nitropyrene	25.0	12.0	23.0	n.d.
4-Nitropyrene	18.0	16.0	44.0	10.0
3-Nitrofluoranthene	7.0	16.0	41.0	2.0
Dinitrated PAHs				
Compound (pg/mg DEP)	**B0**	**B30**	**B100**	**NEXBTL100**
1,3-Dinitropyrene	1.6	2.4	17.7	0.4
1,6-Dinitropyrene	1.2	5.6	65.0	n.d.
1,8-Dinitropyrene	0.9	4.6	48.0	n.d.

* Human carcinogens (IARC). PAHs, polycyclic aromatic hydrocarbons; DEP, diesel exhaust particles; n.d., not detectable.

2.2. Cytotoxicity Assessment

Cytotoxicity was evaluated upon 24 h exposure using the WST-1 Proliferation Assay. The range of concentrations from 22 μg/mL to 1000 μg/mL of each DEP extract was applied to obtain a dose–response proliferation capacity of the cells. The results for individual extracts were expressed as a percentage of increase/decrease of the potency to convert tetrazolium dye by mitochondrial dehydrogenase enzymes compared to the untreated control (Figure 2). We detected a substantial increase of absorbance up to the dose 68.7 μg/mL (154.5%–182.7%) while higher doses gradually decreased the absorbance upon all DEP extract treatments. Dose 134.2 μg/mL already caused inhibition of metabolic activity indicating decreased cell viability below the control level (95%–62.8%). NEXBTL100 extract exhibited the highest but not significant rate of dye conversion up to the dose 134.2 μg/mL compared to other treatments, however, the rapid decrease at higher doses was consequently observed. For all DEP extracts, a non-toxic concentration of 50 μg/mL was selected for further testing.

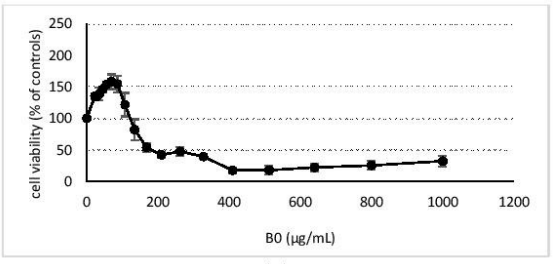

(A)

Figure 2. *Cont.*

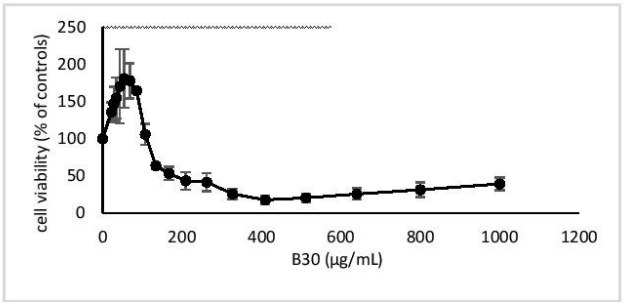

(**B**)

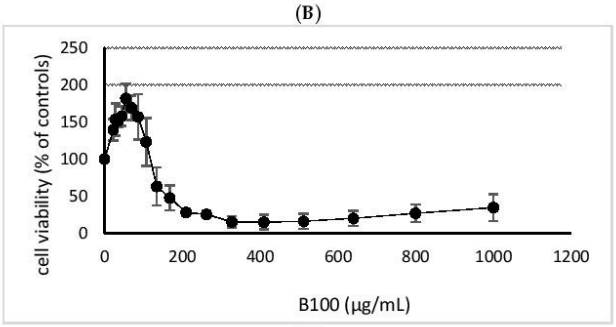

(**C**)

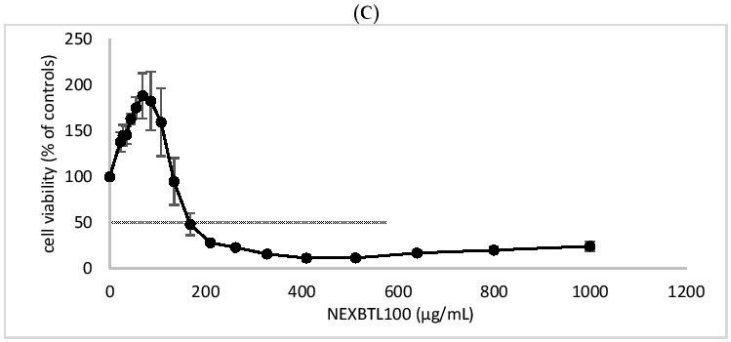

(**D**)

Figure 2. Cell viability evaluated by WST-1 Proliferation Assay. Cells were exposed to 18 different concentrations of: (**A**) B0; (**B**) B30; (**C**) B100; and (**D**) NEXBTL100 extracts for 24 h and the results were expressed as a percentage of increased/decreased activity of mitochondrial dehydrogenases to metabolize tetrazolium dye compared to the untreated control.

2.3. Quantification of Intracellularly Generated Reactive Oxygen Species and Reduced Glutathione Level

We measured the oxidative potency of DEP extracts, intracellular ROS production and levels of reduced glutathione in BEAS-2B cells. After 4 h incubation with 50 µg/mL dose of each DEP extract, we did not observe any significant increase of fluorescence indicating ROS production. Instead, NEXBTL100 and B30 rather slightly decreased (31% and 23%, respectively) ROS levels compared to untreated controls. B100 exhibited a subtle increase (11%) and B0 had no effect (Figure 3). Similar

to ROS production, we did not find significant changes in reduced glutathione (GSH) levels among DEP-treated cells (Figure 4).

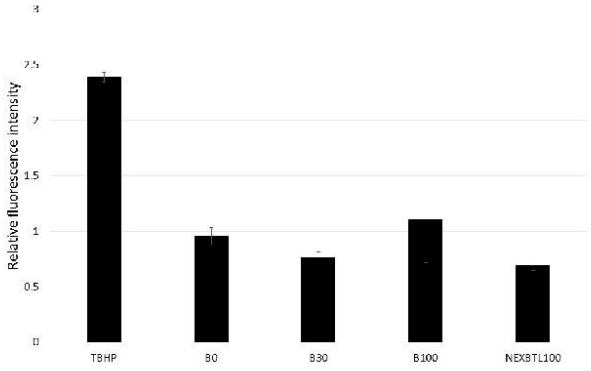

Figure 3. Relative intracellular ROS production upon 4 h exposure to DEP extract. Results are expressed as ratios of fluorescence intensity of treated and untreated cells. Cells were incubated with 50 μg/mL of different DEP extracts and 250 μM *tert*-butyl hydroperoxide (TBHP) as a positive control. No significant changes between the samples treated with individual DEP extracts and the control sample were found.

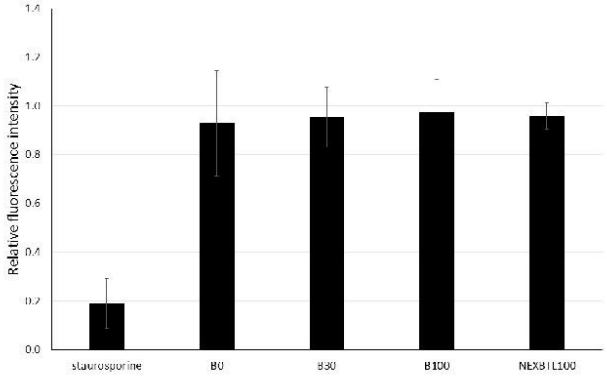

Figure 4. Relative GSH levels upon 4 h exposure to DEP extracts. Results are expressed as ratios of fluorescence intensity of treated and untreated cells. Cells were incubated with 50 μg/mL of different DEP extracts and staurosporine (1 μg/mL) as a positive control. No significant changes between the samples treated with individual DEP extracts and the control sample were found.

2.4. Gene Expression Profiling in BEAS-2B Exposed to Diverse DEP Extracts

2.4.1. Identification of Differentially Expressed Genes

We performed differential gene expression analysis to explore the impact of DEP extract exposure on mRNA expression levels. Results showed that all DEP extracts induced significant changes in expression of various genes following both 4 and 24 h exposure. The number of upregulated and downregulated genes varied among all samples. After 4 h exposure, B100 extract elicited the most pronounced response and modulated the highest number of genes, while NEXBTL100 exhibited the lowest potency to induce gene expression changes. Interestingly, the number of deregulated genes

increased with the increasing ratio of biocomponent in the fuel. After 24 h exposure, B30 extract yielded an increase of considerably higher number of deregulated genes compared to other treatments. Similar to 4 h treatment, 24 h exposure to NEXBTL100 resulted in the weakest response in terms of gene numbers. Venn diagrams were generated to visualize the common genes identically modulated by all DEP extracts as well as unique transcripts affected by individual treatments. The analysis revealed 27 common genes deregulated following 4 h exposure (Figure 5A). Several genes were common for other combinations of DEP extract treatments while each individual DEP extract induced a relatively higher number of specifically deregulated genes (22 for B0, 36 for B30, 58 for B100 extract treatment and 27 genes for NEXBTL100). Twenty-four hour exposure resulted in deregulation of 19 genes common for all treatments (Figure 5B). A substantially higher number of genes was modulated in response to individual DEP extracts, particularly B30 induced changes in expression of 232 genes compared to other extracts: NEXBTL100 extract induced deregulation of 15 genes; B0, 74 genes; and B100, 10 genes. A list of differentially deregulated genes is included in Table S1.

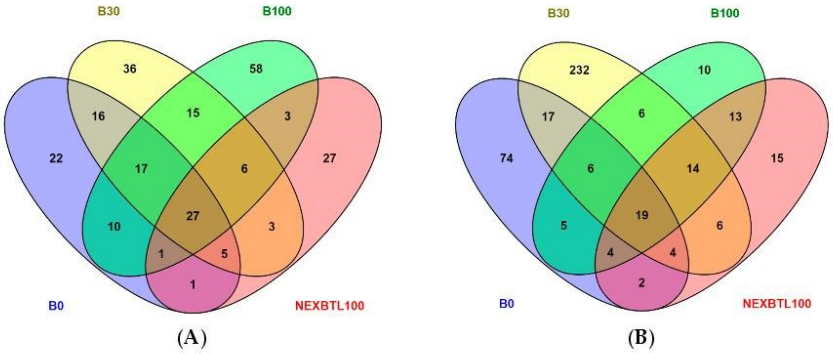

Figure 5. Venn diagrams illustrating the overlap of genes commonly modulated in response to all DEP extract treatments as well as numbers of specifically modulated genes by each individual DEP extract upon: (**A**) 4 h; and (**B**) 24 h incubation.

2.4.2. Functional Analysis

Commonly Modulated Pathways

We performed functional analysis of significantly deregulated genes using the ToppFun tool to discover common processes and pathways identically modified by all DEP extract treatments. Table 2 shows the rank of pathways enriched in the list of 27 common genes deregulated after 4 h exposure. The top represented pathway was "Benzo[a]pyrene metabolism" with aldo-keto reductases (*AKRs*) *AKR1C3* and *AKR1C2* as the most important contributing genes. It was the only pathway with significance below 0.05 after Bonferroni correction. However, numerous other pathways were found with high significance after False Discovery Rate Benjamini–Hochberg (FDR B&H) correction. *AKR1C3* and *AKR1C2* were further involved in "Synthesis of bile acids and bile salts via 27-hydroxycholesterol", "Synthesis of bile acids and bile salts via 24-hydroxycholesterol", "Synthesis of bile acids and bile salts via 7α-hydroxycholesterol", "Synthesis of bile acids and bile salts", "Bile acid and bile salt metabolism" and together with thioredoxin reductase (*TXNRD1*), glioma pathogenesis-related protein 1 (*GLIPR1*), connective tissue growth factor (*CTGF*), low density lipoprotein receptor (*LDLR*) in "Metabolism of lipids and lipoproteins". A combination of genes *TXNRD1*, *GLIPR1* and *CTGF* also played a role in "Regulation of Lipid Metabolism by Peroxisome proliferator-activated receptor alpha (PPARalpha)" and "PPARA Activates Gene Expression" pathways. *AKR1C3* together with *LDLR* were also involved in "Retinoid metabolism and transport" and "Ovarian steroidogenesis".

"Keap1-Nrf2 pathway" was enriched by heme oxygenase 1 (*HMOX1*) and glutamate-cysteine ligase regulatory subunit (*GCLM*) genes; *HMOX1* also contributed together with *TXNRD1* to "Oxidative stress" pathway enrichment and dominated as the only gene in the "Heme catabolic" pathway. *HMOX1* only contributed to the "Validated transcriptional targets of AP1 family members Fra1 and Fra2".

Urokinase-type plasminogen activator (*PLAU*) and serpin peptidase inhibitor, clade B (ovalbumin), member 2 (*SERPINB2*) were genes contributing to over-representation of multiple pathways ("Dissolution of Fibrin Clot", "Fibrinolysis Pathway", "Plasminogen activating cascade", "Blood clotting cascade", "Blood coagulation" and together with *IL24* in "Senescence and autophagy"). *PLAU* itself further contributed to numerous pathways in cooperation with a variety of other genes such as *LDLR* and *BIK*, BCL2-interacting killer ("DNA damage response (only ATM dependent)"), *CTGF* ("amb2 Integrin signaling"), E2F transcription factor 2 (*E2F2*), fibroblast growth factor receptor 3 (*FGFR3*) and *HMOX1* ("MicroRNAs in cancer").

FGFR3 was the only gene contributing to "t(4;14) translocations of FGFR3" and together with *E2F2* was involved in "Bladder cancer". Heat shock 27 kDa protein 1 (*HSPB1*) and stratifin (*SFN*) were involved in "p38 signaling mediated by MAPKAP kinases" pathway enrichment.

Different responses were observed after 24 h incubation: fewer genes were shared by all treatments and generally only several genes contributed to the deregulation of specific pathways (Table 3). Among top ranked pathways belonged "Benzo[a]pyrene metabolism" with the contribution of *AKR1C2* and *AKR1C4*. These two genes also played a role in over-representation of other pathways such as "Synthesis of bile acids and bile salts via 27-hydroxycholesterol", "Synthesis of bile acids and bile salts via 24 hydroxycholesterol", "Synthesis of bile acids and bile salts via 7alpha-hydroxycholesterol", "Synthesis of bile acids and bile salts", "Bile acid and bile salt metabolism", "Steroid hormone biosynthesis", "Metabolism of xenobiotics by cytochrome P450" and together with *TXNRD1* and 3-hydroxy-3-methylglutaryl-CoA synthase 1 (soluble) (*HMGCS1*) to "Metabolism of lipids and lipoproteins". *TXNRD1* was also important for "thioredoxin pathway" and together with further contribution of kynureninase (*KYNU*) and interleukin 1 beta (*IL1B*) for "Selenium pathway". *COL7A1* and *COL8A1* were genes involved in deregulation of "Genes encoding collagen proteins", "Assembly of collagen fibrils and other multimeric structures", "Collagen biosynthesis and modifying enzymes", "Collagen formation". "Protein digestion and absorption" was modulated due to the *COL7A1* and solute carrier family 3 (amino acid transporter heavy chain), member 2 (*SLC3A2*) action and "ketone bodies metabolic" due to *HMGCS1*.

Table 2. Top ranked over-represented pathways shared by all DEP extract treatments following 4 h incubation. Functional enrichment was performed using ToppFun tool integrating numerous annotation databases. Significant upregulation resp. downregulation of genes: ↑↓.

Name	Genes from Input
"Benzo[a]pyrene metabolism", "Synthesis of bile acids and bile salts via 27-hydroxycholesterol", "Synthesis of bile acids and bile salts via 24-hydroxycholesterol", "Synthesis of bile acids and bile salts via 7α-hydroxycholesterol", "Synthesis of bile acids and bile salts", "Bile acid and bile salt metabolism"	↑ *AKR1C3, AKR1C2*
"Metabolism of lipids and lipoproteins"	↑ *TXNRD1, GLIPR1, AKR1C3, AKR1C2*; ↓ *LDLR, CTGF*
"PPARA Activates Gene Expression", "Regulation of Lipid Metabolism by Peroxisome proliferator-activated receptor alpha (PPARalpha) "	↑ *TXNRD1, GLIPR1*; ↓ *CTGF*
"Retinoid metabolism and transport, Ovarian steroidogenesis"	↑ *AKR1C3*; ↓ *LDLR*
"Oxidative Stress"	↑ *TXNRD1, HMOX1*
"Keap1-Nrf2 Pathway"	↑ *HMOX1, GCLM*
"Validated transcriptional targets of AP1 family members Fra1 and Fra2"	↑ *PLAU, HMOX1*
"heme catabolic"	↑ *HMOX1*
"Dissolution of Fibrin Clot", Fibrinolysis Pathway", "Plasminogen activating cascade", "Blood Clotting Cascade", "Blood coagulation"	↑ *PLAU, SERPINB2*
"Senescence and Autophagy"	↑ *IL24, PLAU, SERPINB2*
"amb2 Integrin signaling"	↑ *PLAU*; ↓ *CTGF*
"DNA damage response (only ATM dependent) "	↑ *PLAU, BIK*; ↓ *LDLR*
"intrinsic apoptotic"	↑ *BIK*; ↓ *BNIP3*
"t(4;14) translocations of FGFR3"	↑ *FGFR3*
"Bladder cancer"	↑ *FGFR3*; ↓ *E2F2*
"MicroRNAs in cancer"	↑ *PLAU, FGFR3, HMOX1*; ↓ *E2F2*
"p38 signaling mediated by MAPKAP kinases"	↑ *HSPB1, SFN*

Table 3. Top ranked over-represented pathways shared by all DEP extract treatments following 24 h incubation. Significant upregulation resp. downregulation of genes: ↑↓.

Name	Genes from Input
"Benzo[a]pyrene metabolism", "Synthesis of bile acids and bile salts via 27-hydroxycholesterol", "Synthesis of bile acids and bile salts via 24-hydroxycholesterol", "Synthesis of bile acids and bile salts via 7α-hydroxycholesterol", "Synthesis of bile acids and bile salts", "Bile acid and bile salt metabolism", "Steroid hormone biosynthesis", "Metabolism of xenobiotics by cytochrome P450"	↑ *AKR1C4, AKR1C2*
"Metabolism of lipids and lipoproteins"	↑ *TXNRD1, AKR1C4, AKR1C2*; ↓ *HMGCS1*
"ketone bodies metabolic"	↓ *HMGCS1*
"Selenium Pathway"	↑ *TXNRD1, IL1B, KYNU*
"thioredoxin pathway"	↑ *TXNRD1*
"Genes encoding collagen proteins", "Assembly of collagen fibrils and other multimeric structures", "Collagen biosynthesis and modifying enzymes", "Collagen formation"	↑ *COL7A1*; ↓ *COL8A1*
"Protein digestion and absorption"	↑ *COL7A1, SLC3A2*

Analysis of Variance

One-way ANOVA was employed to discover differently modulated gene expression levels across all groups of treatment (NEXBTL100, B0, B30 and B100). After 4 h exposure, a significant alteration in expression levels of 99 genes was found. The vast majority of detected genes was distinctively modulated in response to NEXBTL100 compared to other treatments (Figure S1A). The functional annotation of the NEXBTL100-specific gene set revealed genes associated with the regulation of cell cycle. Genes involved in cell cycle (*MCM8*, *RBL1*, *RPS27*, *CDC25C*, *ENSA*, *ZWINT*) exhibited elevated expression levels, while other regulators were rather suppressed (*RAE1*, *CDKN2A*, *CCNB2*). The NEXBTL100 gene set further indicated the enhanced folding of actin by CCT/TriC (*CCT6A*, *TCP1*), purine metabolism (*ADSS*, *GART*) and repressed expression levels of genes participated in oxidative stress (*HMOX1*, *TXNRD1*, *GPX1*) or respiratory electron transport and mitochondrial function (*CYC1*, *UQCRFS1*, *NDUFV2*, *NDUFS3*).

ANOVA also revealed significant differences in expression levels of 152 genes across all groups of treatment upon 24 h incubation. We identified a distinctive pattern of modulated genes involved in the regulation of cell cycle (*KIF20A*, *AURKA*, *ACTR1A*, *UBA52*, *LMNA*, *CENPA*, *PSMC1*, *GINS2* or *MCM4*). Expression levels of these genes were almost exclusively elevated by NEXBTL100, while the lowest levels were detected upon B0 and B30 treatment. Expression levels of *RANBP1* and *TPX2*, genes involved in Ran-mediated regulation of mitotic spindle assembly were lowest upon B0 treatment compared to B30 displaying the highest potency to induce these genes (Figure S1B).

2.4.3. Quantitative RT-PCR Validation of Selected Genes

For verification of gene expression changes in microarray analysis, qRT-PCR of eleven selected genes was performed (Figure 6). We focused on genes involved in processes and pathways related to the metabolism of xenobiotics (*AKR1C2*, *CYP1A1* and *CYP1B1*), activation of antioxidant defense (*HMOX1* and *TXNRD1*), AP-1 transcription, induction of plasminogen activator urokinase and modulation of cell adhesion (*FOSL1*), modulation of cell cycle (*CCNB2*), apoptosis (*CDKN2A* and *BNIP3*), regulation of spindle function (*TPX2*), endoplasmic reticulum stress and unfolded protein response (*HSPE1*).

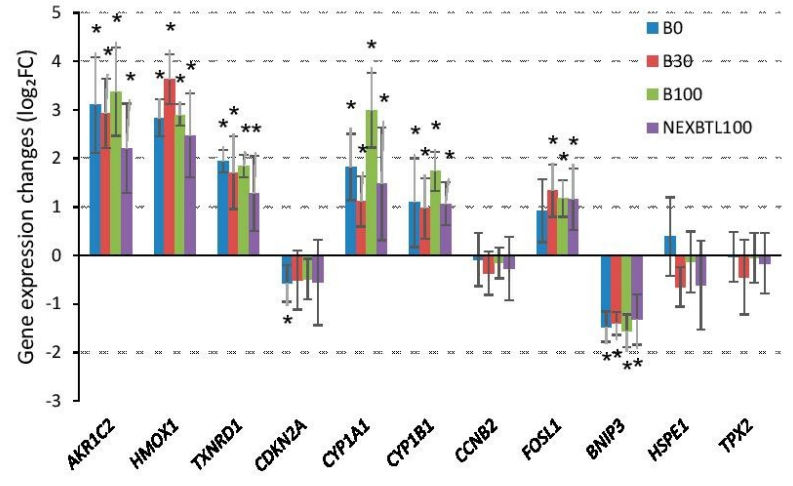

(A)

Figure 6. *Cont.*

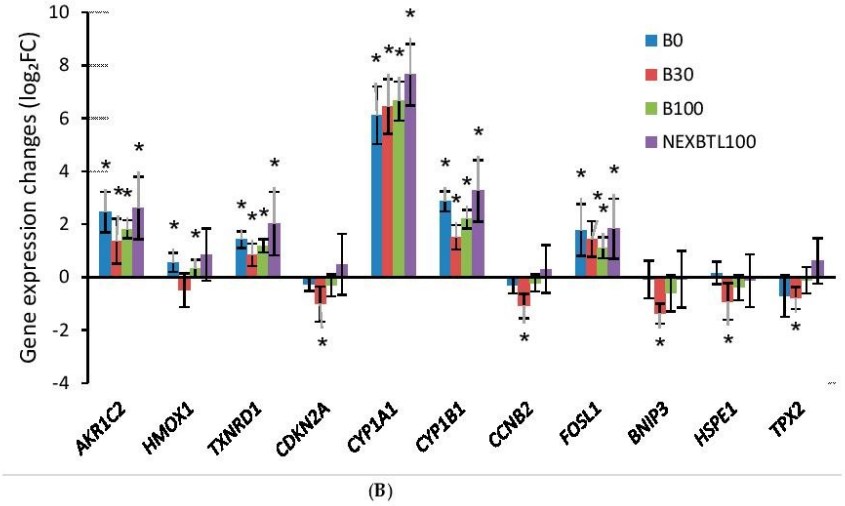

Figure 6. Quantitative RT-PCR verification of gene expression data obtained by microarray analysis. Eleven significantly deregulated genes were selected across all results and their gene expression levels were determined using qRT-PCR. Gene expression changes ($\log_2$ FC) were obtained by normalization to control samples ($2^{-\Delta\Delta Ct}$ method). Expression changes of selected genes upon: (**A**) 4 h exposure; and (**B**) 24 h exposure. * Indicates a statistically significant difference (p-value < 0.05).

3. Discussion

In the present study, we aimed to reveal a molecular signature of the toxicity induced by different organic compound mixtures extracted from diesel exhaust particles produced by diesel/renewable fuels in human lung BEAS-2B cells. A comparative analysis of gene expression changes was used to characterize the common mode of action underlying DEP extract exposure as well as specific effects of individual DEP extract treatments.

Recent studies on the toxicity of different diesel and biodiesel exhaust particles suggest inconsistent data due to different running conditions of engines and experimental approaches [23,24]. Here, we used a standardized procedure providing the same conditions for particle collection, extraction and cell treatment thus enabling the accurate comparison of DEP extracts on gene expression changes. Although in vitro exposure to whole particles is more relevant in terms of simulation of real world conditions, many difficulties arising from intact particle collection, the characterization of particles and their behavior in culture medium may consequently complicate the interpretation of results. It has been documented that organic compounds bound to DEP are responsible to a large extent for its genotoxicity and other effects [12,25]. To the best of our knowledge, a study investigating effects of organic extracts from various fuels engine emissions on global gene expression changes in a model cell line system has not been published yet, so comparable data are not available. However, several authors reported the results of genotoxicity/mutagenicity of similar organic extracts. Bulky DNA adduct formation in a cellular calf thymus DNA system was consistently increased after treatment of the samples with extracts containing higher levels of PAHs [12,25]. In another study that investigated mutagenic properties of organic extracts of diesel and biodiesel fuels, higher PAHs content was associated with increased mutagenicity and bactericidal effects in *Salmonella typhimurium* TA98 and YG1041 strains [19]. These reports are in line with our observation that application of NEXBTL100 extract that contains lower levels of PAHs results in weaker biological response. This suggests that not

only genotoxicity/mutagenicity, but also global gene expression changes are strongly affected by the presence of PAHs in the samples.

3.1. Common Cellular Response—4 h Cell Exposure

Despite the variability in chemical composition of individual DEP extracts, we revealed numerous genes and pathways altered in the same manner. Commonly deregulated genes following 4 h exposure were mostly involved in oxidative stress response and consequent events, such as activation of Nrf-2 and AP-1 transcription, antioxidant defense and DNA damage response.

The most significantly deregulated genes were *AKR1C2* and *AKR1C3*. A wide substrate specificity of these enzymes determines their implication in the metabolism of various exogenous and endogenous compounds such as steroids, sugars, carbonyls and others. They have a dual role in toxicity: under the control of Nrf-2 transcription factor they exhibit a detoxifying function by conversion of toxic aldehydic products [26] or catalyze the NADPH-dependent reduction of the *o*-quinone products to catechols and thus exacerbating ROS formation [27]. Induction of *AKR1C1*, *1C2* and *1C3* was also observed in BEAS-2B cells exposed to urban particulate matter in the study of Longhin et al., 2016 [28].

Polycyclic aromatic hydrocarbons and other organic compounds are capable of producing a substantial amount of ROS, which consequently lead to stabilization and activation of transcription factor Nrf-2 and induction of antioxidants and detoxifying enzymes [27]. Nrf-2 participates in the regulation of oxidant-stimulated functions, such as autophagy, inflammasome assembly, ER stress/UPR, mitochondrial biogenesis or stem cell regulation as well as protects against toxicity and chronic diseases in normal cells or through pharmacological interventions [29].

In our study, we observed elevated expression levels of *HMOX1*, *GCLM* and *TXNRD1* suggesting anti-oxidant response against ROS production. Surprisingly, we were not able to detect an increase in ROS production by carboxy-H_2DCFDA assay. The same effect was reported in the study of Li et al., 2002 [30] where DEP extract treatment failed to induce DCF fluorescence in BEAS-2B, while the same treatment and detection method was effective in different cells. However, the authors confirmed the pro-oxidative potential by using a different method reflecting mostly production of superoxide radical. They also demonstrated a decrease of the GSH/GSSG ratio in BEAS-2B cells but not in THP-1 macrophages, as well as increased expression of *HMOX1*, pro-inflammatory cytokine *IL-8*, activation of JNK and decreased cell viability. In contrast, we observed no effect on reduced glutathione levels, suggesting effective replenishment of depleted GSH stores possibly due to the enhanced expression of *GLCM*. Moreover, other recent studies have demonstrated the pro-oxidative and pro-inflammatory effect in BEAS-2B and other cell lines upon exposure to DEP chemicals [31]. Importantly, the authors underscore the close relation of increasing oxidative potential of DEP extracts and the higher content of PAHs.

An excessive amount of ROS can further activate intracellular signaling cascades, including the mitogen-activated protein kinase. We detected significant upregulation of *HSPB1*, a protein chaperon involved in stress resistance and regulation of apoptosis. *HSPB1* maintains glutathione in its reduced form and decreases the amount of reactive oxygen species (ROS) produced in cells exposed to oxidative stress or tumor necrosis factor TNFα [32]. This could further support the hypothesis of a vigorous antioxidant response, which effectively neutralizes ROS and restores GSH levels.

ROS generation by DEP extracts arising from enzymatic metabolism of organic compounds as well as formation of reactive intermediates possibly cause DNA damage with consequent cell cycle arrest, senescence and cell death. Our data strongly suggest activation of p53 signaling due to the modulation of genes involved in "DNA damage response (ATM induced) pathway" (*BIK*, *LDLR*, *PLAU*). We also observed the induction of *SFN*, a direct p53 effector, suggesting cell cycle arrest in response to DNA double strand breaks. Suppression of *CCNB2* by all extract treatments, as confirmed by qRT-PCR, may indicate inhibition of cell cycle. It has been shown that the activity of *CCNB2*, a key factor essential for transition from G2 to mitosis, is under the control of p53 which represses transcription of *CCNB2* and causes arrest in G2 phase upon DNA damage [33]. Elevated

expression of *GLIPR1*, another p53 target, could further contribute to increased ROS production, promote cell cycle arrest and apoptosis, as observed in prostatic cancer cells [34]. On the other hand, pro-apoptotic *BNIP3* was significantly downregulated by all treatments. This suppression of *BNIP3* might be mediated by p53 acting in favor of the protection against hypoxia-induced cell death as documented in Feng et al. [35]. Suppression of *CDKN2A*, a stabilizer of p53 protein, *BIK* and *BNIP3* may suggest the suppression of p53 activity and anti-apoptotic response of the cells. *FOSL1* induction might be related to AP-1 transcription, induction of plasminogen activator urokinase (*PLAU*) and modulation of cell adhesion [36]. Other genes contributing to DNA damage response indicated cellular senescence and/or autophagy (*PLAU*, *SERPINB2*).

The role of plasminogen activator (*PLAU*) and its inhibitor (*SERPINB2*) in senescence is not fully understood; however, the study of West et al. [37], described alterations in plasminogen activator activity during replicative senescence leading to the disruption of extracellular matrix maintenance with possible deleterious consequences on tissue homeostasis. According to our results, in the study of Longhin et al. [28], the authors also found a strong induction of *SERPINB2* and *PLAU* in BEAS-2B cells exposed to whole airborne particles. Exposure to air pollution may cause acute exacerbation of idiopathic pulmonary fibrosis [38]. Interestingly, enhanced expression of *PLAU* and *SERPINB2* and simultaneous suppression of *CTGF*, a growth factor promoting the fibrosis, observed in our study, may suggest the anti-fibrotic response. Plasminogen activator and plasminogen activator-inhibitor are components of the plasminogen activation system, which has been implicated in fibrosis reduction [39]. Similarly, a defensive role of Nrf2 target, *TXNRD1*, against fibrosis has also been described [40]. Moreover, activation of peroxisome proliferator-activated receptor α (PPARα) participating in the processes of both physiological and toxicological response to various endogenous or exogenous substances may also protect against lung fibrosis [41]. The multiple regulatory role of PPARα in various processes related to oxidative stress, lipid metabolism and inflammation has been documented [42].

3.2. Differential Response Detected by Analysis of Variance—4 h Cell Exposure

A vast majority of genes detected by ANOVA among all treatments were distinctively modulated in response to NEXBTL100 treatment and exhibited more than 1.5-fold change in expression levels compared to a group median involving other gene sets (B0, B30 and B100). Most of the NEXBTL100-specific genes were involved in DNA replication, cyclin B2 related events and entry into mitosis. Elevated expressions of *MCM8*, *RBL1*, *RPS27*, *CDC25C*, *ENSA* and *ZWINT* may suggest deregulation towards enhanced proliferation compared to other DEP extract treatment. Accordingly, repression of *RAE1*, a mitotic checkpoint regulator, as well as *CDKN2A*, a tumor suppressor that inhibits G1/S transition and establishes cell cycle arrest, could further support the hypothesis of enhanced proliferative potential of NEXBTL100 extract.

Analysis of top-ranked over-represented pathways specific for each DEP extract treatment showed that "Keap-Nrf2 pathway" and "Glutathione biosynthesis pathway" were the most significantly affected by NEXBTL100 4 h exposure. However, NEXBTL100 induced the lowest levels of *HMOX1*, *TXNRD1* and *GPX1* suggesting modest anti-oxidative response, possibly caused by the lowest production of ROS. It should be stressed that changes were not significant compared to unexposed controls. However, subtle changes in gene expression levels detected by ANOVA may also contribute to distinctive gene expression patterns of individual DEP extracts treatments. These results indicate that NEXBTL100 induced the weakest oxidative stress response and DNA damage and exhibited elevated expression of genes possibly contributing to increased proliferation compared to other treatments.

On the other hand, the list of the most over-represented pathways modulated by B0, B30 and B100 was similar to each other and involved "Benzo[a]pyrene metabolism" and similar pathways (with *AKR1C2* and *CYP1B1* being the most contributing deregulated genes) and "Plasminogen activating cascade" (with a significant contribution of *SERPINB2*, *PLAU*, *PLAT*). Additionally, B100 extract, which contained the highest concentrations of carcinogenic PAHs, also affected most

significantly the "Cell cycle", "p38 signaling" and "Senescence and autophagy" pathways (data not presented here).

3.3. Common Cellular Response—24 h Cell Exposure

The major toxic response following 24 h exposure to all DEP extracts was the metabolic activation of PAHs. The key enzymes contributing to modulation of "Benzo[a]pyrene metabolism" and "Metabolism of xenobiotics by cytochrome P450" as well as numerous other pathways were *AKR1C2* and *AKR1C4*. AKRs participate in *o*-quinone pathway by conversion of PAH-diols into redox active PAH *o*-quinones, but also facilitate the redox cycling of the PAH *o*-quinones to catechols. Catechols are able to conjugate with a wide range of conjugating enzymes. Conjugation terminates the redox cycling, eliminates formation of electrophilic products and prevents formation of covalent adducts [43]. We also confirmed significantly elevated expression of other important PAH-metabolic enzymes *CYP1A1* and *CYP1B1* by qRT-PCR, although microarray data did not indicate a significant increase, possibly due to the high variability among replicates. CYP enzymes are involved in the formation of *trans*-dihydrodiols, the first step of PAH activation and also in the consequent event when dihydrodiols are converted into diol-epoxides, which can covalently bind to DNA and form persistent DNA adducts. The competing role of CYP and AKR enzymes in the metabolic activation of PAH-diols has been observed in human bronchoalveolar cell extracts [44].

The induction of CYP enzymes is dependent on the activation of AhR. Our recent data of AhR-mediated activity performed in human AZ-AhR cells (Stable HepG2 Luciferase Reporter Cell Line) by CALUX assay, suggest similar TEQ values for B0, B30 and B100 extracts and lower TEQ value for NEXBTL100 extract (see Figure S2), which accordingly reflected a lower PAH content. The similar trend could be also expected for BEAS-2B cell line. Our previous findings indicate that concentration of PAHs in a mixture of organic compounds extracted from reference urban dust particulate matter is higher [45] than in similar organic extracts from standard reference diesel exhaust particle material [25]. Therefore, also AhR-mediated activity of DEP extracts was lower. These results are in line with our present findings where only partial induction of CYP1A1 and CYP1B1 mRNA confirmed the low activation of the AhR-dependent gene expression. Interestingly, a recent study of Palkova et al., 2015 [25] analyzing the toxicity of organic fraction extracted from reference material of diesel exhaust particles (SRM 1650b) consistently evidenced its high AhR-inducing activity and potency to induce metabolic enzymes, trigger DNA damage response and disrupt cell cycle progression and proliferation in rat lung epithelial cells RLE-6TN and rat liver epithelial cells WB-F344 in the concentration range of 100–1000 and 50–1000 μg/mL, respectively, suggesting a higher potency to metabolize PAHs compared to other cell lines.

Interestingly, a higher metabolic rate of organic compounds probably caused the interference with WST-1 assay and gave false positive results of "enhanced" proliferation upon low dose exposures to DEP extracts. Since WST-1 assay is based on conversion of tetrazolium dye by mitochondrial dehydrogenases, the results obtained by WST-1 assay more likely imply enhanced metabolic activity of cells due to the effect of organic compounds and not increased number of cells.

3.4. Differential Response Detected by Analysis of Variance—24 h Cell Exposure

Similar to 4 h incubation, ANOVA also revealed distinct gene expression patterns following 24 h incubation across all treatments. Functional annotation of genes identified by ANOVA revealed that the most distinctive signature was induced by NEXBTL100 extract treatment. Specifically, we found a marked difference in expression levels of genes associated with regulation of chromosome segregation and cytokinesis. Among them, *AURKA* is critical for the proper formation of mitotic spindle [46], while *CENPA* controls kinetochore assembly and chromosome segregation [47] and *KIF20A*, a mitotic kinesin, is required for chromosome passenger complex (CPC)-mediated cytokinesis [48]. It has been demonstrated that p53 acts as a negative regulator of *AURKA* activity and reduces its expression level after DNA damage [49]. Deletion of *AURKA* may consequently cause cell cycle arrest. *AURKA* requires

a number of co-factors for its activation such as microtubule associated protein *TPX2* and GTPase Ran. Ran releases *TPX2* to bind and activate *AURKA* by changing its conformation, stimulating its autophosphorylation and targeting it to spindle microtubules at the pole [50]. Importantly, overexpression of *AURKA* and *TPX2* has been linked to tumor development at different levels [51]. We confirmed the elevated expression of *TPX2* upon NEXBTL100 extract treatment by RT-qPCR, while other treatments rather slightly suppressed gene expression level. *TPX2* is an essential regulator of spindle function and may indicate the possible negative effect of DEP extracts (excepting NEXBTL100) on mitosis and generally on cell cycle progression [52].

3.5. Study Limitations

Although our study represents a comprehensive analysis of toxic effects of organic extracts from various fuels engine emissions, there are several limitations that should be acknowledged.

The first limitation is related to the nature of the samples used for in vitro tests. The results reported here are based on exposing the cells to the extracts from comparable masses of particles. The results therefore represent the "quality" of the particles, expressed as some metric of effect per mg of particulate matter, a metric suitable for attempting to comprehend the mechanisms of the effects of particles on human health. For realistic evaluation of fuels, however, the effects of fuels should be compared based on distance driven, amount of useful work performed by the engine, fuel consumed, or similar metric. Since the total mass of particles emitted varied among the fuels (see Figure 1B), and the effects are believed to be nonlinear, the results do not necessarily represent the realistic effects of a fuel substitution on human health. In addition, due to the anticipated nonlinearity of effects with respect to dose, expressing the effects per kg of fuel would be of limited use. The real exposure is not to raw, undiluted exhaust, and the effective dilution ratio (reciprocal of the fraction of raw exhaust in inhaled air) considerably varies with conditions (mainly proximity of vehicles to population and atmospheric conditions). Evaluation of "realistic" fuel effects would therefore necessitate an arbitrary and difficult to justify assumption of a certain dilution ratio.

Another limitation is the fact, that we used organic extracts rather than exhaust particles to investigate biological effects of various fuel emissions. Although particles mediate some unique effects, particularly oxidative stress induction that cannot be directly mimicked by extracts, organic fraction contains PAHs, i.e., compounds with highest genotoxic activity and most immediate impact on human health. It should be also noted that the use of organic extracts increase the bioavailability of PAHs compared to whole particles experiments therefore the results may overestimate the effects of DEP-associated PAHs. Oxidative stress induction measured in our study yielded mostly negative results, although this may be caused by technical limitations of the test methods.

Finally, although gene expression profiling is a robust tool that covers simultaneously whole-genome gene expression changes, it still measures a single endpoint (mRNA levels). To get more insight into the mechanism of action of tested toxicant(s), gene expression profiling experiments should be integrated into larger studies examining multiple end-points at the molecular, cellular, tissue, and physiological levels in the context of the whole organism. Therefore, our study does not aim to reveal the precise mechanism of action (e.g., cell cycle regulation or other fundamental cellular processes) but rather provides new testable hypothesis that could be subsequently confirmed by further experiments.

4. Materials and Methods

4.1. Chemicals and Biochemicals

Bronchial Epithelial Basal Medium and BEGM™ BulleKit™ were purchased from Lonza (Basel, Switzerland); Human bronchial epithelial cells BEAS-2B from ATCC (Manassas, VA, USA); *tert*-butyl hydroperoxide, Glutathione Fluoriometric Assay Kit, $NaHCO_3$, HEPES, and non-essential amino acids were obtained from Sigma-Aldrich (St. Louis, MO, USA); WST-1 Proliferation Assay and High Fidelity cDNA synthesis Kit from Roche (Mannheim, Germany); 5-(and-6)-carboxy-2′,

7′-dichlorodihydrofluorescein diacetate and Hank's Balanced Salt Solution from Thermo Fisher Scientific (Waltham, MA, USA); NucleoSpin RNA II from Macherey-Nagel (Düren, Germany); Illumina Human-HT12 v4 Expression BeadChips were from Illumina (San Diego, CA, USA); Illumina TotalPrep RNA Amplification Kit from Ambion (Austin, TX, USA); RT-qPCR master mix, PerfectProbe assays and geNorm Reference Gene Selection Kit from Primerdesign (Southampton, UK); Dulbecco's Modified Eagle's Medium and Gentamicin Sulfate from Gibco (Paisley, UK) and Luciferase Assay kit from BioThema (Handen, Sweden).

4.2. Test Vehicle and Exhaust Particles Collection

Engine tests and particle collection were performed on a transient engine dynamometer test stand at the laboratories of the Czech Technical University in Prague in VTP Roztoky. An Iveco Tector 5.9 L, 176 kW engine commonly used in the EU (and similar in design to Cummins ISB engine used widely in the U.S.) was utilized as a representative of a common diesel engine of a small truck. The engine was operated without after treatment to represent the type of engines responsible for the majority of particulate matter in the air. Exhaust gases were transferred into a full-flow dilution tunnel where the gases were mixed with fresh air filtered through active carbon and high-efficiency particulate air (HEPA) filters. A constant volume sampler system kept the flow rate through the dilution tunnel to 50 m^3/min. DEP samples were taken from the dilution tunnel by two high volume Ecotech 3000 samplers with installed impactor (cut off particle diameter 2.5 μm). The sample flow rate was set to 67.8 m^3/h. The samplers were normally used for atmospheric sampling and were modified for use with diluted exhaust and subsequently augmented with an auxiliary three-stage blower to increase the filter capacity. Borosilicate filters (8″ × 10″, Emfab, TX40HI20-WW, Pall, Port Washington, NY, USA) were used to collect hundreds of milligrams of DEP for the extraction procedure and toxicity testing. The World Harmonized Transient Cycle (WHTC) used for type-approval of heavy-duty engines was chosen as a test cycle. This cycle was run once with a cold start and nine times with a hot start (it should be noted the engine was not fully warmed up after one WHTC). Four different fuels were used: pure diesel (B0, Cepro, a.s., Prague, Czech Republic), neat fuel-grade biodiesel (B100, methylesters of rapeseed oil, Cepro, a.s., Prague, Czech Republic), a blend of 70% B0 and 30% B100 (v/v) mixed from B0 and B100, and pure hydrotreated vegetable oils and waste animal fats (NEXBTL100, Neste Oil, Espoo, Finland). Before sampling, the engine ran 3 WHTC in order to adapt to a new fuel. The engine was then left overnight at 23 °C as a preconditioning for the cold start WHTC to prepare it for the sampling with a cold start the next day. DEPs collected within 10 WHTCs for every fuel was used for chemical and toxicological analysis.

4.3. Particle Characterization and Chemical Analysis

Particle size distributions were measured using a fast mobility particle sizer (EEPS, Engine Exhaust Particle Sizer, model 3090, TSI, St. Paul, MN, USA), coupled to a rotating disc microdiluter (model MD-11, Matter Engineering Inc., Wohlen, Switzerland) set to a dilution ratio of 150:1, with the dilution head heated to 150 °C. Fuel consumption was recorded using an AVL 735S Fuel Mass Flow Meter (AVL, Graz, Austria).

Organic compounds from diesel exhaust particles produced by different fuels (B0, B30, B100 and NEXBTL100 were extracted with 70 mL of dichloromethane in an automated extraction apparatus (Behr EF, BEHR, Stuttgart, Germany) for 4 h (3 h in boiled solvent and 1 h in condensed solvent). Requested aliquots of the extract were re-dissolved in required volume of acetonitrile for HPLC/DAD and LC/MS-MS; and in dimethylsulfoxide (DMSO) for biological in vitro assays. Identification of compounds was performed by comparison of their retention times with authentic standards. The method of external standardization was used for quantification of contaminants. The accuracy and precision of the analytical methods was determined by analyzing of the standard reference material SRM 1650b (Diesel Particulate Matter, NIST, Gaithersburg, MD, USA). Further details on chemical analysis are described elsewhere [45].

4.4. Cell Cultures and Exposure Conditions

Human bronchial epithelial cells BEAS-2B were cultured in Bronchial Epithelial Basal Medium (BEBM) supplemented with the standardized set of growth factors provided by the manufacturer (BEGM™ BulleKit™). All cultivation flasks and plates were coated with BEBM containing fibronectin, collagen and bovine serum albumin. All tested DEP extracts were diluted in complete BEBM and cells were incubated in triplicates for 4 h or 24 h, respectively. Control cells were incubated with DMSO extracts from blank filters. Cell cultures and cell-based assays were maintained in a humidified atmosphere with 5% CO_2 at 37 °C.

4.5. Cytotoxicity

To assess the viability of cells, the WST-1 Proliferation Assay was performed 24 h after exposure to DEP extracts following the manufacturer's protocol. BEAS-2B were cultivated in 96-well plates 24 h before treatment in a density of 7500 cells per well. For dose–response curve and threshold cytotoxicity assessment, cells were incubated in 18 concentrations (22–1000 μg/mL) of each DEP extract obtained by serial dilution in BEGM. Positive controls were incubated with 0.1% Triton X-100 and negative controls with complete medium.

4.6. Cell Culture Conditions, RNA Isolation and Quality Control

For gene expression profiling, cells suspended in complete BEBM were seeded in pre-coated Petri dishes (surface area 22.1 cm^2). Cell seeding density was 27,000 and 18,000 cells/cm^2 for 4 and 24 h exposure period, respectively. After 44 hours, media was removed, cells were washed with PBS and 3 mL of fresh dilutions of DEP extracts in complete BEBM (50 μg/mL) and controls (complete BEBM and 0.1% DMSO) were added to the cells. Triplicates were prepared for each DEP extract and control. Cells were incubated in humidified atmosphere with 5% CO_2 at 37 °C for 4 and 24 h.

Total RNA from lysed BEAS-2B cells was obtained using NucleoSpin RNA II according to the manufacturer's instructions. RNA concentration was quantified with a Nanodrop ND-1000 Spectrophotometer (Thermo Fisher Scientific, Waltham, MA, USA). The integrity of RNA was assessed using an Agilent 2100 Bioanalyzer (Agilent Technologies Inc., Santa Clara, CA, USA). All samples had an RNA Integrity Number (RIN) greater than 9. Isolated RNA was stored at −80 °C until processing.

4.7. Microarray Analysis

Illumina Human-HT12 v4 Expression BeadChips were used to generate gene expression profiles. Biotinylated complementary RNA (cRNA) was prepared from 200 ng of total RNA using the Illumina TotalPrep RNA Amplification Kit (Thermo Fisher Scientific, Waltham, MA, USA). Next, 1000 ng of biotinylated cRNA targets was hybridized to the beadchips. The steps of hybridization and the subsequent washing, staining and drying of the beadchips were performed according to standard instructions from Illumina. The hybridized beadchips were then scanned on the Illumina iScan and bead level data were summarized by Illumina GenomeStudio Software v2011.1 (Illumina Inc., San Diego, CA, USA).

4.8. Real-Time Quantitative PCR (RT-qPCR) Verification

One microgram of RNA from each sample was used for complementary DNA (cDNA) synthesis using the Transcriptor High Fidelity cDNA synthesis Kit (Roche, Basel, Switzerland). cDNA synthesis was performed twice for each sample to obtain a technical replicate. The original protocol was modified by using 2.5 μM oligo(dT) and 10 μM random hexamers for priming in a 20 μL reaction volume. cDNA synthesis was run according to the following conditions: 30 min at 55 °C and 5 min at 85 °C. Quantitative PCR measurements were performed using the 7900HT Fast Real-Time PCR System (Applied Biosystems, Carlsbad, CA, USA). Each RT-qPCR reaction was carried out in a final volume of 14 μL containing 3.5 μL of diluted cDNA, 2.8 μL of water and 7 μL of master mix. To determine the

level of each target gene, 0.7 µL of a specifically designed assay (Custom designed real-time PCR assay with Double-Dye probe, Primerdesign, Eastleigh, UK) was added to the reaction mixture. Cycling conditions were: 2 min at 95 °C followed by 40 cycles of amplification (10 s at 95 °C and 60 s at 60 °C). The baseline and threshold values of RT-qPCR experiments raw data were assessed with SDS Relative Quantification Software version 2.3 (Applied Biosystems, Waltham, MA, USA) to determine Ct values. Expression levels of target genes were normalized to the reference genes (*B2M* and *ACTB*). Reference genes were selected according to the stability of gene expression during experimental conditions using the geNorm Reference Gene Selection Kit. Relative changes in normalized gene levels were calculated using the $2^{-\Delta\Delta Ct}$ method [53]. The sequences of primers used in RT-qPCR are shown in Table S2.

4.9. Quantification of Intracellular ROS

The intracellular ROS levels upon DEP extracts treatments were detected by using 5-(and-6)-carboxy-2′,7′-dichlorodihydrofluorescein diacetate (carboxy-H_2DCFDA). Cells were plated into black 96-well plates one day before treatment in the density of 30,000 cells per well and each measurement was performed using a cell triplicate. Before treatments, cells were loaded with Hank's Balanced Salt Solution containing 40 µM carboxy-H_2DCFDA for 30 min. After dye loading, cells were washed two times with BEGM and incubated with 50 µg/mL of each DEP extract or 250 µM of *tert*-butyl hydroperoxide as a positive control for 4 h. Fluorescence was measured with a SpectraMax M5 plate reader (Molecular Devices, Sunnyvale, CA, USA) with an excitation and emission wavelength of 494 nm and 525 nm, respectively.

4.10. Quantification of Glutathione Levels

The total amount of reduced glutathione (GSH) in the cell cultures exposed to 50 µg/mL of DEP extracts for 4 h was quantified with a Glutathione Fluorimetric Assay Kit according to the manufacturer's recommendations for a 96-well plate format. Absorbance was measured by a SpectraMax M5 plate reader at 494 nm. Concentrations of reduced GSH were calculated using a standard calibration curve; positive controls were treated with staurosporine (1 µg/mL). Each measurement was performed using a cell triplicate.

4.11. Statistical Analysis

Gene expression levels were compared with control BEAS-2B cell cultures treated with extract from blank filter only. Bead summary data were imported into R statistical environment (https://www.r-project.org/) and normalized using the quantile method in the Lumi package [54]. Only probes with a detection p-value < 0.01 in more than 50% of arrays were included for further analyses. Differential gene expression was analyzed in the Limma package using the moderated t-statistic. A linear model was fitted for each gene given a series of arrays using lmFit function [55]. A multiple testing correction was performed using the Benjamini and Hochberg method. To analyze lists of significantly deregulated genes after DEP extract treatments (cut-off p-value < 0.05, fold change > 1.5, or < 0.6), a ToppFun tool was used [56]. Functional analysis identified numerous over-represented terms in several categories; pathways as a functional category were considered for the analysis.

The detection of differential gene expression was performed using the parametric one-way ANOVA test. We employed the R Stats package [57] implementation using the design described in [58]. The p-values were adjusted for multiple comparisons using the BH method [59]. The Tukey's "Honest Significant Difference" method [60] served as a "post-hoc" test. The data of ROS generation, reduced glutathione levels and expression of selected genes verified by RT-qPCR were expressed as mean values ± S.D. To detect significant changes between means of treated groups and the control group, the two-tail Student's t-tests were used.

5. Conclusions

In conclusion, equal concentrations of organic extracts of diesel and biodiesel exhaust particles induced similar molecular response in BEAS-2B cells, although specific gene expression patterns were also observed. Following 4 h exposure, we found altered processes related to oxidative stress response (mostly antioxidant defense activation only), suppression of pro-apoptotic stimuli, regulation of cell cycle and plasminogen activating cascade. NEXBTL100 extract distinctively exhibited a modest antioxidant response, suggesting weaker stress response probably due to the less harmful nature of the organic compounds compared to other extracts. The key common events after 24 h incubation were metabolism of lipids and xenobiotics, including PAHs, and oxidative stress-induced pathways; however, no increase in ROS production was detected. Importantly, no pro-inflammatory genes (with the exception of *IL24*) and pathways were affected, cancer-related pathways were modulated minimally and only a low AhR-mediated activity was found at sub-cytotoxic concentration of DEP extracts. Biological effects of induction of plasminogen activating cascade (*SERPINB2*, *PLAU* and other genes) in human bronchial cells should be further studied.

This study used the toxicogenomic approach to identify biological processes and pathways affected by organic components of diesel exhaust particles produced by four commonly used fuels. Although NEXBTL100 extract exhibited the weakest toxic response, our findings indicate subtle differences in overall toxic effects induced by different diesel or alternative fuels' DEPs, or their blends when the equal amount of particles and qualitative composition of organic compound mixtures was considered. Other factors, such as fuel consumption, total amount of produced particles or particle size distribution may influence substantially the resulting toxic effects.

Supplementary Materials: Supplementary materials can be found at www.mdpi.com/1422-0067/17/11/1833/s1.

Acknowledgments: The authors would like to thank Zdenek Dvorak (Palacky University, Olomouc, Czech Republic) for kindly supplying the AZ-AhR cell line. The work was supported by the Czech Science Foundation (Project No. 13-01438S and 14-22016S) and by the Czech Ministry of Youth, Education and Sports Projects No. LO1305, LO1311 (Czech Technical University in Prague) and LO1508. The authors also acknowledge the assistance provided by the Research Infrastructure NanoEnviCz, supported by the Ministry of Education, Youth and Sports of the Czech Republic under Project No. LM2015073.

Author Contributions: Helena Libalova contributed to data analyses, performed ROS detection experiments and wrote the substantial part of the manuscript; Pavel Rossner, Jr. participated on the interpretation of the results and preparation of the manuscript; Tana Brzicova and Kristyna Vrbova cultivated cells, performed gene expression analysis using microarrays and verified microarray results using qPCR; Jiri Klema performed statistical analysis of gene expression data; Michal Vojtisek-Lom, Vit Beranek and Jitka Sikorova have designed the engine tests and test setup including the high volume sampling system and run the engine tests, including online measurements and sampling of emissions and contributed to the data interpretation and preparation of the manuscript; Miroslav Ciganek and Jiri Neca performed DEP extraction and chemical analysis (HPLC/DAD, LC/MS/MS); Katerina Pencikova measured AhR-mediated activity (DR-CALUX); Miroslav Machala contributed to a design of experiments, interpretation of data and preparation of the manuscript and Jan Topinka designed the study, participated on results interpretation and coordinated the whole project.

Conflicts of Interest: The authors declare no conflict of interest.

References

1. Aatola, H.; Larmi, M.; Sarjovaara, T.; Mikkonen, S. Hydrotreated vegetable oil (HVO) as a renewable diesel fuel: Trade-off between nox, particulate emission, and fuel consumption of a heavy duty engine. *SAE Int. J. Engines* **2009**, *1*, 1251–1262. [CrossRef]
2. Moser, B.R. Impact of fatty ester composition on low temperature properties of biodiesel–petroleum diesel blends. *Fuel* **2014**, *115*, 500–506. [CrossRef]
3. Kim, D.; Kim, S.; Oh, S.; No, S.-Y. Engine performance and emission characteristics of hydrotreated vegetable oil in light duty diesel engines. *Fuel* **2014**, *125*, 36–43. [CrossRef]
4. Omidvarborna, H.; Kumar, A.; Kim, D.-S. Variation of diesel soot characteristics by different types and blends of biodiesel in a laboratory combustion chamber. *Sci. Total Environ.* **2016**, *544*, 450–459. [CrossRef] [PubMed]

5. Prokopowicz, A.; Zaciera, M.; Sobczak, A.; Bielaczyc, P.; Woodburn, J. The effects of neat biodiesel and biodiesel and HVO blends in diesel fuel on exhaust emissions from a light duty vehicle with a diesel engine. *Environ. Sci. Technol.* **2015**, *49*, 7473–7482. [CrossRef] [PubMed]
6. Rakopoulos, D.C.; Rakopoulos, C.D.; Giakoumis, E.G. Impact of properties of vegetable oil, bio-diesel, ethanol and n-butanol on the combustion and emissions of turbocharged hddi diesel engine operating under steady and transient conditions. *Fuel* **2015**, *156*, 1–19. [CrossRef]
7. Singh, D.; Subramanian, K.A.; Singal, S.K. Emissions and fuel consumption characteristics of a heavy duty diesel engine fueled with hydroprocessed renewable diesel and biodiesel. *Appl. Energy* **2015**, *155*, 440–446. [CrossRef]
8. Woo, C.; Kook, S.; Hawkes, E.R.; Rogers, P.L.; Marquis, C. Dependency of engine combustion on blending ratio variations of lipase-catalysed coconut oil biodiesel and petroleum diesel. *Fuel* **2016**, *169*, 146–157. [CrossRef]
9. Xue, J.; Grift, T.E.; Hansen, A.C. Effect of biodiesel on engine performances and emissions. *Renew. Sustain. Energy Rev.* **2011**, *15*, 1098–1116. [CrossRef]
10. Millo, F.; Debnath, B.K.; Vlachos, T.; Ciaravino, C.; Postrioti, L.; Buitoni, G. Effects of different biofuels blends on performance and emissions of an automotive diesel engine. *Fuel* **2015**, *159*, 614–627. [CrossRef]
11. Lapuerta, M.; Armas, O.; Rodríguez-Fernández, J. Effect of biodiesel fuels on diesel engine emissions. *Prog. Energy Combust. Sci.* **2008**, *34*, 198–223. [CrossRef]
12. Vojtisek-Lom, M.; Pechout, M.; Dittrich, L.; Beranek, V.; Kotek, M.; Schwarz, J.; Vodicka, P.; Milcova, A.; Rossnerova, A.; Ambroz, A.; et al. Polycyclic aromatic hydrocarbons (PAH) and their genotoxicity in exhaust emissions from a diesel engine during extended low-load operation on diesel and biodiesel fuels. *Atmos. Environ.* **2015**, *109*, 9–18. [CrossRef]
13. Tang, S.; LaDuke, G.; Chien, W.; Frank, B.P. Impacts of biodiesel blends on pm2.5, particle number and size distribution, and elemental/organic carbon from nonroad diesel generators. *Fuel* **2016**, *172*, 11–19. [CrossRef]
14. IARC Working Group on the Evaluation of Carcinogenic Risks to Humans. Chemical agents and related occupations. *IARC Monogr. Eval. Carcinog. Risks Hum.* **2012**, *100*, 9–562.
15. IARC Working Group on the Evaluation of Carcinogenic Risks to Humans. Diesel and gasoline engine exhausts and some nitroarenes. IARC monographs on the evaluation of carcinogenic risks to humans. *IARC Monogr. Eval. Carcinog. Risks Hum.* **2014**, *105*, 9–699.
16. Claxton, L.D. The history, genotoxicity and carcinogenicity of carbon-based fuels and their emissions: Part 4—Alternative fuels. *Mutat. Res. Rev. Mutat. Res.* **2015**, *763*, 86–102. [CrossRef] [PubMed]
17. Schins, R.P.; Knaapen, A.M. Genotoxicity of poorly soluble particles. *Inhal. Toxicol.* **2007**, *19*, 189–198. [CrossRef] [PubMed]
18. Topinka, J.; Milcova, A.; Schmuczerova, J.; Mazac, M.; Pechout, M.; Vojtisek-Lom, M. Genotoxic potential of organic extracts from particle emissions of diesel and rapeseed oil powered engines. *Toxicol. Lett.* **2012**, *212*, 11–17. [CrossRef] [PubMed]
19. André, V.; Barraud, C.; Capron, D.; Preterre, D.; Keravec, V.; Vendeville, C.; Cazier, F.; Pottier, D.; Morin, J.P.; Sichel, F. Comparative mutagenicity and genotoxicity of particles and aerosols emitted by the combustion of standard vs. Rapeseed methyl ester supplemented bio-diesel fuels: Impact of after treatment devices: Oxidation catalyst and particulate filter. *Mutat. Res. Genet. Toxicol. Environ. Mutagen.* **2015**, *777*, 33–42. [CrossRef] [PubMed]
20. Steiner, S.; Heeb, N.V.; Czerwinski, J.; Comte, P.; Mayer, A.; Petri-Fink, A.; Rothen-Rutishauser, B. Test-methods on the test-bench: A comparison of complete exhaust and exhaust particle extracts for genotoxicity/mutagenicity assessment. *Environ. Sci. Technol.* **2014**, *48*, 5237–5244. [CrossRef] [PubMed]
21. Iba, M.M.; Caccavale, R.J. Genotoxic bioactivation of constituents of a diesel exhaust particle extract by the human lung. *Environ. Mol. Mutagen.* **2013**, *54*, 158–171. [CrossRef] [PubMed]
22. Bao, L.; Xu, A.; Tong, L.; Chen, S.; Zhu, L.; Zhao, Y.; Zhao, G.; Jiang, E.; Wang, J.; Wu, L. Activated toxicity of diesel particulate extract by ultraviolet a radiation in mammalian cells: Role of singlet oxygen. *Environ. Health Perspect.* **2009**, *117*, 436–441. [CrossRef] [PubMed]
23. Jalava, P.I.; Tapanainen, M.; Kuuspalo, K.; Markkanen, A.; Hakulinen, P.; Happo, M.S.; Pennanen, A.S.; Ihalainen, M.; Yli-Pirila, P.; Makkonen, U.; et al. Toxicological effects of emission particles from fossil- and biodiesel-fueled diesel engine with and without doc/poc catalytic converter. *Inhal. Toxicol.* **2010**, *22*, 48–58. [CrossRef] [PubMed]

24. Kooter, I.M.; van Vugt, M.A.T.M.; Jedynska, A.D.; Tromp, P.C.; Houtzager, M.M.G.; Verbeek, R.P.; Kadijk, G.; Mulderij, M.; Krul, C.A.M. Toxicological characterization of diesel engine emissions using biodiesel and a closed soot filter. *Atmos. Environ.* **2011**, *45*, 1574–1580. [CrossRef]
25. Palkova, L.; Vondracek, J.; Trilecova, L.; Ciganek, M.; Pencikova, K.; Neca, J.; Milcova, A.; Topinka, J.; Machala, M. The aryl hydrocarbon receptor-mediated and genotoxic effects of fractionated extract of standard reference diesel exhaust particle material in pulmonary, liver and prostate cells. *Toxicol. In Vitro* **2015**, *29*, 438–448. [CrossRef] [PubMed]
26. Lou, H.; Du, S.Y.; Ji, Q.; Stolz, A. Induction of AKR1C2 by phase II inducers: Identification of a distal consensus antioxidant response element regulated by Nrf2. *Mol. Pharmacol.* **2006**, *69*, 1662–1672. [CrossRef] [PubMed]
27. Penning, T.M. Human aldo-keto reductases and the metabolic activation of polycyclic aromatic hydrocarbons. *Chem. Res. Toxicol.* **2014**, *27*, 1901–1917. [CrossRef] [PubMed]
28. Longhin, E.; Capasso, L.; Battaglia, C.; Proverbio, M.C.; Cosentino, C.; Cifola, I.; Mangano, E.; Camatini, M.; Gualtieri, M. Integrative transcriptomic and protein analysis of human bronchial BEAS-2B exposed to seasonal urban particulate matter. *Environ. Pollut.* **2016**, *209*, 87–98. [CrossRef] [PubMed]
29. Ma, Q. Role of Nrf2 in oxidative stress and toxicity. *Annu. Rev. Pharmacol. Toxicol.* **2013**, *53*, 401–426. [CrossRef] [PubMed]
30. Li, N.; Wang, M.Y.; Oberley, T.D.; Sempf, J.M.; Nel, A.E. Comparison of the pro-oxidative and proinflammatory effects of organic diesel exhaust particle chemicals in bronchial epithelial cells and macrophages. *J. Immunol.* **2002**, *169*, 4531–4541. [CrossRef] [PubMed]
31. Totlandsdal, A.I.; Lag, M.; Lilleaas, E.; Cassee, F.; Schwarze, P. Differential proinflammatory responses induced by diesel exhaust particles with contrasting pah and metal content. *Environ. Toxicol.* **2015**, *30*, 188–196. [CrossRef] [PubMed]
32. Arrigo, A.P. The cellular "networking" of mammalian hsp27 and its functions in the control of protein folding, redox state and apoptosis. *Adv. Exp. Med. Biol.* **2007**, *594*, 14–26. [PubMed]
33. Krause, K.; Wasner, M.; Reinhard, W.; Haugwitz, U.; Dohna, C.L.Z.; Mossner, J.; Engeland, K. The tumour suppressor protein p53 can repress transcription of cyclin B. *Nucleic Acids Res.* **2000**, *28*, 4410–4418. [CrossRef] [PubMed]
34. Karantanos, T.; Tanimoto, R.; Edamura, K.; Hirayama, T.; Yang, G.; Golstov, A.A.; Wang, J.X.; Kurosaka, S.; Park, S.; Thompson, T.C. Systemic GLIPR1-ΔTM protein as a novel therapeutic approach for prostate cancer. *Int. J. Cancer* **2014**, *134*, 2003–2013. [CrossRef] [PubMed]
35. Feng, X.; Liu, X.; Zhang, W.; Xiao, W.H. P53 directly suppresses BNIP3 expression to protect against hypoxia-induced cell death. *EMBO J.* **2011**, *30*, 3397–3415. [CrossRef] [PubMed]
36. Galvagni, F.; Orlandini, M.; Oliviero, S. Role of the AP-1 transcription factor FOSL1 in endothelial cell adhesion and migration. *Cell Adhes. Migr.* **2013**, *7*, 408–411. [CrossRef] [PubMed]
37. West, M.D.; Shay, J.W.; Wright, W.E.; Linskens, M.H.K. Altered expression of plasminogen activator and plasminogen activator inhibitor during cellular senescence. *Exp. Gerontol.* **1996**, *31*, 175–193. [CrossRef]
38. Johannson, K.A.; Vittinghoff, E.; Lee, K.; Balmes, J.R.; Ji, W.; Kaplan, G.G.; Kim, D.S.; Collard, H.R. Acute exacerbation of idiopathic pulmonary fibrosis associated with air pollution exposure. *Eur. Respir. J.* **2014**, *43*, 1124–1131. [CrossRef] [PubMed]
39. Hattori, N.; Mizuno, S.; Yoshida, Y.; Chin, K.; Mishima, M.; Sisson, T.H.; Simon, R.H.; Nakamura, T.; Miyake, M. The plasminogen activation system reduces fibrosis in the lung by a hepatocyte growth factor-dependent mechanism. *Am. J. Pathol.* **2004**, *164*, 1091–1098. [CrossRef]
40. Cho, H.Y.; Reddy, S.P.; Yamamoto, M.; Kleeberger, S.R. The transcription factor Nrf2 protects against pulmonary fibrosis. *FASEB J.* **2004**, *18*, 1258–1260. [CrossRef] [PubMed]
41. Lakatos, H.F.; Thatcher, T.H.; Kottmann, R.M.; Garcia, T.M.; Phipps, R.P.; Sime, P.J. The role of ppars in lung fibrosis. *PPAR Res.* **2007**, *2007*, 71323. [CrossRef] [PubMed]
42. Devchand, P.R.; Ziouzenkova, O.; Plutzky, J. Oxidative stress and peroxisome proliferator-activated receptors: Reversing the curse? *Circ. Res.* **2004**, *95*, 1137–1139. [CrossRef] [PubMed]
43. Zhang, L.; Jin, Y.; Huang, M.; Penning, T.M. The role of human Aldo-Keto reductases in the metabolic activation and detoxication of polycyclic aromatic hydrocarbons: Interconversion of pah catechols and pah o-quinones. *Front. Pharmacol.* **2012**, *3*, 193. [CrossRef] [PubMed]

44. Jiang, H.; Vudathala, D.K.; Blair, I.A.; Penning, T.M. Competing roles of Aldo-Keto reductase 1A1 and cytochrome P4501B1 in benzo[a]pyrene-7,8-diol activation in human bronchoalveolar H358 cells: Role of akrs in p4501b1 induction. *Chem. Res. Toxicol.* **2006**, *19*, 68–78. [CrossRef] [PubMed]
45. Andrysik, Z.; Vondracek, J.; Marvanova, S.; Ciganek, M.; Neca, J.; Pencikova, K.; Mahadevan, B.; Topinka, J.; Baird, W.M.; Kozubik, A.; et al. Activation of the aryl hydrocarbon receptor is the major toxic mode of action of an organic extract of a reference urban dust particulate matter mixture: The role of polycyclic aromatic hydrocarbons. *Mutat. Res. Fund. Mol. M* **2011**, *714*, 53–62. [CrossRef] [PubMed]
46. Crane, R.; Gadea, B.; Littlepage, L.; Wu, H.; Ruderman, J.V. Aurora A, meiosis and mitosis. *Biol. Cell* **2004**, *96*, 215–229. [CrossRef] [PubMed]
47. Kunitoku, N.; Sasayama, T.; Marumoto, T.; Zhang, D.W.; Honda, S.; Kobayashi, O.; Hatakeyama, K.; Ushio, Y.; Saya, H.; Hirota, T. Cenp-a phosphorylation by aurora-A in prophase is required for enrichment of aurora-b inner centromeres and for kinetochore function. *Dev. Cell* **2003**, *5*, 853–864. [CrossRef]
48. Neef, R.; Preisinger, C.; Sutcliffe, J.; Kopajtich, R.; Nigg, E.A.; Mayer, T.U.; Barr, F.A. Phosphorylation of mitotic kinesin-like protein 2 by polo-like kinase 1 is required for cytokinesis. *J. Cell Biol.* **2003**, *162*, 863–875. [CrossRef] [PubMed]
49. Wu, C.C.; Yang, T.Y.; Yu, C.T.; Phan, L.; Ivan, C.; Sood, A.K.; Hsu, S.L.; Lee, M.H. P53 negatively regulates aurora a via both transcriptional and posttranslational regulation. *Cell Cycle* **2012**, *11*, 3433–3442. [CrossRef] [PubMed]
50. Eyers, P.A.; Erikson, E.; Chen, L.G.; Maller, J.L. A novel mechanism for activation of the protein kinase aurora A. *Curr. Biol.* **2003**, *13*, 691–697. [CrossRef]
51. Garrido, G.; Vernos, I. Non-centrosomal tpx2-dependent regulation of the aurora a kinase: Functional implications for healthy and pathological cell division. *Front. Oncol.* **2016**, *6*, 88. [CrossRef] [PubMed]
52. Aguirre-Portoles, C.; Bird, A.W.; Hyman, A.; Canamero, M.; de Castro, I.P.; Malunnbres, M. Tpx2 controls spindle integrity, genome stability, and tumor development. *Cancer Res.* **2012**, *72*, 1518–1528. [CrossRef] [PubMed]
53. Livak, K.J.; Schmittgen, T.D. Analysis of relative gene expression data using real-time quantitative PCR and the $2^{-\Delta\Delta Ct}$ method. *Methods* **2001**, *25*, 402–408. [CrossRef] [PubMed]
54. Du, P.; Kibbe, W.A.; Lin, S.M. Lumi: A pipeline for processing illumina microarray. *Bioinformatics* **2008**, *24*, 1547–1548. [CrossRef] [PubMed]
55. Smyth, G.K. Linear models and empirical bayes methods for assessing differential expression in microarray experiments. *Stat. Appl. Genet. Mol. Biol.* **2004**, *3*, Article 3. [CrossRef] [PubMed]
56. Chen, J.; Bardes, E.E.; Aronow, B.J.; Jegga, A.G. Toppgene suite for gene list enrichment analysis and candidate gene prioritization. *Nucleic Acids Res.* **2009**, *37*, W305–W311. [CrossRef] [PubMed]
57. R Core Team. *R: A Language and Environment for Statistical Computing*; R foundation for Statistical Computing: Vienna, Austria, 2015. Available online: http://www.R-project.org/ (accessed on 8 August 2016).
58. Chambers, J.M.; Freeny, A.; Heiberger, R.M. *Analysis of Variance*; Designed Experiments; Wadsworth & Brooks/Cole: Pacific Grove, CA, USA, 1992.
59. Benjamini, Y.; Hochberg, Y. Controlling the false discovery rate: A practical and powerful approach to multiple testing. *J. R. Stat. Soc.* **1995**, *57*, 289–300.
60. Yandell, B.S. *Practical Data Analysis for Designed Experiments*; Crc Press, Chapman & Hall: London, UK, 1997; Volume 39.

Článek 3

Toxicology in Vitro 48 (2018) 329–341

Contents lists available at ScienceDirect

Toxicology in Vitro

journal homepage: www.elsevier.com/locate/toxinvit

Transcriptional response to organic compounds from diverse gasoline and biogasoline fuel emissions in human lung cells

Helena Libalova[a], Pavel Rossner Jr[a], Kristyna Vrbova[a], Tana Brzicova[a,b], Jitka Sikorova[a,c], Michal Vojtisek-Lom[d], Vit Beranek[d], Jiri Klema[e], Miroslav Ciganek[f], Jiri Neca[f], Miroslav Machala[f], Jan Topinka[a,*]

[a] Department of Genetic Toxicology and Nanotoxicology, Institute of Experimental Medicine AS CR, Videnska 1083, 142 20 Prague, Czech Republic
[b] Faculty of Safety Engineering, VSB-Technical University of Ostrava, Lumirova 13, 700 30 Ostrava, Czech Republic
[c] Institute for Environmental Studies, Faculty of Science, Charles University in Prague, Benatska 2, 128 01 Prague 2, Czech Republic
[d] Center of Vehicles for Sustainable Mobility, Faculty of Mechanical Engineering, Czech Technical University in Prague, Technicka 4, 166 07 Prague, Czech Republic
[e] Department of Cybernetics, Faculty of Electrical Engineering, Czech Technical University in Prague, Karlovo namesti 13, 121 35 Prague, Czech Republic
[f] Department of Chemistry and Toxicology, Veterinary Research Institute, Hudcova 296/70, 621 00 Brno, Czech Republic

ARTICLE INFO

Keywords:
Gasoline exhaust particles
Alternative fuels
Organic extracts
Gene expression profiling
DNA damage response

ABSTRACT

Modern vehicles equipped with Gasoline Direct Injection (GDI) engine have emerged as an important source of particulate emissions potentially harmful to human health. We collected and characterized gasoline exhaust particles (GEPs) produced by neat gasoline fuel (E0) and its blends with 15% ethanol (E15), 25% n-butanol (n-But25) and 25% isobutanol (i-But25). To study the toxic effects of organic compounds extracted from GEPs, we analyzed gene expression profiles in human lung BEAS-2B cells. Despite the lowest GEP mass, n-But25 extract contained the highest concentration of polycyclic aromatic hydrocarbons (PAHs), while i-But25 extract the lowest. Gene expression analysis identified activation of the DNA damage response and other subsequent events (cell cycle arrest, modulation of extracellular matrix, cell adhesion, inhibition of cholesterol biosynthesis) following 4 h exposure to all GEP extracts. The i-But25 extract induced the most distinctive gene expression pattern particularly after 24 h exposure. Whereas E0, E15 and n-But25 extract treatments resulted in persistent stress signaling including DNA damage response, MAPK signaling, oxidative stress, metabolism of PAHs or pro-inflammatory response, i-But25 induced changes related to the metabolism of the cellular nutrients required for cell recovery. Our results indicate that i-But25 extract possessed the weakest genotoxic potency possibly due to the low PAH content.

1. Introduction

Air pollution has emerged as a worldwide problem and numerous studies have raised concerns about environmental and health effects of particulate matter (PM) in the atmosphere. A crucial portion of particles is derived from anthropogenic activities, such as the burning of fossil fuels in vehicle engines, domestic heating, power plants and industrial processes.

It has been demonstrated that long- and short-term exposure to the PM of aerodynamic diameter (d_{ae}) < 2.5 μm (PM2.5) can cause premature death and health disorders, such as adverse implications on the cardiovascular system and respiratory effects including asthma attacks (Pope III and Dockery, 2006). PM from anthropogenic activities consists of the aggregated nuclei composed largely of elemental carbon, with high concentrations of toxic substances adsorbed on the surface, such as acid sulphates, soluble metals, and organic compounds including carcinogenic polycyclic aromatic hydrocarbons (c-PAHs). The serious health risks are posed not only by PM2.5 but particularly by the ultrafine fraction (d_{ae} < 100 nm). PM2.5 are potentially more harmful than larger particles because they can deposit deeper into the lungs, and ultrafine particles may even penetrate into the bloodstream and reach target organs (Xia et al., 2016).

Motor vehicle emissions are among the major sources of air pollutants in many urban areas. Although emissions have been reduced over the last few decades due to the development of new fuels, improvement of engine exhaust after-treatment technology and due to the

Abbreviations: E0, Neat gasoline fuel; E15, Blend of gasoline and 15% ethanol; GDI, Gasoline Direct Injection; GEPs, Gasoline Exhaust Particles; i-but25, Blend of gasoline and 25% isobutanol; n-but25, Blend of gasoline and 25% n-butanol; PAHs, Polycyclic Aromatic Hydrocarbons

* Corresponding author.
E-mail address: jtopinka@biomed.cas.cz (J. Topinka).

https://doi.org/10.1016/j.tiv.2018.02.002
Received 23 October 2017; Received in revised form 30 January 2018; Accepted 5 February 2018
Available online 09 February 2018

increasingly stringent emission controls, the number of vehicles is still growing and studies of the toxic effects associated with exposure to vehicle engine exhaust are often complicated by a various composition of emissions. Modern gasoline engines with the innovative direct fuel injection system known as Gasoline Direct Injection (GDI) or Direct Injection Spark Ignition (DISI) offers numerous benefits including improved fuel efficiency and thus reduced CO_2 emissions, compared to conventional port fuel injection technology (PFI). Currently, emission limits for new cars are becoming more stringent every 3–5 years, so GDI is gradually replacing the historically dominant PFI engines. However, GDI engines also have several shortcomings such as the production of a substantial amount of particulate emission due to the direct fuel injection technology (Tripathy et al., 2017).

Increasing demands for alternative fuels produced from renewable sources attempting to reduce greenhouse gas emissions, energy dependency and to diversify energy resources have raised an interest in numerous biofuels and their blends. Apart from ethanol, the most prominent bioadditive worldwide, butanol might represent a competitive alternative offering further benefits (Jin et al., 2011). However, the use of bio-additives to supplement neat gasoline fuel may cause profound changes in emission properties such as particle morphology, size distribution and chemical composition, thus complicating the assessment of health and environmental risks. Importantly, compared to extensive research dealing with the toxicity of diesel and biodiesel fuel emissions, studies on the comparative toxicity of fossil gasoline and biogasoline exhaust particles or their organic extracts are very scarce. Acute exposure to emissions from neat gasoline and gasoline-ethanol blends was examined in human lung cells (Bisig et al., 2016). The authors found no adverse cell responses in this exposure; however, they pointed out that chronic and in vivo studies are missing. Moreover, no study exists on the toxicity of butanol-gasoline blends.

We recently reported a study on the comparative toxicity of organic compound mixtures extracted from diverse diesel and biodiesel particulate emissions in human lung BEAS-2B cells. Our results suggested that biofuels (conventional biodiesel fuel B100 and new generation of biodiesel fuel NexBTL) and the blend B30 considerably changed the particulate emission properties including chemical composition and affected various cellular processes on transcriptional level thus causing distinctive molecular responses in BEAS-2B cells (Libalova et al., 2016).

The present study addresses the important issue concerning the toxicity of particles emitted by gasoline direct injection engines. We aimed to compare chemical properties and toxic effects of organic extracts from GEPs produced by the combustion of conventional gasoline fuel and currently used (ethanol) or candidate (butanol) biofuels. Whole-genome gene expression profiling in human lung BEAS-2B cells was used to identify the major processes and genes which were commonly modulated after the exposure to all GEP extracts, as well as those specific for each treatment. This integrated approach, linking the characteristics of gasoline and alcohol-gasoline blends of particulate emissions with their toxic effects may improve the current knowledge of their impact on health and the environment.

2. Materials and methods

2.1. Chemicals and biochemicals

Agilent RNA 6000 Nano Kit was purchased from Agilent Technologies (Waldbronn, Germany), Bronchial Epithelial Basal Medium and BEGM™ BulleKit™ from Lonza (Basel, Switzerland); human bronchial epithelial cells BEAS-2B from ATCC (Manassas, VA, USA); dimethylsulphoxide (DMSO) from Sigma-Aldrich (St. Louis, MO, USA); WST-1 Proliferation Assay, Cytotoxicity Detection Kit (LDH) and High Fidelity cDNA synthesis Kit from Roche (Mannheim, Germany); NucleoSpin RNA II Isolation Kit from Macherey-Nagel (Düren, Germany); Illumina Human-HT12 v4 Expression BeadChips were from Illumina (San Diego, CA, USA); Illumina TotalPrep RNA Amplification Kit from Thermo Fisher Scientific (Waltham, MA, USA); Custom Designed Real-Time PCR Assay, qRT-PCR master mix and geNorm Reference Gene Selection Kit from Primerdesign (Southampton, UK); Standard Reference Material SRM 1650b (diesel particulate matter) from NIST (Gaithersburg, MD, USA).

2.2. Test vehicle, fuels and exhaust particles collection

The tests were carried on a typical European small family car (C-segment production passenger car), 2013 Ford Focus station wagon, with a three-cylinder 1.0 L turbocharged gasoline direct injection EcoBoost engine (92 kW @ 6000 rpm, 170 Nm @ 1400–4500 rpm, certified to Euro 6) and a 6-speed manual transmission, mileage of 7962 km (4948 mi) at the beginning and 10,130 km (6296 mi) at the end of the study.

Non-oxygenated gasoline with a nominal research octane number of 95, meeting ČSN EN228 specifications, was obtained at the local fuel station (EuroOil, Buštěhrad, Hřebečská 695, 27343), and used as the baseline fuel for the testing. Commercially available E85 fuel, also obtained from a local fuel station (LPG-AUTO s.r.o., Michelská 4/11, Prague 14000) and analyzed to contain 70% of ethanol, was mixed with the base fuel to produce a blend containing 15% of ethanol by volume (E15). Technical grade n-butanol (Chemlogistic, Pardubice) and isobutanol (Chemap, Dašice) were also mixed with the baseline fuel to obtain a blend of 25% of n-butanol with gasoline (n-But25) and a blend of 25% isobutanol with gasoline (i-But25). The fuels were metered on a mass basis using their actual densities into 20-liter canisters and splash-blended.

The vehicle was operated on a 4-wheel chassis dynamometer, according to the Common Artemis Driving Cycle, created to represent automobile driving patterns in Europe (André, 2004). The Artemis driving cycle comprises of an urban, rural and motorway section. Several versions of the motorway section, differing in maximum speed, are defined; the version with a maximum speed of 130 km/h (79 mph) was run here. The whole Artemis cycle was repeated four times to collect representative samples of exhaust particulate emissions.

The exhaust was routed into a full-flow dilution tunnel with a constant volume sampler (CVS) operating at 10.8 m^3/min (381 cfm), from which samples were taken for online measurements and offline analyses. The instantaneous dilution ratio, expressed as the ratio of the CVS flow and the instantaneous exhaust flow, varied considerably over the cycle and ranged from about 5:1 at full load to nearly 100:1 at idle. The online measurements included concentrations of hydrocarbons, CO, CO_2, NO_x and particle number concentrations. Particle size distributions were measured online with a fast mobility particle sizer (EEPS, Model 3090, TSI), preceded by a secondary dilution by a rotating disc diluter (MD-19, Matter Engineering) set to 180:1 dilution ratio; the diluter head was heated to 150 °C (Vojtisek-Lom et al., 2015a, 2015b).

For toxicity assays, diluted exhaust from the tunnel was sampled on 8″ × 10″ (203 × 254 mm) Teflon-coated glass fiber filters (Pall TX40HI20-WW), at a 67.8 m^3/h sampling rate using a pair of modified EcoTech 3000 high-volume samplers. The sample from the high-volume sampler was returned to the CVS; the sum of the remaining flows not returned to the CVS was added to the CVS nominal flow, and the emissions calculations were done with the corrected flow.

2.3. Particle characterization and chemical analysis

Organic compounds were extracted with dichloromethane in automated extraction apparatus Behr EF (BEHR, Germany) for 4 h. Aliquot parts of the crude extract were re-dissolved in the required volume of acetonitrile for HPLC/DAD and LC/MS-MS; and in dimethyl sulfoxide (DMSO) for bioassays. The method of external standardization was used for quantification of all PAH contaminants. The accuracy and precision of the analytical methods was determined by analysis of the standard

reference material SRM 1650b. Further details on the chemical analysis are described elsewhere (Andrysik et al., 2011).

2.4. Cell cultures and exposure conditions

Human bronchial epithelial cells BEAS-2B were cultured in Bronchial Epithelial Basal Medium (BEBM), supplemented with the standardized set of growth factors provided by the manufacturer (BEGM™ BulleKit™). All cultivation flasks and plates were coated with BEBM containing fibronectin, collagen and bovine serum albumin. All tested GEP extracts were diluted in complete BEBM (concentration of DMSO did not exceeded 0.1% *w*/w) and cells were incubated in triplicates for 4 h or 24 h, respectively. Control cells were incubated with extracts from blank filters. Cell cultures and cell-based assays were maintained in a humidified atmosphere with 5% CO_2 at 37 °C.

2.5. Cytotoxicity

To assess the viability of cells, the WST-1 Proliferation Assay and LDH Cytotoxicity Assay were performed 24 h after exposure to GEP extracts following the manufacturer's protocol. BEAS-2B cells were seeded in 96-well plates 24 h before treatment at a density of 7500 cells per well. For the dose-response curve and threshold cytotoxicity assessment, cell triplicates were incubated with six concentrations (1, 10, 50, 100, 500 and 1000 µg/mL) of each GEP extract. Triton X-100 (0.1%) was used as a positive control. The absorbance was measured at 440 nm (WST-1 assay) and at 490 nm (LDH assay), respectively.

2.6. RNA isolation and quality control

Total RNA from lysed BEAS-2B cells was obtained using NucleoSpin RNA II according to the manufacturer's instructions. The RNA concentration was quantified with a Nanodrop ND-1000 Spectrophotometer (Thermo Fisher Scientific, USA). The integrity of RNA was assessed using an Agilent 2100 Bioanalyzer (Agilent Technologies Inc., USA) and Agilent RNA 6000 Nano Kit. All samples had an RNA Integrity Number (RIN) > 9. Isolated RNA was stored at −80 °C until processing.

2.7. Microarray analysis

Illumina Human-HT12 v4 Expression BeadChips were used to generate gene expression profiles of cell triplicates exposed to all tested GEP extracts for 4 and 24 h. Biotinylated complementary RNA (cRNA) was prepared from 500 ng of total RNA using the Illumina TotalPrep RNA Amplification Kit. Next, 900 ng of biotinylated cRNA targets was hybridized to the beadchips. The steps of hybridization and the subsequent washing, staining and drying of the beadchips were performed according to standard instructions from Illumina. The hybridized beadchips were then scanned on the Illumina iScan and bead level data were summarized by GenomeStudio Software v2 (Illumina, San Diego, CA, USA).

2.8. Quantitative RT-PCR verification

One µg of RNA obtained from each sample replicate was transcribed into the complementary DNA (cDNA) using the High Fidelity cDNA synthesis Kit (Roche). The original protocol was modified by using 2.5 µM oligo(dT) and 10 µM random hexamers for priming in a 20 µl reaction volume. cDNA synthesis was performed according to the following conditions: 30 min at 55 °C and 5 min at 85 °C. Quantitative RT-PCR (qRT-PCR) measurements were carried out using the Light Cycler 480 (Roche, Germany). A final reaction qPCR mix (14 µl) contained 2.5 µl of diluted cDNA, 3.8 µl of water, 7 µl of master mix (Primerdesign, UK)., 0.7 µl of a specifically designed assay (Custom Designed Real-Time PCR Assay, Primerdesign, UK) to determine the level of each target gene. Cycling conditions were the following: 2 min at 95 °C and 40 cycles of amplification (10 s at 95 °C and 60 s at 60 °C). The sequences of primers used in qRT-PCR are shown in Supplementary file 1.

2.9. Statistical analysis

Gene expression levels in GEP extract-treated cells were compared with control BEAS-2B cell cultures treated with extract from blank filter only. BeadChip summary data were imported into an R statistical environment (https://www.r-project.org/) and normalized using the quantile method in the Lumi package (Du et al., 2008). Only probes with a detection p-value < 0.01 in > 50% of arrays were included for further analyses. Differential gene expression was analyzed in the Limma package using the moderated t-statistic. A linear model was fitted for each gene given a series of arrays using lmFit function (Smyth, 2004). A multiple testing correction was performed using the Benjamini & Hochberg method. To analyze lists of significantly deregulated genes after GEP extract treatments (cut-off p-value < 0.05, fold change > 1.5 and < 0.67), ToppFun tool was used (Chen et al., 2009). Functional analysis identified numerous over-represented terms in several categories; pathways as a functional category were considered for the analysis. Only pathways with a corrected p-value (Benjamini & Hochberg method) below 0.05 were selected. Venn diagrams were prepared in Bioinformatics & Evolutionary Genomics tool (http://bioinformatics.psb.ugent.be/webtools/Venn/).

The baseline and threshold values of qRT-PCR experiments raw data were obtained from GenEx software version 6.1 (MultiD Analyses AB, Goteborg, Sweden). Expression levels of target genes were normalized to the reference genes (*TOP1* and *ACTB*). Reference genes were selected according to the stability of gene expression during experimental conditions using the geNorm Reference Gene Selection Kit. Relative changes in normalized gene levels were calculated using the $2^{-\Delta\Delta Ct}$ method (Livak and Schmittgen, 2001). For the assessment of significant changes between the means of treated groups and the control group, the two-tail Student's t-test was used. Graphs were constructed in Graphpad Prism v5 (GraphPad Software Inc., La Jolla, CA, USA).

3. Results

3.1. Characteristics of collected gasoline exhaust particles and chemical analysis of organic extracts

The total mass of particles emitted varied among fuels and is listed in Table 1. Emissions of gaseous compounds, total number of non-volatile particles and other results have been reported in Vojtisek-Lom et al. (2015a, 2015b). Compared to conventional gasoline E0 with production of 1.70 mg GEP/km, GEP mass emissions were slightly higher for E15 (1.76 mg/km), lower for i-But25 (1.26 mg/km), and approximately half for n-But25 (0.86 mg/km). We further determined the content of PAHs and their derivatives in dichloromethane extracts of GEPs from individual fuels. All results of chemical analyses and toxicological assays are reported per mg of GEPs, reflecting the properties of the GEP. Since toxic effects are non-linear with the dose, and the dilution of the exhaust prior to inhalation varies considerably, expression of toxic effects per km driven would be subject to considerable uncertainties. In general, chemical analysis revealed the substantial amount of PAHs and their derivatives such as oxy-, nitro- or dinitro-PAHs in all GEP extracts (Table 1). The sum of analyzed PAHs in the i-But25 extract was approximately 30% lower than in n-But25 (815.7 ng per mg of i-But25 GEPs versus 1293.6 ng per mg of n-But25 GEPs) and 15–20% lower than in E0 and E15 extracts (959 and 999 ng per mg of E0 or E15 GEPs, respectively). This was particularly true for low molecular weight PAHs such as phenanthrene, fluoranthene or pyrene which elicit significantly lower toxic potencies than high-molecular weight PAHs. The sum of PAHs classified by IARC as carcinogenic, or

Table 1
Emission characteristics of GEPs and chemical analysis of PAH compounds and their oxygenated, nitrated and dinitrated derivatives in GEP extracts.

Total emissions, Artemis cycle				
GEPs	E0	E15	n-But25	i-But25
Mass [mg/km]	1.70	1.76	0.86	1.26
Standard deviation	0.54	1.76	0.23	0.86
PAH analysis				
PAHs (ng/mg GEP)				
Compound [molecular weight]	E0	E15	n-But25	i-But25
Phenanthrene [178]	111.3	127.1	201.1	75.4
Anthracene [178]	30.5	38.8	46.3	24.1
4H-Cyclopenta[*def*]phenathrene [190]	15.8	5.6	3.4	1.9
Fluoranthene [202]	164.7	204.3	286.8	174.4
Pyrene [202]	182.9	201.3	291.5	170.5
1-Methylpyrene [216]	8.8	9.1	12.0	7.0
Benzo[*c*]phenanthrene [228]	21.4	21.5	26.8	18.6
Triphenylene [228]	13.3	12.2	15.6	12.0
Benz[*a*]anthracene* [228]	74.9	72.2	89.1	66.4
Chrysene* [228]	65.6	63.3	74.2	58.8
7-Methylbenz[*a*]anthracene [242]	1.0	0.9	1.9	1.2
9-Methylbenz[*a*]anthracene [242]	0.6	0.7	0.9	0.6
1-Methylchrysene [242]	2.3	2.6	2.7	2.0
Benzo[*a*]fluoranthene [252]	15.3	14.2	14.9	9.8
Benzo[*j*]fluoranthene [252]	25.7	23.2	22.4	17.9
Benzo[*e*]pyrene [252]	18.0	17.2	16.8	13.1
Perylene [252]	5.3	5.3	6.0	4.0
Benzo[*b*]fluoranthene* [252]	40.3	37.6	34.6	27.2
Benzo[*k*]fluoranthene* [252]	19.5	17.3	15.6	14.6
Benzo[*a*]pyrene* [252]	29.2	28.3	24.5	20.2
1-Methylbenzo[*a*]pyrene [266]	n.d.	n.d.	n.d.	n.d.
Benzo[*g,h,i*]perylene [276]	54.4	42.8	51.5	51.9
Indeno[1,2,3-*cd*]pyrene* [276]	27.1	25.6	23.8	18.2
Dibenz[*a,c*]anthracene [278]	1.8	1.9	1.7	1.4
Benzo[*c*]chrysene [278]	0.9	1.1	n.d.	n.d.
Dibenz[*a,j*]anthracene [278]	1.2	1.3	1.3	1.0
Dibenz[*a,h*]anthracene* [278]	0.5	0.5	n.d.	0.4
Benzo[*b*]chrysene [278]	n.d.	n.d.	n.d.	n.d.
Picene [278]	1.4	1.8	1.2	1.4
Coronene [300]	18.3	12.9	20.6	15.2
Dibenzo[*a,l*]pyrene [302]	n.d.	n.d.	n.d.	n.d.
Dibenzo[*j,l*]fluoranthene [302]	n.d.	n.d.	n.d.	n.d.
Naphtho[1,2-*b*]fluoranthene [302]	2.6	2.6	2.9	1.8
Dibenzo[*a,e*]fluoranthene [302]	n.d.	n.d.	n.d.	n.d.
Dibenzo[*a,k*]fluoranthene [302]	n.d.	n.d.	n.d.	n.d.
Naphtho[2,3-*e*]pyrene [302]	1.3	1.2	n.d.	0.9
Dibenzo[*a,e*]pyrene [302]	n.d.	n.d.	n.d.	n.d.
Dibenzo[*e,l*]pyrene [302]	n.d.	n.d.	n.d.	n.d.
Dibenzo[*b,k*]fluoranthene [302]	n.d.	1.3	n.d.	n.d.
Naphtho[2,3-*b*]fluoranthene [302]	n.d.	n.d.	n.d.	n.d.
Naphtho[2,1-*a*]pyrene [302]	0.9	1.1	n.d.	1.1
Dibenzo[*a,i*]pyrene [302]	n.d.	n.d.	n.d.	n.d.
Naphtho[2,3-*a*]pyrene [302]	n.d.	n.d.	n.d.	n.d.
Dibenzo[*a,h*]pyrene [302]	n.d.	n.d.	n.d.	n.d.
Naphtho[1,2,3,4-*ghi*]perylene [326]	n.d.	n.d.	n.d.	n.d.
Benzo[*a*]coronene [350]	2.2	2.2	3.5	2.7
Sum of PAHs (ng/mg GEP)	959	999	1293.6	815.7
Sum of carcinogenic PAHs (ng/mg GEP)	257.1	244.8	261.8	205.8
Oxygenated PAHs (ng/mg GEP)				
Compound	E0	E15	n-But25	i-But25
1,8-Naphthalic Anhydride	19.1	10.8	28.9	43.7
Phenanthrene-9,10-dione	3.5	4.0	5.8	4.6
9H-Fluoren-9-one	68.0	72.2	149.4	88.8
Anthrone	1.1	1.0	1.4	1.2
Anthracene-9,10-dione (anthraquinone)	86.8	100.5	189.8	127.9
7H-Benz[*de*]anthracene-7one (benzanthrone)	26.4	24.3	47.2	27.9
9-Hydroxybenzo[*a*]pyrene	0.4	0.5	0.7	0.6
Benz[*a*]anthracene-7,12-dione	2.2	2.3	2.7	2.5
3-Hydroxybenzo[*a*]pyrene	n.d.	0.1	0.3	0.3
Sum of oxygenated PAHs (ng/mg GEP)	207.5	215.7	426.2	297.5
Nitrated PAHs (pg/mg GEP)				
Compound	E0	E15	n-But25	i-But25
1-Nitropyrene	129	86	171	66
2-Nitropyrene	n.d.	n.d.	n.d.	n.d.
4-Nitropyrene	97	54	101	119
3-Nitrofluoranthene	5	2	4	2
Sum of nitrated PAHs (ng/mg GEP)	231	142	276	187
Dinitrated PAHs (pg/mg GEP)				
Compound	E0	E15	n-But25	i-But25
1,3-Dinitropyrene	n.d.	n.d.	n.d.	n.d.
1,6-Dinitropyrene	n.d.	n.d.	4.5	3.5
1,8-Dinitropyrene	n.d.	n.d.	4.4	n.d.
Sum of dinitrated PAHs (ng/mg GEP)	0	0	8.9	3.5

* Carcinogenic according to IARC (Groups 1, 2A and 2B).

probably/possibly carcinogenic to humans (c-PAHs; Group 1, 2A or 2B) including benzo[*a*]pyrene, benz[*a*]anthracene, chrysene, benzo[*b*]fluoranthene, benzo[*k*]fluoranthene, dibenz[*a,h*]anthracene, and indeno[1,2,3-*cd*]pyrene ranged from 205.8 ng/mg for i-But25 to 261.8 ng/mg for n-But25; the carcinogenic PAH content in i-But25 extract was approx. 21%, 20% and 16% lower than in n-But25, E0 and E15 extracts, respectively. Importantly, E0 and E15 extracts contained the highest concentration of carcinogenic PAHs and methyl PAHs such as methylbenz[*a*]anthracenes, benzofluoranthenes, benzo[*a*]pyrene and indeno[1,2,3-*cd*]pyrene. On the other hand, a higher content of several oxygenated PAHs was found in i-But25 and n-But25 extracts compared to E0 and E15 (Table 1).

3.2. Cytotoxicity

Cytotoxicity was assessed using LDH and WST-1 assays after 24 h exposure to six doses (1, 10, 50, 100, 500 and 1000 µg/mL) of each GEP extract (Fig. 1). Both assays established a dose of 50 µg/mL as non-cytotoxic for all tested extracts. A dose of 100 µg/mL of n-But25 extract was already toxic and decreased the number of viable cells to 3% (measured by WST-1 assay) or 50% (measured by LDH assay), respectively. Other extracts exhibited decreased viability at a concentration of 500 µg/mL. Thus, 50 µg/mL was used as the common non-toxic dose for further experiments.

3.3. Gene expression profiling

3.3.1. Four hour exposure

After 4 h exposure, each GEP extract induced a specific gene expression pattern in BEAS-2B cells. The n-But25 extract altered the expression of the highest number of genes, both up- and downregulated (427) while other extracts were less effective (E0–257, E15–240 and i-But25–215, respectively; Fig. 2). Fifty-six genes were common for all treatments (for complete list of commonly deregulated genes see Supplementary file 2). Gene set enrichment analysis revealed a list of pathways that were significantly overrepresented across the gene set. Four clusters of these pathways were identified to share similar genes. Modulation of “SREBP signaling”, “C5 isoprenoid biosynthesis, mevalonate pathway”, “Cholesterol biosynthesis”, “Terpenoid backbone biosynthesis” and other related pathways were mainly affected by downregulated *HMGCR* and *HMGCS1* genes. *LPIN1*, *INSIG1*, *LDLR* additionally contributed to “SREBP signaling”, “SREBF and miR33 in cholesterol and lipid homeostasis” or “Regulation of Cholesterol Biosynthesis by SREBP (SREBF)” and together with upregulated *SPHK1* and *PTGES* also to “Metabolism of lipids and lipoproteins”. Other classes of overrepresented processes associated with plasminogen activating cascade such as “Blood coagulation”, “Dissolution of fibrin clot”, “Fibrinolysis pathway”, “Plasminogen activating cascade” and “Blood Clotting Cascade” were enriched with upregulated *SERPINB2*, *PLAT* and *F3*. These genes also contributed to “Senescence and autophagy” together with *IL24* and *IL1B* and “Ensemble of genes encoding ECM-

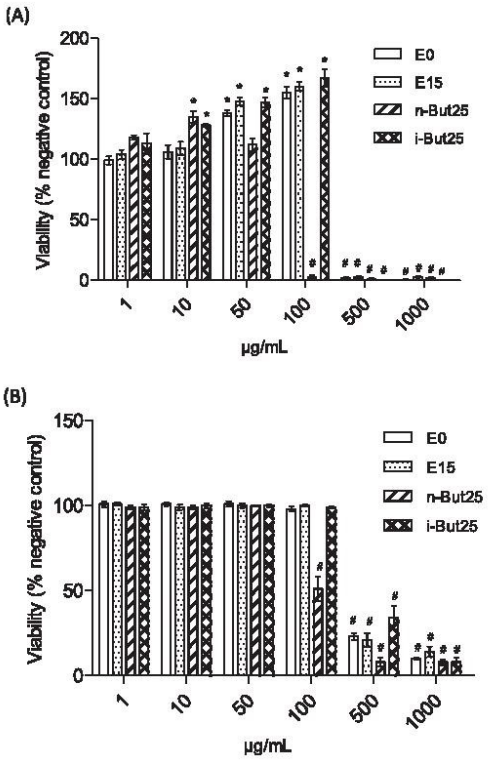

Fig. 1. Cytotoxicity evaluated by (A) WST-1 and (B) LDH Assay. BEAS-2B cells were exposed to six different concentrations of E0, E 15, n-But25 and i-But25 GEP extracts for 24 h and the results were expressed as a percentage of increased or decreased viability compared to the untreated control. *p-value < 0.05 (significant increase); #p-value < 0.05 (significant decrease) compared with negative control (unpaired t-test, two-tailed p-values).

associated proteins including ECM-affiliated proteins, ECM regulators and secreted factors" which were also accompanied by an increased expression of *IL24*, *GPC1*, *S100A9*, *ANXA8*, *IL1B*, *IL1B*, *FST* and *TGFA*. The combination of *PLAT*, *FGFR3* and *HMGCS1* affected "Endochondral Ossification". The alteration of cell junctions was characterized by modulated "Cell-cell junction organization", "Cell junction organization" and "Nectin adhesion pathway" (upregulated *CDH1*, *CDH3* and *CLDN1*) and finally, a combination of *LDLR* (downregulated) and *FOSL1*, *CCND2* (both upregulated) caused modulation of the "Wnt Signaling Pathway" and "DNA damage response (only ATM dependent)"(Table 2).

Importantly, the upregulation of cell cycle regulators such as *CDKN1A* (coding p21 protein), *GADD45* and pro-apoptotic *BIK* after exposure to E0 and E15, and n-But25 extracts supported the identification of the DNA damage response pathway.

The highest number of specific pathways was modulated by the n-But25 extract. These pathways include those involved in cell-cell junction and communication ("Anchoring fibril formation", "Collagen formation", "Stabilization and expansion of the E-cadherin adherens junction" and others), "TGF-β signaling", "Activin signaling","HIF-1α and HIF-2α transcription factor network", "Validated transcriptional targets of AP1 family members Fra1 and Fra2", several infectious

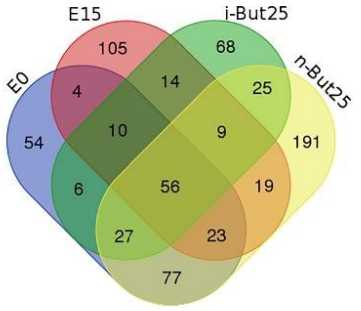

Fig. 2. Venn diagrams illustrating the overlap of common genes significantly deregulated in response to all GEP extract treatments, as well as numbers of specifically modulated genes by each individual GEP extract after 4 h incubation of BEAS-2B cells (cut-off p-value < 0.05, fold change > 1.5 and < 0.67).

diseases (Salmonella infection, Chagas disease), "Pathways in cancer" or "Direct p53 effectors" and many others. E0 and E15 additionally modulated "Regulation of Lipid Metabolism by Peroxisome proliferator-activated receptor alpha (PPARalpha)", and E0 itself induced changes in "Apoptotic cleavage of cell adhesion proteins" and related pathways. Complete lists of all significantly deregulated genes and over-represented pathways with the most contributing genes specific for each individual treatment after 4 h exposure are presented in Supplementary file 3.

3.3.2. Twenty-four hour exposure

The numbers of deregulated genes after 24 h exposure were more consistent across all treatments; we found 298, 254, 389 and 327 genes modulated in response to the exposure to E0, E15, i-But25 and n-But25 extracts, respectively. However, in contrast to 4 h, 24 h exposure to individual organic extracts induced more distinctive gene expression patterns (Fig. 3). Fewer genes (40) were found as commonly deregulated for all treatments (Supplementary file 2). This set contained different deregulated genes compared to the 4 h exposure set, and included the genes of biotransformation of xenobiotics (*CYP1A1*, *ALDH3A1*), intracellular signaling (several phosphatases and kinases such as *PPP1R15A*, *PHACTR3*, *RASIP1*, *CSK* and *CAMK2B*), DNA damage responses and cell cycle regulators (*GADD45A*, *CKS2*). The list also includes several genes, in which deregulation is associated with tumor promotion (upregulated *TAGLN*, *ID1*, *ARTN* and downregulated *BEX1* and *PRICKLE1*). However, gene set enrichment analysis identified only one pathway "Alanine, aspartate and glutamate metabolism" significantly overrepresented in the set of common genes with a contribution of upregulated *GTP2*, *ASS1* and *ASNS* genes.

Since the most distinctive gene expression pattern was exhibited by cells exposed to i-But25 extract (containing the lowest concentrations of PAHs), we focused on genes and pathways induced separately by three other GEP extracts. We identified 97 common genes shared by E0, E15 and n-But25 extract treatments only (Fig. 4, for the complete list of genes see Supplementary file 2) and numerous overrepresented pathways. A wide range of pathways related to cholesterol biosynthesis, mevalonate pathway and SREBP signaling ("Cholesterol biosynthesis", "Regulation of cholesterol biosynthesis by SREBP (SREBF)" and others) was deregulated due to diverse combinations of *HMGCR*, *HMGCS1*, *FDFT* and *ELOVL6* genes with suppressed expression. "Fatty acid, triacylglycerol and ketone body metabolism" pathway was modulated by downregulated *HMGCR*, *HMGCS1*, *FDFT* and *ELOVL6*, and upregulated *CYP1A1*, *ACADVL* and *AGPAT2*. *CYP1A1* and *CYP1B1* genes, both upregulated, contributed to the deregulation of "Bioactivation via cytochrome P450", "Synthesis of epoxy (EET) and dihydroeicosatrienoic acids (DHET)", "Synthesis of (16-20)-hydroxyeicosatetraenoic acids

Table 2
Top ranked common overrepresented pathways and contributing genes after 4 h exposure to all GEP extracts (cut-off corrected *p*-value < 0.05).

ID	Name	Source	Genes in annotation
219802	SREBP signaling	BioSystems: WikiPathways	↓ *LPIN1*, *INSIG1*, *HMGCR*, *HMGCS1*, *LDLR*
755438	SREBF and miR33 in cholesterol and lipid homeostasis	BioSystems: WikiPathways	↓ *HMGCR*, *HMGCS1*, *LDLR*
685551	Regulation of cholesterol biosynthesis by SREBP (SREBF)	BioSystems: REACTOME	↓ *INSIG1*, *HMGCR*, *HMGCS1*
413387	C5 isoprenoid biosynthesis, mevalonate pathway	BioSystems: KEGG	↓ *HMGCR*, *HMGCS1*
P00014	Cholesterol biosynthesis	PantherDB	↓ *HMGCR*, *HMGCS1*
142207	Mevalonate pathway I	BioSystems: BIOCYC	↓ *HMGCR*, *HMGCS1*
545288	Superpathway of geranylgeranyldiphosphate biosynthesis I (via mevalonate)	BioSystems: BIOCYC	↓ *HMGCR*, *HMGCS1*
198809	Cholesterol biosynthesis	BioSystems: WikiPathways	↓ *HMGCR*, *HMGCS1*
PW:0000454	Cholesterol biosynthetic	Pathway Ontology	↑ *PLAT*, *F3*
83022	Terpenoid backbone biosynthesis	BioSystems: KEGG	↓ *HMGCR*, *HMGCS1*
106142	Cholesterol biosynthesis	BioSystems: REACTOME	↓ *HMGCR*, *HMGCS1*
198812	Endochondral ossification	BioSystems: WikiPathways	↑ *PLAT*, *FGFR3* ↓ *HMGCS1*
160976	Metabolism of lipids and lipoproteins	BioSystems: REACTOME	↑ *SPHK1*, *PTGES* ↓ *HMGCS1*, *HMGCR*, *LDLR*, *LPIN1*, *INSIG1*
P00011	Blood coagulation	PantherDB	↑ *SERPINB2*, *PLAT*, *F3*
106061	Dissolution of fibrin clot	BioSystems: REACTOME	↑ *SERPINB2*, *PLAT*
M2842	Fibrinolysis pathway	MSigDB C2 BIOCARTA (v5.1)	↑ *SERPINB2*, *PLAT*
P00050	Plasminogen activating cascade	PantherDB	↑ *SERPINB2*, *PLAT*
198840	Blood clotting cascade	BioSystems: WikiPathways	↑ *SERPINB2*, *PLAT*
198825	Selenium pathway	BioSystems: WikiPathways	↑ *PLAT*, *IL1B* ↓ *LDLR*
198780	Senescence and autophagy	BioSystems: WikiPathways	↑ *IL24*, *SERPINB2*, *PLAT*, *IL1B*
M5885	Ensemble of genes encoding ECM-associated proteins including ECM-affiliated proteins, ECM regulators and secreted factors	MSigDB C2 BIOCARTA (v5.1)	↑ *IL24*, *GPC1*, *S100A9*, *SERPINB2*, *PLAT*, *ANXA8*, *IL1B*, *FST*, *TGFA*
119532	Cell-cell junction organization	BioSystems: REACTOME	↑ *CDH1*, *CDH3*, *CLDN1*
160966	Cell junction organization	BioSystems: REACTOME	↑ *CDH1*, *CDH3*, *CLDN1*
138054	Nectin adhesion pathway	BioSystems: Pathway Interaction Database	↑ *CDH1*, *CLDN1*
198789	Wnt signaling pathway	BioSystems: WikiPathways	↑ *FOSL1*, *CCND2* ↓ *LDLR*
198827	DNA damage response (only ATM dependent)	BioSystems: WikiPathways	↑ *FOSL1*, *CCND2* ↓ *LDLR*

↑upregulated ↓downregulated.

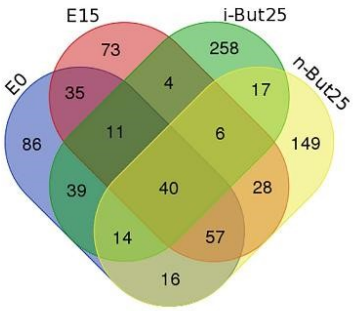

Fig. 3. Venn diagrams illustrating the overlap of common genes significantly deregulated in response to all GEP extract treatments, as well as the numbers of specifically modulated genes by each individual GEP extract after 24 h incubation of BEAS-2B cells (cut-off *p*-value < 0.05, fold change > 1.5 and < 0.67).

(HETE)" and "gamma-hexachlorocyclohexane degradation" pathways. Upregulated *IL1A* and *IL1B* were involved in "Interleukin-1 processing" pathway and together with *EGR1* in "Prion disease" pathway. Both *IL1A* and *IL1B* in combinations with upregulated *FOS*, *CYBA*, *ASS1* or downregulated *TGBR2* also played a role in "Leishmaniasis", "Osteoclast differentiation" and "Fluid shear stress and atherosclerosis" pathways. "Amino acid synthesis and interconversion (transamination)" and "Alanine, aspartate and glutamate metabolism" were pathways modulated due to the combination of upregulated *PSAT1*, *ASNS*, *ASS1* and *GPT2*. "Glucocorticoid receptor regulatory network" with a contribution of upregulated *CDKN1A*, *EGR1*, *FOS* and *PCK2* also appeared among the significantly altered processes. Upregulated *CYP1B1* and downregulated *CYP4X1* contributed to the overrepresentation of "melatonin degradation I" and "superpathway of melatonin degradation" (Table 3).

E0 and E15 extracts (which contained the highest concentrations of carcinogenic PAHs and methyl-PAHs with molecular weight range 242–276) specifically modulated "Oxidative stress", "Validated targets of C-MYC transcriptional repression" or "Protein processing in ER" and "Unfolded protein response" pathways while E15 altered the expression of genes contributing to "MAPK signaling pathway", "IFN-gamma pathway", "IL6-mediated signaling events", "Alpha6-Beta4 Integrin Signaling Pathway" or "Pertussis". "AhR pathway" and "Benzo(a) pyrene metabolism" were shared by E15 and n-But25; n-But25 further modulated "TGF-β receptor signaling", "Integrin signaling pathway", "E-cadherin signaling in the nascent adherens junction" or "eNOS activation". Beside pathways related to amino acid synthesis, conversions and glucose metabolism, i-But25 specifically deregulated "Protein processing in endoplasmic reticulum" pathway. "AhR activation" and "bioactivation via cytochrome P450" pathways were not significantly modulated, which is in accordance with the lowest PAH content compared to other tested extracts. Complete lists of significantly deregulated genes and pathways specific for each individual GEP extract treatment with the most contributing genes after 24 h exposure are presented in Supplementary file 4.

3.4. Quantitative RT-PCR validation of selected genes

For verification of gene expression changes detected by microarray analysis, we performed qRT-PCR of selected genes (Fig. 5). We focused

Table 3
Top ranked common overrepresented pathways and contributing genes after 24 h exposure to E0, E15 and n-but25.

ID	Name	Source	Genes in annotation
1270039	Activation of gene expression by SREBF (SREBP)	BioSystems: REACTOME	↓ *HMGCR, HMGCS1, FDFT, EVLOV6*
1270038	Regulation of cholesterol biosynthesis by SREBP (SREBF)	BioSystems: REACTOME	↓ *HMGCR, HMGCS1, FDFT, EVLOV6*
PW:0000454	Cholesterol biosynthetic	Pathway Ontology	↓ *HMGCR, HMGCS1, FDFT*
1270037	Cholesterol biosynthesis	BioSystems: REACTOME	↓ *HMGCR, HMGCS1, FDFT*
142269	Superpathway of cholesterol biosynthesis	BioSystems: BIOCYC	↓ *HMGCR, HMGCS1, FDFT*
P00014	Cholesterol biosynthesis	PantherDB	↓ *HMGCR, HMGCS1, FDFT*
MAP00100	MAP00100 sterol biosynthesis	GenMAPP	↓ *HMGCR, HMGCS1*
142207	Mevalonate pathway	BioSystems: BIOCYC	↓ *HMGCR, HMGCS1*
545288	Superpathway of geranylgeranyldiphosphate biosynthesis I (via mevalonate)	BioSystems: BIOCYC	↓ *HMGCR, HMGCS1*
413387	C5 isoprenoid biosynthesis, mevalonate pathway	BioSystems: KEGG	↓ *HMGCR, HMGCS1*
1270010	Fatty acid, triacylglycerol, and ketone body metabolism	BioSystems: REACTOME	↑ *CYP1A1, ACADVL, AGPAT2* ↓ *HMGCR, HMGCS1, FDFT1, ELOVL6*
1270159	Amino acid synthesis and interconversion (transamination)	BioSystems: REACTOME	↑ *PSAT1, ASNS, GPT2*
PW:0000375	Bioactivation via cytochrome P450	Pathway Ontology	↑ *CYP1A1, CYP1B1*
1270096	Synthesis of epoxy (EET) and dihydroxyeicosatrienoic acids (DHET)	BioSystems: REACTOME	↑ *CYP1A1, CYP1B1*
1270095	Synthesis of (16-20)-hydroxyeicosatetraenoic acids (HETE)	BioSystems: REACTOME	↑ *CYP1A1, CYP1B1*
PW:0000111	Gamma-hexachlorocyclohexane degradation	Pathway Ontology	↑ *CYP1A1, CYP1B1*
1269319	Interleukin-1 processing	BioSystems: REACTOME	↑ *IL1A, IL1B*
101144	Prion diseases	BioSystems: KEGG	↑ *EGR1, IL1A, IL1B*
144181	Leishmaniasis	BioSystems: KEGG	↑ *FOS, IL1A, IL1B, CYBA*
193147	Osteoclast differentiation	BioSystems: KEGG	↑ *FOS, IL1A, IL1B, CYBA* ↓ *TGFBR2*
1474302	Fluid shear stress and atherosclerosis	BioSystems: KEGG	↑ *FOS, ASS1, IL1A, IL1B, CYBA*
101142	Alanine, aspartate and glutamate metabolism	BioSystems: KEGG	↑ *ASNS, ASS1, GPT2*
138014	Glucocorticoid receptor regulatory network	BioSystems: Pathway Interaction Database	↑ *CDKN1A, FOS, EGR1, PCK2*
545356	Melatonin degradation I	BioSystems: BIOCYC	↑ *CYP1B1* ↓ *CYP4X1*
545359	Superpathway of melatonin degradation	BioSystems: BIOCYC	↑ *CYP1B1* ↓ *CYP4X1*

↑upregulated ↓downregulated.

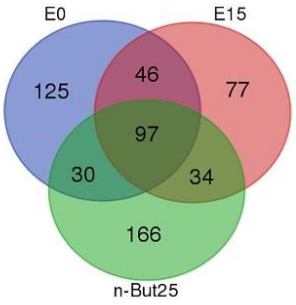

Fig. 4. Venn diagrams illustrating the overlap of common genes significantly deregulated in response to E0, E15 and n-But25 extract treatments, as well as the numbers of specifically modulated genes by selected GEP extract after 24 h incubation (cut-off *p*-value < 0.05, fold change > 1.5 and < 0.67).

on p53 target genes involved in the processes and pathways related to the cell cycle arrest, apoptosis and repair (*CDKN1A*, *BIK*, *GADD45A*), senescence (*GLB1*), immediate early stress response and activation of mitogen-activated protein kinase (MAPK) signaling (*FOS* and *EGR1*), remodeling of extracellular matrix (*SERPINB2*), modulation of cell adhesion (*CDH1*), metabolism of cholesterol and SREBP signaling (*HMGCR*), TGF-β signaling (*TGFBR2*) and activation of aryl hydrocarbon receptor and metabolism of PAHs (*TIPARP*, *CYP1A1*). We observed the strongest significant upregulation of *SERPINB2* (up to 25-fold induction) after 4 h exposure to all GEP extracts. Expression levels of *CDKN1A* and *CYP1A1* were also commonly significantly induced by all GEP extracts while the *HMGCR* mRNA level exhibited significant suppression. The expression of *BIK* and *TIPARP* was significantly elevated after E0 and n-But25 extracts treatments, and *CDH1* after E0 and E15. *TGFBR2* expression was significantly inhibited by i-But25 only. Generally, n-But25 induced the most profound changes in expression of upregulated genes. After 24 h exposure, abundant expression of *FOS*, *EGR1*, *SERPINB2* and particularly *CYP1A1* was detected. Similarly, *TIPARP*, *GADD45A*, *CDKN1A* and *BIK* (excluding E0 treatment) exhibited significant induction of mRNA levels. The expression level of *TGFBR2* was significantly reduced by the n-But25 extract treatment and *HMGCR* showed subtle downregulation (significant for E0 and i-But25 extract treatments). *GLB1* was slightly increased after all GEP extract treatments, and E15 extract induced a significant change.

Generally, the qRT-PCR method confirmed the significance of changes in the expression of selected genes and verified the validity of microarray results.

4. Discussion

4.1. GEP characteristics

Our results demonstrated that GEP mass concentration was substantially affected by the supplementation of gasoline fuel with bio-additives. Although some studies have documented that the addition of ethanol decreases particulate emissions (Maricq et al., 2012; Mulawa et al., 1997), we did not observe any significant effects of the E15 blend on GEP mass when compared to E0 (1.84 mg of particles produced by E15 vs 1.77 mg produced by E0 per km). A possible explanation could be that while oxygenated fuels tend to decrease particulate emissions, the two-carbon structure of ethanol is prone to increased production of particles via the ethylene pathway. On the other hand, the addition of both n-butanol and i-butanol resulted in a significant decrease of total particulate mass (i-But25 produced 1.32 mg particles and n-But25 generated the lowest mass, 0.90 mg per km), confirming the GEP mass reduction suggested by other relevant studies, where the decrease of GEP mass with increasing alcohol content in gasoline has been shown (Karavalakis et al., 2014). Partial inconsistency with the results achieved by other studies might be caused by many factors such as

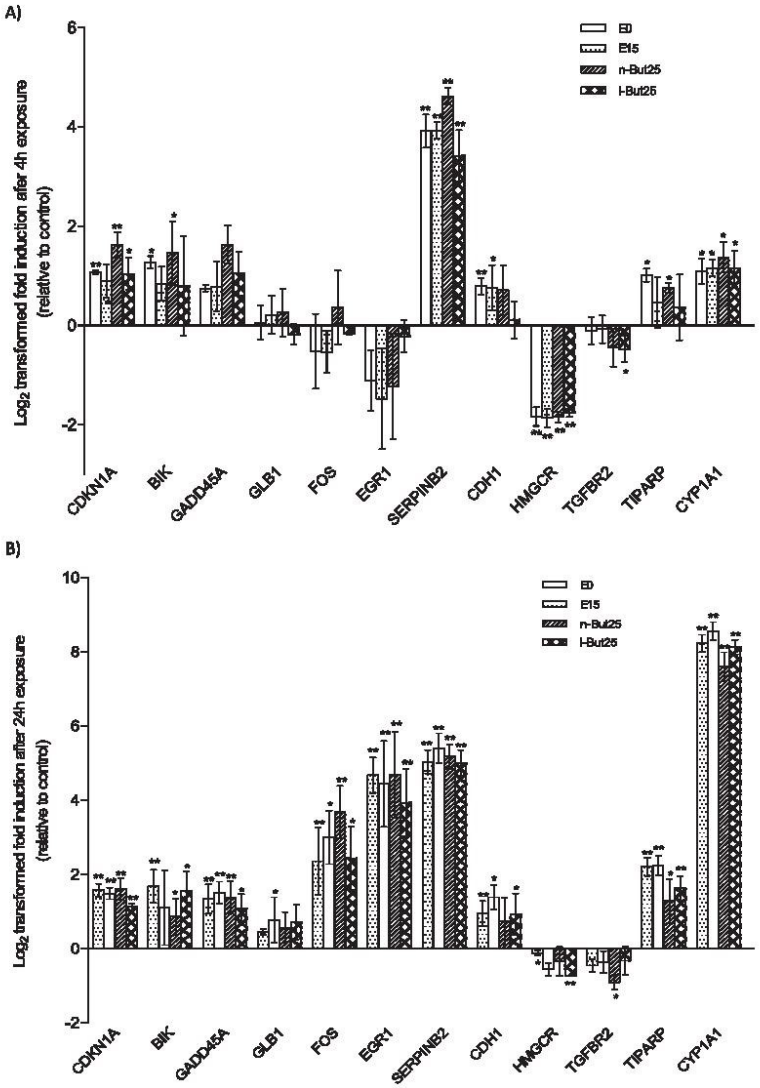

Fig. 5. Quantitative RT-PCR verification of changes in the expression of selected genes after (A) 4 h and (B) 24 h exposure of BEAS-2B cells. The fold induction was calculated using $2^{-\Delta\Delta Ct}$ method; genes with log-transformed fold induction value above 0 were considered as upregulated, and the value below 0 as downregulated. $^{*}p$-value < 0.05, $^{**}p$-value < 0.01 (unpaired *t*-test, two-tailed *p*-values).

differences among engine design, calibration, condition and operating conditions.

As chemical analysis revealed, the content of PAHs relative to an equal amount of GEPs (ng/mg) varied among extracts. Regardless of the lowest GEP mass production, n-But25 contained the highest amount of low-molecular-weight PAHs and their oxygenated derivatives, while i-But25 had the lowest; E15 contained a comparable content of PAHs as E0. It has been observed that the blending of gasoline with alcohol may lead to a lowering of PAH concentration due to the higher oxygen content affecting the combustion chemistry (Muñoz et al., 2016). In our study, the tested fuels were mixed so that the oxygen content was comparable among the individual blends. However, despite this fact, the PAH content in GEP extracts differed. We thus could not confirm the observation reported in (Muñoz et al., 2016).

4.2. Gene expression profiling

PAHs have been identified by many studies as the most prominent

genotoxic and carcinogenic components of polluted urban air. They are known to undergo a metabolic activation; a reaction involving a generation of highly reactive intermediates which interact with DNA, and form DNA adducts (Vojtisek-Lom et al., 2015a, 2015b). Furthermore, alternative pathways of PAH metabolism resulting in reactive oxygen species (ROS) generation and oxidative DNA damage also contribute to their genotoxic potential (Xue and Warshawsky, 2005). Besides genotoxic properties, the toxicity of PAHs involves an activation of the aryl hydrocarbon receptor (AhR), a multifunctional transcription factor which induces the expression of enzymes participating in PAH metabolic activation and detoxification, and also a wide range of other genes. Crosstalk of AhR with a variety of cellular processes and signaling pathways has been documented (Kung et al., 2009; Nebert et al., 2000; Puga et al., 2009). Additionally, disruption of cell-cell junctions and communication is the major nongenotoxic effect of lower-molecular weight PAHs such as phenanthrene, fluoranthene and pyrene leading to tumor promotion (Blaha et al., 2002). Also PAH derivatives, such as nitro- and oxygenated PAHs as well as additional compounds associated with GEPs, may contribute to multiple toxic events induced by GEPs.

To elucidate the possible mechanisms of toxic actions and molecular fingerprints of the complex mixture of organic compounds in extracts, we used gene expression profiling in human lung cells as a target tissue exposed to engine emissions. Although we identified numerous processes and pathways affected by the GEP treatment, we discuss below only those which are mostly attributed to the PAH exposure.

4.2.1. Activation of AhR, DNA damage response, cell cycle arrest

All GEP extracts induced expression of the AhR target genes *CYP1A1* and *TIPARP*, as confirmed by qRT-PCR. Inducibility of their expression was significantly higher after 24 h exposure. Expression of the other AhR-dependent gene, *CYP1B1*, was enhanced by nBut25, E0, E15, but not by iBut25. "Bioactivation via cytochrome P450" with the contribution of *CYP1A1* and *CYP1B1* was the pathway shared by n-But25, E0, E15. E0 and n-But25 additionally exhibited modulation of "AhR pathway". Induction of AhR gene battery including *CYP1A1*, *CYP1B1* and *ALDH3A1* play a crucial role in the biotransformation and toxicity of PAHs. CYP1 enzymes participate mainly in the conversion of PAHs to reactive intermediates (PAH diolepoxides or o-quinones) during the phase 1 of PAH activation, while *ALDH3A1* is involved in the detoxification of peroxides and aldehydes (Black et al., 2012).

In the case of i-But25, neither "AhR pathway" nor "bioactivation via cytochrome P450" was found. Although increased expression of *CYP1A1* and *TIPARP* implicates activation of AhR and the metabolism of PAHs, the i-But25 extract exerted a weaker genotoxic effect due to the lower content of AhR-inducing PAHs with molecular weight 252 (see Table 2), and possibly triggered a different stress response.

One of the key common events recognized in response to all GEP extract treatments after 4 h exposure was the deregulation of genes associated with DNA damage response (DDR), possibly due to the high content of PAHs in all extracts as detected by chemical analysis. DDR is triggered after exposure to various genotoxic compounds including PAHs. Activation of p53 is the key regulator mediating cell cycle arrest, DNA repair, senescence, and apoptosis. The transcriptional output of p53 target genes regulating the broad spectrum of DNA damage responses depends, beside other factors, on the stabilization levels of p53 and the persistence of its activation (Roos et al., 2016).

Transcriptional activation of *CDKN1A* and *GADD45A*, direct targets of p53, is associated with the arresting and anti-proliferative function (Bieging et al., 2014). As confirmed by qRT-PCR, all GEP extracts had already significantly upregulated *CDKN1A* and *GADD45A* expression by 4 h exposure, and mRNA levels also remained increased after 24 h. These results strongly suggest a cell cycle arrest following DNA damage. Although expression of *BIK*, a pro-apoptotic p53-dependent regulator, was enhanced after 4 h exposure and even more profound upregulation was detected after 24 h exposure, no transcription of other pro-apoptotic markers was found. "DNA damage response (only ATM dependent)" was the pathway commonly modulated by all GEP extracts after 4 h exposure, and it was characterized by upregulated *FOSL1* and *CCND2* and downregulated *LDLR*. *FOSL1*, a member of the Fos gene family, belongs to a group of immediate early response genes that can dimerize with proteins of the JUN family to form the transcription factor complex AP-1. Increased activity of AP-1 is linked to modulation of cellular fate such as proliferation, differentiation, cell cycle arrest, death or senescence. AP-1 activated by a low dose of a DNA-damaging agent in immediate-early response manner causes stimulation of DNA repair genes and maintains nucleotide excision repair capacity, thus preventing cell death (Christmann and Kaina, 2013).

In addition to the common DDR pathway, n-But25 and E15 extracts, which contained higher PAH concentration, modulated the expression of various other genes involved in "Direct p53 effectors pathway". This may support the fact that each GEP extract treatment induced a different level of DNA damage and triggered a slightly different response to DNA damage, which could consequently affect the cell fate decision.

Importantly, the "Glucocorticoid receptor regulatory network" modulated by E0, E15 and n-But25, comprised of upregulated *CDKN1A*, *EGR1*, *FOS* and *PCK2* genes after 24 h exposure. It has been documented that the glucocorticoid receptor has an important role in mediating the cell cycle arrest, and cooperates with the DNA damage response pathway by acting as a tumor suppressor (Rogatsky et al., 1997). *EGR1* and *FOS*, immediate-early response genes, are activated by p38/JNK mitogen-activated protein kinases (MAPK) in response to stress stimuli and regulate the transcription of downstream genes and adaptation (Bahrami and Drablos, 2016). In our data, a strong induction of these genes was found after 24 h exposure to all GEP extracts, suggesting the activation of MAPK signaling. Consistently, "MAPK signaling" was the pathway modulated after E15 exposure, and contained upregulated *GADD45A*, *DDIT3*, *AKT1*, *FOS*, *ATF4*, *IL1A*, *IL1B* and downregulated *HSPA1B* and *TGFBR2*. After exposure to stressful stimuli, a crosstalk between p53 and MAPK signaling occurs. *GADD45A* is an established p53 target but is also associated with p38/JNK signaling and activated AP-1 complex, and coordinates the repair function. It has been demonstrated that GADD45A reciprocally contribute to the activation and stabilization of p53 via p38 (Salvador et al., 2013).

As confirmed by qRT-PCR, the crucial p53 target mediating cell cycle arrest, *CDKN1A*, was significantly upregulated after 24 h exposure to all GEP extracts, thus indicating the persistence of DDR signaling. Specifically for E0 and n-But25 exposure, expression of other known p53 targets implicates the orchestrated cellular response under the p53 control, including signaling of growth arrest (upregulated *NDRG1*), apoptosis (upregulated *GDF15*, *TP73L*, downregulated *DKK1*), DNA repair (upregulated *GDF15*) and many others.

After 24 h exposure, more distinctive responses to individual GEP extract treatments in BEAS-2B cells were found. A set of 40 genes common for all treatments was enriched with the only pathway, "Alanine, aspartate and glutamate metabolism" comprising of upregulated *GPT2*, *ASNS* and *ASS1* genes. Regardless of the common genes, each GEP extract modulated a variety of metabolic pathways. Alterations of gene expression were mostly in favor of enhanced glycolysis and pentose phosphate production, biosynthesis and interconversion of amino acids or carbon metabolism (see Supplementary file 3). Upon DNA damage, cells use extracellular nutrients such as glucose and glutamine to generate NADPH and glycolytic intermediates for nucleotide synthesis, DNA repair and antioxidant defense, including the replenishment of glutathione. In the study of Bensaad and Vousden (2007), the role of p53 in the regulation of glucose metabolism after DNA damage was established. Interestingly, a mechanistic connection between p53-coordinated DNA repair and nucleotide synthesis, and the promotion of pentose phosphate pathway has been observed (Franklin et al., 2016).

4.2.2. Metabolism of lipids and steroids

Another important finding was modulation of pathways related to cholesterol and lipid biosynthesis in cells exposed to all GEP extracts. SREBP is a key transcription factor that regulates the transcription of genes encoding mevalonate pathway, an essential metabolic process that uses acetyl-CoA to produce steroid and isoprenoid lipids. Homeostatic control of sterols and isoprenoids are closely related to cell proliferation and activation of p53. Proliferating cells exhibit an increased consumption of nucleotides synthesized from the cholesterol and isoprenoid sources to sustain the replication, thereby the inhibition mediated by p53 represents the mechanism by which damaged cells maintain the cell cycle arrest and prevent aberrant replication (Sanchez-Alvarez et al., 2015). In our data, suppressed expression of SREBP signaling-downstream genes (*HMGCS1*, *HMGCR*, *INSIG1*, *LPIN1* or *LDLR*) involved in the mevalonate pathway may indicate inhibition of cholesterol and fatty acid synthesis, due to the PAH exposure-mediated cell cycle arrest. Accordingly, Tanos et al. (2012), demonstrated that AhR regulates the cholesterol biosynthetic pathway in a dioxin response element-independent manner in mice. Another study confirmed the role of PAHs in the disruption of cholesterol metabolism, and showed that B[*a*]P exposure induced a depletion of cholesterol and modulation of lipid composition in cholesterol-rich membrane microdomaines (lipid rafts), that was linked to a reduced expression of *HMGCR*. The authors established the role of AhR and reactive oxygen species (ROS) formation in the regulation of the expression of genes involved in lipid biosynthesis, leading to membrane remodeling and intracellular alkalinization, which is an early apoptotic event in F258 cells (Tekpli et al., 2010). In contrast, study of Sun et al. (2012) showed activation of the SREBP transcription factor and upregulation of several downstream genes in BEAS-2B cells after 4-days lasting exposure to PM10.

Apart from i-But25, all other GEP extracts further induced several changes after 24 h, similar as observed for 4 h exposure. The inhibition of sterol biosynthesis, SREBP signaling and other related pathways was mainly driven by the downregulation of *HMGCR*, *HMGCS1* and *FDFT1* genes. Apart from the evidence of SREBP signaling being most likely regulated as a consequence of DNA damage, a different line of evidence suggests a link between ER stress and lipid metabolism. Cholesterol accumulation in endoplasmic reticulum (ER) membranes can cause ER stress. Protein kinase RNA (PKR)-like ER kinase (PERK)-mediated phosphorylation of eukaryotic translation initiation factor-2 (eIF2) antagonizes sterol-regulated enhancer binding protein (SREBP) activation, to decrease cholesterol synthesis (Ron and Walter, 2007).

4.2.3. Senescence-associated secretory phenotype, modulation of extracellular matrix, cell adhesion and intercellular communication

"Senescence and autophagy" pathway was another commonly modulated process upon all GEP extract treatments. Senescence is characterized by a naturally irreversible cell-cycle arrest due to persistent DNA damage response signaling followed by changes in morphology, heterochromatin formation and alteration of gene expression. Senescent cells secrete a number of proteins such as pro-inflammatory cytokines, chemokines and proteases known as senescence-associated secretory phenotype (SASP) factors that alter the local tissue environment. Apart from the protective role (attracting of immune cells, cell cycle arrest prevents tumor development), senescent cells also facilitate tumor cell invasion by degradation of extracellular matrix (ECM) and inducing an epithelial-to-mesenchymal transition (EMT) (Coppe et al., 2010).

In our study, the expression of several SASP biomarkers contributing to the deregulation of "Senescence and autophagy" and "Ensemble of genes encoding ECM-associated proteins including ECM-affiliated proteins, ECM regulators and secreted factors" after 4 h exposure to all GEP extracts was found. Tissue-type plasminogen activator *PLAT* and its inhibitor *SERPINB2* (*PAI-2*) were massively upregulated after all GEP extract treatments. Plasminogen activators and their inhibitors are important regulators of extracellular proteolysis, and act in the blood coagulation cascade. Recently, they have been implicated in paracrine activities of SASP due to the ability to alter the ECM and consequent EMT and cancer cell invasion (Laberge et al., 2012). In line with our results, other studies have reported the induction of *SERPINB2* in response to PAH exposure. (Oeder et al., 2012) observed increased expression of *SERPINB2* upon exposure to PAH containing outdoor PM_{10} and linked the changes with activated AhR. The serine proteases are also targets of the AhR pathway; its role in the regulation of cell adhesion and matrix metabolism has been discussed in the review of Kung et al. (2009).

Importantly, we detected a slight but not significant increase in the expression of *GLB1*, a widely used senescent biomarker, by qRT-PCR after 24 h exposure to all GEP extracts. Although the secretion of several SASP factors was observed, the development of senescence requires long-lasting DNA damage signaling, and 24 h exposure might not be sufficient.

Altered expression of several genes involved in cell junction and adhesion was detected in our study. E-cadherin (*CDH1*) and claudin (*CLDN1*) are key components of cell-to-cell adhesion; downregulation of E-cadherin is considered as a hallmark of EMT that leads to destabilization of adherens junctions (Yilmaz and Christofori, 2009). The link between EMT and senescence, where EMT factors regulate senescence and vice versa, has been described (Smit and Peeper, 2010). Moreover, activation of AhR has been linked to disruption of the contact inhibition and downregulation of E-cadherin level in liver epithelial cells, thus stimulating EMT (Dietrich and Kaina, 2010; Prochazkova et al., 2011). In contrast, our data showed significant upregulation of E-cadherin and P-cadherin (*CDH1* and *CDH3*), claudin and several keratins in lung bronchial BEAS-2B cells; significant upregulation of *CDH1* was also verified by qRT-PCR. Numerous studies have evidenced that E-cadherin is a growth and proliferation suppressor and is regulated by Rb; loss of Rb function results in E-cadherin deletion and causes EMT and tumor invasiveness. Several lines of evidence suggest possible effects of various stressful conditions (hypoxia, mechanical stress or genotoxic stress) on the enhancement of ECM integrity and cell survival (Jean et al., 2011).

Out of all the treatments, n-But25 extract containing the highest levels of low-molecular-weight PAHs exhibited the most robust changes in cell junction, adhesion and communication pathways, as well as actin cytoskeleton reorganization, characterized by increased expression of numerous adhesion and cytoskeletal molecules such as cadherins, laminins and integrins (see Table 2 and Supplementary file 2). The increased expression of non-soluble extracellular matrix proteins is probably associated with SASP (Coppe et al., 2010), and also, the enhanced regulation of intercellular contacts and cell adhesion might be linked to a protective mechanism of DDR against loss of sensitivity to pro-apoptotic stimuli (Lewis et al., 2002). Possibly, the AhR pathway can further contribute to altered matrix metabolism and deposition, through interactions with other signaling pathways (Kung et al., 2009).

Notably, the amino acid metabolic pathways discussed above, together with "Protein processing in endoplasmic reticulum (ER)" were the only processes modulated by i-But25. During physiological and pathological or stressful conditions such as DNA damage, an accumulation of unfolded proteins may occur causing ER stress and unfolded protein response (UPR). When the stress persists and homeostasis is not mitigated, cell death is triggered (Hetz, 2012; Ron and Walter, 2007). Similar to the i-But25 extract, also E0 and E15 modulated pathways "Protein processing and folding in ER", "Activation of Chaperone Genes by ATF6-alpha" and "Unfolded protein response", respectively. However, a difference exists among the i-But25, E0 and E15 responses. Unlike iBut25, E0 and E15 extracts elevated the expression of genes employed in the ER stress response (*DDIT3*, *XBP1*, *ATF4*), while iBut25 rather upregulated the genes involved in ubiquitination and degradation of unfolded proteins (*FBOX2*, *CUL1*, *UBQLN2* or *SYVN1*), indicating a shift towards re-establishment of the homeostasis. It has been

widely proposed that the functional insufficiency of cellular cleaning and housekeeping mechanisms for protein and organelle degradation, including proteasome and autophagy pathways, play a pivotal role in the accumulations of deleterious cellular components and the regulation of cell senescence (Ravid and Hochstrasser, 2008; Ron and Walter, 2007).

4.2.4. Proinflammatory and tumor promotion-related pathways

Importantly, oxidative stress and other tumor promotion-related genes and pathways such as NF-κB, Wnt, TGF-β were also modulated by E0, E15 and n-But25 extracts but not by i-But25 extract. Oxidative stress leads to many cytoplasmic and nuclear responses, a number of genes and cellular pathways are known to be regulated by redox changes. To name a few examples, the transcription of many "redox-sensitive" genes is mediated through the activation of stress-activated MAP kinases such as JUN, ERK and p38-MAPK and activation of NF-κB, a central mediator of the immune and inflammatory response.

We observed increased expression of *IL24* and *IL1β* after 4 h exposure to all GEP extract treatments and *IL1β* with *IL1α* after 24 h exposure. Genotoxic stress and DDR activate various inflammatory signaling pathways to mediate innate immune responses. NF-κB is a key pro-inflammatory transcription factor activated via different stress-induced pathways, and has been linked to the induction of SASP (Salminen et al., 2012). Interestingly, *IL1α*, upregulated by all GEP extracts, has been demonstrated to sense directly the DNA lesions in the damage focus, and its ability to report and communicate danger signals to the surrounding tissue was established as a novel signaling cascade (Idan et al., 2015).

Regulation of TGF-β signaling pathway and other tumor promotion-related genes and pathways were detected after all GEP extract exposures. Apart from the canonical TGF-β pathway involving the activation of SMADs, TGF-β can also activate other pathways such as PI3K/AKT, p38MAPK, MAPK–ERK, JNK and others to regulate directly or indirectly apoptosis, extracellular matrix production and differentiation. Although TGF-β signaling is very complex and determination of the resulting effects depends on the intensity and duration of activation of the pathways, or by differential activation of Smad vs. nonSmad signaling pathways, TGF-β receptors seems to play a crucial role in the specificity of the response. A critical role of the TGFBR2 expression level in modulation of CDKN1A-mediated apoptosis has been proposed (Rojas et al., 2009). Therefore, suppressed *TGFBR2* expression by all GEP extracts observed in our study may substantially regulate the specific cellular response and exert a pro-survival effect. Upregulation of *ID1* (effector of TGF-β/Smad signaling) and *ARTN* (secreted ligand of TGF-β receptors involved in the recruitment and activation of the Smad family transcription factors) may also contribute to the deregulation of TGF-β signaling. Moreover, upregulation of *JAG2* (an activator of Notch signaling) and downregulation of *PRICKLE1* (a negative regulator of Wnt/β-catenin pathway), suggests possible deregulation of additional developmental processes linked, after "unwanted" non-physiological activation, to tumor promotion and progression. Also, upregulation of *TAGLN* whose overexpression has been associated with tumor progression in lung adenocarcinoma (Wu et al., 2014), was identified in this study. Taken together, gene expression data suggest that GEP extracts may deregulate tumor-promoting processes such as TGF-β, Notch and Wnt signaling pathways. In contrast to other extracts, none of these pathways were significantly overrepresented among genes modulated by i-But25.

4.3. Study limitations

Overall, this study has several limitations similar to those described in detail in our previous work (Libalova et al., 2016): 1. The exposure of cell culture to organic extracts may have a different impact on cellular response compared to whole particles, since they cause many other adverse effects. We focused on gene expression profiles specific for organic compounds only. 2. This study compares a qualitative composition of GEP extracts but does not take into account the total amount of produced particles; although GEP released from n-But25 fuel contained the highest concentration of PAHs, n-But25 simultaneously produced much lower GEP mass, which should be considered in a potential risk assessment. 3. Our interpretation of the results covers the most profound effects; however, other effects which are not involved in the Discussion may also be important. Moreover, gene expression profiling is only the first step to reveal the precise mechanisms of the action. Despite that, we believe that the results reported here are useful base for further studies investigating the mechanisms in more detail.

5. Conclusions

Our findings indicate that the supplementation of neat gasoline fuel with different biofuels substantially influenced the particle mass, the chemical composition and the toxic properties of GEP emissions. The addition of isobutanol and n-butanol reduced particulate emission, while ethanol exhibited no effect. The n-But25 extract contained the highest concentration of PAHs, and together with E0 and E15 exerted stronger genotoxic potency and other AhR-mediated effects than the i-But25 extract.

Functional analysis of gene expression changes in BEAS-2B cells revealed many common deregulated processes and pathways for all GEP extracts. DNA damage response as the key modulated process after 4 h exposure, common for all GEP extract treatments. Although altered expression of common genes implicates the induction of subsequent events following DNA damage such as cell cycle arrest, cellular senescence, remodeling of ECM, cell adhesion and suppressed metabolism of steroids and SREBP signaling, the differences among treatments were found on a pathway level. 24 h exposure to E0, E15 and n-But25 extracts resulted in an elevated expression of DDR-related genes, activation of genes involved in PAH metabolism, pro-inflammatory response, stress response related to MAPK signaling, endoplasmic reticulum stress and unfolded protein response or enhanced metabolism of cellular nutrients such as amino acids, glucose and nucleotides. The n-But25 modulated specifically TGFβ receptor, integrin, cadherin and eNOS signaling pathways linked to tumor promotion; E0 and E15 extracts containing the highest concentrations of PAHs with molecular weight 252 and 276 induced then most significantly oxidative stress. Fewer processes were modulated the by i-But25 extract compared to other treatments. The distinctive gene expression pattern of i-But25 was more profound after 24 h exposure when the only pathway Alanine, aspartate and glutamate metabolism was shared by all GEP extract treatments. While gene expression profiles of E0, E15 and n-But25 extracts showed persistent DNA damage response and stress signaling, i-But25 indicated a shift towards homeostasis restoration and cell recovery. This may implicate that the i-But25 extract induced a lower level of DNA damage, probably due to the lower content of genotoxic PAHs, and triggered a different cellular response.

Supplementary data to this article can be found online at https://doi.org/10.1016/j.tiv.2018.02.002.

Conflicts of interest

The authors declare no conflict of interest.

Transparency document

The Transparency document associated with this article can be found, in online version.

Acknowledgments

The study was supported by the Czech Science Foundation (Projects No. P503-12-G147 and 14-22016S) and by the Czech Ministry of Youth,

Education and Sports Projects No. LO1305, LO1311 (Czech Technical University in Prague) and LO1508. The authors also acknowledge the assistance provided by the Research Infrastructure NanoEnviCz, supported by the Ministry of Education, Youth and Sports of the Czech Republic under Project No. LM2015073 and Operational Program Prague–Competitiveness (CZ.2.16/3.1.00/21528 and CZ.2.16/3.1.00/24507).

References

André, M., 2004. The ARTEMIS European driving cycles for measuring car pollutant emissions. Sci. Total Environ. 334, 73–84. http://dx.doi.org/10.1016/j.scitotenv.2004.04.070.

Andrysik, Z., Vondracek, J., Marvanova, S., Ciganek, M., Neca, J., Pencikova, K., Mahadevan, B., Topinka, J., Baird, W.M., Kozubik, A., Machala, M., 2011. Activation of the aryl hydrocarbon receptor is the major toxic mode of action of an organic extract of a reference urban dust particulate matter mixture: the role of polycyclic aromatic hydrocarbons. Mutat. Res. Fundam. Mol. Mech. Mutagen. 714 (1–2), 53–62.

Bahrami, S., Drablos, F., 2016. Gene regulation in the immediate-early response process. Adv. Biol. Regul. 62, 37–49. http://dx.doi.org/10.1016/j.jbior.2016.05.001.

Bensaad, K., Vousden, K.H., 2007. p53: new roles in metabolism. Trends Cell Biol. 17 (6), 286–291. http://dx.doi.org/10.1016/j.tcb.2007.04.004.

Bieging, K.T., Mello, S.S., Attardi, L.D., 2014. Unravelling mechanisms of p53-mediated tumour suppression. Nat. Rev. Cancer 14 (5), 359–370. http://dx.doi.org/10.1038/nrc3711.

Bisig, C., Roth, M., Müller, L., Comte, P., Heeb, N., Mayer, A., Czerwinski, J., Petri-Fink, A., Rothen-Rutishauser, B., 2016. Hazard identification of exhausts from gasoline-ethanol fuel blends using a multi-cellular human lung model. Environ. Res. 151, 789–796. http://dx.doi.org/10.1016/j.envres.2016.09.010.

Black, W., Chen, Y., Matsumoto, A., Thompson, D.C., Lassen, N., Pappa, A., Vasiliou, V., 2012. Molecular mechanisms of ALDH3A1-mediated cellular protection against 4-hydroxy-2-nonenal. Free Radic. Biol. Med. 52 (9), 1937–1944. http://dx.doi.org/10.1016/j.freeradbiomed.2012.02.050.

Blaha, L., Kapplova, P., Vondracek, J., Upham, B., Machala, M., 2002. Inhibition of gap-junctional intercellular communication by environmentally occurring polycyclic aromatic hydrocarbons. Toxicol. Sci. 65 (1), 43–51.

Chen, J., Bardes, E.E., Aronow, B.J., Jegga, A.G., 2009. ToppGene Suite for gene list enrichment analysis and candidate gene prioritization. Nucleic Acids Res. 37, W305–W311.

Christmann, M., Kaina, B., 2013. Transcriptional regulation of human DNA repair genes following genotoxic stress: trigger mechanisms, inducible responses and genotoxic adaptation. Nucleic Acids Res. 41 (18), 8403–8420. http://dx.doi.org/10.1093/nar/gkt635.

Coppe, J.P., Desprez, P.Y., Krtolica, A., Campisi, J., 2010. The senescence-associated secretory phenotype: the dark side of tumor suppression. Annu. Rev. Pathol. 5, 99–118. http://dx.doi.org/10.1146/annurev-pathol-121808-102144.

Dietrich, C., Kaina, B., 2010. The aryl hydrocarbon receptor (AhR) in the regulation of cell-cell contact and tumor growth. Carcinogenesis 31 (8), 1319–1328. http://dx.doi.org/10.1093/carcin/bgq028.

Du, P., Kibbe, W.A., Lin, S.M., 2008. lumi: a pipeline for processing Illumina microarray. Bioinformatics 24 (13), 1547–1548.

Franklin, D.A., He, Y., Leslie, P.L., Tikunov, A.P., Fenger, N., Macdonald, J.M., Zhang, Y., 2016. p53 coordinates DNA repair with nucleotide synthesis by suppressing PFKFB3 expression and promoting the pentose phosphate pathway. Sci. Rep. 6, 38067. http://dx.doi.org/10.1038/srep38067.

Hetz, C., 2012. The unfolded protein response: controlling cell fate decisions under ER stress and beyond. Nat. Rev. Mol. Cell Biol. 13 (2), 89–102. http://dx.doi.org/10.1038/nrm3270.

Idan, C., Peleg, R., Elena, V., Martin, T., Cicerone, T., Mareike, W., Lydia, B., Marina, F., Gerhard, M., Elisa, F.-M., Dinarello, C.A., Ron, A.N., Robert, S., 2015. IL-1α is a DNA damage sensor linking genotoxic stress signaling to sterile inflammation and innate immunity. Sci. Rep. 5, 14756. http://dx.doi.org/10.1038/srep14756.

Jean, C., Gravelle, P., Fournie, J.J., Laurent, G., 2011. Influence of stress on extracellular matrix and integrin biology. Oncogene 30 (24), 2697–2706. http://dx.doi.org/10.1038/onc.2011.27.

Jin, C., Yao, M., Liu, H., Lee, C.-f.F., Ji, J., 2011. Progress in the production and application of n-butanol as a biofuel. Renew. Sust. Energ. Rev. 15 (8), 4080–4106. http://dx.doi.org/10.1016/j.rser.2011.06.001.

Karavalakis, G., Short, D., Chen, V., Espinoza, C., Berte, T., Durbin, T., Asa-Awuku, A., Jung, H., Ntziachristos, L., Amanatidis, S., Bergmann, A., 2014. Evaluating Particulate Emissions from a Flexible Fuel Vehicle with Direct Injection when Operated on Ethanol and Iso-butanol Blends. http://dx.doi.org/10.4271/2014-01-2768.

Kung, T., Murphy, K.A., White, L.A., 2009. The aryl hydrocarbon receptor (AhR) pathway as a regulatory pathway for cell adhesion and matrix metabolism. Biochem. Pharmacol. 77 (4), 536–546. http://dx.doi.org/10.1016/j.bcp.2008.09.031.

Laberge, R.M., Awad, P., Campisi, J., Desprez, P.Y., 2012. Epithelial-mesenchymal transition induced by senescent fibroblasts. Cancer Microenviron. 5 (1), 39–44. http://dx.doi.org/10.1007/s12307-011-0069-4.

Lewis, J.M., Truong, T.N., Schwartz, M.A., 2002. Integrins regulate the apoptotic response to DNA damage through modulation of p53. Proc. Natl. Acad. Sci. U. S. A. 99 (6), 3627–3632. http://dx.doi.org/10.1073/pnas.062698499.

Libalova, H., Rossner, Pavel, Vrbova, K., Brzicova, T., Sikorova, J., Vojtisek-Lom, M., Beranek, V., Klema, J., Ciganek, M., Neca, J., Pencikova, K., Machala, M., Topinka, J., 2016. Comparative analysis of toxic responses of organic extracts from diesel and selected alternative fuels engine emissions in human lung BEAS-2B cells. Int. J. Mol. Sci. 17 (11), 1833.

Livak, K.J., Schmittgen, T.D., 2001. Analysis of relative gene expression data using real-time quantitative PCR and the 2−ΔΔCT method. Methods 25 (4), 402–408. http://dx.doi.org/10.1006/meth.2001.1262.

Maricq, M.M., Szente, J.J., Jahr, K., 2012. The impact of ethanol fuel blends on PM emissions from a light-duty GDI vehicle. Aerosol Sci. Technol. 46 (5), 576–583. http://dx.doi.org/10.1080/02786826.2011.648780.

Mulawa, P.A., Cadle, S.H., Knapp, K., Zweidinger, R., Snow, R., Lucas, R., Goldbach, J., 1997. Effect of ambient temperature and E-10 fuel on primary exhaust particulate matter emissions from light-duty vehicles. Environ. Sci. Technol. 31 (5), 1302–1307. http://dx.doi.org/10.1021/es960514r.

Muñoz, M., Heeb, N.V., Haag, R., Honegger, P., Zeyer, K., Mohn, J., Comte, P., Czerwinski, J., 2016. Bioethanol blending reduces nanoparticle, PAH, and alkyl- and nitro-PAH emissions and the genotoxic potential of exhaust from a gasoline direct injection flex-fuel vehicle. Environ. Sci. Technol. 50 (21), 11853–11861. http://dx.doi.org/10.1021/acs.est.6b02606.

Nebert, D.W., Roe, A.L., Dieter, M.Z., Solis, W.A., Yang, Y., Dalton, T.P., 2000. Role of the aromatic hydrocarbon receptor and [Ah] gene battery in the oxidative stress response, cell cycle control, and apoptosis. Biochem. Pharmacol. 59 (1), 65–85.

Oeder, S., Jorres, R.A., Weichenmeier, I., Pusch, G., Schober, W., Pfab, F., Behrendt, H., Schierl, R., Kronseder, A., Nowak, D., Dietrich, S., Fernandez-Caldas, E., Lintelmann, J., Zimmermann, R., Lang, R., Mages, J., Fromme, H., Buters, J.T., 2012. Airborne indoor particles from schools are more toxic than outdoor particles. Am. J. Respir. Cell Mol. Biol. 47 (5), 575–582. http://dx.doi.org/10.1165/rcmb.2012-0139OC.

Pope III, C.A., Dockery, D.W., 2006. Health effects of fine particulate air pollution: lines that connect. J. Air Waste Manage. Assoc. 56 (6), 709–742.

Prochazkova, J., Kabatkova, M., Bryja, V., Umannova, L., Bernatik, O., Kozubik, A., Machala, M., Vondracek, J., 2011. The interplay of the aryl hydrocarbon receptor and beta-catenin alters both AhR-dependent transcription and Wnt/beta-catenin signaling in liver progenitors. Toxicol. Sci. 122 (2), 349–360. http://dx.doi.org/10.1093/toxsci/kfr129.

Puga, A., Ma, C., Marlowe, J.L., 2009. The aryl hydrocarbon receptor cross-talks with multiple signal transduction pathways. Biochem. Pharmacol. 77 (4), 713–722. http://dx.doi.org/10.1016/j.bcp.2008.08.031.

Ravid, T., Hochstrasser, M., 2008. Diversity of degradation signals in the ubiquitin-proteasome system. Nat. Rev. Mol. Cell Biol. 9 (9), 679–690. http://dx.doi.org/10.1038/nrm2468.

Rogatsky, I., Trowbridge, J.M., Garabedian, M.J., 1997. Glucocorticoid receptor-mediated cell cycle arrest is achieved through distinct cell-specific transcriptional regulatory mechanisms. Mol. Cell. Biol. 17 (6), 3181–3193.

Rojas, A., Padidam, M., Cress, D., Grady, W.M., 2009. TGF-beta receptor levels regulate the specificity of signaling pathway activation and biological effects of TGF-beta. Biochim. Biophys. Acta 1793 (7), 1165–1173. http://dx.doi.org/10.1016/j.bbamcr.2009.02.001.

Ron, D., Walter, P., 2007. Signal integration in the endoplasmic reticulum unfolded protein response. Nat. Rev. Mol. Cell Biol. 8 (7), 519–529. http://dx.doi.org/10.1038/nrm2199.

Roos, W.P., Thomas, A.D., Kaina, B., 2016. DNA damage and the balance between survival and death in cancer biology. Nat. Rev. Cancer 16 (1), 20–33. http://dx.doi.org/10.1038/nrc.2015.2.

Salminen, A., Kauppinen, A., Kaarniranta, K., 2012. Emerging role of NF-κB signaling in the induction of senescence-associated secretory phenotype (SASP). Cell. Signal. 24 (4), 835–845. http://dx.doi.org/10.1016/j.cellsig.2011.12.006.

Salvador, J.M., Brown-Clay, J.D., Fornace Jr., A.J., 2013. Gadd45 in stress signaling, cell cycle control, and apoptosis. Adv. Exp. Med. Biol. 793, 1–19. http://dx.doi.org/10.1007/978-1-4614-8289-5_1.

Sanchez-Alvarez, M., Zhang, Q., Finger, F., Wakelam, M.J., Bakal, C., 2015. Cell cycle progression is an essential regulatory component of phospholipid metabolism and membrane homeostasis. Open Biol. 5 (9), 150093. http://dx.doi.org/10.1098/rsob.150093.

Smit, M.A., Peeper, D.S., 2010. Epithelial-mesenchymal transition and senescence: two cancer-related processes are crossing paths. Aging (Albany NY) 2 (10), 735–741. http://dx.doi.org/10.18632/aging.100209.

Smyth, G.K., 2004. Linear models and empirical bayes methods for assessing differential expression in microarray experiments. Stat. Appl. Genet. Mol. Biol. 3http://dx.doi.org/10.2202/1544-6115.1027. (Article3).

Sun, H., Shamy, M., Kluz, T., Munoz, A.B., Zhong, M., Laulicht, F., Alghamdi, M.A., Khoder, M.I., Chen, L.C., Costa, M., 2012. Gene expression profiling and pathway analysis of human bronchial epithelial cells exposed to airborne particulate matter collected from Saudi Arabia. Toxicol. Appl. Pharmacol. 265 (2), 147–157. http://dx.doi.org/10.1016/j.taap.2012.10.008.

Tanos, R., Patel, R.D., Murray, I.A., Smith, P.B., Patterson, A.D., Perdew, G.H., 2012. Aryl hydrocarbon receptor regulates the cholesterol biosynthetic pathway in a dioxin response element-independent manner. Hepatology 55 (6), 1994–2004. http://dx.doi.org/10.1002/hep.25571.

Tekpli, X., Rissel, M., Huc, L., Catheline, D., Sergent, O., Rioux, V., Legrand, P., Holme, J.A., Dimanche-Boitrel, M.T., Lagadic-Gossmann, D., 2010. Membrane remodeling, an early event in benzo[a]pyrene-induced apoptosis. Toxicol. Appl. Pharmacol. 243 (1), 68–76. http://dx.doi.org/10.1016/j.taap.2009.11.014.

Tripathy, S., Sahoo, S., Srivastava, D.K., 2017. Gasoline direct injection—challenges. In: Agarwal, A.K., De, S., Pandey, A., Singh, A.P. (Eds.), Combustion for Power Generation and Transportation: Technology, Challenges and Prospects. Springer Singapore, Singapore, pp. 367–379.

Vojtisek-Lom, M., Beranek, V., Stolcpartova, J., Pechout, M., Klir, V., 2015a. Effects of n-butanol and Isobutanol on particulate matter emissions from a euro 6 direct-injection spark ignition engine during laboratory and on-road tests. SAE Int. J. Engines 8 (5), 2338–2350. http://dx.doi.org/10.4271/2015-24-2513.

Vojtisek-Lom, M., Pechout, M., Dittrich, L., Beránek, V., Kotek, M., Schwarz, J., Vodička, P., Milcová, A., Rossnerová, A., Ambrož, A., Topinka, J., 2015b. Polycyclic aromatic hydrocarbons (PAH) and their genotoxicity in exhaust emissions from a diesel engine during extended low-load operation on diesel and biodiesel fuels. Atmos. Environ. 109, 9–18. http://dx.doi.org/10.1016/j.atmosenv.2015.02.077.

Wu, X., Dong, L., Zhang, R., Ying, K., Shen, H., 2014. Transgelin overexpression in lung adenocarcinoma is associated with tumor progression. Int. J. Mol. Med. 34 (2), 585–591. http://dx.doi.org/10.3892/ijmm.2014.1805.

Xia, T., Zhu, Y., Mu, L., Zhang, Z.-F., Liu, S., 2016. Pulmonary diseases induced by ambient ultrafine and engineered nanoparticles in twenty-first century. Nat. Sci. Rev. 3 (4), 416–429. http://dx.doi.org/10.1093/nsr/nww064.

Xue, W., Warshawsky, D., 2005. Metabolic activation of polycyclic and heterocyclic aromatic hydrocarbons and DNA damage: a review. Toxicol. Appl. Pharmacol. 206 (1), 73–93. http://dx.doi.org/10.1016/j.taap.2004.11.006.

Yilmaz, M., Christofori, G., 2009. EMT, the cytoskeleton, and cancer cell invasion. Cancer Metastasis Rev. 28 (1–2), 15–33. http://dx.doi.org/10.1007/s10555-008-9169-0.

International Journal of
Molecular Sciences

MDPI

Article

Toxic Effects of the Major Components of Diesel Exhaust in Human Alveolar Basal Epithelial Cells (A549)

Pavel Rossner Jr. [1,*], Simona Strapacova [2], Jitka Stolcpartova [1,3], Jana Schmuczerova [1], Alena Milcova [1], Jiri Neca [2], Veronika Vlkova [1], Tana Brzicova [1], Miroslav Machala [2] and Jan Topinka [1]

1 Institute of Experimental Medicine, Academy of Sciences of the Czech Republic, Videnska 1083, 142 20 Prague, Czech Republic; jitka.stolcpartova@biomed.cas.cz (J.St.); schmucze@yahoo.com (J.Sc.); milcova@biomed.cas.cz (A.M.); veronika.vlkova@biomed.cas.cz (V.V.); tana.brzicova@biomed.cas.cz (T.B.); jtopinka@biomed.cas.cz (J.T.)

2 Veterinary Research Institute, Hudcova 70, 621 00 Brno, Czech Republic; strapacova@vri.cz (S.S.); neca@vri.cz (J.N.); machala@vri.cz (M.M.)

3 Institute for Environmental Studies, Faculty of Science, Charles University, Benatska 2, 128 01 Prague 2, Czech Republic

* Correspondence: prossner@biomed.cas.cz; Tel.: +42-024-106-2763; Fax: +42-024-106-2785

Academic Editor: Marcello Iriti
Received: 1 July 2016; Accepted: 17 August 2016; Published: 26 August 2016

Abstract: We investigated the toxicity of benzo[a]pyrene (B[a]P), 1-nitropyrene (1-NP) and 3-nitrobenzanthrone (3-NBA) in A549 cells. Cells were treated for 4 h and 24 h with: B[a]P (0.1 and 1 μM), 1-NP (1 and 10 μM) and 3-NBA (0.5 and 5 μM). Bulky DNA adducts, lipid peroxidation, DNA and protein oxidation and mRNA expression of *CYP1A1*, *CYP1B1*, *NQO1*, *POR*, *AKR1C2* and *COX2* were analyzed. Bulky DNA adducts were induced after both treatment periods; the effect of 1-NP was weak. 3-NBA induced high levels of bulky DNA adducts even after 4-h treatment, suggesting rapid metabolic activation. Oxidative DNA damage was not affected. 1-NP caused protein oxidation and weak induction of lipid peroxidation after 4-h incubation. 3-NBA induced lipid peroxidation after 24-h treatment. Unlike B[a]P, induction of the aryl hydrocarbon receptor, measured as mRNA expression levels of *CYP1A1* and *CYP1B1*, was low after treatment with polycyclic aromatic hydrocarbon (PAH) nitro-derivatives. All test compounds induced mRNA expression of *NQO1*, *POR*, and *AKR1C2* after 24-h treatment. *AKR1C2* expression indicates involvement of processes associated with reactive oxygen species generation. This was supported further by *COX2* expression induced by 24-h treatment with 1-NP. In summary, 3-NBA was the most potent genotoxicant, whereas 1-NP exhibited the strongest oxidative properties.

Keywords: benzo[a]pyrene; 1-nitropyrene; 3-nitrobenzanthrone; bulky DNA adducts; oxidative damage; gene expression

1. Introduction

Environmental air pollution affects most of the human population. In industrialized countries, air pollutants originate from three major sources: domestic heating, industrial activities, and traffic. Despite substantial technological advances resulting in decreased fuel consumption and lower emissions, road traffic remains a significant source of air pollution, particularly in metropolitan areas. Recently, the International Agency for Research on Cancer (IARC) classified outdoor air pollution as "carcinogenic to humans" (Group 1) [1,2].

From a complex mixture of chemicals and particles produced by incomplete combustion of organic material, including oil and oil products, polycyclic aromatic hydrocarbons (PAHs) are noteworthy due to their metabolism to reactive compounds that can bind to nucleic acids and proteins, cause their damage and/or loss of function, and induce mutations. Apart from binding to macromolecules resulting in formation of PAH–DNA adducts or protein adducts, some PAHs may generate reactive oxygen species (ROS) and thus induce oxidative stress. Nitro-PAHs may be produced by direct sources (diesel and gasoline exhaust), but may also be generated by reactions of PAHs with oxides of nitrogen in the atmosphere [3]. Nitro-PAHs are characterized by persistence in the environment and high mutagenic and carcinogenic activities in model systems. Their concentrations in the environment are lower than those of parent PAHs, but some nitro-PAHs have been shown to act as direct mutagens that do not require metabolic activation [3].

Benzo[a]pyrene has been classified as carcinogenic to humans (IARC, Group 4) [4]. Three pathways have been proposed for metabolic activation of B[a]P: (i) cytochrome P450-catalyzed conversion of B[a]P to epoxide that is further metabolized by epoxide hydrolase and CYP1A1 to diol epoxide, which binds to DNA; (ii) P450 peroxidase-catalyzed activation to reactive radical cations that bind to DNA; (iii) dihydrodiol dehydrogenase-catalyzed conversion of dihydrodiols to catechol. The latter is unstable and undergoes auto-oxidation first to a semiquinone radical and hydrogen peroxide followed by formation of *o*-quinone and the superoxide anion. Eventually, these events lead to redox-cycling and induction of oxidative stress [5].

1-Nitropyrene (1-NP) is the most abundant nitro-PAH in emissions from diesel engines. It is considered to be the main contributor of direct-acting mutagenicity of diesel exhaust as assessed by the Ames test [6]. 1-NP is metabolized by three major pathways. The first pathway utilizes cytochrome P450-mediated ring oxidation to non-K-region phenols and K-region oxides; K-region oxides are converted further to trans-dihydrodiols or phenols that bind to macromolecules. The second pathway involves nitroreduction in one- or two-electron steps to form 1-nitrosopyrene and *N*-hydroxy-1-aminopyrene or 1-aminopyrene. The third pathway is a combination of ring oxidation and nitroreduction followed by acetylation [7,8]. 1-NP also induces ROS production by induction of endoplasmic reticulum (ER) stress mediated by 1-NP metabolites formed during nitroreduction [9]. Another source of ROS is a reactive intermediate of 1-NP, the *N*-hydroxy radical, which undergoes auto-oxidation coupled with generation of the superoxide radical and hydrogen peroxide [10]. 1-NP has been classified as "probably carcinogenic to humans" (IARC, Group 2A, [11]).

3-Nitrobenzanthrone (3-NBA) is one of the most potent mutagens and a potential human carcinogen (IARC Group 2B, possibly carcinogenic to humans, [2]). Apart from incomplete combustion of fossil fuels, 3-NBA can also originate from the reaction of benzanthrone (a pollutant abundant in exhaust gas and particles from diesel engines) with nitrogen oxides in the atmosphere [11]. In organisms, 3-NBA is metabolized by nitroreduction catalyzed by xanthine oxidase (XO), NAD(P)H:quinone oxidoreductase (NQO1) and NAPDH:cytochrome P450 oxidoreductase (POR) to *N*-hydroxy-3-aminobenzanthrone (N-OH-ABA). The latter can be metabolized further by two pathways: the major pathway results in formation of non-acetylated 3-NBA DNA adducts, whereas the minor pathway leads to acetylated 3-NBA DNA adducts [12,13]. Furthermore, N-OH-ABA can induce production of the superoxide radical and hydrogen peroxide as well as subsequent oxidative damage to macromolecules [13]. Unlike B[a]P and 1-NP, CYP enzymes do not contribute significantly to 3-NBA activation [14].

Inhalation is a primary route of exposure of humans to PAHs and their derivatives. Hence, studies on cell models derived from lung tissue could provide the most relevant information on the negative effects of these compounds to humans. A549 is a human lung adenocarcinoma cell line commonly used as a model in genetic toxicology. Being a cancer cell line, this model is not suitable for cytogenetic applications, or studies of cell cycle regulation. However, its morphology and many basic cellular functions are comparable with normal alveolar epithelial type-II cells. Hence, these cells are useful for studies of metabolic processes associated with exposure to xenobiotics and their toxic effects [15,16].

Here, we aimed to compare toxic effects (including damage to DNA, lipids and proteins as well as mRNA expression of selected relevant genes) in A549 cells treated with model PAH (B[a]P) and nitro-PAHs (1-NP, 3-NBA). The genes included those encoding enzymes participating in the metabolism of xenobiotics (CYP1A1, CYP1B1, NQO1, POR) and/or associated with oxidative stress (aldo-keto reductase (AKR1C2), cyclooxygenase-2 (COX2)). We tested two concentrations of each compound. To account for the different kinetics of biologic effects induced by test compounds, we treated cells for two different time intervals (4 h and 24 h).

2. Results

2.1. Bulky DNA Adducts

Four-hour treatment of A549 cells with 0.1 and 1 μM of B[a]P induced one major adduct spot whereas, after 24-h treatment with 1 μM of B[a]P, three additional minor spots representing three other adduct types were detected (Figure 1). With the exception of the 10-μM concentration after 24-h incubation (when multiple DNA adduct spots were visible on autoradiographs), 1-NP induced weak adduct spots. In contrast, 0.5 μM and 5 μM 3-NBA induced 3–4 strong adduct spots after 4-h and 24-h treatment (Figure 1). Levels of bulky DNA adducts after treatment with 3-NBA (5 μM) exceeded 275 adducts/10^8 nucleotides (Figure 2A). After 24-h treatment with 1 μM B[a]P, levels of DNA adducts reached 175 adducts/10^8 nucleotides, whereas the 0.1 μM concentration of B[a]P induced much lower levels of DNA adducts (≈10 adducts/10^8 nucleotides). Interestingly, although levels of DNA adducts induced by 3-NBA after 24-h treatment were high, we observed almost 50% reduction in their levels after incubation with 3-NBA (0.5 μM). Levels of DNA adducts induced by 1-NP were low even after 24-h incubation with the compound, when the higher test dose (10 μM) induced almost 30 adducts/10^8 nucleotides (Figure 2B).

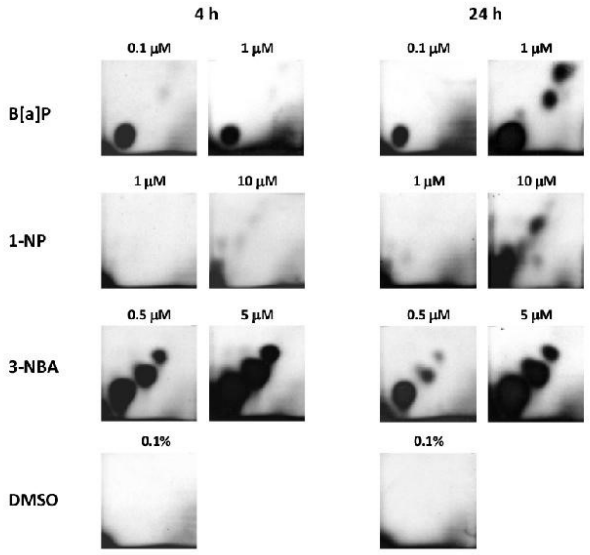

Figure 1. Autoradiographs of TLC maps of ^{32}P-labeled DNA digests after incubation of A549 cells with various concentrations of benzo[a]pyrene, 1-nitropyrene and 3-nitrobenzanthrone for 4 h and 24 h. Control panels depict analyses of A549 cells treated withdimethylsulfoxide. DNA (5 μg) was analyzed using the nuclease P1 method of sensitivity enhancement. Screen-enhanced autoradiography was performed at −80 °C for 24 h.

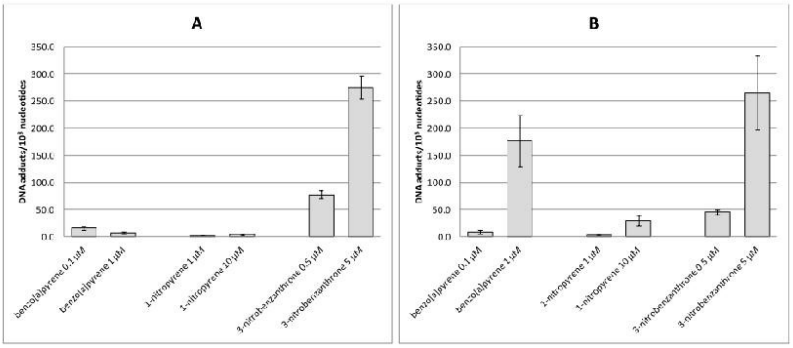

Figure 2. Levels of bulky DNA adducts/10^8 nucleotides induced after treatment of A549 cells with benzo[a]pyrene, 1-nitropyrene and 3-nitrobenzanthrone for 4 h (**A**) and 24 h (**B**). Data represent mean values ± standard deviation from two triplicates from two independent experiments (analyzed as $n = 6$) (negative control subtracted). Based on the comparison with autoradiographs (Figure 1), bulky DNA adduct levels induced by 1-nitropyrene were negligible.

2.2. Oxidative Damage to DNA, Lipids and Proteins

Analyses of oxidative damage (Figures 3–5) indicate relatively weak and non-consistent effects of test compounds on markers of oxidative damage. None of the time intervals and test (non-cytotoxic) doses of B[a]P increased levels of oxidative damage to DNA (8-oxodG, Figure 3A,B), lipids (15-F_{2t}-IsoP, Figure 4A,B) or proteins (protein carbonyls, Figure 5A,B) significantly. Most of the significant biological effects could be ascribed to 1-NP treatment. This compound increased levels of lipid peroxidation after 4-h treatment (Figure 4A) and induced protein oxidation after 4-h and 24-h incubation (Figure 5A,B). However, no significant effect on DNA oxidation (Figure 3A,B) or lipid peroxidation after 24-h treatment (Figure 4B) was detected. 3-NBA significantly induced lipid peroxidation after 24-h treatment; levels of 15-F_{2t}-IsoP increased to 200% of the relative control level, and were comparable for both test concentrations (Figure 4B). Levels of lipid peroxidation after 4-h treatment with 3-NBA were elevated, but the increase was not significant (Figure 4A). We did not detect an effect of this compound on oxidation of DNA or protein (Figures 3A,B and 5A,B).

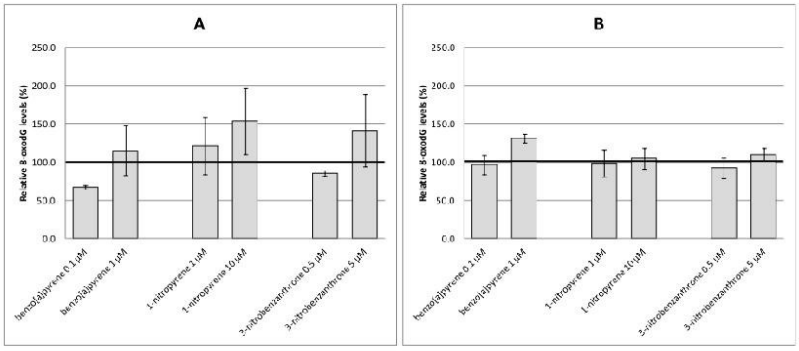

Figure 3. 8-oxodG levels relative to the control (%) induced after treatment of A549 cells with benzo[a]pyrene, 1-nitropyrene and 3-nitrobenzanthrone for 4 h (**A**) and 24 h (**B**). Data represent mean values ± standard deviation from two triplicates from two independent experiments (analyzed as $n = 6$). The control level of 8-oxodG is represented by an emboldened horizontal line.

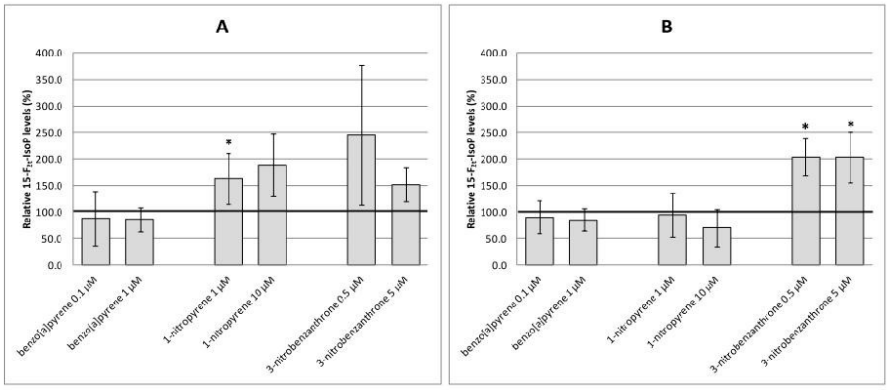

Figure 4. 15-F2t-IsoP levels relative to the control (%) induced after treatment of A549 cells with benzo[a]pyrene, 1-nitropyrene and 3-nitrobenzanthrone for 4 h (**A**) and 24 h (**B**). Data represent mean ± standard deviation from two triplicates from two independent experiments (analyzed as $n = 6$). Asterisks denote significant (* $p < 0.05$) changes. The control level of 15-F2t-IsoP is represented by an emboldened horizontal line. 1-nitropyrene (1 μM, 4 h) and 3-nitrobenzanthrone (0.5 μM and 5 μM, 24 h) significantly increased 15-F2t-IsoP levels.

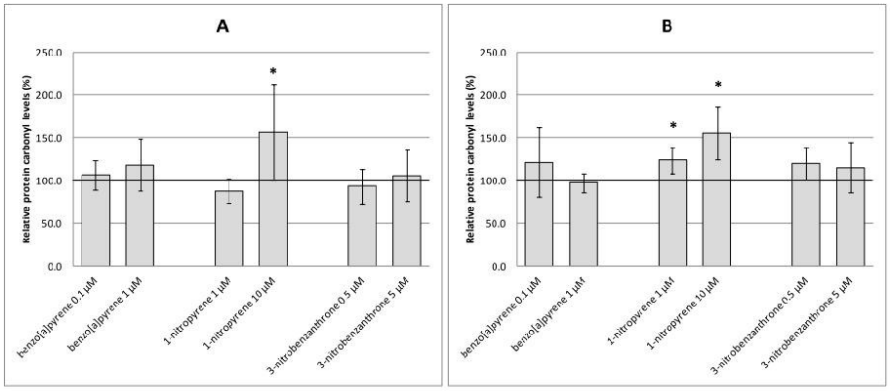

Figure 5. Levels of protein carbonyls relative to the control (%) induced after treatment of A549 cells with benzo[a]pyrene, 1-nitropyrene and 3-nitrobenzanthrone for 4 h (**A**) and 24 h (**B**). Data represent mean ± standard deviation from two triplicates from two independent experiments (analyzed as $n = 6$). Asterisks denote significant (* $p < 0.05$) changes. The control level of protein carbonyls is represented by an emboldened horizontal line. 1-nitropyrene (10 μM, 4 h; 1 μM and 10 μM, 24 h) significantly increased protein carbonyl levels.

2.3. mRNA Expression of Selected Genes

Expression levels of genes encoding metabolic activation enzymes are shown in Figure 6. As expected, B[a]P induced *CYP1A1* expression in both tested doses and intervals (Figure 6A,B). Similarly, this compound induced *CYP1B1* expression, although no significant effect was observed for the 4-h treatment with 0.1 μM B[a]P. Both tested nitro-PAHs required the 24-h treatment to exert consistent induction of *CYP1A1* and *CYP1B1* expression (Figure 6B,D), although 3-NBA (5 μM) induced *CYP1A1* expression (Figure 6A) and 1-NP (1 μM) induced *CYP1B1* expression (Figure 6C) after the

4-h treatment. However, the induction levels were weak compared to those after the B[a]P treatment. None of the tested compounds had significant effect on *NQO1* and *POR* expression after the 4-h treatment (Figure 6E,G). In most cases, the longer treatment period increased expression of these mRNAs significantly (Figure 6F,H). For *NQO1*, no effects were observed for 1-NP at 10 μM (Figure 6F). Substantial differences in induction levels between compounds were not observed, but B[a]P tended to induce higher expression of *NQO1*. Highest levels of *POR* expression were induced after 1-NP treatment; for B[a]P and 3-NBA, only the lower test dose induced significant changes in gene expression (Figure 6H).

Although none of the test compounds increased *AKR1C2* expression after 4-h treatment (Figure 7A), induction was observed for all chemicals and doses after the longer treatment period. 1-NP was identified as the most potent inducer of *AKR1C2* expression (Figure 7B). Four-hour treatment of A549 cells with B[a]P and 3-NBA resulted in a significant decrease in *COX2* expression (Figure 7C). This decrease was also observed after 24-h treatment with 1 μM B[a]P. 1-NP, particularly at the higher test dose, was a strong inducer of *COX2* after 24-h incubation (Figure 7D).

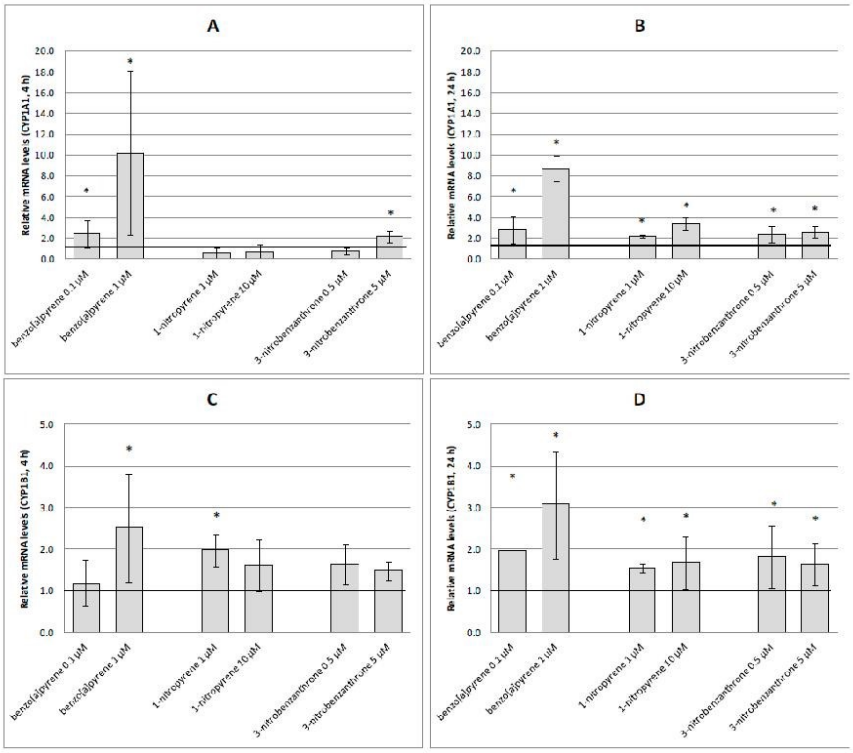

Figure 6. *Cont.*

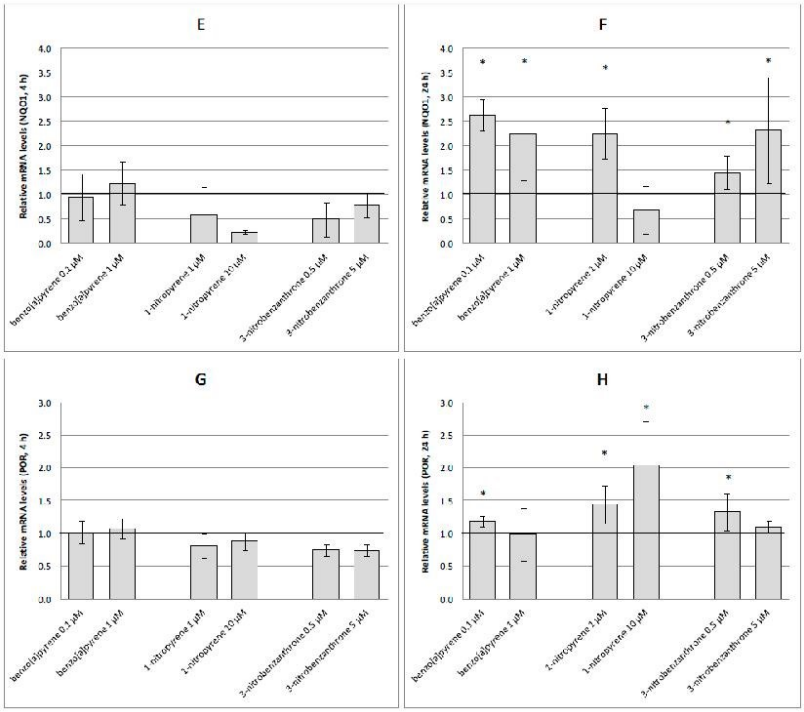

Figure 6. Relative mRNA levels (fold changes relative to the control) induced after treatment of A549 cells with benzo[a]pyrene, 1-nitropyrene and 3-nitrobenzanthrone. (**A**) *CYP1A1*, 4 h; (**B**) *CYP1A1*, 24 h; (**C**) *CYP1B1*, 4 h; (**D**) *CYP1B1*, 24 h; (**E**) *NQO1*, 4 h; (**F**) *NQO1*, 24 h; (**G**) *POR*, 4 h; (**H**) POR, 24 h. Data represent mean values ± standard deviation from two triplicates from two independent experiments (analyzed as $n = 6$). Asterisks denote significant (* $p < 0.05$) gene expression changes relative to the control. Control expression level of the respective gene is represented by an emboldened horizontal line.

3. Discussion

In the present study, we aimed to characterize differences in the response of A549 cells treated with a model PAH (B[a]P) and nitro-PAHs (1-NP, 3-NBA), i.e., compounds with different metabolism. We selected bulky DNA adducts and markers of oxidative damage as endpoints for the comparison of toxic effects of test compounds. Furthermore, we analyzed mRNA expression of selected genes to identify potential mechanisms responsible for changes in levels of studied endpoints. The rationale behind the selection of compounds was the fact that B[a]P was the only PAH classified by IARC as being carcinogenic to humans (Group 1) and nitro-PAHs were pollutants associated mostly with diesel exhaust and thus with traffic.

Selection of a suitable cell model is critical for interpretation of the results of in vitro toxicity testing. Lungs are the primary target for air pollutants, so cells of lung-tissue origin are a logical choice for investigation of the toxic effects of PAHs and nitro-PAHs. Results are affected mainly by the activity of metabolic activation enzymes in a selected cell line. A recent study compared genotoxic responses to B[a]P in three human cell lines (including A549 cells) and observed extreme variability for various markers (including DNA adducts) [17]. Authors observed a moderate increase in levels of BPDE–N^2–dGuo adducts in A549 cells after 24-h treatment, but only for low doses of the compound

(0.2 μM); at higher B[a]P concentrations, levels of DNA adducts decreased. While is not in agreement with our present data, it should be noted that in our study not only specific BPDE-N^2-dGuo, but bulky DNA adducts, were analyzed. Furthermore, previously we analyzed levels of bulky DNA adducts after treatment of A549 cells with B[a]P concentrations ranging from 1 nM to 10 μM, and detected a decrease in levels of DNA adducts but only at >1 μM [18]. The decrease probably reflects general toxicity of high B[a]P doses negatively impacting cellular functions. On the other hand, after 4-h treatment, levels of bulky DNA adducts were low for both test concentrations of B[a]P. In general, levels of bulky DNA adducts are dependent upon the activity of CYP1A1, a key enzyme responsible for the metabolism of B[a]P [5]. Its expression is further modulated by the activity of transcription factor Nrf2 [19,20]. Although at the 4-h time-point we detected a significant increase in the expression of *CYP1A1* mRNA at a low B[a]P dose, the metabolic activity of cells (i.e., levels of the active CYP1A1 protein) was not probably sufficient to increase levels of bulky DNA adducts.

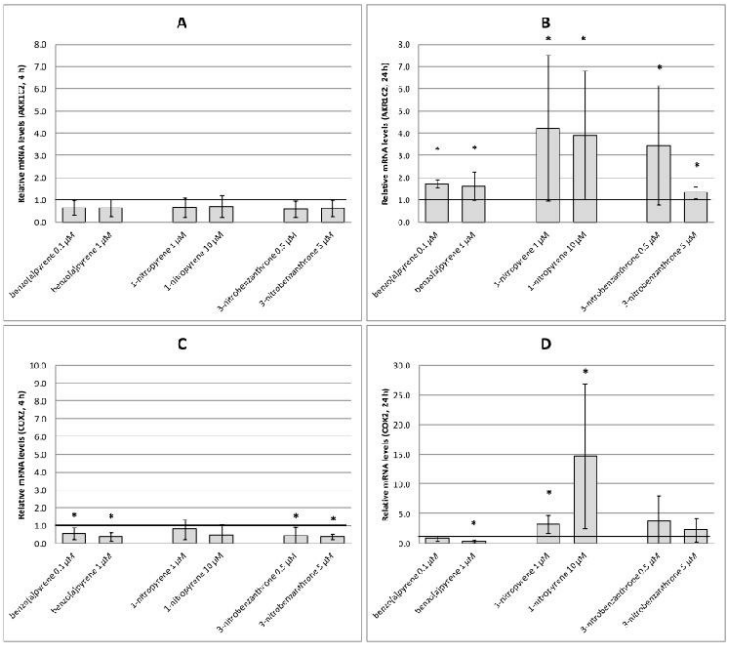

Figure 7. Relative mRNA levels (fold changes relative to the control) induced after treatment of A549 cells with benzo[a]pyrene, 1-nitropyrene and 3-nitrobenzanthrone. (**A**) *AKR1C2*, 4 h; (**B**) *AKR1C2*, 24 h; (**C**) *COX2*, 4 h; (**D**) *COX2*, 24 h. Data represent mean values ± standard deviation from two triplicates from two independent experiments (analyzed as $n = 6$). Asterisks denote significant (* $p < 0.05$) gene expression changes relative to the control. The control expression level of the respective gene is represented by an emboldened horizontal line.

We observed very low levels of bulky DNA adducts induced by 1-NP, even after 24-h treatment with a higher dose of the compound. It has been demonstrated that 1-NP is activated by human CYP1 enzymes (especially CYP1B1) to exert genotoxicity in the *umu* test [21]. 1-NP induces only low DNA adduct formation and also low levels of *CYP1A1* and *CYP1B1* mRNA in human bronchial epithelial (BEAS-2B) cells [22]; another study showed that induction of expression of *CYP1A1* and *CYP1B1* in these cells was very weak [23]. This observation is in agreement with our data, which indicated low induction of *CYP1B1* mRNA even after 24-h treatment with 10 μM 1-NP. Interestingly, this treatment,

which resulted in the highest levels of bulky DNA adducts induced by 1-NP, was also associated with almost fourfold induction of *CYP1A1* expression. Thus, the low DNA adduct levels induced by 1-NP in A549 cells could be caused by low expression of the gene encoding the CYP1B1 enzyme in this cell line. Our data also suggest that CYP1A1 may play a part in the formation of 1-NP-induced bulky DNA adducts.

3-NBA is a potent mutagen and has been shown repeatedly to induce DNA adducts in various model systems (reviewed in [11]). However, we identified only two studies analyzing this endpoint in A549 cells. Nagy et al. observed a linear dose–response relationship between 24-h exposure to 3-NBA (2, 5, 10 and 20 μM) and levels of DNA adducts [24]. In another study, 18-h exposure of A549 cells to 3-NBA (10 μM) also resulted in induction of DNA adducts [25]. It is worth mentioning that in our study, a 3-NBA concentration as low as 0.5 μM increased levels of DNA adducts. In addition, unlike other test compounds, the effect was observed after 4-h treatment. Theoretically, greater genotoxic potency, consistent with similar observations in BEAS-2B cells [22], may be associated with a different type of metabolic activation of 3-NBA, in which NQO1 and POR enzymes play an important part in conversion of 3-NBA to N-OH-ABA [12,14], whereas CYP enzymes are not considered to contribute significantly to 3-NBA activation [14]. 3-aminobenzanthrone, a product of the metabolic activation of 3-NBA, has been shown to be converted further by CYP1A1 to N-OH-ABA, thereby enhancing its genotoxicity [26,27]. The authors demonstrated that 3-NBA induces the protein expression and activity of CYP1A1 in rats [26]. However, our results did not show a significant increase in levels of *NQO1* and *POR* mRNA after 4-h treatment with 3-NBA; CYP1A1 expression showed a modest increase only after treatment with higher doses of the compound. Thus, in our experimental system, high levels of bulky DNA adducts induced by the 4-h treatment with 3-NBA are not likely to be associated with mRNA expression of *NQO1*, *POR* and *CYP1A1* genes. Twenty-four-hour treatment with 3-NBA resulted in a significant induction in levels of *NQO1*, *CYP1A1* and (for the lower dose of compound) *POR*, although the increase was modest and cannot probably explain strong induction of bulky DNA adducts. Further information might be obtained from analyses of protein expression because basal levels of these enzymes sufficient for metabolic activation of 3-NBA might be present in A549 cells.

Theoretically, all test compounds could induce ROS generation and, therefore, oxidative damage to macromolecules, though the mechanism of action differs. For B[a]P, this mechanism includes the activity of dihydrodiol dehydrogenases, including AKR1C2 [5]. Indeed, in our study, we observed a significant increase in expression of *AKR1C2* mRNA after 24-h treatment with both doses of B[a]P, although the increase is relatively modest (~1.8-fold) and its biological meaning might be limited. Moreover, similar effects were found after treatment with nitro-PAHs. These observations may be because regulation of *AKR1C2* expression is probably mediated by the antioxidant response of cells rather than by a xenobiotic response [5]. Thus, our results on *AKR1C2* expression indicate that some levels of ROS are generated after treatment of A549 cells with B[a]P and nitro-PAHs. These processes may be responsible for the induction of lipid peroxidation and oxidative damage to proteins after treatment with nitro-PAHs. Considering the fact that B[a]P had no effect on oxidative damage of either macromolecule, we may conclude that nitro-PAHs tested were stronger pro-oxidants under our experimental conditions. 1-NP clearly induces oxidative stress by ROS production [9,28], but the mechanisms by which ROS are produced are not conclusively identified. It has been reported that 1-nitrosopyrene, a metabolite of 1-NP, can induce oxidative damage [10]. The authors of another study [9] argued that increased ROS levels upon 1-NP treatment were associated with ER stress induced by metabolites of 1-NP during nitroreduction. 3-NBA may contribute to ROS generation due to the activity of enzymes participating in its metabolic activation. Xanthine oxidase reduces molecular oxygen to the superoxide radical and hydrogen peroxide, thus generating ROS [16]. In another study, a mechanism of ROS generation involving N-OH-ABA was proposed [13]. N-OH-ABA is formed from 3-NBA by the action of NQO1, POR or XO [11]; in the presence of NADH and Cu(II), N-OH-ABA may be auto-oxidized, resulting in superoxide generation and further dismutation of superoxide to hydrogen peroxide.

Despite the findings mentioned above, we did not detect oxidative DNA damage after treatment with any compound. The literature suggests that, in A549 cells, DNA is oxidized only after application

of higher doses of the compound (i.e., 2 μM for 14 h; [17]). ROS production induced by B[a]P is also dependent on the cell type because, in our previous study on human embryonic lung fibroblasts, we did not detect 8-oxodG formation even after a 48-h application of 100 μM B[a]P [29]. However, Bolck et al. reported ROS formation in human immortalized keratinocytes even after very short treatment with 1 μM B[a]P [30]. 1-NP can also induce oxidative DNA damage as shown, for example, in human umbilical vein endothelial cells at doses <10 μM [9], or in naked DNA in the presence of NADPH [10]. In HaCaT keratinocytes, 1-NP induced oxidative DNA damage but only in the presence of UV-light [31]. In another study, exposure to 1-NP resulted in formation of 8-OH-dG in A549 cells but only after application of very high doses of the compound (above 250 μM). The authors argue that 1-NP causes ROS generation, but the repair mechanisms of cells can remove oxidized bases provided that 1-NP concentrations are not too high [28]. This observation may explain why, in our study, no increase in oxidative DNA damage was detected, whereas oxidative damage to lipids and proteins that are not actively repaired by cellular mechanisms was found. 3-NBA has also been shown to induce oxidative DNA damage as measured by the Comet assay in A549 cells after treatment with 10 μM of 3-NBA for 18 h [25]. In another study, 1-h incubation of cells with 0.1 and 6 μM 3-NBA did not significantly increase oxidative DNA damage as measured by the Comet assay, though the authors showed that 3-NBA could induce ROS production [16]. The authors suggested that the pro-oxidative properties of 3-NBA are related to the involvement of CYP1A1 and CYP1A2 enzymes in its metabolism. In our study, we used HPLC-MS/MS to measure specifically 8-oxodG, so our results cannot be compared directly with studies that used the Comet assay for analyses of oxidative DNA damage. We did not identify a significant increase in 8-oxodG levels, though there was some indication of possible 8-oxodG induction after 4-h treatment with 1-NP and 3-NBA. The lack of significant induction of oxidative DNA damage in our study may be explained (at least in part) by the fact that A549 cells exhibit greater resistance to this type of damage due to the a higher content of ferritin [32].

Our results further confirm the ability of 1-NP to induce ROS generation because the compound induced protein oxidation and, to a lesser extent, lipid peroxidation. There have been reports on the induction of lipid peroxidation by 1-NP in various experimental systems, including rat hepatocytes, mouse hepatoma cells and methyl linoleate [33–35]. However, our study is the first demonstrating the ability of 1-NP to induce oxidative damage to macromolecules other than DNA in A549 cells. In our study, 1-NP had the strongest pro-oxidant properties. Contrary to 1-NP, we did not observe any effect of 3-NBA exposure upon protein oxidation. Nevertheless, 3-NBA increased levels of lipid peroxidation, particularly after 24-h treatment when 15-F2t-IsoP levels were significantly higher than those in controls. This is the first report focusing on oxidative damage to lipids and proteins induced by 3-NBA in in vitro systems.

Finally, we analyzed mRNA expression of *COX2*, whose protein product catalyzes the synthesis of prostaglandins using arachidonic acid (AA) as a substrate. COX-2 is overexpressed during inflammation, and an association with increased oxidative stress and activation of nuclear factor-kappa B has been proposed [36]. In our study, 1-NP was a strong inducer of *COX2* expression, further confirming the pro-oxidant activity of this compound. However, there may be another role of COX2 that may affect detection of oxidative stress. 15-F2t-IsoP is formed from AA independent of COX2 [37]. We speculate that elevated expression of *COX2* could limit the cellular content of AA that would otherwise be available for 15-F2t-IsoP. This phenomenon would result in lower production of 15-F2t-IsoP after ROS attack. We observed a similar phenomenon in our previous study [29], but we did not have gene expression data to confirm our hypothesis. The present study showed significant down-regulation of *COX2* expression after 4-h treatment with B[a]P and 3-NBA, whereas 24-h treatment with 1-NP elicited very strong up-regulation of expression of this gene. It is interesting to note that twenty four-hour treatment with 1-NP had no effect on 15-F2t-IsoP levels, whereas a significant increase in 15-F2t-IsoP levels after 24-h incubation of cells with 3-NBA was not accompanied by up-regulation of *COX2* expression. This observation suggests that our hypothesis may be correct, but more experiments are needed to confirm it.

Finally, it should be noted that our results represent a typical in vitro study. Such studies are important as they help to investigate the mechanisms of action of various compounds in model systems. However, it is difficult to extrapolate the results to real-life conditions and estimate possible negative health effects in humans. First, in these studies cell lines that lack three-dimensional interactions of cells in tissues/organs of multicellular organisms are used. Second, the concentrations of the tested compounds in the ambient air are orders of magnitude lower than those used for in vitro tests (for B[a]P, the ambient concentrations are usually in the range of 0.1–10 ng/m^3 which corresponds to femtomolar concentrations of the compound in the culture media; the ambient concentrations of 1-NP and 3-NBA are only in the tens of pg/m^3 range). Moreover, these compounds are present in complex mixtures with many other chemicals which affects the interaction with the organism. Thus, our data should be regarded as a valuable contribution to understanding the mechanisms of action of PAHs and nitro-PAHs in a model of alveolar basal epithelial cells that specifically highlighted the role of oxidative damage to macromolecules. This process, along with bulky DNA adduct formation, may contribute to increased cancer risk in humans.

4. Materials and Methods

4.1. Test Compounds

B[a]P, 1-NP and 3-NBA were obtained from Sigma–Aldrich (Saint Louis, MO, USA). These compounds were dissolved in dimethyl sulfoxide (DMSO) and stock solutions were stored at −80 °C. For treatment, non-cytotoxic doses of each compound were used: B[a]P, 0.1 and 1 μM; 1-NP, 1 and 10 μM; 3-NBA, 0.5 and 5 μM.

4.2. Cell Cultures and Treatment

A549 cells (human adenocarcinoma alveolar basal epithelial cells, type II) were grown in Dulbecco's Modified Eagle's medium (DMEM) supplemented with 1.0 g/L glucose and pyruvate, 10% fetal bovine serum (FBS), 200 mM glutamine and gentamicin sulfate (10 mg/mL). Cells were cultivated in plastic cell-culture dishes (21 cm^2) at 37 °C in an atmosphere of 5% CO_2. After reaching 70%–80% confluence, the medium was replaced with fresh medium supplemented with 1% FBS. Test compounds were diluted with DMSO and added to the medium at test concentrations. Cells were treated for 4 h or 24 h. Each concentration was tested in triplicate in two independent experiments including control cell cultures incubated with DMSO only. The final concentration of DMSO was ≤0.1% of the total incubation volume. Harvested cells were washed thrice in phosphate-buffered saline (PBS) and stored at −80 °C until further processing. Cytotoxicity of test concentrations of B[a]P, 1-NP and 3-NBA in A549 cells was analyzed using a Lactate Dehydrogenase Cytotoxicity Assay kit (Bio Vision, Milpitas, CA, USA) according to manufacturer recommendations. Significant cytotoxicity was not observed at any of the test concentrations (Table 1).

Table 1. Cytotoxicity of test compounds after treatment of A549 cells with selected concentrations of B[a]P, 1-NP and 3-NBA for 4 h or 24 h.

Test Compound	Concentration (μM)	Cytotoxicity (%)	
		4 h	24 h
B[a]P	0.1	ND	ND
	1.0	ND	ND
1-NP	1.0	ND	ND
	10	ND	0.6
3-NBA	0.5	ND	ND
	5.0	ND	2.0

ND, not detectable.

4.3. DNA Isolation and DNA Adduct Analysis

DNA was isolated via phenol/chloroform/isoamylalcohol extraction and ethanol precipitation [38], and samples were stored at −80 °C until analysis. DNA adduct analysis was performed using ^{32}P-postlabeling as described previously [39,40]. Briefly, DNA samples (6 µg) were digested with a mixture of micrococcal endonuclease (Sigma-Aldrich) and spleen phosphodiesterase (MP Biomedicals, Strasbourg, France) for 4 h at 37 °C. Nuclease P1 (Yamasa Corporation, Chiba-ken, Japan) was used for adduct enrichment. Labeled DNA adducts were resolved via multidirectional thin-layer chromatography (TLC) on 10 cm × 10 cm polyethylenimine–cellulose plates. The following solvent systems were used for TLC: D-1: 1 M sodium phosphate, pH 6.8; D-2: 3.8 M lithium formate, 8.5 M urea, pH 3.5; D-3: 0.8 M lithium chloride, 0.5 M Tris, 8.5 M urea, pH 8.0. Autoradiography was carried out at −80 °C for 24 h. Radioactivity of distinct adduct spots and diagonal radioactive zones was measured using liquid scintillation counting. To determine the exact amount of DNA in each sample, aliquots of the DNA enzymatic digest (1 µg of DNA hydrolyzate) were analyzed for nucleotide content using reverse-phase high performance liquid chromatography with UV detection, which simultaneously controlled for DNA purity. DNA adduct levels were expressed as relative DNA adduct levels per 10^8 nucleotides. A BPDE-DNA adduct standard was run in duplicate in each postlabeling experiment to control for interassay variability.

4.4. RNA Isolation and Quality Control

Total RNA from lysed A549 cells was obtained using NucleoSpin RNA II (Macherey-Nagel GmbH & Co. KG, Düren, Germany) according to manufacturer instructions. RNA concentrations were quantified with a Nanodrop ND-1000 Spectrophotometer (Thermo Fisher Scientific, Waltham, MA, USA). RNA integrity was assessed using an Agilent 2100 Bioanalyzer (Agilent Technologies, Santa Clara, CA, USA). All samples had an RNA Integrity Number >9. Isolated RNA was stored at −80 °C until processing.

4.5. Analyses of mRNA Expression

Quantitative real-time polymerase chain reaction (qRT-PCR) was performed using a QuantiTect Probe RT-PCR kit (Qiagen, Hilden, Germany) on a 7900HT Fast Real-Time PCR System (Applied Biosystems, Waltham, MA, USA). Each RNA sample (1 µL, 300 ng) was mixed with 1 µL of primers (stock solution, 5 µM; Generi Biotech, Hradec Kralove, Czech Republic), 0.1 µL of fluorescence probe (stock solution: for NQO1, POR, AKR1C2, COX2: 10 µM, Roche, Mannheim, Germany; for CYP1A1 and CYP1B1: 1 µM, Generi Biotech), 0.1 µL RT mix, and 5 µL RT-PCR mix and incubated 30 min at 55 °C. qRT-PCR included a 15-min incubation at 95 °C and 40 cycles of 15-sencond incubation at 95 °C followed by 1-min incubation at 60 °C. Primer sequences are shown in Table 2.

Table 2. Analyzed genes and primer sequences used in qRT-PCR.

Gene	RefSeq ID		Primer Sequence
CYP1A1	NM_000499	Forward Reverse	CACCATCCCCCACAGCAC TTACAAAGACACAACGCCCC
CYP1B1	NM_000104	Forward Reverse	GCTTTTTCTCTTCATCTCCATC TTCATTTTCGCAGGCTCATTTG
ALDH3A1	NM_001135168	Forward Reverse	TCTTGGCTCTTGCCGTTC CGCTGATCTTGCTCATGG
COX2	NM_000963	Forward Reverse	CTTCACGCATCAGTTTTTCAAG TCACCGTAAATATGATTTAAGTCCAC
AKR1C2	NM_001135241	Forward Reverse	AGCACCTCCACCTTCTCTCTC AGGTGAAGGGGAAGTAAGCAT
NQO1	NM_000903	Forward Reverse	ATGTATGACAAAGGACCCTTCC TCCCTTGCAGAGAGTACATGG
POR	NM_000941	Forward Reverse	GAGACCCCACCGACAATG TGGCATTGAAGTGCTCGTAG

4.6. Analyses of 8-oxo-7,8-Dihydro-2′-deoxyguanosine (8-oxodG)

DNA was isolated from cell pellets using a DNeasy Blood and Tissue kit (Qiagen, Hilden, Germany), denaturated by heating, and cooled rapidly on ice. Denatured samples were incubated with 4 µL of Nuclease P1 (1 U/1 µL; Sigma–Aldrich) for 1 h at 37 °C and then with 2 µL of alkaline phosphatase (3.5 mg/30 µL; Sigma–Aldrich) for 1 h at 37 °C. The reaction was terminated by addition of 8 µL of 3 M sodium acetate (pH 5). Samples were stored at −80 °C. The ratio of 8-oxodG/2′-deoxyguanosine (dG) was determined using liquid chromatography-tandem mass spectrometry (LC/MS-MS). A 1200 chromatographic system (Agilent Technologies) comprised a binary pump, vacuum degasser, autosampler, thermostatted column compartment, and a UV detector. Separation of analytes was carried out using a ZORBAX Eclipse Plus C18, 2.1 × 150 mm, 3.5 µm particle-size column (Agilent Technologies) with a 15-min linear gradient from 2.5% to 23% of methanol. The flow rate of the mobile phase was 0.2 mL/min, and the column temperature was set at 45 °C. A triple quadrupole mass spectrometer (6410 Triple Quad LC/MSl Agilent Technologies) with an electrospray interface (ESI) was used for detection of 8-oxodG. The mass spectrometer was operated in positive ion mode. Multiple reaction monitoring (MRM) with the mass transition m/z 284.1 → m/z 168.1 was used for quantification. dG was detected with a UV detector at 260 nm.

4.7. Preparation of Cell Lysates; Analyses of Lipid Peroxidation and Protein Oxidation

Analyses of lipid peroxidation and protein oxidation were carried out using enzyme-linked immunoassays (ELISAs) as described previously [29] with modification. Cells stored at −80 °C were thawed and mixed with 100 µL of CelLytic Reagent (Sigma–Aldrich) and mixed vigorously for 15 min at room temperature on a shaker. Lysates were centrifuged at 18,000× g for 15 min at 4 °C. Supernatants were transferred to a new tube and stored at −80 °C or used directly for analyses of total protein concentration using a Bicinchoninic Acid kit (Sigma–Aldrich). The concentration of 15-F_{2t}-isoprostane (15-F2t-IsoP) in cell lysates was analyzed by use of immunoassay kits from Cayman Chemical Company (Ann Arbor, MI, USA). First, membrane-bound 15-F2t-IsoP was hydrolyzed and samples purified. Cell lysates containing 100 µg of protein were diluted with dH_2O to 100 µL. Then, 100 µL of 15% KOH was added and the samples vortex-mixed and incubated for 60 min at 40 °C. pH of the samples was adjusted by addition of 300 µL of 1 M KH_2PO_4; 100 µL of column buffer (containing 13.6 g KH_2PO_4, 29.2 g NaCl, 0.5 g NaN_3 per 1000 mL, pH 7.4) was added, and samples were mixed. The next step included addition of 50 µL of Isoprostane Affinity Sorbent (Cayman Chemical Company) and incubation for 60 min at room temperature on a shaker. After incubation, samples were centrifuged for 1 min at 5000× g and supernatants removed by pipetting. 15-F_{2t}-isoprostane bound to sorbent was washed with 1 mL of dH_2O and eluted from the sorbent by re-suspension in 0.5 mL of elution solution (95% ethanol). Then, samples were stored in elution solution at −80 °C until analyses. Before the assay, samples were vacuum-dried, re-suspended in 110 µL of enzyme immunoassay (EIA) buffer (supplied with the 15-F_{2t}-IsoP kit) and used immediately for ELISA, which was performed according to manufacturer instructions.

Protein oxidation was analyzed using a published protocol [29]. Briefly, cell lysates were diluted with PBS to a final protein concentration of 2 mg/mL. Ten microliters of samples were mixed with 10 µL of 2,4-dinitrophenylhydrazine (DNPH) solution (derivatization solution). Then, samples were incubated at room temperature in the dark for 45 min and vortex-mixed every 10–15 min. Derivatization was stopped by addition of 30 µL of 2 M Tris, and samples were mixed on a shaker and centrifuged briefly. Of the derivatized samples, 6.25 µL were added to 1.25 mL of coating buffer, mixed and used for coating ELISA plates. The ELISA was performed as described in [29].

To account for the biological variability of markers of oxidative stress within triplicates, results were normalized to the basal level of oxidative damage in the negative control sample, and these relative numbers were used for statistical analyses. In addition, data in the figures are shown as relative values of oxidative damage.

4.8. Statistical Analyses

Raw data from qRT-PCR were analyzed using SDS Relative Quantification v2.3 (Applied Biosystems). Expression levels of analyzed genes were normalized to those of the reference gene porphobilinogendeaminase (PBDG; obtained from a kit from Generi Biotech). mRNA expression was compared to that in control samples treated with DMSO only. Changes in relative gene expression were calculated using the $2^{-\Delta\Delta Ct}$ method [41].

For statistical analyses of data on DNA adducts, oxidative stress, and mRNA expression, SPSS v20.0 (IBM, Armonk, NY, USA) was used. Data followed a normal distribution, so the Student's *t*-test was used for comparisons between groups. Figures showed the mean value of DNA adducts, relative value of markers of oxidative damage, and the mean fold-change ± standard deviation of mRNA expression.

5. Conclusions

Our data demonstrated the very strong genotoxic effects of 3-NBA in A549 cells even after short incubation; the effect of 1-NP was limited. All test compounds seemed to induce ROS generation, though oxidative damage to macromolecules was inconsistent. The most pronounced effects were observed for protein oxidation induced by 1-NP and for 15-F2t-IsoP induced by 3-NBA. In our experimental system, nitro-PAHs (particularly 1-NP) were stronger oxidants than B[a]P.

Acknowledgments: The study was supported by the Czech Science Foundation (grant number 13-01438S, 16-14631S), the Ministry of Education, Youth and Sports of the Czech Republic (grant number LO1508) and Operational Program Prague–Competitiveness (CZ.2.16/3.1.00/21528). The authors acknowledge the assistance provided by the Research Infrastructure NanoEnviCZ, supported by the Ministry of Education, Youth and Sports of the Czech Republic under Project No. LM2015073.

Author Contributions: Pavel Rossner Jr.—Analysis of oxidative stress, data analysis and preparation of the manuscript; Simona Strapacova, Veronika Vlkova—mRNA expression analysis; Jitka Stolcpartova, Jiri Neca—Oxidative stress analysis; Jana Schmuczerova, Alena Milcova—Analysis of DNA adducts; Tana Brzicova—Cell treament; Miroslav Machala, Jan Topinka—Overall design and concept of the study.

Conflicts of Interest: The authors declare no conflict of interest.

Abbreviations

AA	Arachidonic Acid
AKR1C2	Aldo-Keto Reductase
B[a]P	Benzo[a]pyrene
COX2	Cyclooxygenase-2
ER stress	Endoplasmic Reticulum Stress
15-F2t-IsoP	15-F_{2t}-Isoprostane
3-NBA	3-nitrobenzanthrone
N-OH-ABA	*N*-hydroxy-3-aminobenzanthrone
1-NP	1-nitropyrene
NQO1	NAD(P)H:QuinoneOxidoreductase
8-oxodG	8-oxo-7,8-dihydro-2′-deoxyguanosine
PAHs	Polycyclic Aromatic Hydrocarbons
POR	NAPDH: Cytochrome P450 Oxidoreductase
ROS	Reactive Oxygen Species
XO	Xanthine Oxidase

References

1. Loomis, D.; Grosse, Y.; Lauby-Secretan, B.; El Ghissassi, F.; Bouvard, V.; Benbrahim-Tallaa, L.; Guha, N.; Baan, R.; Mattock, H.; Straif, K. The carcinogenicity of outdoor air pollution. *Lancet Oncol.* **2013**, *14*, 1262–1263. [CrossRef]
2. IARC. Diesel and gasoline engine exhausts and some nitroarenes. In *IARC Monographs on the Evaluation of the Carcinogenic Risk of Chemicals to Humans*; IARC Publications: Lyon, France, 2013; Volume 105, p. 467.

3. Bamford, H.A.; Bezabeh, D.Z.; Schantz, S.; Wise, S.A.; Baker, J.E. Determination and comparison of nitrated-polycyclic aromatic hydrocarbons measured in air and diesel particulate reference materials. *Chemosphere* **2003**, *50*, 575–587. [CrossRef]
4. IARC. Chemical agents and related occupations. In *IARC Monographs on the Evaluation of the Carcinogenic Risk of Chemicals to Humans*; IARC Publications: Lyon, France, 2012; Volume 100, pp. 137–138.
5. Penning, T.M.; Burczynski, M.E.; Hung, C.F.; McCoull, K.D.; Palackal, N.T.; Tsuruda, L.S. Dihydrodiol dehydrogenases and polycyclic aromatic hydrocarbon activation: Generation of reactive and redox active o-quinones. *Chem. Res. Toxicol.* **1999**, *12*, 1–18. [CrossRef] [PubMed]
6. Toriba, A.; Kitaoka, H.; Dills, R.L.; Mizukami, S.; Tanabe, K.; Takeuchi, N.; Ueno, M.; Kameda, T.; Tang, N.; Hayakawa, K.; et al. Identification and quantification of 1-nitropyrene metabolites in human urine as a proposed biomarker for exposure to diesel exhaust. *Chem. Res. Toxicol.* **2007**, *20*, 999–1007. [CrossRef] [PubMed]
7. Silvers, K.J.; Couch, L.H.; Rorke, E.A.; Howard, P.C. Role of nitroreductases but not cytochromes P450 in the metabolic activation of 1-nitropyrene in the HepG2 human hepatoblastoma cell line. *Biochem. Pharmacol.* **1997**, *54*, 927–936. [CrossRef]
8. WHO. Selected nitro and nitrooxy-polycyclic-aromatic hydrocarbons. In *Environ. Health Criteria*; World Health Organization: Geneva, Switzerland, 2003; Volume 229, pp. 125–140.
9. Andersson, H.; Piras, E.; Demma, J.; Hellman, B.; Brittebo, E. Low levels of the air pollutant 1-nitropyrene induce DNA damage, increased levels of reactive oxygen species and endoplasmic reticulum stress in human endothelial cells. *Toxicology* **2009**, *262*, 57–64. [CrossRef] [PubMed]
10. Ohnishi, S.; Murata, M.; Fukuhara, K.; Miyata, N.; Kawanishi, S. Oxidative DNA damage by a metabolite of carcinogenic 1-nitropyrene. *Biochem. Biophys. Res. Commun.* **2001**, *280*, 48–52. [CrossRef] [PubMed]
11. Arlt, V.M. 3-Nitrobenzanthrone, a potential human cancer hazard in diesel exhaust and urban air pollution: A review of the evidence. *Mutagenesis* **2005**, *20*, 399–410. [CrossRef] [PubMed]
12. Arlt, V.M.; Cole, K.J.; Phillips, D.H. Activation of 3-nitrobenzanthrone and its metabolites to DNA-damaging species in human B lymphoblastoid MCL-5 cells. *Mutagenesis* **2004**, *19*, 149–156. [CrossRef] [PubMed]
13. Murata, M.; Tezuka, T.; Ohnishi, S.; Takamura-Enya, T.; Hisamatsu, Y.; Kawanishi, S. Carcinogenic 3-nitrobenzanthrone induces oxidative damage to isolated and cellular DNA. *Free Radic. Biol. Med.* **2006**, *40*, 1242–1249. [CrossRef] [PubMed]
14. Oya, E.; Ovrevik, J.; Arlt, V.M.; Nagy, E.; Phillips, D.H.; Holme, J.A. DNA damage and DNA damage response in human bronchial epithelial BEAS-2B cells following exposure to 2-nitrobenzanthrone and 3-nitrobenzanthrone: Role in apoptosis. *Mutagenesis* **2011**, *26*, 697–708. [CrossRef] [PubMed]
15. Foster, K.A.; Oster, C.G.; Mayer, M.M.; Avery, M.L.; Audus, K.L. Characterization of the A549 cell line as a type II pulmonary epithelial cell model for drug metabolism. *Exp. Cell Res.* **1998**, *243*, 359–366. [CrossRef] [PubMed]
16. Hansen, T.; Seidel, A.; Borlak, J. The environmental carcinogen 3-nitrobenzanthrone and its main metabolite 3-aminobenzanthrone enhance formation of reactive oxygen intermediates in human A549 lung epithelial cells. *Toxicol. Appl. Pharmacol.* **2007**, *221*, 222–234. [CrossRef] [PubMed]
17. Genies, C.; Maitre, A.; Lefebvre, E.; Jullien, A.; Chopard-Lallier, M.; Douki, T. The extreme variety of genotoxic response to benzo[a]pyrene in three different human cell lines from three different organs. *PLoS ONE* **2013**, *8*, e78356. [CrossRef]
18. Libalova, H.; Krckova, S.; Uhlirova, K.; Milcova, A.; Schmuczerova, J.; Ciganek, M.; Klema, J.; Machala, M.; Sram, R.J.; Topinka, J. Genotoxicity but not the AhR-mediated activity of PAHs is inhibited by other components of complex mixtures of ambient air pollutants. *Toxicol. Lett.* **2014**, *225*, 350–357. [CrossRef] [PubMed]
19. Aoki, Y.; Sato, H.; Nishimura, N.; Takahashi, S.; Itoh, K.; Yamamoto, M. Accelerated DNA adduct formation in the lung of the Nrf2 knockout mouse exposed to diesel exhaust. *Toxicol. Appl. Pharmacol.* **2001**, *173*, 154–160. [CrossRef] [PubMed]
20. Aoki, Y.; Hashimoto, A.H.; Amanuma, K.; Matsumoto, M.; Hiyoshi, K.; Takano, H.; Masumura, K.; Itoh, K.; Nohmi, T.; Yamamoto, M. Enhanced spontaneous and benzo(a)pyrene-induced mutations in the lung of Nrf2-deficient gpt delta mice. *Cancer Res.* **2007**, *67*, 5643–5648. [CrossRef] [PubMed]

21. Yamazaki, H.; Hatanaka, N.; Kizu, R.; Hayakawa, K.; Shimada, N.; Guengerich, F.P.; Nakajima, M.; Yokoi, T. Bioactivation of diesel exhaust particle extracts and their major nitrated polycyclic aromatic hydrocarbon components, 1-nitropyrene and dinitropyrenes, by human cytochromes P450 1A1, 1A2, and 1B1. *Mutat. Res.* **2000**, *472*, 129–138. [CrossRef]
22. Ovrevik, J.; Arlt, V.M.; Oya, E.; Nagy, E.; Mollerup, S.; Phillips, D.H.; Lag, M.; Holme, J.A. Differential effects of nitro-PAHs and amino-PAHs on cytokine and chemokine responses in human bronchial epithelial BEAS-2B cells. *Toxicol. Appl. Pharmacol.* **2010**, *242*, 270–280. [CrossRef] [PubMed]
23. Iwanari, M.; Nakajima, M.; Kizu, R.; Hayakawa, K.; Yokoi, T. Induction of CYP1A1, CYP1A2, and CYP1B1 mRNAs by nitropolycyclic aromatic hydrocarbons in various human tissue-derived cells: Chemical-, cytochrome P450 isoform-, and cell-specific differences. *Arch. Toxicol.* **2002**, *76*, 287–298. [CrossRef] [PubMed]
24. Nagy, E.; Johansson, C.; Zeisig, M.; Moller, L. Oxidative stress and DNA damage caused by the urban air pollutant 3-NBA and its isomer 2-NBA in human lung cells analyzed with three independent methods. *J. Chromatogr. B Anal. Technol. Biomed. Life Sci.* **2005**, *827*, 94–103. [CrossRef] [PubMed]
25. Nagy, E.; Adachi, S.; Takamura-Enya, T.; Zeisig, M.; Moller, L. DNA adduct formation and oxidative stress from the carcinogenic urban air pollutant 3-nitrobenzanthrone and its isomer 2-nitrobenzanthrone, in vitro and in vivo. *Mutagenesis* **2007**, *22*, 135–145. [CrossRef] [PubMed]
26. Stiborova, M.; Dracinska, H.; Mizerovska, J.; Frei, E.; Schmeiser, H.H.; Hudecek, J.; Hodek, P.; Phillips, D.H.; Arlt, V.M. The environmental pollutant and carcinogen 3-nitrobenzanthrone induces cytochrome P450 1A1 and NAD(P)H:quinoneoxidoreductase in rat lung and kidney, thereby enhancing its own genotoxicity. *Toxicology* **2008**, *247*, 11–22. [CrossRef] [PubMed]
27. Mizerovska, J.; Dracinska, H.; Arlt, V.M.; Schmeiser, H.H.; Frei, E.; Stiborova, M. Oxidation of 3-aminobenzanthrone, a human metabolite of carcinogenic environmental pollutant 3-nitrobenzanthrone, by cytochromes P450—Similarity between human and rat enzymes. *Neuro Endocrinol. Lett.* **2009**, *30*, 52–59. [PubMed]
28. Kim, Y.D.; Ko, Y.J.; Kawamoto, T.; Kim, H. The effects of 1-nitropyrene on oxidative DNA damage and expression of DNA repair enzymes. *J. Occup. Health* **2005**, *47*, 261–266. [CrossRef] [PubMed]
29. Hanzalova, K.; Rossner, P., Jr.; Sram, R.J. Oxidative damage induced by carcinogenic polycyclic aromatic hydrocarbons and organic extracts from urban air particulate matter. *Mutat. Res.* **2010**, *696*, 114–121. [CrossRef] [PubMed]
30. Bolck, B.; Ibrahim, M.; Steinritz, D.; Morguet, C.; Duhr, S.; Suhr, F.; Lu-Hesselmann, J.; Bloch, W. Detection of key enzymes, free radical reaction products and activated signaling molecules as biomarkers of cell damage induced by benzo[a]pyrene in human keratinocytes. *Toxicol. in Vitro* **2014**, *28*, 875–884. [CrossRef] [PubMed]
31. Fullove, T.P.; Yu, H. DNA damage and repair of human skin keratinocytes concurrently exposed to pyrene derivatives and UVA light. *Toxicol. Res. Camb.* **2013**, *2*, 193–199. [CrossRef] [PubMed]
32. Persson, H.L.; Nilsson, K.J.; Brunk, U.T. Novel cellular defenses against iron and oxidation: Ferritin and autophagocytosis preserve lysosomal stability in airway epithelium. *Redox. Rep.* **2001**, *6*, 57–63. [CrossRef] [PubMed]
33. De Mejia, E.G.; Ramirez-Mares, M.V. Leaf extract from Ardisiacompressa protects against 1-nitropyrene-induced cytotoxicity and its antioxidant defense disruption in cultured rat hepatocytes. *Toxicology* **2002**, *179*, 151–162. [CrossRef]
34. Landvik, N.E.; Gorria, M.; Arlt, V.M.; Asare, N.; Solhaug, A.; Lagadic-Gossmann, D.; Holme, J.A. Effects of nitrated-polycyclic aromatic hydrocarbons and diesel exhaust particle extracts on cell signalling related to apoptosis: Possible implications for their mutagenic and carcinogenic effects. *Toxicology* **2007**, *231*, 159–174. [CrossRef] [PubMed]
35. Fullove, T.P.; Johnson, B.; Yu, H. Structure-dependent lipid peroxidation by photoirradiation of pyrene and its mono-substituted derivatives. *J. Environ. Sci. Health Toxic Hazard. Subst. Environ. Eng.* **2013**, *48*, 233–241. [CrossRef] [PubMed]
36. Lu, Y.; Wahl, L.M. Oxidative stress augments the production of matrix metalloproteinase-1, cyclooxygenase-2, and prostaglandin E2 through enhancement of NF-kappa B activity in lipopolysaccharide-activated human primary monocytes. *J. Immunol.* **2005**, *175*, 5423–5429. [CrossRef] [PubMed]
37. Morrow, C.S.; Chiu, J.; Cowan, K.H. Posttranscriptional control of glutathione S-transferase pi gene expression in human breast cancer cells. *J. Biol. Chem.* **1992**, *267*, 10544–10550. [PubMed]

38. Gupta, R.C. Enhanced Sensitivity of 32P-Postlabeling Analysis of Aromatic Carcinogen: DNA Adducts. *Cancer Res*. **1985**, *45*, 5656–5662. [PubMed]
39. Phillips, D.H.; Castegnaro, M. Standardization and validation of DNA adduct postlabelling methods: Report of interlaboratory trials and production of recommended protocols. *Mutagenesis* **1999**, *14*, 301–315. [CrossRef] [PubMed]
40. Randerath, E.; Avitts, T.A.; Reddy, M.V.; Miller, R.H.; Everson, R.B.; Randerath, K. Comparative 32P-postlabeling analysis of cigarette smoke-induced DNA damage in human tissues and mouse skin. *Cancer Res*. **1986**, *46*, 5869–5877. [PubMed]
41. Livak, K.J.; Schmittgen, T.D. Analysis of relative gene expression data using real-time quantitative PCR and the $2^{-\Delta\Delta Ct}$ Method. *Methods* **2001**, *25*, 402–408. [CrossRef] [PubMed]

Článek 5

Fuel 197 (2017) 407–421

Contents lists available at ScienceDirect

Fuel

journal homepage: www.elsevier.com/locate/fuel

Full Length Article

Blends of butanol and hydrotreated vegetable oils as drop-in replacement for diesel engines: Effects on combustion and emissions

Michal Vojtisek-Lom [a,*], Vít Beránek [a], Pavel Mikuška [b], Kamil Křůmal [b], Pavel Coufalík [b], Jitka Sikorová [c,d], Jan Topinka [c]

[a] Center for Sustainable Mobility, Faculty of Mechanical Engineering, Czech Technical University in Prague, Přílepská 1920, 252 63 Roztoky u Prahy, Czech Republic
[b] Institute of Analytical Chemistry, The Czech Academy of Sciences, Veveří 97, 602 00 Brno, Czech Republic
[c] Institute of Experimental Medicine, The Czech Academy of Sciences, Vídeňská 1083, 142 20 Prague 4, Czech Republic
[d] Institute for Environmental Studies, Faculty of Science, Charles University, Benátská 2, 12801 Prague 2, Czech Republic

HIGHLIGHTS

- 30% n-butanol or isobutanol blended into HVO as economic oxygenated "extenders".
- No adverse effects on combustion, performance, efficiency, NO_x or other emissions.
- Butanol-HVO blends result in less particle mass, black soot, PAHs vs. diesel and vs. HVO.
- Biodiesel, HVO & blends lower emissions of EC, OC, PAHs and phytane vs. diesel.
- Butanol-HVO blends reduced carcinogenic PAHs by 75–78% and soot by 79–80% vs. diesel.

ARTICLE INFO

Article history:
Received 8 June 2016
Received in revised form 10 February 2017
Accepted 13 February 2017
Available online 25 February 2017

Keywords:
Butanol
Renewable diesel
HVO
Particulate matter
Polyaromatic hydrocarbons (PAH)
Combustion
Hopanes
Steranes
Speciation

ABSTRACT

This work investigates the performance of a mix of two emerging biofuels, butanol and hydrotreated vegetable oil (HVO), in an Iveco Tector diesel engine with no aftertreatment. HVO, a possible drop-in fuel for diesel engines, features excellent combustion and emissions characteristics yet is relatively expensive, while two isomers of butanol, n-butanol and isobutanol, are less expensive oxygenated fuels with a drawback to their use in diesel engines in the form of their increased ignition delay and, on some engines, higher emissions of nitrogen oxides.

Blends of 30% of either n-butanol or isobutanol into HVO had, compared to diesel fuel, resulted in a 70–80% decrease in the emissions of elemental carbon and carcinogenic polycyclic aromatic hydrocarbons (cPAHs) and a moderate decrease in the emissions of nitrogen oxides, without showing an adverse effect on combustion timing, heat release rates, engine maximum torque, thermal efficiency, and other measured pollutants.

Particulate matter from biodiesel, HVO, their blends with diesel fuel, and the above mentioned blends was also analysed for elemental carbon (EC) and organic carbon (OC), polycyclic aromatic hydrocarbons (PAHs), nitrated PAHs, n-alkanes and organic tracer compounds, including hopanes, steranes, and isoprenoids. n-Alkanes were the most abundant class among the analysed particulate organic compounds in emissions of all fuels. All biofuels exhibited, relative to diesel fuel, a decrease in the concentration of particulate PAHs and n-alkanes in emissions, while the concentrations of hopanes and steranes originated from lubricating oil were comparable across all fuels. Cold starts yielded about 15% higher concentrations of both particulate matter and particulate organic compounds in emissions than hot starts. The vast majority of EC and OC, studied organic compounds, and mass of $PM_{2.5}$ was included in the size fraction PM_1.

1. Introduction

Diesel engines have become a practical, efficient, reliable, and cost-effective prime mover of virtually all heavy vehicles and mobile machinery. The downsides of traditional petroleum diesel

* Corresponding author.
E-mail address: michal.vojtisek@fs.cvut.cz (M. Vojtisek-Lom).

http://dx.doi.org/10.1016/j.fuel.2017.02.039
0016-2361/

Nomenclature

ANOVA	analysis of variance
B0	neat diesel
B100	biodiesel
B30	blends by volume of 30% biodiesel with 70% of diesel fuel
CAD	crank angle degrees
cPAHs	carcinogenic polycyclic aromatic hydrocarbons
CPI	carbon preference index
EC	elemental carbon
HC	hydrocarbons
HVO	hydrotreated (hydrodeoxygenated) vegetable oil
HVO100	neat hydrotreated (hydrodeoxygenated) vegetable oil
HVO30	blends by volume of 30% hydrotreated vegetable oil blended with 70% of diesel fuel
iBu30	blends by volume of 30% iso-butanol with 70% hydrotreated vegetable oil
MFB	mass fraction burned
nBu30	blends by volume of 30% n-butanol with 70% hydrotreated vegetable oil
NExBTL30	blends by volume of 30% hydrotreated vegetable oil blended with 70% of diesel fuel
nitro-PAHs	nitrated polycyclic aromatic hydrocarbons
NO_X	nitrogen oxides
OC	organic carbon
PAHs	polycyclic aromatic hydrocarbons
PM	particulate matter
PM_1	particulate matter with aerodynamic diameter less then 1 μm
$PM_{2.5}$	particulate matter with aerodynamic diameter less then 2.5 μm
TC	total carbon
WHSC	World Harmonized Steady-State Cycle
WHTC	World Harmonized Transient Cycle

fuel are concerns about petroleum availability and cost, energy security and independence, international trade balance, and climatic changes arising out of fossil fuel combustion. Its current replacement, biodiesel (methylesters of mostly vegetable oils), is coming under scrutiny as according to some it is produced mostly from edible oils and hence competes with food production. This study investigates a blend of two candidate replacements, butanol and hydrotreated (hydrodeoxygenated) vegetable oil (HVO), as a drop-in fuel for existing diesel engines.

Hydrotreated vegetable oils, also termed "renewable diesel" are produced from biomass-based triacylglycerides (such as vegetable oils) through catalytic hydrodeoxygenation, resulting in mostly non-oxygenated aliphatic compounds (terminology and production reviewed by Knothe in [1]).

Traditionally, vegetable oils have been converted to biodiesel (n-alkyl-esters, typically methylesters, of fatty acids), and to a lesser extent used as fuel in their neat form. Biodiesel, both neat and in blends with diesel fuel, offers a substantial reduction of the emissions of particulate matter (PM) [1,2], with minor effect, typically but not always an increase, on the emissions of nitrogen oxides (NO_x) [2]. Biodiesel also tends to reduce the emissions of polycyclic aromatic hydrocarbons (PAHs) [3,4], although the effects on PAHs are not always consistent [4,5]. Possible downsides of biodiesel are cold flow properties and stability of the fuel.

HVO has higher cetane number and higher stability than methylesters of vegetable oils (biodiesel) produced by their transesterification. HVO has been reported to simultaneously reduce PM, NO_x, hydrocarbons (HC) and CO, with cold flow properties being its potential downside [6]. Westphal also claims reductions in NO_x, PAHs and PM, however, the PM reduction was not as high as that achieved with first-generation biodiesel [7,8]. Lapuerta recommends using HVO in a blend of up to 50%, due to lower lubricity, high cetane number and worse cold flow properties of HVO [9]. Aatola also recommends engine optimization for high-concentration blends to compensate for high cetane number and lower density of HVO, but confirms both NO_x and PM benefits even with original fuel injection timing [10]. Knothe [1] reports that cold flow properties can be improved by including branched chain alkanes and that cloud points comparable to diesel fuel were obtained with HVO. Nylund reports on a successful use of neat HVO in a bus fleet without any engine adjustments [11]. Two distinct disadvantages of HVO are that it uses similar feedstocks as biodiesel, and that its cost is presently much higher compared to diesel fuel and biodiesel.

Alcohols have been used primarily in spark ignition engines: Ethanol produced from biomass is blended in small concentration into gasoline as well as sold in high-concentration blends for flexible fuel vehicles. Ethanol and two isomers of butanol, n-butanol and isobutanol, can be produced from biomass at relatively comparable costs and energy inputs [12]. Alcohols, in general, have lower viscosity, higher volatility, and lower cetane number (ethanol 5–8, n-butanol 17 to around 25) than diesel fuel [13,14]. Two alcohols have been considered in diesel engines, ethanol and n-butanol, with n-butanol being more suitable than ethanol due to its (relative to ethanol) higher density, viscosity, lubricity, and cetane number. Butanol, unlike ethanol, is miscible with diesel fuel without additional co-solvents. The addition of alcohols into diesel fuel, in general, has been found to decrease the emissions of particulate matter [14,15], with the exception of cold start, where the observed outcomes are not consistent, due to the opposing effect of lower cetane number [14]. The emissions of PAHs were also reduced by addition of water-containing n-butanol [15]. Addition of 16% n-butanol into diesel fuel has been reported to delay the combustion by several crank angle degrees [16]. Addition of butanol into diesel fuel has lead to an increase [17], a decrease [18] or inconsistent effect [19] on the emissions of NO_x. Lin reported an increase in NO_x for smaller and decrease in NO_x for larger concentrations of water containing n-butanol in diesel fuel [15]. The addition of butanol to biodiesel or vegetable oil has increased the ignition delay and possibly the variability of combustion among individual engine working cycles [20]. Simultaneous addition of biodiesel and butanol to diesel fuel has reduced both NO_x and PM, shifting the smoke-NO_x curve towards lower levels [21].

Overall, HVO is a suitable but expensive fuel, and n-butanol is a cost-effective fuel with a high potential to reduce PM emissions, but has a low cetane number of around 25 [1] and may increase the emissions of NO_x. This study investigates the potential of a blend of HVO and butanol as a drop-in replacement for petroleum diesel fuel, or, the potential of butanol as an extender of the (currently costly) HVO.

Adding an oxygenate into HVO has been reported to reduce NO_x emissions by about 5% and PM emissions by 25–30% [22]. It is

therefore expected that by blending HVO with butanol, a significant reduction in PM will be achieved, without an increase in NO_x emissions.

2. Experimental

2.1. Engine, fuels and test conditions

A widely used heavy-duty watercooled inline six-cylinder turbocharged 2001 model year 5.9-liter Iveco Tector F4a E0681B C109 diesel engine with intercooler, bore 102 mm, stroke 120 mm, compression ratio 17:1, max power 176 kW @ 2700 min^{-1}, max torque 810 Nm @ 1250–2100 min^{-1}, common rail, Euro3 compliant, ECU Iveco RDC7 ELT 3.1, operated without any exhaust aftertreatment devices, with approximately 1900 operating hours accumulated, was operated on a four-quadrant transient heavy-duty engine dynamometer (DynoExact 220 kW, AVL) at the Czech Technical University in Prague, in the following test sequence:

- WHTC (World Harmonized Transient Cycle) [23] as preconditioning
- Cold WHTC
- Subsequent WHTC (a "warm" but not a "fully stabilized warm")
- Multiple hot-start WHTC
- WHSC (World Harmonized Steady-State Cycle).

Several renewable fuels were tested: a market-grade biodiesel (methylesters of primarily rapeseed oil, obtained from a fueling station KM Prona, Strančice, Czech Rep.), a paraffinic diesel fuel made from renewable sources (NExBTL, Neste Oil, Finland, provided directly by Neste Oil), and two isomers of butanol, n-butanol and isobutanol. Biodiesel (further referred to as B100) and NExBTL (further referred to as HVO) were used both neat (B100 and HVO100) and blended at 30% by volume with diesel fuel (B30 and HVO30). NExBTL was also used in blends of 30% n-butanol with 70% HVO (referred to as nBu30), and 30% isobutanol with 70% HVO (referred to as iBu30).

Neat diesel fuel used as a reference (referred to as B0) and for blending was a non-oxygenated EU market-grade petroleum diesel fuel without bioadditives. Blends were splash blended in barrels. The laboratory fuel system (a small transfer tank, fuel balance, fuel temperature conditioning system) and the engine fuel system, including fuel filter, were emptied prior to the change of the fuels. Following each fuel change, the engine was run at full load for at least 10 min to complete the fuel change and to combust deposits in the combustion chamber, and a WHTC cycle was run as preconditioning.

All fuels were circulated multiple times through the laboratory fuel conditioning system. The fuel consumption was measured by AVL 735S Fuel Mass Flow Meter (declared instrument accuracy 0.12%) as well as calculated from CO_2 emissions using the fuel carbon fractions listed in Table 1. The exhaust was transferred to a full-flow dilution tunnel with a constant flow of 50, 90 and 110 m^3/min, depending on the test cycle.

2.2. On-line measurement and sampling of emissions

Continuous measurements of the concentrations of the following pollutants were made in the diluted exhaust:

- Solid particle number concentrations per the Particle Measurement Programme (PMP) requirements (non-volatile particles, 50% counting efficiency at 23 nm diameter)
- Particle size distributions (EEPS, Engine Exhaust Particle Sizer, model 3090, TSI, coupled to a rotating disc microdiluter, model MD-11, Matter Engineering)
- HC, CO, CO_2, NO_x by typical type-approval grade methods (HC - heated flame ionization detector, CO CO_2 – non-dispersive infrared analyzers, NO_x – chemiluminiscence analyzer, AMA i60, AVL; total uncertainty of g/kWh measurement estimated to 5–10%, repeatability to 2–3%)
- Various unregulated pollutants by Fourier Transform Infra Red (FTIR) analyzer (Nicolet Antaris IGS, 5 meter optical length cell, liquid nitrogen cooled MCT detector, operating at 0.5 cm^{-1} optical resolution and temperature of sample cell and the entire sampling train at 165 C; measurement interpreted as qualitative only)

The diluted exhaust was sampled

- With a standard gravimetric sampling system on 47 mm diameter Teflon-coated glass fiber (TX40HI20-WW, Pall), quartz fiber (Tissuquartz, Pall) and Teflon membrane (Teflo, Pall) filters, at a nominal flow rate of 40 dm^3/min
- With a high-volume sampler (DH-77, Digitel), with PM_1 and $PM_{2.5}$ impactor (a specially modified inlet for a direct sampling from the constant volume sampling (CVS) tunnel), at a nominal flow rate of 0.50 m^3/min, on 150 mm diameter quartz fiber (Whatman QM-A). To remove organic contaminants, the quartz filters were burned at 500 °C for 24 h before sampling.

Mass concentrations of collected aerosols were determined by weighing filters, using a microbalance M5P (±1 μg; Sartorius, Germany) equipped with a special large plate to allow weighing of 150 mm filters. Filters were equilibrated before weighing for 48 h in air-conditioned room under constant conditions (temperature 20 ± 1 °C, relative humidity 50 ± 3%).

2.3. Organic compounds analysis

Quartz filters were analysed on the content of n-alkanes, acyclic isoprenoids (pristane, phytane), hopanes, steranes, PAHs, nitrated PAHs and organic (OC) and elemental (EC) carbon. Prior to extraction, recovery standards, deuterated PAHs (1,4-dichlorbenzene-D8, naphthalene-D8, acenaphthene-D10, phenanthrene-D10, chrysene-D12 and perylene-D12), 6-nitrochrysene-D11 and ααα (20R)-cholestane-D2, were added to filters. The filters were extracted three times for 30 min under ultrasonic agitation; once with 20 mL of mixture of dichloromethane with hexane (v/v 1:1) and then twice with 20 mL of dichloromethane. The extracts were pooled and then dried under a stream of nitrogen to 1 mL.

Table 1
Selected properties of tested fuels.

	Diesel fuel	Biodiesel	NExBTL [16]	n-butanol	Isobutanol	Bu30-NExBTL
Density	830	890	780	808	808	800
LHV [MJ/kg]	42	37	44	33.3	33.3	40.8
LHV [MJ/dm^3]	35	32.9	34	26.9	26.9	32.6
Carbon content [%]	85.7	77.5	84.9	65	65	78.9

The extracts were then fractionated by flash chromatography in a glass column filled with 10 g of Al_2O_3 (Aluminium oxide 90 standardized, for column chromatographic adsorption analysis according to Brockmann, activity II - III). Three fractions were taken after elution with different solvents; hexane, mixture of dichloromethane/hexane (v/v 1:1) and dichloromethane. The first hexane fraction (20 mL) contained non-polar organic compounds (alkanes, isoprenoids, hopanes and steranes), the second dichloromethane/hexane fraction (20 mL) contained PAHs and the third dichloromethane fraction contained nitrated PAHs. All fractions were dried separately under a stream of nitrogen to 1 mL and then were analysed by GC–MS.

Quantification of all organic compounds was carried out by GC–MS (Agilent, 7890A, 5975C). A capillary column HP5-MS, 1 μm film thickness, 0.32 mm i.d., 30 m length was used.

A sample volume of 2 μL was injected into a split/splitless injector, operated in the splitless mode at a temperature of 280 °C for non-polar compounds and at 260 °C for other compounds. The carrier gas was helium at a flow rate of 4 ml min^{-1}. A detailed information concerning the GC–MS analysis is reported in recent papers [24,25]. For analysis of nitrated PAHs, the temperature program was started at 70 °C for 2 min, a gradient of 20 °C min^{-1} was used up to 150 °C, then a gradient of 5 °C min-1 was used up to 300 °C and then the temperature was held for 14 min. The MS was operated in SIM mode with *m/z* 173, 211, 223, 247, 273, 275, 284, 292 and 297. The other MS settings were the same as during analysis of non-polar organic compounds and PAHs.

The identification of all organic compounds and recovery standards was based on the comparison with retention times and mass spectra of standards

2.4. Organic carbon and elemental carbon (OC/EC) analysis

Small parts of filters (1.5 cm^2) were analysed for the OC/EC contents by thermal-optical method using a semi-continuous OC/EC analyzer (Model 4, Sunset Laboratory Inc.) at Institute of Chemical Process Fundamentals of the CAS,v.v.i., Prague. A EUSAAR2 protocol was applied [26].

2.5. Statistical analysis

Statistical analysis was made using statistical software R [27–29]; used tests: Shapiro–Wilk and Bartlett test of homogeneity of variances test for assumptions determinations, two Sample *t*-test or Wilcoxon rank sum test, and analysis of variance (ANOVA) coupled with multiple comparisons of means (Tukey contrasts) or Kruskal-Wallis rank sum test coupled multiple comparison between treatments. A significance level was set to 0.05.

3. Results

3.1. Maximum engine torque

The maximum engine torque for all fuels for different engine rpm, relative to diesel fuel, is plotted in Fig. 1. The average reductions in maximum engine torque were 0.3% for HVO30, 0.7% for neat HVO, 2.2% for B30, 6.9% for nBu30-HVO and 8.0% for iBu30-HVO. For butanol blends, the approximately 7–8% decrease in maximum torque corresponds to the lower volumetric energy density of the fuel (32.1 MJ/dm^3 for butanol-HVO blend is 8% lower than 34.9 MJ/dm^3 for diesel fuel), as fuel is metered on a volumetric basis.

3.2. Combustion analysis – WHSC

For each fuel, indicated pressures were measured over 150 consecutive combustion cycles during the 13 steady-state operating points within the WHSC test. The test modes are given in Table 2.

The crank angle degrees (CAD) corresponding to 5%, 10% and 50% mass fraction burned (MFB) and to the occurrence of maximum combustion pressure, are given, along with the peak combustion pressures, as mean values, with error bars denoting standard deviations, in Fig. 2. The calculations were done by the AVL software. The calculation assumptions, formulaes, parameters, and uncertainty were not provided by the manufacturer and are not known to the authors. The standard deviations of 5%, 10% and 50% MFB were in tenths of CAD, except for idle, where they were up to several CAD, but on no fuel during both idle modes (1 and 13). The differences between the two idles were 1–2 or even more CAD. The heat release rate appears to be higher for both HVO-butanol blends at idle and full load, and somewhat lower at low speed, but overall, no significant changes in the MFB (Wilcox test at $p < 0.05$) were observed, suggesting that the combustion of all fuels is comparable within the measurement uncertainty, or more precisely, no anomalies or major differences among the fuels were observed.

3.3. Fuel consumption and engine efficiency

The brake-specific fuel consumption (mass of fuel consumed per kWh of engine output) at maximum load, shown in Fig. 3, was, compared to diesel fuel, about 1% lower for HVO30. about 3% lower for neat HVO, about 3% higher for B30, and about 4% higher for butanol-HVO blends. These differences are comparable to the differences in lower heating values, which are, compared to diesel fuel, about 2–3% higher for HVO, about 3% lower for B30, and about 3% lower for butanol-HVO blends.

Brake-specific fuel consumption at maximum torque at various rpm is shown in Fig. 4. The differences relative to diesel fuel mostly stem out of differences in lower heating values, however, some patterns can be observed. At lower rpm, HVO efficiency seems to improve by up to 1% (not statistically significant given the measurement uncertainty), while B30 efficiency seems to be lower. At high rpm, the relative fuel consumption increases, and efficiency therefore seems to decrease, for all oxygenated fuels, B30, nBu30 and iBu30.

The variances in measured brake-specific fuel consumption correspond to the differences in the lower heating values (in MJ/kg) among the fuels, given in Table 1. The average engine efficiency during the cycle was 34.55%, with differences among fuels not being significantly higher than differences within multiple sets of runs on each fuel. The fuel consumption derived from CO_2 emissions measurements, using fuel mass carbon fractions given in Table 1, is in general agreement with measured fuel consumption (no statistical difference per Wilcoxon test), with a potential exception for butanol-HVO blends, where about 3% of the fuel consumed was not accounted for in CO_2 (or any other) emissions.

3.4. Regulated pollutants – WHTC hot start stabilized

The brake-specific fuel consumption, NO_x, HC, CO and PM emissions are given in Fig. 5. The PM represent total mass as determined by gravimetric analysis of a pair of $8 \times 10''$ fluorocarbon-coated glass fiber filters collected by two high-volume samplers running in parallel during each test. The error bars represent standard deviation from multiple (the count for each run is noted on the charts) consecutive runs of hot start WHTC, and are therefore more of a measure of test reproducibility than of the total measurement uncertainty. To shed a light on the measurement uncer-

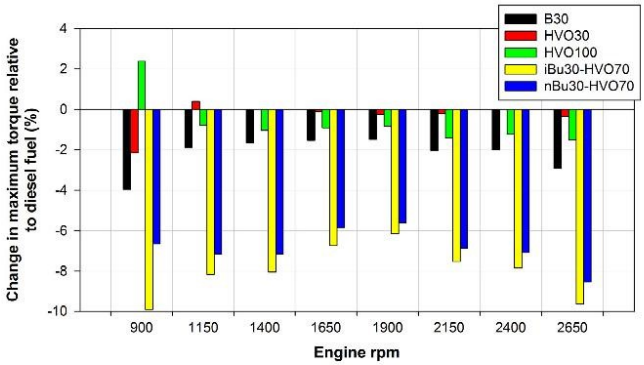

Fig. 1. Maximum engine torque relative to diesel fuel.

Table 2
WHSC test modes.

test mode	engine rpm	torque [Nm]	Bmep [kPa]	Fuel pressure [MPa]	Injection timing °BTDC
1	650	0	0	50	13, 5
2	1833	847	1804	105	29, 4
3	1833	215	4579	78	22, 3
4	1833	604	1286	103	29, 3
5	1403	847	1804	115	34, 5
6	1188	210	447	81	30, 6
7	1618	593	1263	115	29, 3
8	1618	212	451	87	25, 3
9	1833	432	920	86	29, 3
10	2263	764	1627	113	30, 4
11	1403	428	912	102	33, 4
12	1403	213	454	82	28, 4
13	650	0	0	50	13, 5

Note: Injection timing is given in degrees before top dead center (BTDC) for pilot and main injection. Fuel pressure in the common rail is estimated from the base fuel pressure map stored in the engine control unit.

tainty, data from other WHTC tests on the same engine on diesel and biodiesel have been added to the graph. Samples during which material for subsequent chemical analysis was obtained are denoted with (∗). Variances were highest for a set of only two diesel runs on January 16, one of which being run at 110 m^3/min, more than twice the normal dilution tunnel flow of 50 m^3/min. Variances among sets of biodiesel runs may also reflect the fact that different batches of biodiesel were used for each set. The patterns were similar, however less conclusive due to absence of multiple repeated runs, for the cold start WHTC.

Butanol-HVO blends had NO_x emissions comparable to the neat HVO, and slightly lower compared to diesel fuel. Out of three sets of neat biodiesel data, relative to the closest set of diesel tests, NO_x was once apparently (significantly per *t*-test, $p = 0.02$) lower (Dec. 9 vs. Dec. 15), and twice (Jan 5 vs. Jan 9, Mar 3 vs. Mar 6) apparently (significantly per Wilcoxon non-parametric test, $p = 0.03$ for January and $p < 0.001$ for March) higher, owing possibly to three different batches of commercially supplied biodiesel being tested. HC and CO emissions for butanol-HVO blends were higher compared to the neat HVO (for CO this difference was significant per one-way ANOVA at $p < 0.01$), not overly different from diesel fuel, and, in their absolute values, relatively low. Application of the non-parametric Kruskal-Wallis multiple comparison test has shown no significant ($p < 0.05$) differences between any set of diesel fuel data and any other fuel for CO or NO_x except for NO_x and CO being lower for neat HVO. NO_x was also significantly lower for HVO30, HVO100 and HVO-butanol blends compared to B30 and B100.

3.5. Particle size distributions

The particle size distributions were measured in a sample taken from undiluted exhaust, which was diluted by a rotating disc microdiluter at a dilution ratio of 150:1. The measured concentrations in each second were multiplied by the corresponding intake air flow to obtain second-by-second emissions data, which were then integrated to obtain total emissions per cycle. These were divided by the total intake air flow, resulting in flow-weighted average concentrations over the WHTC cycle, which are given, for each fuel, in Fig. 6. The results for butanol-HVO blends are virtually identical for both butanol isomers. The variance among multiple runs was on the order of units of percent to ten percent, is comparable among the fuels, and is shown, as an example, for diesel fuel and nBu30-HVO fuels. Given that all, not just non-volatile, particles were measured, it is believed that size channels below approximately 20 nm are subject to additional uncertainty. The difference between diesel fuel and HVO was relatively small, while the difference between non-oxygenated fuels and butanol-HVO blends was considerable: the addition of 30% of butanol has resulted in about one half decrease in total particle number emissions, and nearly 60% decrease of particles larger than approximately 23 nm. Data

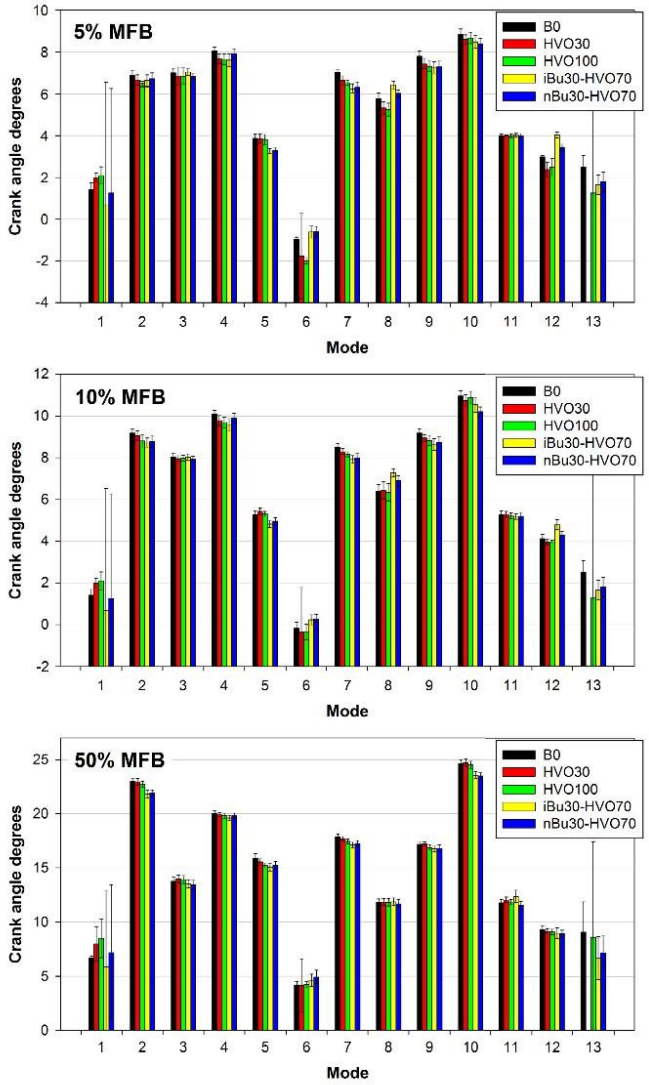

Fig. 2. Crank angle degrees at which 5%, 10% and 50% of the heat content of the fuel was released, maximum combustion pressure and the angle of max. combustion pressure for all fuels and 13 WHSC test modes listed in Table 2.

for cold starts was similar, with very little if any "excess" attributable to the cold start.

3.6. EC/OC and polycyclic aromatic hydrocarbons

The total particulate mass as determined by gravimetric analysis on quartz filters and the results of EC/OC analysis are given in Fig. 7. Separate results are given for WHTC for $PM_{2.5}$ and for PM_1, and for selected fuels, also for cold WHTC for $PM_{2.5}$. Total carbon (TC = OC + EC) comprises a significant part of the exhaust mass. The TC contribution to PM mass was relatively stable in all samples with mean value of 74% and range 66–86% for $PM_{2.5}$, hot start WHTC, and mean value of 76% and range 55–94% for all tests. EC serves as a marker of diesel particles [30]. For HVO and hot B0 samples the concentrations of EC exceeded the concentrations of OC whereas in other samples the concentrations of EC were smaller than the corresponding concentrations of OC.

In all cases, gravimetric mass exceeds, by approximately one fifth to one quarter, the sum of elemental and organic carbon, most likely due to hydrogen and oxygen content of the organic carbon. Also, in all cases, the "excess" PM mass, EC and OC from cold start, determined as a difference between cold and hot WHTC, is from

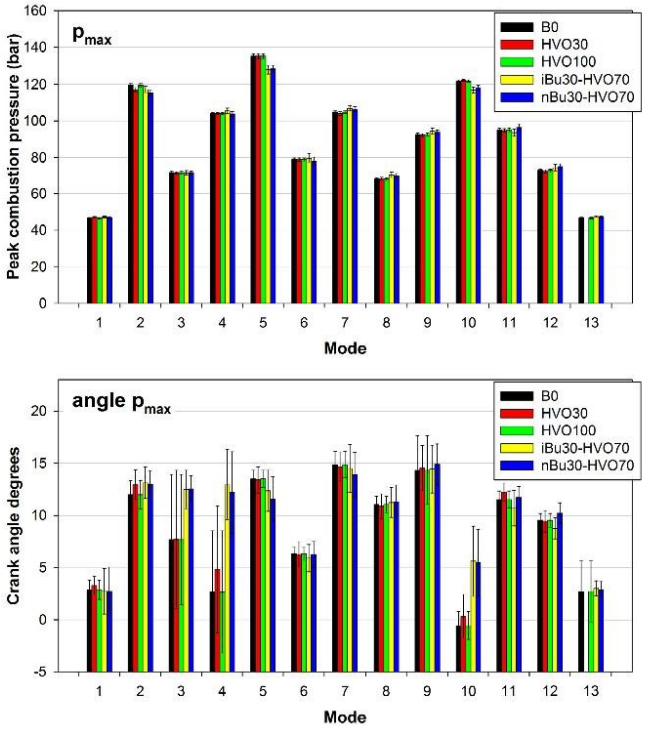

Fig. 2 (*continued*)

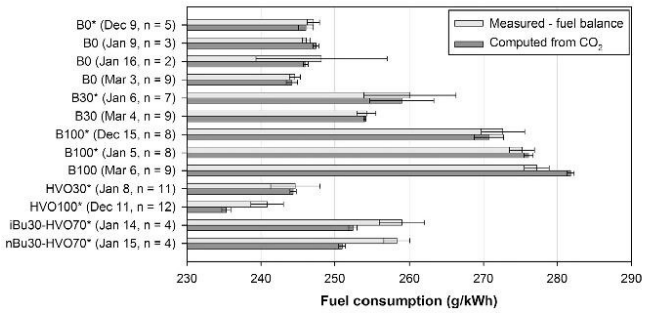

Fig. 3. Brake-specific fuel consumption – average of multiple runs of WHTC test cycle – as determined by direct measurement (fuel balance) and by inference from CO2 emissions.

insignificant for HVO and B100 to tens of percent. There is also very little difference in EC and OC, suggesting that nearly all EC and OC, and vast majority of total (i.e., $PM_{2.5}$) particulate mass, is in the PM_1 fraction.

HVO and its blends with butanol all provided a moderate reduction of 30–40% in OC. While neat HVO provided a moderate reduction of EC of about 30%, butanol-HVO blends resulted in a considerable, 75–80% reduction in EC, more than around 70% for B100.

Decrease of OC and EC in emissions of biodiesel and its blends in comparison with those of classical diesel is in agreement with data in literature [31]. The reduced concentrations of EC found for both butanol blends in this study agrees with the results of another study dealing with the effect of n-butanol addition [32]. However, the course of the concentration of OC for the fuels with addition of butanol differ in both studies, the OC decreases in this study while increases in previous study [32] in comparison with those without butanol.

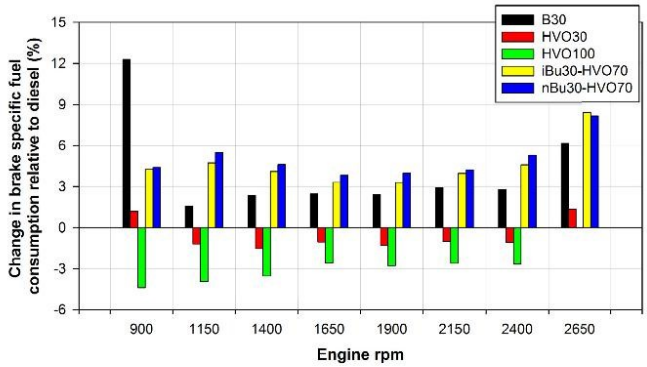

Fig. 4. Brake-specific fuel consumption at maximum torque relative to diesel fuel.

PAHs in emission of diesel vehicles originate partly from lubricating oil or pyrosynthesis but predominant part of PAHs is derived from the incomplete combustion of diesel fuel [33,34]. Many polycyclic aromatic hydrocarbons are suspected or known carcinogens and mutagens [35]. The sum of the concentrations of nine of the PAHs regarded by the IARC [36] as carcinogenic (cPAHs) in experimental animals (the US EPA simultaneously classifies them as probable human carcinogens [35]), namely benz[a]anthracene, chrysene, benzo[b]fluoranthene, benzo[k]fluoranthene, benzo[e]pyrene, benzo[a]pyrene, dibenz[a,h]anthracene, indeno[1,2,3-cd]pyrene and benzo[g,h,i]perylene, is referred to as cPAHs.

For the same conditions as in Fig. 7, the emissions of all PAHs and cPAHs are plotted in Fig. 8.

With the exception of diesel fuel, where cold start resulted in more than twice carcinogenic PAHs (9 PAHs per US EPA) than hot run, there is no consistent effect of cold start, and no consistent difference between $PM_{2.5}$ and PM_1. Carcinogenic PAHs represent an average 8.7% of the total content of PAHs. The concentration of cPAHs increases at cold starts to mean ratio of 11.2% while at hot starts the amount of formed cPAHs is smaller (mean ratio of 7.9%). For hot starts, the highest sum of cPAHs was found at exhaust of B0 and B30 wheres amount of cPAHs in exhausts of HVO100, iBu30 and nBu30 decreased to only 29, 26 and 22%, respectively, of those in B0. In cold starts we observed even larger difference when the highest concentrations of cPAHs was found again in B0 exhaust and amount of cPAHs in exhausts of HVO100, iBu30 and nBu30 decreased to 26, 9 and 11%, respectively, of those in B0.

The lowest content of sum of PAHs was found in exhausts of mixture HVO with nBu and iBu containing only 20% and 27%, respectively, of sum of PAHs in diesel (B0) exhaust. Content of PAHs in biodiesel (B100) or in HVO100 was also smaller than those in classical diesel (B0).

The emissions of individual PAHs are given in Fig. 9, and the relative abundance of three- and four-ring PAHs is given in Fig. 10. Light three- (fluorene, phenathrene, anthracene) and four-ring (pyrene, fluoranthene, benz[a]anthracene, chrysene) PAHs comprise a dominant part of PAHs in all samples forming in average 97.8% of detected PAHs (range 93.2–98.8%). The most abundant PAHs for all fuels (with exception of HVO100) was pyrene while phenanthrene prevailed in HVO100 samples. The relative abundance of all PAHs is compared in Fig. 11.

Overall, butanol-HVO blends have resulted in a considerable reduction of 70–80% in total PAHs, while other fuels exhibited inconsistent effects. PAHs in emissions of pure biodiesel and pure HVO were reduced, while PAHs in emissions of their 30% blends increased. Similarly, butanol-HVO blends have resulted in a considerable reduction of 70–80% in the sum of the 9 carcinogenic PAHs, compared to moderate and not always consistent effects of other fuels.

Unlike other studied organic compounds, PAHs are relatively more frequently analysed components in diesel and biodiesel emissions [31–32,37–42]. Decrease of PAHs found in this study for pure biodiesel fuels (B100 and HVO100) in comparison with B0 is in agreement with previous studies [31,37–40] but a few papers [41,42] reported no significant differences in PAHs amount in biodiesel emissions, so the influence of alternative fuels on PAHs emissions is variable. Regarding the effect of butanol addition, only blends of n-butanol with diesel were tested in literature resulting in increase of PAHs emissions [32,37]. These results are thus the opposite of the findings from this study although we examined of n-butanol or isobutanol blends with HVO and not with diesel as in other studies.

3.7. Nitrated polycyclic aromatic hydrocarbons

Nitrated polycyclic aromatic hydrocarbons (nitro-PAHs) could be more harmful to humans than the unsubstituted-PAHs [43]. The 1-nitropyrene has been used as marker of diesel exhaust [44]. A total of 15 nitro-PAH compounds were analysed in this study (including 1-nitronaphthalene, 2-nitronaphthalene, 2-nitrofluorene, 9-nitroanthracene, 9-nitrophenanthrene, 3-nitrophenanthrene, 3-nitrofluoranthene, 1-nitropyrene, 7-nitrobenz[a]anthracene, 6-nitrochrysene, 3-nitrobenzanthrone, 1,3-, 1,6-, and 1,8-dinitropyrenes, 6-nitrobenzo[a]pyrene), however, the concentrations of all nitro-PAHs in all samples were below the limit of detection (range of 0.018–0.286 μg/kWh).

3.8. Alkanes

Particulate n-alkanes in diesel exhaust emissions were reported to result from engine lubricating oil and also from unburned diesel fuel itself [45]. n-Alkanes identified in exhaust emissions of Iveco engine were the most abundant class of organic compounds analysed. n-Alkanes constitute 1.4% of organic carbon in emissions. The emissions of n-alkanes and the abundance of different alkanes, grouped by number of carbon atoms, are compared in Fig. 12. The highest sum of n-alkanes was found for B0 while for HVO100 and its mixtures with n-butanol and isobutanol the sum

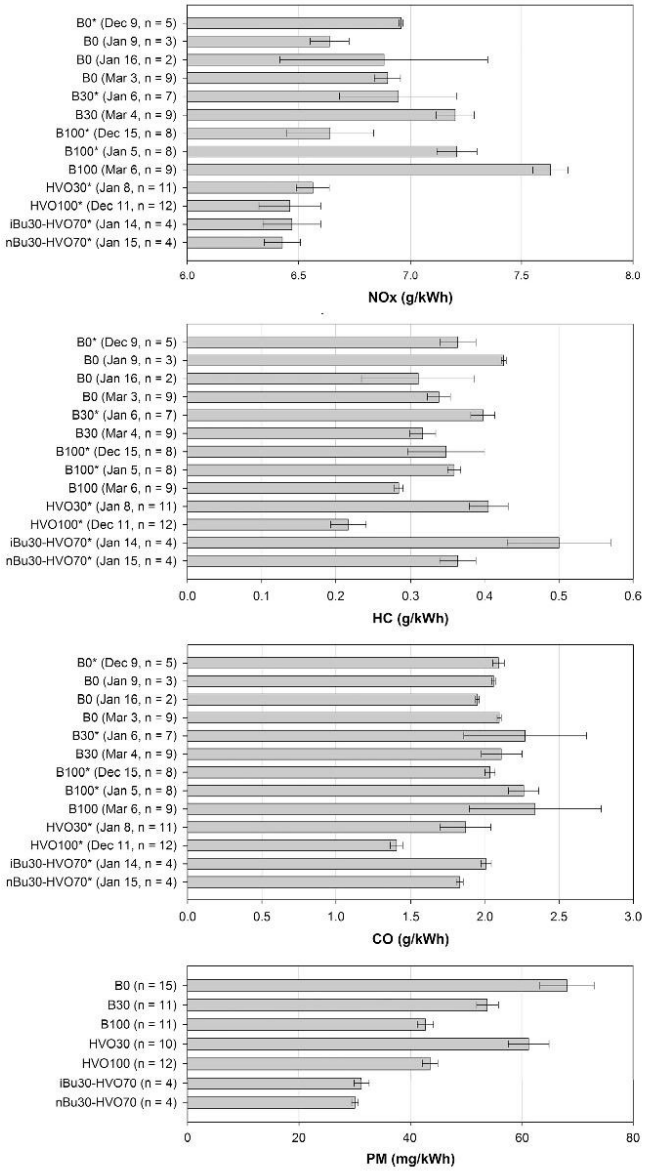

Fig. 5. Comparison of NOx, HC and CO emissions during different sets – each point represent an average of multiple runs of the hot WHTC cycle. Multiple runs on the same fuel but on different days were inluded to assess variability.

was nearly two times smaller, which indicates effect of fuel composition on exhaust composition.

In dependence on the fuel used, the homologue distribution of the n-alkanes (C_{10}-C_{36}) shows a unimodal or bimodal distribution. The carbon number with maximum detected concentration (C_{max}) is used as an indication of relative source input [46]. Heneicosane (C_{21}) was the most abundant n-alkane at the unimodal distribution of classical diesel (B0), which is in agreement with diesel data in literature [47]. The same maximum was observed also at bimodal distributions of other tested fuels when another maximum was

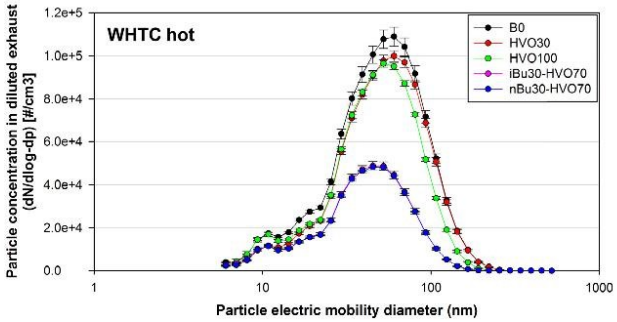

Fig. 6. Exhaust-flow-weighted average particle size distributions (raw exhaust diluted by a factor of 150) during hot WHTC cycle for different fuels. Error bars represent standard deviation of multiple consecutive runs of the cycle. Data for two butanol isomers are practically identical.

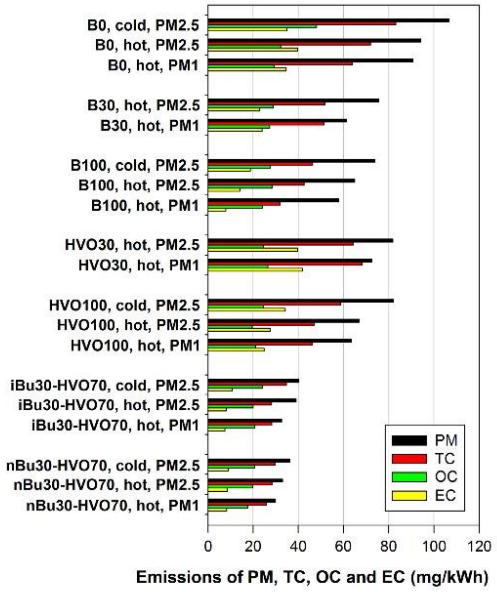

Fig. 7. Comparison of emissions of PM, elemental (EC), organic (OC) and total (TC = OC + EC) carbon: PM2.5 for cold start WHTC and in PM2.5 and PM1 for hot start WHTC across different fuels.

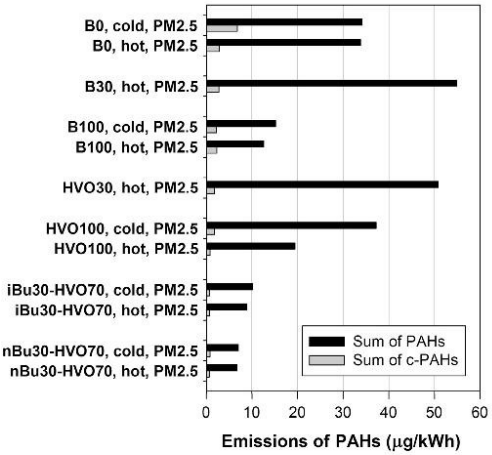

Fig. 8. Comparison of emissions of 9 carcinogenic PAHs (benz[a]anthracene, chrysene, benzo[b]fluoranthene, benzo[k]fluoranthene, benzo[e]pyrene, benzo[a]pyrene, dibenz[a,h]anthracene, indeno[1,2,3-cd]pyrene and benzo[g,h,i]perylene) and total PAHs in PM2.5 for cold and hot start WHTC across different fuels.

found at hexacosane (C_{26}) or heptacosane (C_{27}) (Fig. 12). The second maximum probably results from the addition of bio components of vegetable oils into used fuel.

Alkane molecular diagnostic ratio, the so called carbon preference index (CPI), is applied for the identification of emission source of n-alkanes. The CPI values calculated as the ratio of the sums of odd over even n-alkanes in the range C_{14} – C_{32} were for examined fuels close to unity (mean value 0.99, range 0.89 – 1.09), which proves petroleum residues as the main source of n-alkanes found in exhausts from Iveco engine [47,48].

3.9. Isoprenoids

Isoprenoids, pristane and phytane, are formed mainly during diagenesis of phytol [46] or are emitted from biological sources [48]. Pristane and phytane are present in fuel and in lubricating oil [49,50]. The concentration of pristane in all Iveco exhaust samples was smaller than corresponding concentration of phytane. The concentration of pristane was similar in all Iveco exhaust samples while the concentration of phytane changed for different fuels (Fig. 13). The highest content of phytane was found in exhaust of petroleum diesel (B0). The lower concentrations of phytane in emissions from all biofuels is probably connected with the biological origin of these fuels. The lowest emissions of phytane were for B100 and for both HVO-butanol blends, and for these, it cannot be readily discerned whether the phytane originates from the combustion of engine lubricating oil or from the fuels.

3.10. Hopanes and steranes

Fossil petroleum markers such as steranes and hopanes (pentacyclic triterpanes) are present in lubricating oils [49]. They are used to track the presence of the vehicle emissions in the ambient

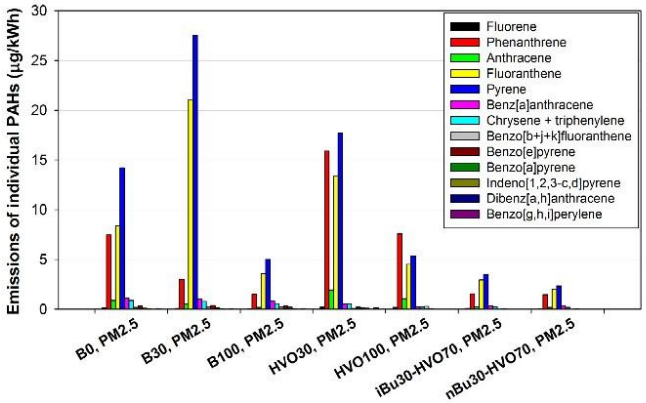

Fig. 9. Emissions of individual PAHs across different fuels (PM2.5, WHTC hot).

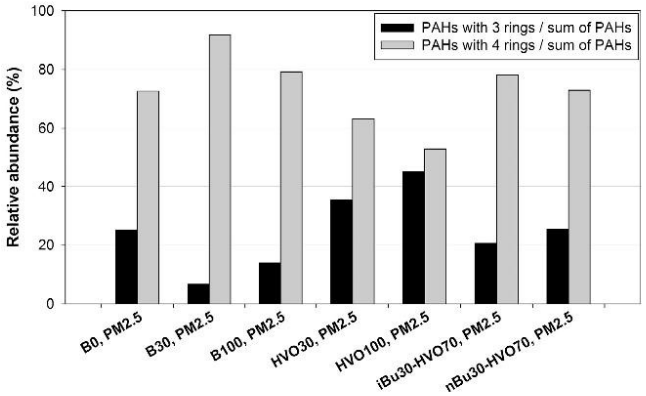

Fig. 10. Relative abundance of three- and four-ring PAHs across different fuels (PM2.5, WHTC hot).

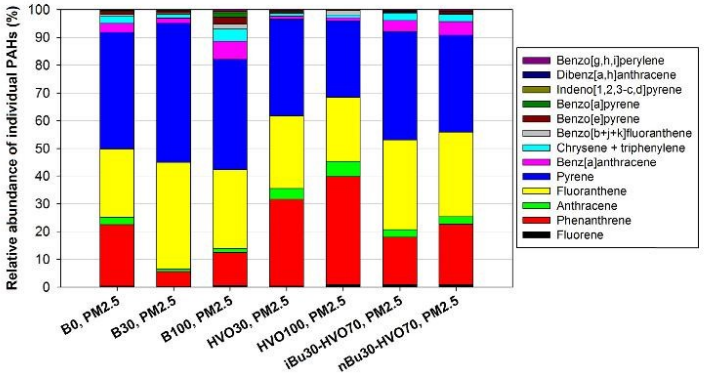

Fig. 11. Relative abundance of individual PAHs across different fuels (PM2.5, WHTC hot).

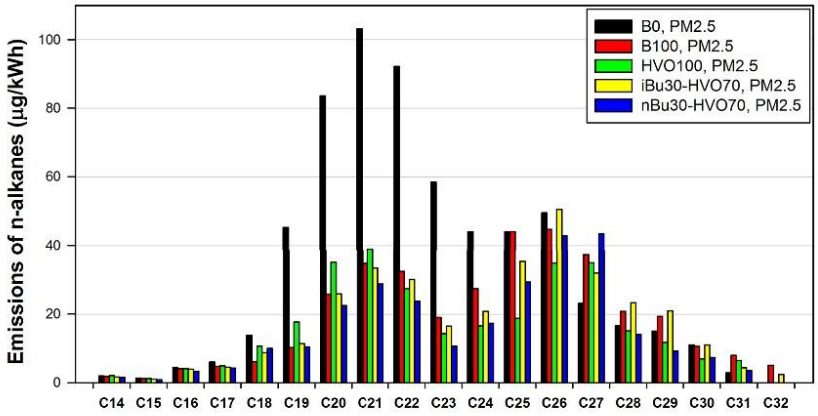

Fig. 12. Emissions of n-Alkane (C14 – C32) homologue distribution across different fuels (PM2.5, WHTC hot).

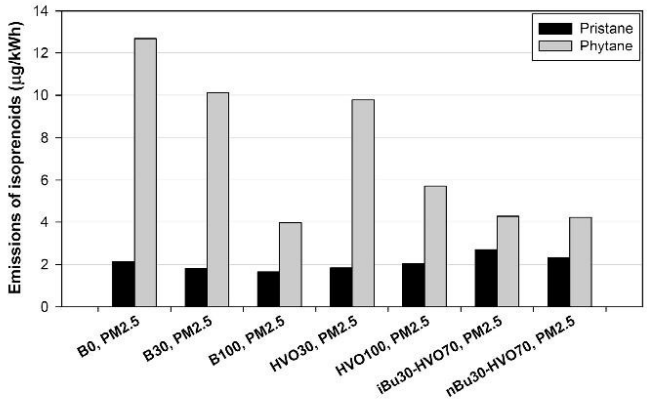

Fig. 13. Emissions of isoprenoids across the fuels (PM2.5, WHTC hot).

atmosphere [51] as well as for estimation of exhaust contributions from vehicular sources to the atmosphere [45].

Hopanes and steranes were identified in all exhaust samples. In general, no significant differences in the concentrations of hopanes and steranes in the emissions for studied diesel and biodiesel fuels were observed. 17α(H),21β(H)-norhopane, a tracer for motor vehicle exhaust [52], was the most abundant hopane in all samples (Fig. 14). The similar concentrations of R and S isomer of 17α(H), 21β(H)-homohopane in all samples are in concordance with data in literature indicating that their concentrations in vehicular emissions should be equal [50]. The mean value of homohopane index [S/(S + R)], the ratio of the concentration of R- and S- isomer of the 17α(H),21β(H)-homohopane, was 0.46 (the range of 0.44–0.48). The most abundant sterane in all samples was ααα(20R)-choles tane, the concentrations of other steranes (i.e., ααα(20R,24S)-24-methylcholestane and ααα(20R,24R)-24-ethylcholestane) were smaller (Fig. 14). Comparison of the percentual compositional variations of hopanes and steranes between the fuels show stable ratios of hopanes and steranes associated with studied fuels. Our findings hence differ from results of previous study [31] where % profiles of hopanes and steranes varied between the fuels and levels of hopanes/steranes associated with B100 were lower than those of B0.

The exhaust mass and sums of concentrations of analysed PAHs, n-alkanes, isoprenoids, hopanes and steranes for fine fraction of Iveco exhaust are compared in Fig. 15 for all fuels. n-Alkanes were the most abundant class among the analysed organic compounds comprising in average of 1.4% of OC in emissions for all fuels. Hopanes and steranes together with isoprenoids were only minor compounds in Iveco emissions, however, these compounds, so-called molecular biomarkers, are important components of vehicular emissions because they serve as petroleum tracers for airborne PM [48]. PAHs were the most toxic compounds analysed in Iveco emissions.

Cold starts yielded in average about 15% higher concentrations of particulate matter and higher concentrations of particulate organic compounds in emissions than hot starts.

The vast majority of EC and OC, studied organic compounds, and mass of $PM_{2.5}$ was included in the size fraction PM_1.

4. Discussion

There is no apparent indication of any substantial difference in the combustion process among the fuels. As there were no differences in the crankshaft angles at which 5%, 10% and 50% of the fuel

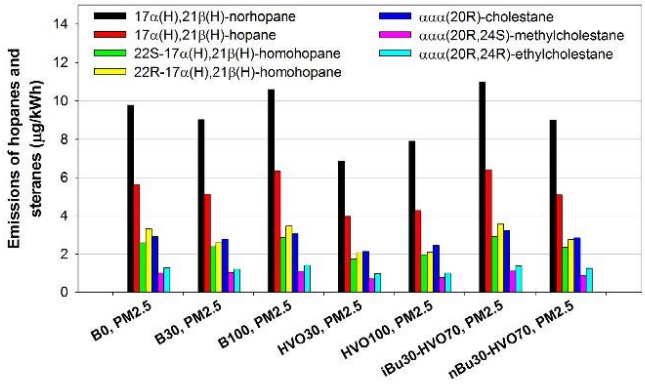

Fig. 14. Emissions of hopanes and steranes across the fuels (PM2.5, WHTC hot).

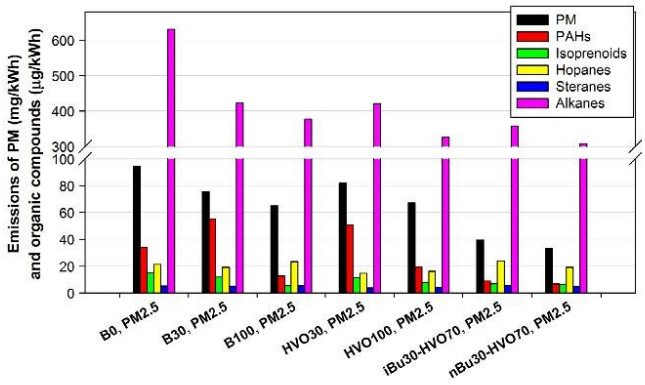

Fig. 15. Overview of fuel effects on the emissions of PM, PAHs, n-alkanes, isoprenoids, hopanes and steranes (PM2.5, WHTC hot).

energy was released, and there were no substantial differences in the cycle-to-cycle variance, it appears that the timing of the combustion was comparable for all fuels. As a difference in the ignition delay would likely lead to a difference in 5% or 10% MFB, it can be argued that there was no difference in the ignition delay across the fuels. This is especially important for the butanol-HVO blends, as an increase in the ignition delay would be expected (and was observed in [16]) should butanol be blended with diesel fuel.

The differences in maximum torque were commensurate to the differences in the heating values of the fuels. The engine brake thermal efficiency, assessed at various operating conditions, was comparable across all fuels. Differences in fuel consumption were attributed primarily to the different heating values. The differences in the CO_2 emissions were mostly affected by the fuel heating value and carbon content, except for butanol-HVO blends, where approximately 3% of the fuel consumed was not accounted for in CO_2 emissions; this difference is, however, within the uncertainty of emissions measurement.

Regarding exhaust emissions, the main effect of butanol-HVO blends with respect to diesel fuel were small changes, often on the borderline of significance, in NO_x emissions, major and significant decreased in total PM mass, and large decreases in practically all PM metrics and major decreases in the PM emissions. Relative to diesel fuel, NO_x were slightly higher for biodiesel (B30 and B100) and slightly lower for HVO and its blends with diesel fuel and with butanol; however, only the differences between HVO-containing fuels and biodiesel-containing fuels were large enough to be statistically significant. This is in line with the general trend of biodiesel slightly increasing and HVO slightly decreasing NO_x emissions. The addition of butanol to HVO did not produce a difference in NO_x relative to neat HVO, which is in line with relatively small and inconsistent effects on NO_x of addition of butanol to diesel fuel.

The highest difference was in the PM emissions. For both n-butanol and isobutanol blends with HVO, the emissions of total PM mass have decreased by more than one half according to the gravimetric measurement on fluorocarbon-coated glass fiber filters (Fig. 5) and slightly more according to the gravimetry on uncoated glass fiber filters (Fig. 7) which are more prone to the retention of gaseous organic compounds. Also, elemental carbon, organic carbon and PAHs have all decreased relative to diesel fuel considerably, by approximately 75–80% for EC and cPAHs (Fig. 7), by far the highest reduction achieved by any of the fuels tested in this study.

The total PM mass was lower for biodiesel and for HVO relative to diesel fuel, which is in line with the general findings (see Introduction) on biodiesel and HVO, and the PM mass was also lower for HVO-butanol blends relative to neat HVO, which is in agreement

with the reported decrease in PM by addition of butanol into diesel fuel. Addition of butanol into HVO has decreased, relative to neat HVO, PAHs, while addition of butanol into diesel fuel has been reported to increase PAHs relative to diesel fuel [32,37].

The usage of vegetable oils results in bimodal distributions of n-alkanes and decrease in the concentration of n-alkanes and phytane in emissions of B100, HVO and butanol-HVO blends in comparison with those in B0, suggesting that the fuel is a considerable source of these compounds, and that fuel composition affects the composition of emissions. The concentrations of hopanes and stearanes were comparable across the fuels, suggesting that their primary source might have been engine lubricating oil, which was the same for all fuels.

Overall, HVO-butanol blends did not exhibit any negative consequences in terms of combustion, engine efficiency, or emissions, while yielding a very considerable reduction in what is believed to be the most harmful pollutants, ultrafine particles and particle-bound carcinogenic PAHs. The HVO-butanol blends therefore appear to combine the best of both blend components – high cetane number and superior ignition properties of HVO, and oxygen content and relatively low cost of butanol – while the potential negative aspects of each of the fuels (high cost of HVO, low cetane number of butanol) are reduced by the presence of the other fuel.

5. Conclusions

The potential of n-butanol and isobutanol as economic oxygenate extenders of hydrogenated vegetable oils (HVO) was examined experimentally on a turbocharged diesel engine with common rail injection. HVO and biodiesel, neat and blended with diesel fuel, and diesel fuel were used as reference.

The addition of 30% of either isomer into HVO has not caused a marked change in the combustion timing, peak combustion pressure, efficiency, or NO_x, both with respect to diesel fuel and to neat HVO. While blending of butanol into diesel fuel has been reported to increase the ignition delay and the production of PAHs, blending of either n-butanol or isobutanol at 30% into HVO has resulted in lower emissions of total particle mass, elemental carbon, and polyaromatic hydrocarbons both with respect to neat HVO and with respect to diesel fuel. The effect on peak torque was commensurate to the differences in the fuel heating values.

Butanol-HVO blends have resulted in a 75–78% reduction in elemental carbon and 79–80% reduction in carcinogenic PAHs relative to diesel fuel, a substantially higher reduction compared to both neat HVO and neat biodiesel.

The usage of vegetable oils results in bimodal distributions of n-alkanes and decrease in the concentration of n-alkanes and phytane in emissions of B100, HVO and butanol-HVO blends in comparison with those in B0, suggesting that the fuel is a considerable source of these compounds, and that fuel composition affects the composition of emissions. The concentrations of hopanes and stearanes were comparable across the fuels, suggesting that their primary source might have been engine lubricating oil, which was the same for all fuels.

The HVO-butanol blends therefore appear to combine the best of both blend components – high cetane number and superior ignition properties of HVO, and oxygen content and relatively low cost of butanol – while the potential negative aspects of each of the fuels (high cost of HVO, low cetane number of butanol) are reduced by the presence of the other fuel.

Acknowledgement

The combustion analysis was supported by project NPU LO1311 and the purchase of analytical equipment by project CZ.1.05/2.1.00/19.04.08, both funded by the Czech Ministry of Education, Youth and Sports. The NExBTL fuel (HVO) was provided by Neste Oil, Espoo, Finland. The remaining part of experimental work was supported by Czech Science Foundation under project P503/13/1438S and by the Institute of Analytical Chemistry of the CAS under the Institutional Research Plan RVO: 68081715.

References

[1] Knothe G. Biodiesel and renewable diesel: a comparison. Prog Energ Combust 2010;36:364–73.
[2] Szybist JP, Song J, Alam M, Boehman AL. Biodiesel combustion, emissions and emission control. Fuel Process Technol 2007;88(7):679–91.
[3] Correa SM, Arbilla G. Aromatic hydrocarbons emissions in diesel and biodiesel exhaust. Atmos Environ 2006;40:6821–6.
[4] Vojtisek-Lom M, Pechout M, Dittrich L, Beranek V, Kotek M, Schwarz J, et al. Polycyclic aromatic hydrocarbons (PAH) and their genotoxicity in exhaust emissions from a diesel engine during extended low-load operation on diesel and biodiesel fuels. Atmos Environ 2015;109:9–18.
[5] Karavalakis G, Fontaras G, Ampazouglou D, Kousoulidou M, Stournas S, Samaras Z, et al. Effects of low concentration biodiesel blends application on modern passenger cars. Part 3: impact on PAH, nitro-PAH, and oxy-PAH emissions. Environ Pollut 2010;158:1584–94.
[6] No SY. Application of hydrotreated vegetable oil from triglyceride based biomass to CI engines – a review. Fuel 2014;115:88–96.
[7] Westphal GA, Krahl J, Munack A, Rosenkranz N, Schröder O, Schaak J, et al. Combustion of hydrotreated vegetable oil and jatropha methyl-ester in a heavy duty engine: emissions and bacterial mutagenicity. Environ Sci Technol 2013;47(11):6038–46.
[8] Murtonen T, Aakko-Saksa P, Kuronen M, Mikkonen S, Lehtoranta K. Emissions with heavy-duty diesel engines and vehices using FAME, HVO, and GTL with and without DOC-POC aftertreatment. SAE Technical Papers 2010; 2:147-166.
[9] Lapuerta M, Villajos M, Agudelo JR, Boehman AL. Key properties and blending strategies of hydrotreated vegetable oil as biofuel for diesel engines. Fuel Process Technol 2011;92:2406–11.
[10] Aatola H, Larmi M, Sarjovaara T. Hydrotreated vegetable oil (HVO) as a renewable diesel fuel: trade-off between NOx, particulate emission, and fuel consumption of a heavy duty engine. SAE Int J Engines 2010;1(1):1251–62.
[11] Nylund NO, Erkkilä K, Ahtiainen M, Murtonen T, Saikkonen P, Amberla A, et al. Optimized usage of NExBTL renewable diesel fuel. OPTIBIO. [Internet].VTT Tiedotteita – Research Notes 2604:p.167 [cited 2016 May 6] Available from: http://www.vtt.fi/inf/pdf/tiedotteet/2011/T2604.pdf.
[12] Tao L, Tan ECD, McCormick R, Zhang M, Aden A, He X, et al. Techno-economic analysis and life-cycle assessment of cellulosic isobutanol and comparison with cellulosic ethanol and n-butanol. Biofuel Bioprod Bior 2014;8(1):30–48.
[13] Kumar NS. Influence of ethanol–gasoline blends on performance parameters and combustion characteristics of copper coated two stroke spark ignition engine with gasohol. IJIRSET 2014;3(3):10787–94.
[14] Giakoumis EG, Rakopoulos CD, Dimaratos AM, Rakopoulos DC. Exhaust emissions with ethanol or n-butanol diesel fuel blends during transient operation: a review. Renew Sust Energ Rev 2013;17:170–90.
[15] Lin SL, Lee WJ, Lee CF, Wu Y. Reduction in emissions of nitrogen oxides, particulate matter, and polycyclic aromatic hydrocarbon by adding water-containing butanol into a diesel-fueled engine generator. Fuel 2012;93:364–72.
[16] Rakopoulos DC, Rakopoulos CD, Papagiannakis RG, Kyritsis DC. Combustion heat release analysis of ethanol or n-butanol diesel fuel blends in heavy-duty DI diesel engine. Fuel 2011;90(5):1855–67.
[17] Rakopoulos CD, Dimaratos AM, Giakoumis EG, Rakopoulos DC. Investigating the emissions during acceleration of a turbocharged diesel engine operating with biodiesel or n-butanol diesel fuel blends. Energy 2010;35:5173–84.
[18] Rakopoulos DC, Rakopoulos CD, Giakoumis EG, Papagiannakis RG, Kyritsis DC. Influence of properties of various common bio-fuels on the combustion and emission characteristics of high-speed DI (direct injection) diesel engine: vegetable oil, bio-diesel, ethanol, n-butanol, diethyl ether. Energy 2013;73:354–66.
[19] Miers SA, Carlson RW, McConnell SS, Ng HK, Wallner T, Esper JL. Drive cycle analysis of butanol/diesel blends in a light-duty vehicle. SAE technical paper 2008; 2008-01-2381.
[20] Rakopoulos DC, Rakopoulos CD, Kyritsis DC. Butanol or DEE blends with either straight vegetable oil or biodiesel excluding fossil fuel: comparative effects on diesel engine combustion attributes, cyclic variability and regulated emissions trade-off. Energy 2016;115:314–25.
[21] Rakopoulos DC, Rakopoulos CD, Giakoumis EG. Impact of properties of vegetable oil, bio-diesel, ethanol and n-butanol on the combustion and emissions of turbocharged HDDI diesel engine operating under steady and transient conditions. Fuel 2015;156:1–19.
[22] Happonen M, Heikkilä J, Aakko-Saksa P, Murtonen T, Lehto K, Rostedt A, et al. Diesel exhaust emissions and particle hygroscopicity with HVO fuel-oxygenate blend. Fuel 2013;103:380–6.
[23] United Nations Agreement Concerning the Adoption of Uniform Technical Prescriptions for Wheeled Vehicles, Equipment and Parts which can be fitted and/or be used on Wheeled Vehicles and the Conditions for Reciprocal

Recognition of Approvals Granted on the Basis of these Prescriptions. Regulation no. 49, revision 6, Appendix I. [cited 2017 January 30] Online at: https://www.unece.org/fileadmin/DAM/trans/main/wp29/wp29regs/2013/R049r6e.pdf.
[24] Křůmal K, Mikuška P, Večeřa Z. Polycyclic aromatic hydrocarbons and hopanes in PM1 aerosols in urban areas. Atmos Environ 2013;67:27–37.
[25] Mikuška P, Křůmal K, Večeřa Z. Characterization of organic compounds in the PM2.5 aerosols in winter in an industrial urban area. Atmos Environ 2015;105:97–108.
[26] Cavalli F, Viana M, Yttri KE, Genberg J, Putaud J-P. Toward a standardised thermal-optical protocol for measuring atmospheric organic and elemental carbon: the EUSAAR protocol. Atmos Meas Tech 2010;3:79–89.
[27] R Core Team. R: A language and environment for statistical computing. R Foundation for Statistical Computing. Vienna, Austria; 2016. URL https://www.R-project.org/.
[28] Fox J, Bouchet-Valat M. Rcmdr: R Commander. R package version 2.3-2; 2017.
[29] Giraudoux P. pgirmess: data Analysis in Ecology. R package version 1.6.5; 2016 https://CRAN.R-project.org/package=pgirmess.
[30] Schauer JJ, Kleeman MJ, Cass GR, Simoneit BR. Measurement of emissions from air pollution sources. 2. C1 through C30 organic compounds from medium duty diesel trucks. Environ Sci Technol 1999;3336:1578–87.
[31] Jedynska A, Tromp PC, Houtzager MMG, Kooter IM. Chemical characterization of biofuel exhaust emissions. Atmos Environ 2015;116:172–82.
[32] Zhang ZH, Balasubramanian R. Influence of butanol–diesel blends on particulate emissions of a non-road diesel engine. Fuel 2014;118:130–6.
[33] Marr LC, Kirchstetter TW, Harley RA, Miguel AH, Hering SV, Hammond SK. Characterization of polycyclic aromatic hydrocarbons in motor vehicle fuels and exhaust emissions. Environ Sci Technol 1999;33:3091–9.
[34] Kleeman MJ, Riddle SG, Robert MA, Jakober CA. Lubricating oil and fuel contributions to particulate matter emissions from light-dutygasoline and heavy-duty diesel vehicles. Environ Sci Technol 2008;42:235–42.
[35] WHO. Health risks of persistent organic pollutants from long-range transboundary air pollution. Copenhagen: World Health Organization, WHO Regional Office for Europe; 2003.
[36] IARC. International Agency for Research on Cancer and World Health Organization, IARC Monographs on the Evaluation of Carcinogenic Risks to Humans, vol. 92. Some non-heterocyclic polycyclic aromatic hydrocarbons and some related exposures; 2010.
[37] Yilmaz N, Davis SM. Polycyclic aromatic hydrocarbon (PAH) formation in a diesel engine fueled with diesel, biodiesel and biodiesel/n-butanol blends. Fuel 2016;181:729–40.
[38] Ballesteros R, Hernández JJ, Lyons LL. An experimental study of the influence of biofuel origin on particle-associated PAH emissions. Atmos Environ 2010;44:930–8.
[39] He C, Ge Y, Tan J, You K, Han X, Wang J. Characteristics of polycyclic aromatic hydrocarbons emissions of diesel engine fueled with biodiesel and diesel. Fuel 2010;89:2040–6.
[40] Sharp C, Howell S, Jobe J. The effect of biodiesel fuels on transient emissions from modern diesel engines, Part II Unregulated emissions and chemical characterization. SAE Technical Paper; 2000-01-1968.
[41] Tang L, Frank B, Lanni T, Rideout G, Meyer N, Beregszaszy C. Unregulated emissions from a heavy-duty diesel engine with various fuels and emission control systems. Environ Sci Technol 2007;41:4043–5037.
[42] Turrio-Baldassarri L, Battistelli C, Conti L, Crebelli R, De Berardis B, Iamiceli A, et al. Emission comparison of urban bus engine fueled with diesel oil and biodiesel blend. Sci Total Environ 2004;327:147–62.
[43] Durant JL, Busby WF, Lafleur AL, Penman BW, Crespi CL. Human cell mutagenicity of oxygenated, nitrated and unsubstituted polycyclic aromatic hydrocarbons associated with urban aerosols. Mutat Res/Genet Toxicol 1996;371:123–57.
[44] Scheepers PTJ, Martens MHJ, Velders DD, Fijneman P, Van Kerkhoven M, Noordhoek J, et al. 1-nitropyrene as a marker for the mutagenicity of diesel exhaust-derived particulate matter in workplace atmospheres. Environ Mol Mutagen 1995;25:134–47.
[45] Rogge WF, Hildemann LM, Mazurek MA, Cass GR, Simoneit BRT. Sources of fine organic aerosol. 2. Noncatalyst and catalyst-equipped automobiles and heavy-duty diesel trucks. Environ Sci Technol 1993;27:636–51.
[46] Simoneit BRT. Organic-matter of the troposphere. 5. Application of molecular marker analysis to biogenic emissions into the troposphere for source reconciliations. J Atmos Chem 1989;8:251–75.
[47] Mazurek MA, Cass GR, Simoneit BRT. Interpretation of high resolution gas chromatography and high resolution gas chromatography/mass spectrometry data acquired from atmospheric organic aerosol samples. Aerosol Sci Technol 1989;10:408–20.
[48] Andreou G, Rapsomanikis S. Origins of n-alkanes, carbonyl compounds and molecular biomarkers in atmospheric fine and coarse particles of Athens. Greece. Sci Total Environ 2009;407:5750–60.
[49] Simoneit BRT. Application of molecular marker analysis to vehicular exhaust for source reconciliations. Int J Environ Anal Chem 1985;22:203–33.
[50] Křůmal K, Mikuška P, Večeřa Z. In Czech: Využití organických markerů pro identifikaci zdrojů atmosférických aerosolů (in English: Application of organic markers in identification of sources of organic aerosols). Chemické Listy. 106: 95–103.
[51] Schauer JJ, Rogge WF, Hildemann LM, Mazurek MA, Cass GR, Simoneit BRT. Source apportionment of airborne particulate matter using organic compounds as tracers. Atmos Environ 1996;30:3837–55.
[52] Schauer JJ, Kleeman MJ, Cass GR. Simoneit BRT. Measurement of emissions from air pollution sources. 5.C-1-C-32 organic compounds from gasoline-powered motor vehicles. Aerosol Sci Technol 2002;36:1169–80.

Článek 6

Toxicology in Vitro 54 (2019) 178–188

Contents lists available at ScienceDirect

Toxicology in Vitro

journal homepage: www.elsevier.com/locate/toxinvit

Nano-TiO_2 stability in medium and size as important factors of toxicity in macrophage-like cells

T. Brzicova[a,b,1], J. Sikorova[a,c,1], A. Milcova[a], K. Vrbova[a], J. Klema[d], P. Pikal[e], Z. Lubovska[f], V. Philimonenko[f,g], F. Franco[a,h], J. Topinka[a], P. Rossner Jr[a,*]

[a] Department of Genetic Toxicology and Nanotoxicology, Institute of Experimental Medicine of the Czech Academy of Sciences, Prague 14220, Czech Republic
[b] Laboratory for Risk Reesearch and Management, Faculty of Safety Engineering, VSB – Technical University of Ostrava, Ostrava 700 30, Czech Republic
[c] Institute for Environmental Studies, Faculty of Science, Charles University, Benatska 2, Prague 2 12801, Czech Republic
[d] Department of Computer Science, Czech Technical University in Prague, Prague 121 35, Czech Republic
[e] Precheza, Prerov 751 52, Czech Republic
[f] Microscopy Center, Electron Microscopy Core Facility, Institute of Molecular Genetics ASCR v.v.i. of the Czech Academy of Sciences, Prague 142 20, Czech Republic
[g] Department of Biology of the Cell Nucleus, Institute of Molecular Genetics ASCR v.v.i. of the Czech Academy of Sciences, Prague 142 20, Czech Republic
[h] Genetic and Molecular Biology Graduate Program, Federal University of Goias, Goiás, 74690-900, Brazil

ARTICLE INFO

Keywords:
LASSO
Macrophages
Cytotoxicity
Nano-TiO_2
Polydispersity

ABSTRACT

TiO_2 along with nano-TiO_2 are commonly found in consumer products. In vivo studies have observed an accumulation of nano-TiO_2 in macrophages. However, characteristics of nano-TiO_2 determining toxicity remain unclear. In our study, the cytotoxic effects of 14 diverse nano-TiO_2 on THP-1 macrophage-like cells were measured by 3 cytotoxicity assays (MTS, WST-1 and LDH). Total averaged cytotoxicity was calculated using principal component analysis. Characteristics of all 14 nano-TiO_2 included hydrodynamic diameter, zeta potential, shape, polydispersity index (PDI) and concentration; moreover, crystal form, specific surface area and crystallite size were measured for 10 nano-TiO_2.The variables affecting cytotoxicity were chosen using LASSO (least absolute shrinkage and selection operator). Except for concentration, PDI in media measured within 1 h after preparation of the nanomaterial dispersion was selected as a variable affecting cytotoxicity: stable dispersion resulted in higher cytotoxic effects. Crystallite size has been shown to have nonlinear effects (particles of sizes between 20 and 60 nm were cytotoxic while smaller and larger ones were not) and thus it has been excluded from LASSO. The shape (particles/fibre) and crystal form did not affect the cytotoxicity. PDI and the nonlinear effect of size could be an explanation for the inconsistencies of the cytotoxicity of nano-TiO_2 in various studies.

1. Introduction

Nano-TiO_2 is commonly used in products because of their distinct properties (e.g. ultraviolet radiation absorption, photocatalytic properties or higher specific surface connected with catalytic properties) when compared to those consisting of larger particles. TiO_2 is one of the most widely used materials in nanoparticles production (Vance et al., 2015). Nano-TiO_2 is used in specialised products, mainly in cosmetics for UV absorption or in catalysts. However pigmentary material, used also for food colouring, always contains a part of particles with size below 100 nm; usually < 2% of mass or up to 40% of particle number (EFSA ANS Panel, 2016). Nano-forms of various materials could affect organisms in a different way than micro-forms, which have been considered to be inert and safe for human health for decades (Ophus et al., 1979; Hext et al. 2005; Chen et al., 1988). Nanoparticles are small enough to enter the cells, the blood stream, or to be transferred along the nerve (Elder et al. 2006; Kermanizadeh et al. 2015). TiO_2 nanoparticles administered through various routes can translocate via

Abbreviations: ROS, reactive oxygen species; LASSO, least absolute shrinkage and selection operator; NM, nanomaterial; BSA, bovine serum albumin; RPMI, Roswell Park Memorial Institute medium; FBS, fetal bovine serum; DLS, dynamic light scattering; *Z*-Avg, hydrodynamic size; PDI, polydispersity index; NC, negative control; TEM, transmission electron microscopy; PCA, Principal Component Analysis

* Corresponding author at: Department of Genetic Toxicology and Nanotoxicology, Institute of Experimental Medicine, Videnska 1083, Prague 14220, Czech Republic.
E-mail address: pavel.rossner@iem.cas.cz (P. Rossner).
[1] These authors contributed equally to this work.

https://doi.org/10.1016/j.tiv.2018.09.019
Received 2 October 2017; Received in revised form 30 August 2018; Accepted 26 September 2018
Available online 01 October 2018

systemic circulation to different organs (Shakeel et al. 2016). There is evidence that nano-TiO_2 is more toxic than bulk material (Guichard et al., 2012). OECD identified nano-TiO_2 as one of the priority manufactured nanomaterials for toxicology and risk assessment so as to avoid adverse effects from the use of this material (OECD 2010). Some evidence is arising that broad usage of nano-TiO_2in consumer products (Guo et al., 2017) or as a photocatalyst (Kebede et al., 2013) might not be safe.

The toxicity of various forms of nano-TiO_2 depends on their characteristics, such as shape, size, crystal structure, zeta potential, aggregation and agglomeration tendency, surface characteristics and coatings (Sha et al., 2015; Zhang et al., 2015). However, their contribution to toxicity remains unclear, as evident from inconsistent results from different studies (Shi et al., 2013). For instance, toxicity inversely associated with size was shown for TiO_2 nanoparticles (Xiong et al., 2013); but opposite observations, i.e. higher toxicity of 21 nm TiO_2 nanoparticles in comparison with 12 nm and 98 nm, were also observed (Zhang et al. 2012). Anatase, the less stable crystalline structure (Zhang et al., 2015) of TiO_2, was found to be more toxic to mouse macrophages (Zhang et al., 2012), human lung epithelial cells, human dermal fibroblasts, and human breast cancer cells (Sayes et al., 2006; De Matteiset al., 2016). Although in general, anatase is regarded to be more cytotoxic, De Matteiset al., (2016), Guichard et al. (2012) and Numano et al. (2014) found higher cytotoxicity for rutile rods than anatase particles. In this particular case, however, the result might be affected by the elongated shape of rutile nanomaterial (NM). Particles were also found to be less toxic then nano-belts (Silva et al., 2013; Hamilton et al., 2009), and fibrous nano-TiO_2 (Watanabe et al., 2002). The mechanisms of adverse effects of nano-TiO_2 are associated with reactive oxygen species (ROS) generation, as pointed out by Sayes et al. (2006). ROS generation can be enhanced by nontoxic UV illumination which triggers hydroxyl radical generation (Yin et al., 2012; Zhang et al., 2015). On the other hand, there are opposed findings of the cytotoxic effect of photoactivated (UV irradiated) nano-TiO_2 on human alveolar cell lines (A549) (Numano et al., 2014; Sayes et al., 2006). The characteristics possibly responsible for cytotoxicity of nano-TiO_2 have still not been fully understood.

In vivo studies have revealed the distribution of nano-TiO_2 in the organism. Intravenously administered nano-TiO_2 are mainly accumulated in the liver and spleen of the rat (Xie et al. 2011; Shinohara et al. 2014) due to the high population of macrophages in these organs. High levels of nano-TiO_2 retained in the organs 30 days after the administration indicated accumulation of nano-TiO_2 in these cells. Macrophages, nonspecific immune cells, are responsible for the uptake and degradation of foreign material (Saba, 1970) mainly through phagocytosis. As cleaners of the body environment, they play an irreplaceable role in NMs removal, immune response, and inflammation development, and could be considerably affected by the presence of nano-TiO_2 in the organism.

In the present study, we analyzed the cytotoxic effects of fourteen diverse nano-TiO_2 in the human monocytic cell line THP-1, differentiated into macrophage-like cells. The physical properties possibly affecting cytotoxicity were chosen using LASSO (least absolute shrinkage and selectionoperator), which in contrast to stepwise regression techniques gives consistent results (small changes in samples properties would not result in entirely different models) due to a model complexity penalty and cross-validation (Tibshirani,1996). Former LASSO applications in toxicology can be found in Hamon et al. (2015) or Laaksonen et al. (2006).

To enhance the comparability of our results with the data produced by other European laboratories, as well as to ensure their compatibility with nanotoxicological databases prepared in the scope of several ongoing EU projects (e.g. NANoREG, COST Action TD1204 MODENA), standardised protocols for cell cultivation, preparation of NM dispersion and cytotoxicity assays developed within NANOGENOTOX (https://www.anses.fr/fr/node/120284, Jensen et al. 2011) and NANOVALID projects (http://www.nanovalid.eu/) were used.

Table 1
The physical properties of the nano-TiO_2as provided by the manufacturers.

Technical name	Source	Declared size	Declared crystallinity
A5P-	MK Nano	< 5 nm	Anatase
A15P-	US Research Nanomaterials	15 nm	Anatase
A30P-	US Research Nanomaterials	30 nm	Anatase
A50P-	MK Nano	50 nm	Anatase
A100P-	MK Nano	100 nm	Anatase
A10x1T-	Novarials	10 nm × 1 μm	Anatase
A10x10W-	Novarials	10 nm × 10 μm	Anatase
A100x20W-	Novarials	100 nm × 20 μm	Anatase
R1-3P-	PlasmaChem	1–3 nm	Rutile
R30P-	US Research Nanomaterials	30 nm	Rutile
R30PS	US Research Nanomaterials	30 nm	Rutile
R50P-	US Research Nanomaterials	50 nm	Rutile
R100P-	US Research Nanomaterials	100 nm	Rutile
R165P-	US Research Nanomaterials	165 nm	Rutile

2. Materials and methods

2.1. TiO_2 nanomaterials

To comprehensively assess the cytotoxic potential of various types of nano-TiO_2, 14 commercially available nano-TiO_2 were used in this study. The set consisted of 5 variants of anatase and 5 variants of rutile nanoparticles differing in their diameter (ranging from 3 to 165 nm), 3 variants of anatase with high aspect ratio (tubes and wires) of different widths and lengths, and one silicon coated (hydrophobic) rutile particle. Anatase tubes and the smallest rutile particles were delivered in a paste form, and all the other samples were obtained in a powder form. A summary of nano-TiO_2 characteristics declared by the producers is reported in Table 1. The technical names of nano-TiO_2 used in our study, based on nano-TiO_2 characteristics, were derived as follows:

- For particles: anatase/rutile (A/R), size in nm (number), particles (P), no coating/silica coating (−/S)
- For wires/tubes: anatase/rutile (A/R), size nm x μm(number x number), tubes/wires (T/W), no coating (−)

2.2. Characterisation of raw/untreated nano-TiO_2

Nano-TiO_2 samples in powder form were characterised using X-ray diffraction (crystallinity), and Brunauer Emmet Teller measurements (specific surface area). All samples (powders and paste forms) were analysed thermogravimetrically (mass loss) for impurity determination. As nano-TiO_2 in paste form (R1-3P-, A10x1T-, A10x10W-, A100x20W-) were only available in a limited amount, their thermogravimetric analysis was utilised only for determination of the equivalent dose for cytotoxicity assays.

Crystallinity: The sample of a nano-TiO_2 was pressed into the frame using a hand press and placed in a diffractometer cartridge. CubiX3 (PANalytical, UK) diffractometer with a cobalt cathode was used. The spectral range measurement was set from 28° to 33° 2Θ angle with 0.005° 2Θ steps. Crystallinity (anatase/rutile) and crystallite size (Scherrer's equation) were determined.

Specific surface area: The nano-TiO_2 sample was dried at 105 °C by HG53 halogen moisture analyser (Mettler Toledo, Swiss), then 0.2 g of the dried sample was put into a measuring cell. Sample degassing took

3 h at 105 °C and nitrogen flow of 1–2 bubbles/s and specific surface area of the degassed sample in the cell was measured (Nova 4000e, Quantachrome Instruments, USA).

Mass loss and analysis of evolved gas: STA Jupiter 449C (Netzsch, Germany) with evolved gas QMS 403C analysis was utilised to determine thermal mass loss and volatile impurities. Powder samples were placed in measuring alumina crucibles on TG holder with approx. 100–600 mg of sample. The temperature growth rate was 10 °C/min from 30 °C to 1200 °C. Paste samples were measured with DSC holder in measuring platinum crucibles. The weight of samples was about 10–20 mg and temperature growth rate was 20 °C/min from 30 °C to 1000 °C. Furnace air flow rate used for all samples was set to 50 ml/min, and inert nitrogen flow rate through sample chamber balance was 15 ml/min.

2.3. Preparation of nano-TiO_2 for cell treatment and characterisation in culture media

The NM suspension preparation procedure was adopted from the EU Nanogentox Project. Briefly, 15.36 mg of nano-TiO_2 were weighed in glass vials using a microbalance (RC210D, Sartorious, Germany). Nano-TiO_2 were then pre-wetted with 30 µl of 95% ethanol and diluted in 5.970 ml deionised water (diH_2O) containing 0.05% bovine serum albumin (BSA). Suspensions were sonicated (400 W and 10% amplitude) by a sonifier(S-450d, Branson, USA), equipped with a standard 13-mm disruptor horn for 16 min in an ice bath to prepare batch suspensions at a concentration of 2.56 mg/ml (Jensen et al. 2011). The suspension was gradually diluted by Roswell Park Memorial Institute medium (RPMI, Sigma-Aldrich, St. Louis, MO, USA), supplemented with 10% heat-inactivated fetal bovine serum (FBS) (Gibco) to reach final concentrations of 256, 128, 64, 32, 16, and 8 µg/ml.

As cytotoxicity of TiO_2 had a linear relationship with the concentration, suspensions of selected concentrations were used for further tests. The hydrodynamic size for batch, 256 µg/ml, 128 µg/ml, and 32 µg/ml suspension was measured using a dynamic light scattering technique (DLS) (Zetasizer Nano ZS, Malvern, UK). Hydrodynamic size (*Z*-Avg), and polydispersity index (PDI) were determined according to the ISO method ISO13321:1996, and its newer pendant ISO22412:2008. Batch suspensions were measured within 20 min after sonication. Medium suspensions in concentrations of 256 µg/ml, 128 µg/ml, and 32 µg/ml were measured 1 h and 24 h after preparation. All suspensions were vortexed before measurement. Until the measurements took place, medium suspensions were held under the same conditions as the treated cells (in a humidified incubator at 37 °C and 5% CO_2). Sample solutions were measured in DTS0012 polystyrene cell cuvettes, stabilisation time was set to 120 s, temperature to 25 °C for batch, and 37 °C for media solutions. At least 11 runs were performed per each concentration.

Zeta potentials were measured in DTS 1070 cuvettes for medium suspension of 32 µg/ml 1 h and 24 h after preparation. Sample treatment and instrument settings were the same as for *Z*-Avg measurement.

2.4. Cell cultivation, differentiation and exposure

The THP-1 cell line (human monocytic leukemia cells; ATCC) was cultured in a RPMI 1640 GlutaMAX medium (Gibco) supplemented with 10% (v/v) heat-inactivated fetal bovine serum (FBS HI; Sigma-Aldrich). Cells were cultured at a density ranging from 200,000 to 1,000,000 cells per ml in a humidified incubator at 37 °C and 5% CO_2.

To evaluate cytotoxicity of NMs, THP-1 monocytes were differentiated into macrophage-like cells. Various differentiation protocols are available in the scientific literature that may result in different types and responses of macrophages. In the present study, differentiation was performed using phorbol 12-myristate 13-acetate (PMA; Sigma-Aldrich) according to the protocol that was developed within the NanoValid project (THP-1 cell culture SOP; available at www.nanovalid.eu). For cytotoxicity experiments, cells were seeded in 96-well microtiter plates at a density of 50,000 cells per well in the complete cell culture medium supplemented with 500 nM phorbol 12-myristate 13-acetate (PMA; Sigma-Aldrich). After 24 h, the PMA-containing medium was removed and THP-1 cells differentiated into macrophage-like cells were washed with PBS. Freshly prepared serial dilutions of nano-TiO_2 suspensions in the complete cell culture medium were delivered into the wells, and plates were incubated at 37 °C, 5% CO_2 for 24 h. All treatments were performed in triplicates. To test whether the nano-TiO_2 interfere with the cytotoxicity assays, wells with nano-TiO_2 but without cells were included in the plates. Three independents experiments were performed for each nano-TiO_2 and each assay.

2.5. Cytotoxicity tests

2.5.1. MTS assay

After the exposure period, the cell culture medium was removed and cells were rinsed twice with PBS. The CellTiter 96® AQueous One Solution Reagent (Promega) was mixed with a phenol red free RPMI 1640 medium (Gibco) at a ratio of 1:5 and delivered to the test wells in a volume of 120 µl per well. The plate was incubated at 37 °C for 1 h. To prevent interference of nano-TiO_2 adsorbed on the plate plastic with absorbance reading, plates were centrifuged at 2800 xg for 10 min at room temperature, and supernatants were transferred to a new plate. Absorbance was measured at 490 nm using a SpectraMax® M5 Plate Reader (Molecular Device). To determine the viability, the background values of wells without cells were subtracted. Negative control (NC) cells were defined to be 100% viable and the viability was expressed as a percentage of viability of NC.

2.5.2. WST-1 assay

The Cell Proliferation Reagent WST-1 (Roche Diagnostics) was used as another mitochondrial activity-based assay to evaluate nano-TiO_2 cytotoxicity. The procedure was the same as described above for the MTS assay except that the WST-1 reagent was mixed with the phenol red free RPMI medium at a ratio of 1:10 and the absorbance was read at 440 nm.

2.5.3. LDH

The Cytotoxicity Detection Kit (LDH) (Roche Diagnostics) was used to evaluate the cytotoxic potential of nano-TiO_2 by measuring the degree of cellular membrane damage. At the end of the 24-h incubation period, 50 µl of the supernatant from each well was transferred into a new 96-well microtiter plate for the measurement of released LDH activity (LDH-supernatants). The rest of the medium was discarded. The survived cells were washed with PBS and lysed by incubation with 100 µl/well of 1% Triton X-100 (Sigma-Aldrich) at 37 °C for 30 min. 50 µl of the supernatant from each well with lysed cells was transferred into a new 96-well microtiter plate for the measurement of LDH activity of survived cells (LDH-lysates). Fifty µl of the reaction mixture containing the detection dye and the catalyst from the kit was added to both the LDH-supernatants and the LDH-lysates. Plates were incubated in the dark for 20 min. After adding 25 µl of stop solution to each well to terminate the reaction, the absorbance was measured at 490 nm using the SpectraMax® M5 Plate Reader. As for the other assays, the background values of the wells without cells were subtracted. The cell viability was calculated according to the following formula (1):

$$\%\text{viability} = (\text{LDH} - \text{lysates}/\text{LDH} - \text{lysates} + \text{LDH} - \text{supernatants}) \times 100 \quad (1)$$

The NC represented 100% viability and the results were expressed as a percentage of NC viability.

2.6. Transmission electron microscopy (TEM)

Cells incubated with nanoparticles or control cells were quickly washed with HEPES buffer (0.1 M, pH 7.2) at 37 °C, fixed with 2.5% glutaraldehyde in HEPES for 1 h, washed with the buffer, and postfixed with 1% OsO4 solution in HEPES for 45 min. The cells were dehydrated in a series of ethanol with increasing concentration, subsequently in propyleneoxide, and embedded in Quetol 651 resin. After polymerisation for 72 h at 60 °C, blocks were cut into 80 nm ultrathin sections and collected on 200 mesh size copper grids. The sections were examined in FEI Morgagni 268 transmission electron microscope operated at 80 kV. The images were captured using Mega View III CCD camera (Olympus Soft Imaging Solutions).

2.7. Endotoxin contamination

Endotoxin content in nanomaterials (NMs) was measured using the fluorogenic endotoxin detection assay PyroGene™ Recombinant Factor C (Lonza, Walkersville, USA) according to the manufacturers instructions. Assay sensitivity is between 0.005 and 5 EU/ml. Endotoxin contamination was tested in sonicated NM batch dispersions diluted in LAL Reagent Water (endotoxin free). To account for possible interference of NMs with the assay, endotoxin recovery rates were determined in NM samples spiked with 0.5 EU/ml of standard endotoxin.

2.8. Statistical analysis

Statistical analysis was made using R statistical software; in particular glmnet package (Friedman, 2010) was employed. The variables possibly impacting cytotoxicity were identified by the least absolute shrinkage and selection operator analysis (LASSO), which incorporates regularisation that avoids overfitting. The regularisation parameter Lambda was set to the value which gives the most regularised model, such that error is within one standard error of the minimum cross-validation error. Every variable calculation was performed 42 times via repeated 10-fold cross validation with various divisions into folds, and thus into training and testing subsets. Ten folds represent the default and commonly used option, and 42 repetitions were selected because the sample size was 42 and thus enough repetition to obtain stable results. Variables selected by LASSO are referred to as important variables and they are presented as the percentage occurrence of given variables in 42 cross validation models.

Other statistical tests used included nonparametric Wilcoxon signed-rank test with Bonferroni correction of *p*-value, Friedman test with Dunn-Bonferroni post-hoc tests, and Spearman's rank correlation coefficient. The level of significance was set to 0.05.

3. Results

3.1. Nanomaterials characteristics

Results of raw particles characterisation are listed in Table 2. As nanomaterials in the paste form (R1-3P-, A10x1T-, A10x10W-, and A100x20W-) were accessible only in a limited amount, they were characterised only dissolved in the cell culture medium. Their thermogravimetric analysis was utilised for determination of the equivalent mass corresponding to powder nano-TiO_2. Analyses confirmed anatase structure in all samples declared as being anatase by the suppliers. However, one of the rutile samples (30 nm silicon-coated particles, R30PS) was shown to be a mixture of a minority of rutile and prevailing anatase. The surface area measurements detected lower than expected values for 5 nm anatase particles (A5P-) and uncoated anatase 50 nm particles (A50P-), indicating that the size of these particles is actually larger. On the contrary, A100P- had a larger specific surface which should indicate smaller particles. Crystallite size was mostly in accordance with particle diameter calculated for spheres from specific surface area (Fig. 1), however R30P-, R50P- and R100P- showed smaller crystallite size than expected from specific surface area indicating aggregation/agglomeration. Mass losses as measured by the thermogravimetric analysis were generally low (up to 5%, mostly water or CO_2) except for A5P. This sample contains > 10% of a volatile material which was assumed to be an ethylchloride derivative (based on mass spectroscopic analysis of evolved gas).

Table 2
The physical properties of the nano-TiO_2 (nanoparticles).

	Crystal structure	Crystallite size [nm]	Specific surface area [m^2/g]	Mass loss [%]
R30P-	rutile	28.3	26.9	0.97
R30PS	anatase	42.4	41.8	1.34
R50P-	rutile	27.9	27.0	0.95
R100P-	rutile	54.4	17.6	0.44
R165P-	rutile	145.1	9.0	0.61
A5P-	anatase	10.1	135.8	13.74
A15P-	anatase	27.2	87.3	4.23
A30P-	anatase	28.3	50.4	2.01
A50P-	anatase	20.6	78.4	3.04
A100P-	anatase	88.3	19.8	0.77

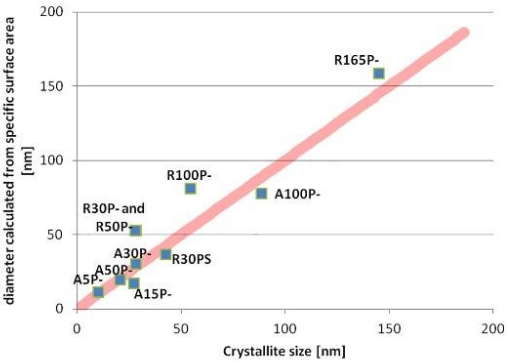

Fig. 1. The relation between crystallite size and particle diameter calculated from the specific surface area. R30P-, R50P- and R100P- showed smaller crystallite size than expected from the specific surface area indicating an aggregation/agglomeration issue.

Table 3 shows hydrodynamic size (Z-Avg), zeta potential (Zeta), and polydispersity index (PDI) of batches (2.56 mg/ml in 0.05% BSA in diH_2O) and suspensions in the cell culture medium at concentrations of 256 µg/ml, 128 µg/ml, and 32 µg/ml, measured 1 h and 24 h after dilution. This method is only suitable for spherical particles; nevertheless, all samples were measured in order to obtain a rough insight into agglomerate formation in the medium. The majority of the nano-TiO_2 had the biggest *Z*-Avg at the highest concentration (batch), and Z-Avg decreased along with the decreasing nano-TiO_2 concentrations in the medium. However, the smallest particles (A5P-, and R1-3P-) behaved differently; at a concentration of 256 µg/ml in the medium they had bigger Z-Avg then their batch dispersions. After 24 h, Z-Avgs remained stable or slightly increased except for A30P- which seemed to decrease in diameter. However, this decrease is most probably caused by the fact that bigger agglomerates settled during the sample stabilization time. It is only detected at the very beginning of the measurement or not detected at all.

PDI is a variable determining the level of polydispersity, with values ranging from 0 to 1. Values smaller than 0.05 correspond to monodisperse suspensions. Samples with PDI larger than 0.7 have a broad size distribution and are probably not suitable for DLS measurement

Table 3
Characterisation of nano-TiO_2 dispersions for batch (2.56 mg/ml in ddH2O + 0.05% BSA) and three concentrations of nano-TiO_2 in RPMI +10% FBS. Measured characteristics: Z-Avg (hydrodynamic diameter), PDI (polydispersity index), Zeta p. (Zeta potential). All characteristics were measured within 1 h after preparation and after 24 h. The samples were kept under the same conditions as the cells (in a humidified incubator at 37 °C and 5% CO_2).

Name	Conc. in liquid	Z-Avg [nm] 1 h	PDI 1 h	Zeta p. [mV] 1 h	Z-Avg [nm] 24 h	PDI 24 h	Zeta p. [mV] 24 h
A10 × 1T-	Batch	107.1	0.48				
	256 μg/ml	68.9	0.45		68.4	0.42	
	128 μg/ml	50.0	0.59		53.5	0.53	
	32 μg/ml	23.4	0.68	−15.9	28.1	0.83	−15.9
A10 × 10W-	Batch	120.7	0.41				
	256 μg/ml	49.7	0.49		40.9	0.53	
	128 μg/ml	27.1	0.56		26.6	0.58	
	32 μg/ml	17.9	0.46	−16.4	99.4	0.69	−20.6
A15P-	Batch	515.3	0.37				
	256 μg/ml	326.5	0.30		344.8	0.35	
	128 μg/ml	357.5	0.40		344.7	0.33	
	32 μg/ml	311.8	0.34	−15.9	332.8	0.39	−15.9
A30P-	Batch	363.2	0.49				
	256 μg/ml	317.7	0.63		207.4	0.50	
	128 μg/ml	222.0	0.53		221.9	0.50	
	32 μg/ml	191.5	0.45	−14	136.2	0.53	−15.5
A50P-	Batch	4188.2	0.60				
	256 μg/ml	140.4	0.24		167.6	0.39	
	128 μg/ml	136.6	0.25		172.3	0.45	
	32 μg/ml	129.8	0.53	−14.6	223.9	0.41	−14.6
A100P-	Batch	479.9	0.32				
	256 μg/ml	439.0	0.32		439.3	0.28	
	128 μg/ml	437.2	0.31		439.5	0.32	
	32 μg/ml	423.3	0.33	−15	437.3	0.36	−15.4
A100 × 20W-	Batch	444.4	0.28				
	256 μg/ml	325.5	0.37		341.2	0.39	
	128 μg/ml	343.5	0.48		343.5	0.45	
	32 μg/ml	428.2	0.56	−13.8	393.2	0.56	−14.8
A5P-	Batch	42.9	0.32				
	256 μg/ml	58.8	0.21		59.2	0.19	
	128 μg/ml	55.3	0.24		55.8	0.23	
	32 μg/ml	41.6	0.47	−16.8	45.1	0.44	−22
R1-3P-	Batch	444.4	0.54				
	256 μg/ml	648.5	0.58		747.4	0.43	
	128 μg/ml	130.5	0.47		145.4	0.48	
	32 μg/ml	49.8	0.65	−17.3	49.0	0.65	−17.4
R30P-	Batch	257.8	0.15				
	256 μg/ml	202.2	0.09		216.7	0.18	
	128 μg/ml	203.1	0.11		212.3	0.13	
	32 μg/ml	212.8	0.15	−14.7	223.1	0.18	−16.4
R30PS	Batch	575.7	0.39				
	256 μg/ml	428.3	0.33		428.0	0.37	
	128 μg/ml	419.9	0.32		560.5	0.44	
	32 μg/ml	389.5	0.33	−15.7	381.3	0.40	−15.7
R50P-	Batch	248.7	0.14				
	256 μg/ml	198.2	0.11		207.8	0.16	
	128 μg/ml	204.5	0.14		205.9	0.13	
	32 μg/ml	211.2	0.17	−15.6	213.1	0.14	−15.4
R100P-	Batch	435.3	0.26				
	256 μg/ml	234.2	0.14		244.2	0.15	
	128 μg/ml	260.9	0.21		249.6	0.14	
	32 μg/ml	267.4	0.21	−15.6	270.8	0.21	−15.7
R165P-	Batch	940.2	0.44				
	256 μg/ml	258.1	0.16		250.9	0.15	
	128 μg/ml	259.9	0.18		251.0	0.17	
	32 μg/ml	259.5	0.21	−19.3	235.9	0.16	−18.2

(Malvern Instruments, 2011). PDIs measured after 1 h and 24 h are reported in Table 3. PDI values exceeding 0.7 were observed only in A10x1T-, however the values for other high aspect ratio nano-TiO_2 were close to this limit (e.g. A10 x 10-).

Zeta potential for nano-TiO_2 in the medium varied between −13.8 and −22 mV and did not change after 24 h.

3.2. Cytotoxicity and endotoxin contamination of nano-TiO_2

Overall, cytotoxicity of all nano-TiO_2 was low, even at the highest tested concentration of 256 μg/ml. Although for some samples the cell viability decreased at the highest concentration (e.g. A15P-, R30P-, R100P-, R30PS), it did not drop below 60% for both the WST-1 and MTS assays, and 80% for the LDH assay (Fig. 2). TEM images (Fig. 3) have shown that nanomaterials (data available for R1-3P-, A15P-, R30P-, R30PS, A10 × 1T-, and A100 × 20W-) are engulfed and internalised as aggregates/agglomerates by THP-1 cells. Images of fibrous nano-TiO_2 revealed that sonication procedure broke the nanomaterials into shorter pieces, which aggregated rapidly (confirmed by the highest PDI). In fact, THP-1 cells were exposed to big agglomerates of nanotubes.

Results of all 3 cytotoxicity tests exhibited good concordance (Fig. 4). This finding was proved by correlation analysis. All *p*-values were under 0.001, correlation coefficients reached: 0.65 (WST-1 vs.

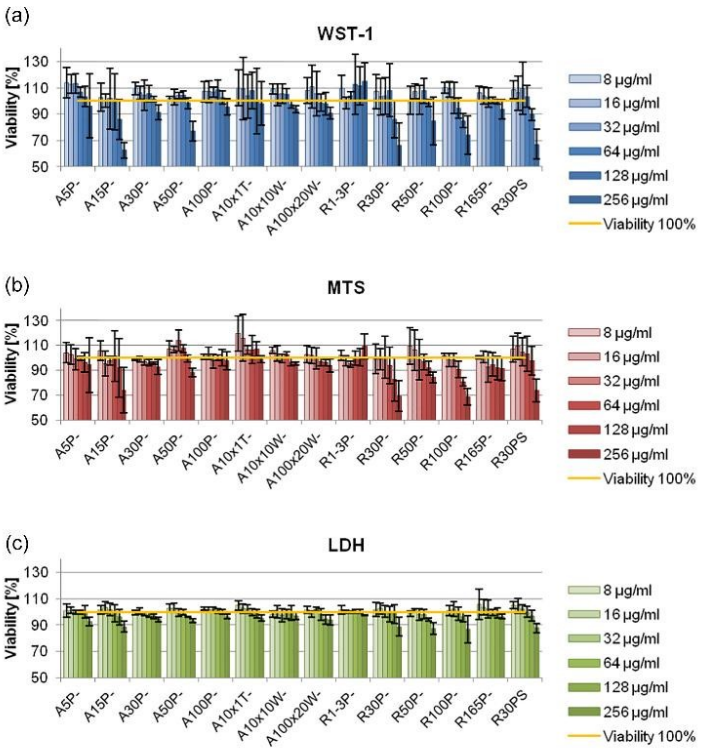

Fig. 2. Cytotoxicity induced by nano-TiO_2 using three different viability tests (WST-1, MTS, LDH). The viability of THP-1 cells exposed for 24 h was calculated as a percentage related to an untreated control. Error bars correspond to standard deviations calculated from three independent repetitions. Values higher than 100% obtained from WST-1 a MTS assays reflect the enhanced metabolic activity of THP-1 cells resulting from low dose nano-TiO_2 treatment.

MTS), 0.6 (WTS-1 vs. LDH) and 0.62 (MTS and LDH). Overall, viabilities measured by WST-1 were significantly lower than those measured by MTS (p-value < .001) and LDH (p-value < .001). There was no significant difference between LDH and MTS data even without Bonferroni correction. However, viabilities for individual nanomaterials did not significantly differ between individual cytotoxicity tests. Further, there were no differences in viabilities between individual nanomaterials for either cytotoxicity test (data not shown).

Overall, even at the highest tested dose of 256 µg/ml, endotoxin concentration in nano-TiO_2 samples was very low (below 0.1 EU/ml), except for A5P- and A10 × 1T-, for which the levels reached 0.271 EU/ml and 0.279 EU/ml, respectively (Supplementary Table 1). As these concentrations were lower than 0.5 EU/ml, a threshold value of the US Food and Drug Administration for eluates of biological products and medical devices, none of the tested TiO_2 nanomaterials contained endotoxin in an extent that could affect viability of the cells (US Department of Health and Human Services, 2012).

3.3. Investigation of variables affecting cytotoxicity

Based on the strong correlation among cytotoxicity tests but significant differences between the data from WST-1 and other assays, we decided to calculate the total averaged cytotoxicity (T.avg) using Principal Component Analysis (PCA) from the cytotoxicity test results. This variable represented overall cytotoxicity regardless of the assay design.

As the extent of the characterisation of four nano-TiO_2 was lower than obtained for the other ten nano-TiO_2, two sets of LASSO models were made. Because all tested nano-TiO_2 were characterised in the culture cell medium by DLS, the first set of models used those data for modelling. Then the second model, containing only the more characterised 10 nanoparticles (listed in Table 2) was made.

3.3.1. LASSO model with all 14 nano-TiO_2 input

The input independent variables used in the first set of models included: concentration of nano-TiO_2, shape (particles/high aspect rationano-TiO_2), batch Z-Avg, batch PDI and variables measured by DLS after 1 and 24 h in the cell culture medium: Z-Avg, PDI, Zeta potential. The occurrence of variables (%) selected as important by 42 cross validation models for cytotoxicity assays and total averaged (T.avg) cytotoxicity are shown in Table 4. The results indicate that higher nano-TiO_2 concentration lead to lower viability of THP-1; at the same time, suspensions of lower stability (i.e. more polydisperse) were found to be less cytotoxic in THP-1 cells.

All models contained nano-TiO_2 concentrations and PDI measured after 1 h of exposure (PDI 1 h). LASSO selected PDI 1 h as the variable affecting cytotoxicity, measured by the WST-1 test only in 69% of cross validation models; on the other hand, all LASSO models for MTS, a test based on the same principle as WST-1, and LDH chose PDI 1 h as an important variable. Additionally, PDI of the batch was detected for MTS and LDH tests. Outputs of the LDH test were also affected by Zeta potential. Due to inconsistency among cytotoxicity tests, the total

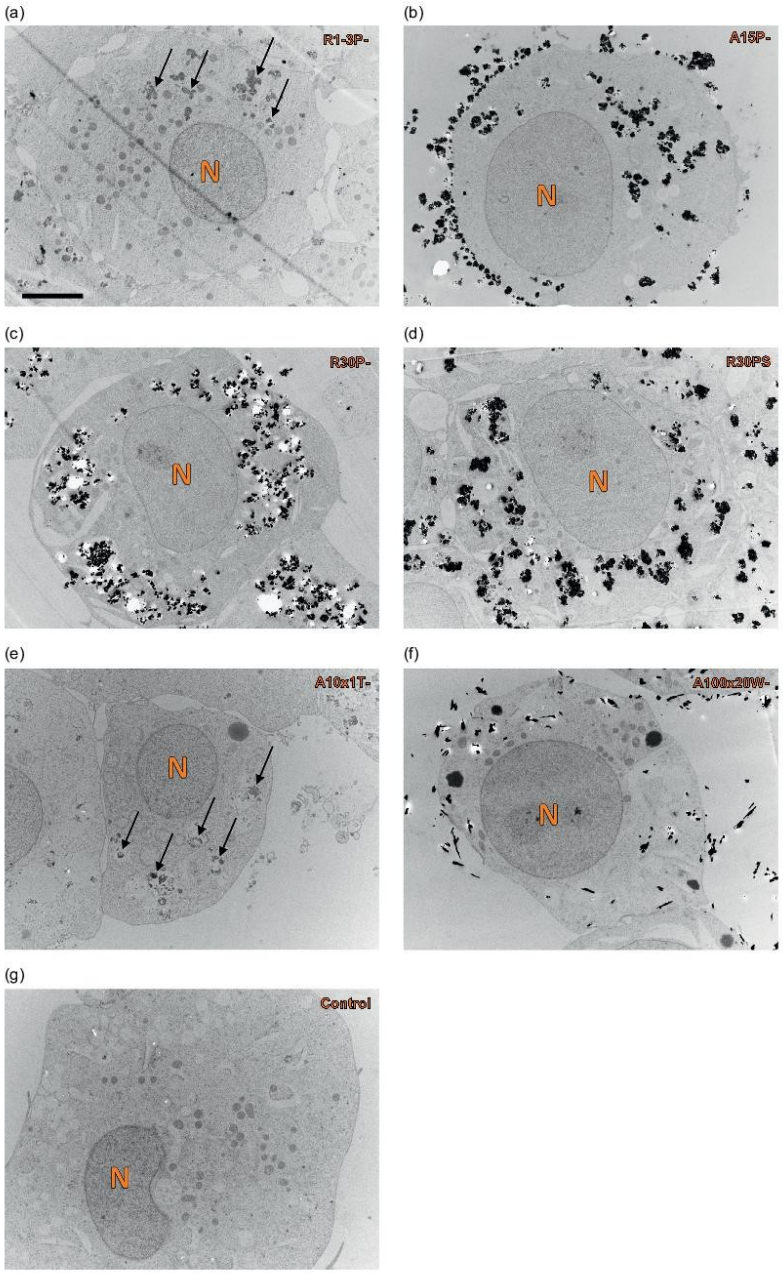

Fig. 3. TEM images of THP-1 cells incubated with nano-TiO_2 for 24 h. The vast majority of engulfed nano-TiO_2 was present in the cells in a form of aggregates/agglomerates, however small clusters were also observed. Nano-TiO_2 was not observed in the cell nucleus. Where needed, nano-TiO_2 are indicated by arrows, N indicates the nucleus. Bar, 5 µm.

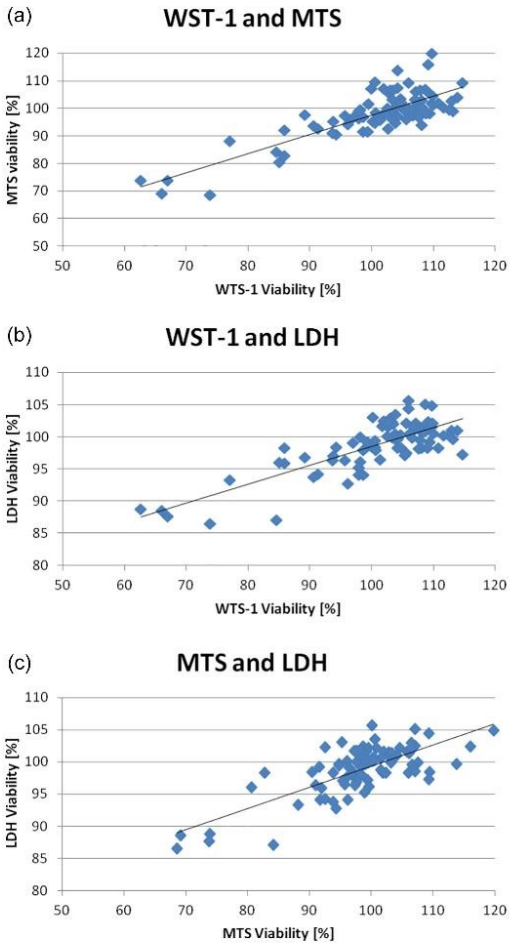

Fig. 4. Correlation between viability detected using different assays. The results show a high degree of concordance - Student correlation coefficients: WST-1 and MTS 0.65, WTS-1 and LDH 0.6, MTS and LDH 0.62; all *p*-values were < 0.001.

Table 4
Occurrence of variables affecting cytotoxicity selected by 42 cross validations. All cross validation models for averaged viability (T.avg) showed two such variables: concentration (averaged index: −0.0523 ± 0.006) and PDI measured after 1 h of exposure (PDI 1 h) (averaged index: 11.618 ± 3.517).

	Concentration	PDI 1 h	Batch PDI	Zeta potential 1 h
WST1	100%	69%	–	–
MTS	100%	100%	23.8%	–
LDH	100%	100%	100%	95.2%
T.avg	100%	100%		

averaged cytotoxicity (T.avg) was further used in the models. All cross validation models for T.avg. showed two variables: concentration (averaged index: −0.0523 ± 0.006) and PDI 1 h (averaged index: 11.618 ± 3.517). PDI indicates the stability of suspended particles; the more stable suspension, the higher cytotoxicity. We did not find any difference between nanoparticles and fibrous nanomaterials.

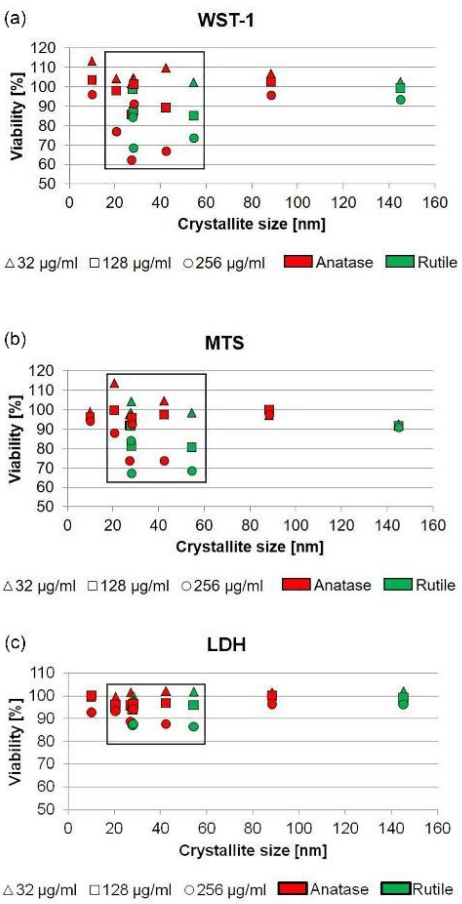

Fig. 5. Relation between crystallite size and cell viability in individual assays. A nonlinear relation is likely with decreased cell viability for particles of size between 20 and 60 nm. No significant difference was observed between anatase and rutile.

Interpretation of other variable, inconsistent over viability tests (batch PDI, Zeta potential), selected by LASSO could be misleading due to relatively small number of samples and low overall toxicity. Larger number of samples would clarify importance of those variables. On the other hand, batch PDI and zeta potential still show an importance of suspension stability.

3.3.2. *LASSO model with selected 10 nano-TiO_2 input*

Prior to the LASSO analysis of 10 more characterised TiO_2 nanoparticles, we looked at the relation between the crystallite size of particles and cytotoxicity, due to inconsistent results between the studies mentioned in the Introduction. Fig. 5 suggests a nonlinear relation; the smallest particles had a low cytotoxic effect, and then cytotoxicity increased for particles with a diameter between 20 and 60 nm, and again there was low cytotoxicity for larger particles. Due to the small sample size (10 types of nanoparticles with PDI values measured in 3

Table 5
Occurrence of variables affecting cytotoxicity selected by 42 cross validations of 10 well characterised nano-TiO_2. The selected variables were highly inconsistent, with the exception of concentration (T.avg. -averaged index: −0.0808 ± 0.009).

	Conc.	Zeta 24 h	PDI	Crystal structure	Batch Z-Avg	Batch PDI	Z-Avg 1 h	Zeta 1 h
WST-1	100%	73.8%	14.3%	–	–	–	–	–
MTS	100%	–	92.9%	88.1%	54.8%	–	–	–
LDH	100%	28.6%	–	7.1%	–	76.2%	23.8%	73.8%
T.avg	100%	–	–	–	–	–	–	–

concentrations) we were not able to properly model the nonlinear relation; thus, we excluded crystallite size from the LASSO analysis.

The second set of models was prepared only for the 10 well characterised nanoparticles listed in Table 2. Input independent variables in these models included: concentration of nano-TiO_2, batch Z-Avg, batch PDI, crystal structure (anatase/rutile), specific surface area, and variables measured after 1 and 24 h in the cell culture medium: Z-Avg, PDI, Zeta potential. The percentage occurrence of the important variables selected by 42 cross validation models for cytotoxicity tests and total averaged cytotoxicity (T.avg) are shown in Table 5.

The only stable variable for all assays is concentration (T.avg. index: −0.0808 ± 0.009). Selection of other variables is highly inconsistent, due to the coincidence of a small number of samples and overall low cytotoxicity of TiO_2 nanoparticles. Thus no conclusion could be made.

Inconsistent results from other studies could be caused by synergy of nonlinear size effect and influence of PDI in the media.

4. Discussion

As recommended by Warheit (2008), a combination of several techniques for NMs characterisation was performed in our study. The results showed differences between the manufacturers' data and real measured characteristics. Overall, there were inconsistencies in the nanoparticle size; moreover, the R30PS sample had different crystallite content. These inconsistencies showed how crucial proper NM characterisation is for overall understanding of nanotoxicity.

Hydrodynamic size and zeta potential were monitored in the cell culture medium after 1 and 24 h. As expected, nano-TiO_2 size measured in the cell culture media by DLS was higher in comparison with crystallite size measured in dry form (Warheit, 2008). Zeta potential fluctuated around -16 mV for all nano-TiO_2. A similar zeta potential of diverse NMs suspended in the same cell culture medium (RPMI +10% FBS) was observed in other studies (Limbach et al., 2005; Pal et al., 2015). The similar zeta potential indicates protein corona formation on the NMs (Maiorano et al., 2010). Zeta potential between 10 and 20 mV above or below zero suggests relatively stable suspension (Patel and Agrawal, 2011). However, suspension stability is also driven by van der Waals forces (Bhattacharjee, 2016), and NMs with mild electrostatic repulsion (zeta potential between 10 and 15 mV) could also be enough to keep a suspension stable. Pal et al. (2015) achieved stable nanoparticle dispersion by adding FBS to RPMI in a 10% proportion. We also observed stable NMs suspensions in RPMI +10% FBS, as the DLS measured diameter (Z-avg) changed only negligibly after 24 h. TEM images showed that nano-TiO_2 have formed aggregates/agglomerates, despite measured stable suspension, which is in concordance with a study by Limbach et al. (2005).

A cell model used in this study is a monocyte cell line THP-1 differentiated into macrophage-like cells using 500 nM PMA. Cytotoxic tests based on measurement of activity of mitochondrial enzymes (WST-1 and MTS) showed higher viability of treated cells than controls at low nano-TiO_2 concentrations. These results of "enhanced" viability likely imply enhanced metabolic activity of cells exposed to nano-TiO_2. A similar response was also observed in cells exposed to organic chemicals by Libalova et al. (2016).

According to TEM images, THP-1 engulfed nano-TiO_2. Particle uptake by macrophages depends mainly on the particle size. Phagocytosis and macropinocytosis take place in particles or agglomerates of size between 0.5 and 10 μm and 0.1–5 μm, respectively. Other types of pinocytosis are responsible for smaller particle engulfment (Hirota and Terada, 2012). Engulfed nanoparticles of different sizes were observed in THP-1 cells (Pang et al., 2016; Naji et al., 2016; Li et al., 2014; Haase et al., 2011), and alveolar macrophages (Ruge et al., 2011, Naji et al., 2016). According to TEM imaging, nano-TiO_2 was present inside the cells in a form of big agglomerates, however small clusters (a few particles) were also observed, indicating that diverse ways of uptake were utilized.

LASSO analysis revealed that cytotoxicity is affected, beside concentration, by PDI measured in the cell culture medium after 1 h of exposure. The stability of suspension (indicated by PDI) is a complex feature driven by a combination of interaction of NMs characteristics and the medium in which they are suspended. This stability does not implicate the stability inside the cell, but rather if the adherent cells are in contact with single particles/small clusters or larger aggregates, we assume that higher PDI led to rapid agglomeration and thus exposure to bigger aggregates. On the other hand, low PDI caused exposure to smaller clusters or even particles alone; this seemed to be associated with higher toxicity. The effect of different nano-TiO_2 characteristics on cytotoxicity found in other studies could be masked by PDI. It would be necessary to ruled out PDI from statistic models to reveal the toxic effect of nano-TiO_2 characteristics.

Surprisingly, we did not observe different toxicity for fibrous forms of TiO_2 as others did (Watanabe et al., 2002). However, as TEM images have shown, cells were exposed to big aggregates of short fibres broken by sonication procedure.

There was a visible nonlinear relationship between crystalline size and cytotoxicity, with the highest toxicity for particles of size between 20 and 60 nm. A nonlinear relationship was also shown by Chang (2013), who concluded that the highest toxicity occurred for particles with a diameter between 10 and 40 nm. Zhang et al. (2012) found TiO_2 nanoparticles with a diameter with a size of 21 ± 3 nm to be more toxic for mouse macrophages than particles of 12 ± 2 nm and 98 ± 20 nm. Increased cytotoxicity in this diameter size range would explain the inconsistent findings for the size and cytotoxicity relationship. In our study, crystal form did not affect cytotoxicity.

Overall, the nano-TiO_2 cytotoxicity was low in the THP-1 model system even at high concentrations which is consistent with other studies (Hanot-Roy et al., 2016; Lanone et al., 2009, Xia et al., 2013).

5. Conclusions

We evaluated the cytotoxic effect of 14 diverse nano-TiO_2 on model macrophage cells, i.e. cells that potentially capture nano-TIO_2 in the body and internalise them. Three assays were used to generate the cytotoxicity data, which were then statistically analysed by LASSO. As LASSO employs cross validation, this approach generates more relevant variables in comparison with stepwise regression.

Except for concentration, polydispersity index (PDI) in media measured within 1 h after exposure was identified as a variable affecting nano-TiO_2 cytotoxicity. Lower PDI led to higher cytotoxicity. Commonly, PDI is often measured only as characteristics for relevant

concentrations of nanoparticles in the media, or it is assessed in water solution, omitting the importance of relevant media for toxicity.

Toxicity of nano-TiO_2 showed a nonlinear relation with crystal size. Particles of size between 20 and 60 nm were more toxic, while smaller and larger ones had low cytotoxicity. We did not find a significant difference between anatase/rutile crystallinity or the effect of aspect ratio of nanomaterials.

Our findings may significantly contribute to the interpretation of some contradictory data on cytotoxicity of nano-TiO_2 published in the last decade.

Overall cytotoxic effects of nano-TiO_2 in THP-1 macrophage-like cells were low.

Supplementary data to this article can be found online at https://doi.org/10.1016/j.tiv.2018.09.019.

Acknowledgements

Supported by the Ministry of Education, Youth and Sports of the Czech Republic (LO1508; CZ.02.1.01/0.0/0.0/16_019/0000765) and the Czech Science Foundation (P503-12-G147). The authors acknowledge the assistance provided by the Research Infrastructure NanoEnviCz, supported by the Ministry of Education, Youth and Sports of the Czech Republic under Project No. LM2015073.

The Microscopy Centre - Electron Microscopy CF, IMG AS CR is supported by the Czech-BioImaging large RI project (LM2015062 funded by MEYS CR) and by OP RDE (CZ.02.1.01/0.0/0.0/16_013/0001775 "Modernization and support of research activities of the national infrastructure for biological and medical imaging Czech-BioImaging").

References

Bhattacharjee, S., 2016. DLS and zeta potential – what they are and what they are not? J. Control. Release 235, 337–351. https://doi.org/10.1016/j.jconrel.2016.06.017.

Chang, X., Zhang, Y., Tang, M., Wang, B., 2013. Health effects of exposure to nano-TiO2: a meta-analysis of experimental studies. Nanoscale Res. Lett. 8 (1), 51. https://doi.org/10.1186/1556-276X-8-51.

Chen, J.L., Fayerweather, W.E., 1988. Epidemiologic study of workers exposed to titanium dioxide. J. Occup. Med. 30 (12), 937–942.

De Matteis, V., Cascione, M., Brunetti, V., Toma, C.C., Rinaldi, R., 2016. Toxicity assessment of anatase and rutile titanium dioxide nanoparticles: the role of degradation in different pH conditions and light exposure. Toxicol. in Vitro 37, 201–210. https://doi.org/10.1016/j.tiv.2016.09.010.

EFSA ANS Panel (EFSA Panel on Food Additives and Nutrient Sources added to Food), 2016. Scientific Opinion on the re-evaluation of titanium dioxide (E 171) as a food additive. EFSA J. 14 (9), 4545. https://doi.org/10.2903/j.efsa.2016.4545.

Elder, A., Gelein, R., Silva, V., Feikert, T., Opanashuk, L., Carter, J., Potter, R., Maynard, A., Finkelstein, J., Oberdorster, G., 2006. Translocation of inhaled ultrafine manganese oxide particles to the central nervous system. Environ. Health Perspect. 114 (8), 1172–1178. https://doi.org/10.1289/ehp.9030.

Friedman, Jerome, Hastie, Trevor, Tibshirani, Robert, 2010. Regularization paths for generalized linear models via coordinate descent. J. Stat. Softw. 33 (1), 1–22.

Guichard, Y., Schmit, J., Darne, C., Gaté, L., Goutet, M., Rousset, D., Rastoix, O., Wrobel, R., Witschger, O., Martin, A., Fierro, V., Binet, S., 2012. Cytotoxicity and genotoxicity of nanosized and microsized titanium dioxide and iron oxide particles in Syrian hamster embryo cells. Ann. OccupHyg. 56 (5), 631–644. https://doi.org/10.1093/annhyg/mes006.

Guo, Z., Martucci, N.J., Moreno-Olivas, F., Tako, E., Mahler, G.J., 2017. Titanium dioxide nanoparticle ingestion alters nutrient absorption in an in vitro model of the small intestine. NanoImpact 5, 70–82. https://doi.org/10.1016/j.impact.2017.01.002.

Haase, A., Arlinghaus, H.F., Tentschert, J., Jungnickel, H., Graf, P., Mantion, A., Draude, F., Galla, S., Plendl, J., Goetz, M.E., Masic, A., Meier, W., Thünemann, A.F., Taubert, A., Luch, A., 2011. Application of laser postionization secondary neutral mass spectrometry/time-of-flight secondary ion mass spectrometry in nanotoxicology: visualization of nanosilver in human macrophages and cellular responses. ACS Nano 5 (4), 3059–3068. https://doi.org/10.1021/nn200163w.

Hamilton, R.F., Wu, N., Porter, D., Buford, M., Wolfarth, M., Holian, A., 2009. Particle length-dependent titanium dioxide nanomaterials toxicity and bioactivity. Part Fibre Toxico 6, 35. https://doi.org/10.1186/1743-8977-6-35.

Hamon, J., Renner, M., Jamei, M., Lukas, A., Kopp-Schneider, A., Bois, F.Y., 2015. Quantitative in vitro to in vivo extrapolation of tissues toxicity. Toxicol. in Vitro 30 (1), 203–216. https://doi.org/10.1016/j.tiv.2015.01.011.

Hanot-Roy, M., Tubeuf, E., Guilbert, A., Bado-Nilles, A., Vigneron, P., Trouiller, B., Braun, A., Lacroix, G., 2016. Oxidative stress pathways involved in cytotoxicity and genotoxicity of titanium dioxide (TiO2) nanoparticles on cells constitutive of alveolo-capillary barrier in vitro. Toxicol. in Vitro 33, 125–135. https://doi.org/10.1016/j.tiv.2016.01.013.

Hext, P.M., Tomenson, J.A., Thompson, P., 2005. Titanium dioxide: inhalation toxicology and epidemiology. Ann. OccupHyg. 49 (6), 461–472. https://doi.org/10.1093/annhyg/mei012.

Hirota, K., Terada, H., 2012. In: Ceresa, Brian (Ed.), "Endocytosis of Particle Formulations by Macrophages and its Application to Clinical Treatment", Molecular Regulation of Endocytosis. InTech. https://doi.org/10.5772/45820. Available online. http://www.intechopen.com/books/molecular-regulation-of-endocytosis/endocytosis-of-particle-formulations-by-macrophages-and-its-application-to-clinical-treatment (accessed 5th November 2016).

Jensen, K.A., Kembouche, Y., Christiansen, E., Jacobsen, N.R., Wallin, H., Guiot, C., Spalla, O., Witschger, O., 2011. "Final Protocol for Producing Suitable Manufactured Nanomaterial Exposure Media", NANOGENOTOX Deliverable Report n3. 34 pp. Availible online. https://www.anses.fr/en/system/files/nanogenotox_deliverable_5.pdf (Accessed 6th September 2016).

Kebede, M.A., Varner, M.E., Scharko, N.K., Gerber, R.B., Raff, J.D., 2013. Photooxidation of ammonia on TiO2 as a source of NO and NO2 under atmospheric conditions. J. Am. ChemSoc. 135 (23), 8606–8615. https://doi.org/10.1021/ja401846x.

Kermanizadeh, A., Balharry, D., Wallin, H., Loft, S., Møller, P., 2015. Nanomaterial translocation–the biokinetics, tissue accumulation, toxicity and fate of materials in secondary organs–a review. Crit. Rev. Toxicol. 45 (10), 837–872. https://doi.org/10.3109/10408444.2015.1058747.

Laaksonen, R., Katajamaa, M., Päivä, H., Sysi-Aho, M., Saarinen, L., Junni, P., Lütjohann, D., Smet, J., Van Coster, R., Seppänen-Laakso, T., Lehtimäki, T., Soini, J., Oresic, M., 2006. A systems biology strategy reveals biological pathways and plasma biomarker candidates for potentially toxic statin-induced changes in muscle. PLoS One 1 (1), e97. https://doi.org/10.1371/journal.pone.0000097.

Lanone, S., Rogerieux, F., Geys, J., Dupont, A., Maillot-Marechal, E., Boczkowski, J., Lacroix, G., Hoet, P., 2009. Comparative toxicity of 24 manufactured nanoparticles in human alveolar epithelial and macrophage cell lines. Part Fibre Toxicol. 6, 14. https://doi.org/10.1186/1743-8977-6-14.

Li, R., Ji, Z., Qin, H., Kang, X., Sun, B., Wang, M., Chang, C.H., Wang, X., Zhang, H., Zou, H., Nel, A.E., Xia, T., 2014. Interference in autophagosome fusion by rare Earth nanoparticles disrupts autophagic flux and regulation of an interleukin-1β producing inflammasome. ACS Nano 8 (10), 10280–10292. https://doi.org/10.1021/nn505002w.

Libalova, H., Rossner, P., Vrbova, K., Brzicova, T., Sikorova, J., Vojtisek-Lom, M., Beranek, V., Klema, J., Ciganek, M., Neca, J., Pencikova, K., Machala, M., Topinka, J., 2016. Comparative analysis of toxic responses of organic extracts from diesel and selected alternative fuels engine emissions in human lung BEAS-2B Cells. Int. J. Mol. Sci. 17 (11), 1833. https://doi.org/10.3390/ijms17111833.

Limbach, L.K., Li, Y., Grass, R.N., Brunner, T.J., Hintermann, M.A., Muller, M., Gunther, D., Stark, W.J., 2005. Oxide nanoparticle uptake in human lung fibroblasts: Effects of particle size, agglomeration, and diffusion at low concentrations. Environ. Sci. Technol. 39 (23), 9370–9376. https://doi.org/10.1021/es051043o.

Maiorano, G., Sabella, S., Sorce, B., Brunetti, V., Malvindi, M.A., Cingolani, R., Pompa, P.P., 2010. Effects of cell culture media on the dynamic formation of protein-nanoparticle complexes and influence on the cellular response. ACSNano 4 (12), 7481–7491. https://doi.org/10.1021/nn101557e.

Malvern Instruments, 2011. Dynamic Light Scattering: Common Terms Defined, Inform White Paper. available online. http://www.biophysics.bioc.cam.ac.uk/wpcontent/uploads/2011/02/DLS_Terms_defined_Malvern.pdf (accessed 23rd November 2016).

Naji, A., Muzembo, B.A., Yagyu, K., Baba, N., Deschaseaux, F., Sensebé, L., Suganuma, N., 2016. Endocytosis of indium-tin-oxide nanoparticles by macrophages provokes pyroptosis requiring NLRP3-ASC-Caspase1 axis that can be prevented by mesenchymal stem cells. Sci. Rep. 6, 26162. https://doi.org/10.1038/srep26162.

Numano, T., Xu, J., Futakuchi, M., Fukamachi, K., Alexander, D.B., Furukawa, F., Kanno, J., Hirose, A., Tsuda, H., Suzui, M., 2014. Comparative study of toxic effects of anatase and rutile type nanosized titanium dioxide particles in vivo and in vitro. Asian Pac. J. Cancer Prev. 15 (2), 929–935. https://doi.org/10.7314/APJCP.2014.15.2.929.

OECD - Series on the Safety of Manufactured Nano No. 27, 2010. List of Manufactured Nano and List of Endpoints for Phase One of the Sponsorship Programme for the Testing of Manufactured Nano: Revision. ENV/JM/MONO/2010/46, available online. http://www.oecd.org/officialdocuments/publicdisplaydocumentpdf/?cote=env/jm/mono(2010)46&doclanguage=en (accessed 20th November 2016).

Ophus, E.M., Rode, L., Gylseth, B., Nicholson, D.G., Saeed, K., 1979. Analysis of titanium pigments in human lung tissue. Scand. J. Work Environ. Health 5 (3), 290–296. https://doi.org/10.5271/sjweh.3104.

Pal, A.K., Bello, D., Cohen, J., Demokritou, P., 2015. Implications of in vitro dosimetry on toxicological ranking of low aspect ratio engineered nanomaterials. Nanotoxicology 9 (7), 871–885. https://doi.org/10.3109/17435390.2014.986670.

Pang, L., Qin, J., Han, L., Zhao, W., Liang, J., Xie, Z., Yang, P., Wang, J., 2016. Exploiting macrophages as targeted carrier to guide nanoparticles into glioma. Oncotarget 7 (24), 37081–37091. https://doi.org/10.18632/oncotarget.9464.

Patel, V.R., Agrawal, Y.K., 2011. Nanosuspension: an approach to enhance solubility of drugs. J. Adv. Pharm. Technol. Res. 2 (2), 81–87. https://doi.org/10.4103/2231-4040.82950.

Ruge, C.A., Kirch, J., Cañadas, O., Schneider, M., Perez-Gil, J., Schaefer, U.F., Casals, C., Lehr, C.M., 2011. Uptake of nanoparticles by alveolar macrophages is triggered by surfactant protein A. Nanomedicine 7 (6), 690–693. https://doi.org/10.1016/j.nano.2011.07.009.

Saba, T.M., 1970. Physiology and Physiopathology of the reticuloendothelial System. Arch. Intern. Med. 126 (6), 1031–1052.

Sayes, C.M., Wahi, R., Kurian, P.A., Liu, Y., West, J.L., Ausman, K.D., Warheit, D.B., Colvin, V.L., 2006. Correlating nanoscale titania structure with toxicity: a

cytotoxicity and inflammatory response study with human dermal fibroblasts and human lung epithelial cells. Toxicol. Sci. 92 (1), 174–185. https://doi.org/10.1093/toxsci/kfj197.
Sha, B., Gao, W., Cui, X., Wang, L., Xu, F., 2015. The potential health challenges of TiO2 nanomaterials. J. Appl. Toxicol. 35 (10), 1086–1101. https://doi.org/10.1002/jat.3193.
Shakeel, M., Jabeen, F., Shabbir, S., Asghar, M.S., Khan, M.S., Chaudhry, A.S., 2016. Toxicity of nano-titanium dioxide (TiO2-NP) through various routes of exposure: a review. Biol. Trace Elem. Res. 172 (1), 1–36. https://doi.org/10.1007/s12011-015-0550-x.
Shi, H., Magaye, R., Castranova, V., Zhao, J., 2013. Titanium dioxide nanoparticles: a review of current toxicological data. Part FibreToxicol. 10, 15. https://doi.org/10.1186/1743-8977-10-15.
Shinohara, N., Danno, N., Ichinose, T., Sasaki, T., Fukui, H., Honda, K., Gamo, M., 2014. Tissue distribution and clearance of intravenously administered titanium dioxide (TiO2) nanoparticles. Nanotoxicology 8 (2), 132–141. https://doi.org/10.3109/17435390.2012.763001.
Silva, R.M., Teesy, C., Franzi, L., Weir, A., Westerhoff, P., Evans, J.E., Pinkerton, K.E., 2013. Biological response to nano-scaletitanium dioxide (TiO2): role of particle dose, shape, and retention. J. Toxicol. Environ. Health A 76 (16), 953–972. https://doi.org/10.1080/15287394.2013.826567.
Tibshirani, R., 1996. Regression shrinkage and selection via the Lasso. J. R. Stat. Soc. Ser. B 58 (1), 267–288.
US Department of Health and Human Services, 2012. Food and Drug Administration. In: Guidance for Industry, Pyrogen and Endotoxins Testing: Questions and Answers.
Vance, M.E., Kuiken, T., Vejerano, E.P., McGinnis, S.P., Hochella Jr., M.F., Rejeski, D., Hull, M.S., 2015. Nanotechnology in the real world: Redeveloping the nanomaterial consumer products inventory. Beilstein J. Nanotechnol. 6, 1769–1780. https://doi.org/10.3762/bjnano.6.181.
Warheit, D.B., 2008. How Meaningful are the results of nanotoxicity studies in the absence of adequate material characterization? Toxicol. Sci. 101 (2), 183–185. https://doi.org/10.1093/toxsci/kfm279.
Watanabe, M., Okada, M., Kudo, Y., Tonori, Y., Niitsuya, M., Sato, T., Aizawa, Y., Kotani, M., 2002. Differences in the effects of fibrous and particulate titanium dioxide on alveolar macrophages of Fischer 344 rats. J. Toxicol. Environ. Health A 65 (15), 1047–1060. https://doi.org/10.1080/15287390276012521 9.
Xia, T., Hamilton, R.F., Bonner, J.C., Crandall, E.D., Elder, A., Fazlollahi, F., Girtsman, T.A., Kim, K., Mitra, S., Ntim, S.A., Orr, G., Tagmount, M., Taylor, A.J., Telesca, D., Tolic, A., Vulpe, C.D., Walker, A.J., Wang, X., Witzmann, F.A., Wu, N., Xie, Y., Zink, J.I., Nel, A., Holian, A., 2013. Interlaboratory evaluation of in vitro cytotoxicity and inflammatory responses to engineered nanomaterials: the NIEHS nano GO consortium. Environ. Health Perspect. 121 (6), 683–690. https://doi.org/10.1289/ehp.1306561.
Xie, G., Wang, C., Sun, J., Zhong, G., 2011. Tissue distribution and excretion of intravenously administered titanium dioxide nanoparticles. Toxicol. Lett. 205 (1), 55–61. https://doi.org/10.1016/j.toxlet.2011.04.034.
Xiong, S., George, S., Yu, H., Damoiseaux, R., France, B., Ng, K.W., Loo, J.S., 2013. Size influences the cytotoxicity of poly (lactic-co-glycolic acid) (PLGA) and titanium dioxide (TiO(2)) nanoparticles. Arch. Toxicol. 87 (6), 1075–1086. https://doi.org/10.1007/s00204-012-0938-8.
Yin, J.J., Liu, J., Ehrenshaft, M., Roberts, J.E., Fu, P.P., Mason, R.P., Zhao, B., 2012. Phototoxicity of nano titanium dioxides in HaCaT keratinocytes—generation of reactive oxygen species and cell damage. Toxicol. Appl. Pharmacol. 263 (1), 81–88. https://doi.org/10.1016/j.taap.2012.06.001.
Zhang, J.Y., Song, W.H., Guo, J., Zhang, J.H., Sun, Z.T., Li, L.Y., Ding, F., Gao, M.L., 2012. Cytotoxicity of different sized TiO2 nanoparticles in mouse macrophages. ToxicolInd Health 29 (6), 523–533. https://doi.org/10.1177/0748233712442708.
Zhang, X.C., Li, W., Yang, Z., 2015. Toxicology of nanosized titanium dioxide: an update. Arch. Toxicol. 89 (12), 2207–2217. https://doi.org/10.1007/s00204-015-1594-6.